FUNCTIONAL NEUROIMAGING OF RESTING-STATE AND STIMULUS-DRIVEN NETWORKS IN THE MACAQUE BRAIN

Dissertation

zur Erlangung des Grades eines
Doktors der Naturwissenschaften

der Mathematisch-Naturwissenschaftlichen Fakultät
und
der Medizinischen Fakultät
der Eberhard-Karls-Universität Tübingen

vorgelegt
von

Frederico Augusto Casarsa de Azevedo
aus Rio de Janeiro, Brazil.

March - 2016

Tag der mündlichen Prüfung: 26.Oktober.2016

Dekan der Math.-Nat. Fakultät: Prof. Dr. W. Rosenstiel

Dekan der Medizinischen Fakultät: Prof. Dr. I. B. Autenrieth

1. Berichterstatter: Prof. Dr. Andreas Bartels

2. Berichterstatter: Tenure-Track Dozent Dr. Georgios A. Keliris

Prüfungskommission: Prof. Dr. Nikos K. Logothetis (Doktorvater)

Prof. Dr. Andreas Bartels

PD. Gabriele Lohmann

Tenure-Track Dozent Dr. Georgios A. Keliris

Declaration:

I hereby declare that I have produced the work entitled “Functional neuroimaging of resting-state and stimulus-driven networks in the macaque brain”, submitted for the award of a doctorate, on my own (without external help), have used only the sources and aids indicated and have marked passages included from other works, whether verbatim or in content, as such. I swear upon oath that these statements are true and that I have not concealed anything. I am aware that making a false declaration under oath is punishable by a term of imprisonment of up to three years or by a fine.

Tübingen, den ....

Date Signature

Dedicated to my family,

Eliane Casarsa, Victor Hugo A. Azevedo,

Leonardo C. Azevedo, Victor Hugo C. Azevedo, and

Katalin A. Kálya.

I love you.

"That which does not kill us, makes us stronger"

- Friedrich Nietzche

ACKNOWLEDGEMENTS

First of all, I would like to specially thank my supervisor, Nikos K. Logothetis, for his trust, patience and support through all those years in his lab. I've developed myself immensely with this unique opportunity, both in personal and in professional terms. Words can't describe how grateful I am.

Unforgettable is my former supervisor, Roberto Lent, who has been always extremely supportive and motivating. Without his trust and additional mentorship, I wouldn't have achieved any of this.

I thank the scientific support of Michael Ortiz-Rios and Vishal Kapoor. Through extreme fruitful discussions with every one of them, my scientific skills improved incredibly and several excellent ideas were born.

Immense thanks to Joachim Werner, our IT-Manager. Without him, chaos would reign. Thank you for being so full of "features", my friend.

To my other family members, Marcos José Marques, Elizabeth Casarsa, Paula Casarsa, André Casarsa, Iracema Casarsa and Jéferson Casarsa. In questa casa siamo tutti nervosi.

And of course, I thank all my friends and colleagues for being there always when I needed, emotionally or professionally: Ricardo Neves, Andrea Zietarska, Ulrike Passlack, Samory Kpotufe, Qinglin Li, Lan Li (and their 2 adorable kids), Cristina Risueno, Hamed Bahmani, Paria Pourriani, Carsten Klein, Agnè Vaic (and little Oliver), Silvia Van Keulen, Paulo Ribeiro, Dávid Balla, Matthias Munk, Gabriele Lohmann, Lewis Chuang, Dong-Seon Chang, Patrice Wegegner, Kasia P., Andriani Rina, Shervin Safavi, María del Mar Ubero, Diana Hernandez, Ali Zaidi, Masataka Watanabe, Shih-pi Ku, Steffen Stoewer, Daniel Zaldivar, Jennifer Smuda, Midea Gierke (and Arlan and Micah), Jonathan Henken, Manuela Liebl, Guo Da, Rasa M., Amit Kumar, Vikram Alva, Michel Besserve, Andre C. Marreiros, Soyoung Kwon, Janina Esins, Nina Gaissert, Elvira Fischer, Amalia Papanikolau, Yibin Shao, Esther Florin, Hannes Goehring, Marcel (Tierstall), Daniel Havel, Silvia Slesiona-Kuenzel, Yusuke Murayama, Axel Oeltermann, Deniz Ipek, Mirko Lindig, Conchy Moya, Mirsat Memaj, Stefano Panzeri, Johannes Boldt, Joshi Walzog, Matthias Arndt, Oliver Holder, Theodor Steffen, Markus Schneller, Glaucia B. Santos, Vinicius Mocaiber, Giani Gotardo, Alvaro S. Peixoto, Diana Cortes, Silvio Martins, Família Altair-Rose Rangel, Anna Carolina Bomfim, Danielle Santiago,

José Martins (Pró-Uni), Carolina Chiao, Ana Terzian, Fabricio and Carla Brasil, Milton Batista, Marcelo Wilde, Theo Marins, Cai Wen Yu, Bruno Buzatto, Bruno Udelsmann, Gustavo Duarte, André Schwambach, Renato Carvalho, Júlia Badur, Vinícius Itatiba and all the others who live in my heart but were betrayed by my poor memory. Without you, this PhD wouldn't have been possible.

Special thanks go to Evi Steinberger, Aline Ivanova, Regine Armann, Juliana N. Gomes and Denise Kobashi for showing me different worlds and ways to live life.

I also thank my fighting partners, Alexandre B. Esperon, Ney Moreira and Emanuel Cardoso, for beating me up even harder every time I thought life was hard enough. OSS!

I have to immensely thank Brigitte and Olga, my two *mulattas*, for having trained me during all this time.

Deutschland, vielen Dank für alles, insbesondere für Wacken und Oktoberfest.

Leo Morita, my Japanese brother, cabah!

CONTENTS

1 ABSTRACT 3

2 INTRODUCTION 5

2.1 ON THE EQUIVALENCE OF INTRINSIC AND EXTRINSIC FUNCTIONAL ARCHITECTURES 6

2.2 LOW-LEVEL AUDIOVISUAL INTEGRATIVE PROCESSES 9

2.3 DUAL STREAM CONCEPT IN VISUAL AND AUDITORY SYSTEMS 10

2.4 AIM OF PROJECTS 13

3 SIMULTANEOUS RESTING-STATE AND VISUALLY-DRIVEN FUNCTIONAL NETWORKS IN THE MACAQUE BRAIN 15

3.1 MOTIVATION 15

3.2 METHODS 16

3.3 RESULTS 17

3.4 CONCLUSIONS 18

4 A POTENTIAL ROLE OF AUDITORY INDUCED MODULATIONS IN PRIMARY VISUAL CORTEX 19

4.1 MOTIVATION 19

4.2 MODEL 20

5 FUNCTIONAL MRI OF THE VOCALIZATION-PROCESSING NETWORK IN THE MACAQUE BRAIN 23

5.1 MOTIVATION 23

5.2 METHODS 23

5.3 RESULTS 25

5.4 CONCLUSIONS 25

6 WIDESPREAD AND OPPONENT FMRI SIGNALS REPRESENT SOUND LOCATION IN MACAQUE AUDITORY CORTEX 27

6.1 MOTIVATION 27

6.2 METHODS 28

6.3 RESULTS 30

6.4 CONCLUSIONS 30

7 DISCUSSION 33

7.1 INTRINSIC AND EXTRINSIC FUNCTIONAL ARCHITECTURES IN THE MACAQUE BRAIN. 33

7.2 A ROLE FOR EXTRINSIC AUDIOVISUAL INTERACTIONS IN PRIMARY VISUAL CORTEX 37
7.3 OBJECT/INDIVIDUAL REPRESENTATION IN MACAQUE AUDITORY SYSTEM 39
7.4 AZIMUTH SPACE REPRESENTATION IN MACAQUE AUDITORY SYSTEM 41
7.5 SUMMARY 42
8 REFERENCES 45
9 LIST OF AUTHOR CONTRIBUTIONS 69
9.1 AZEVEDO F. A. C., ORTIZ-RIOS M., CASARSA, L. A., BALLA D. Z, LI, Q., LOHMANN, G., LOGOTHETIS N. K., AND KELIRIS G. A. (2017). SIMULTANEOUS RESTING-STATE AND VISUALLY-DRIVEN FUNCTIONAL NETWORKS IN THE MACAQUE BRAIN (IN PREPARATION). 69
9.2 AZEVEDO F. A. C., ORTIZ-RIOS M., LI Q., LOGOTHETIS N. K., AND KELIRIS G. A. (2015). A POTENTIAL ROLE OF AUDITORY INDUCED MODULATIONS IN PRIMARY VISUAL CORTEX. MULTISENSORY RESEARCH. 28 (3-4): 331-49. 69
9.3 ORTIZ-RIOS M., KUŚMIEREK P., DEWITT I., ARCHAKOV D., AZEVEDO F. A. C., SAMS M., JÄÄSKELÄINEN I. P., KELIRIS G. A., AND RAUSCHECKER J. P. (2015). FUNCTIONAL MRI OF THE VOCALIZATION-PROCESSING NETWORK IN THE MACAQUE BRAIN. FRONTIERS IN NEUROSCIENCE. 9, 113. 69
9.4 ORTIZ-RIOS M., AZEVEDO F. A. C., KUŚMIEREK P., BALLA D. Z., MUNK M. H., KELIRIS G. A., LOGOTHETIS N. K., AND RAUSCHECKER J. P. WIDESPREAD AND OPPONENT FMRI SIGNALS REPRESENT SOUND LOCATION IN MACAQUE AUDITORY CORTEX. NEURON. 93(4), 971-983. 70
10 APPENDICES 71
10.1 SIMULTANEOUS RESTING-STATE AND VISUALLY-DRIVEN FUNCTIONAL NETWORKS IN THE MACAQUE BRAIN 73
10.2 A POTENTIAL ROLE OF AUDITORY INDUCED MODULATIONS IN PRIMARY VISUAL CORTEX 131
10.3 FUNCTIONAL MRI OF THE VOCALIZATION-PROCESSING NETWORKS IN THE MACAQUE BRAIN 153
10.4 WIDESPREAD AND OPPONENT FMRI SIGNALS REPRESENT SOUND LOCATION IN MACAQUE AUDITORY CORTEX 165
10.5 ILLUSTRATED DESCRIPTION OF THE UNSUPERVISED NETWORK CLASSIFIER DEVELOPED FOR THE STUDY "SIMULTANEOUS RESTING-STATE AND VISUALLY-DRIVEN FUNCTIONAL NETWORKS IN THE MACAQUE BRAIN". 185

1 ABSTRACT

The brain is dynamic. Spontaneous neuronal activity can be observed in cortical and subcortical regions even in the absence of external inputs. At a large scale, long-range coherent spontaneous fluctuations are thought to produce spatially-structured temporal correlations in hemodynamic activity. The set of functional networks observed in the brain during periods of rest, the resting-state networks, constitute what is believed to reflect brain's intrinsic functional architecture. On the other hand, the brain is constantly stimulated by extraneous information. As a consequence, stimulus-driven neuronal activity contributes to shape an extended functional framework, with extrinsic functional topology on top of the intrinsic. How intrinsic and extrinsic network topologies dynamically operate is still unknown. In this thesis, we shed light in this issue after investigating different operational aspects of resting-state and stimulus-driven networks in the macaque brain. We took advantage of the broad coverage at high spatial resolution provided by modern functional neuroimaging to have a global view of brain's functional organization, be it during rest or during sensory stimulation. We started by assessing the topographic relationship of intrinsic and extrinsic functional topologies under different conditions of visual stimulation. Our findings suggest that extrinsic architectures contain an intrinsic component, topographically equivalent to the resting-state architecture, in addition to a stimulus-driven counterpart. Next, we continued our investigation by focusing on the interactions of functional networks evoked by multiple sensory modalities. Specifically, we were interested in the modulatory influences of vision and audition, primate's dominant senses, at early stages of cortical processing. Since no general framework existed concerning auditory influences in early visual cortices, we filled this gap by proposing a novel model for auditory interactions in primary visual cortex, based on recent evidences. Finally, we went beyond early cortical processing and provided evidence supporting the hypothesis of "what" and "where" streams in the auditory cortex specialized in object recognition and spatial representations, respectively. However, we also showed that the analogy between visual and auditory dual streams isn't complete.

2 INTRODUCTION

The primate brain is a complex dynamical system displaying different patterns of oscillatory activity (Penttonen 2003; Buzsáki & Draguhn 2004). These oscillatory patterns have been associated with several neural processes, for example, input selection, plasticity, binding, consolidation; and with various cognitive functions, for instance, salience detection, emotional regulation, attention and memory (Buzsáki & Draguhn 2004; Knyazev 2007; Zuo et al. 2010). Interestingly, even in the absence of external stimulation, intrinsic large-scale temporal correlations in hemodynamic activity can be observed (Biswal et al. 2010). However, intrinsic functional architecture isn't always static. Several studies have shown that extrinsic stimulation and cognitive states are able to modulate intrinsic functional networks (Spadone et al. 2015; Mennes et al. 2013; Astle et al. 2015). How intrinsic and extrinsic functional frameworks dynamically operate is still an open question (Ponce-Alvarez et al. 2015). In this thesis, we investigated different operational aspects of intrinsic (stimulus- and task- free) and extrinsic (stimulus- or task-evoked) functional architectures. We started by assessing the topographical relationship of intrinsic and extrinsic functional configurations (chapter 3). Next, we reconciled recent evidence for extrinsic multisensory modulations at early cortical stages by proposing a novel model for audiovisual interactions (chapter 4). Finally, we explored the concept of a "what" and "where" dual stream, putatively specialized in processing object and spatial representations respectively, within the auditory system (chapters 5 and 6). In our projects, we took advantage of modern functional neuroimaging (fMRI), a technique that provides high spatial coverage at a millimetre scale (Logothetis 2008), to study the brain of anesthetized and awake macaque monkeys at a global scale.

BOLD-fMRI studies performed in macaques are fundamental to bridge the multimodal experimental gap existing between human and non-human primate studies (Logothetis et al. 1999; Logothetis et al. 2001; Hutchison & Everling 2012; Logothetis et al. 2012). Since human experimentation is limited by ethical or practical restrictions that prevent invasive experimentation and manipulation necessary to understand at a neuronal level how the brain processes information, invasive studies are typically performed in

animal models. Consequently, numerous studies using direct interventions, e.g. electrophysiological recordings, microstimulation, ECoG, optical imaging, optogenetics, lesions, etc. have been performed in non-human primates (Krüger & Bach 1981; Vnek et al. 1999; Passingham 2009; Han 2012; Womelsdorf et al. 2014; Logothetis et al. 2010). The macaque brain is a suitable surrogate to the human brain due to their similarities in cellular composition (Azevedo et al. 2009), cytoarchitecture (Petrides & Pandya 1999; Petrides & Pandya 2002; Ongür et al. 2003), structural connectivity (Croxson et al. 2005; Kelly et al. 2010) and functional organization (Rees et al. 2000; Koyama et al. 2004; Petrides et al. 2005; Nakahara et al. 2007). However, in order to confidently derive scientific conclusions, which go beyond the species, data derived from methodologically similar experiments is essential.

2.1 On the equivalence of intrinsic and extrinsic functional architectures

Since its inception, BOLD-fMRI research has been extensively utilized for measuring evoked hemodynamic responses induced by some behavioural manipulation. Traditionally, all signal fluctuations unrelated to the stimulus paradigm were considered noise and thus discarded (Power et al. 2014). However, in 1995, this perspective has changed. In a seminal study, Biswal et al. showed that human subjects who weren't cognitively engaged to any task demonstrated increased temporal correlations among time courses of voxels belonging to particular brain regions. Specifically, they demonstrated that temporal correlations were significantly high among voxels lying in the left and right sensorimotor cortices, the same brain regions active during a finger tapping task (Biswal et al. 1995). Several other studies later confirmed the existence of structured large-scale spontaneous activity in the brain (Lowe et al. 1998; Xiong et al. 1999; Cordes et al. 2000; Raichle et al. 2001; Hampson et al. 2002; Greicius et al. 2003; Hampson et al. 2004). Importantly, temporal coherence of voxel time courses didn't seem to be related to motion, cardiac, respiratory or any other kind of artefact (Power et al. 2014). The term adopted for such functional networks observed in the absence of stimulus or task, i.e. during rest, was resting-state networks.

By definition, resting state networks (RSNs) are spontaneous large-amplitude low frequency fluctuations (<0.1 Hz) of brain activity that happens across functionally related areas in the absence of external stimulation (Biswal et al. 2010). Often measured

with BOLD-fMRI, they are also observed with other techniques, e.g. FDG-PET (Riedl et al. 2014), MEG (van Diessen et al. 2015), fNIRS (Lu et al. 2010), EEG (Deligianni et al. 2014), electrophysiology (Mantini et al. 2007), to cite some. The study of RSNs is interesting for several reasons. They provide important information about anatomical and functional organization of the brain (Power et al. 2014; Sporns 2014) and they are promising non-invasive prognostic/diagnostic tools (Fox 2010). For instance, it has been demonstrated that RSNs span specific functional brain areas, e.g. sensory and motor cortices, language, memory and cognitive systems (Biswal et al. 1995; Lowe et al. 1998; Cordes et al. 2000; Smith et al. 2009; Niazy et al. 2015). In addition, changes in intrinsic network connectivity have been associated with Alzheimer's disease (Li et al. 2002; Greicius et al. 2004; K. Wang et al. 2006; L. Wang et al. 2006; Wang et al. 2007; Allen et al. 2007; Supekar et al. 2008), Parkinson (Lebedev et al. 2014; Baggio et al. 2015), Multiple sclerosis (Lowe et al. 2002; De Luca et al. 2005), ALS (Mohammadi et al. 2009), schizophrenia (Liang et al. 2006; Liu et al. 2006; Liu et al. 2008; Jafri et al. 2008; Whitfield-Gabrieli et al. 2009), autism (Cherkassky et al. 2006; Kennedy & Courchesne 2008; Weng et al. 2010), epilepsy (Waites et al. 2006; Zhang et al. 2009), and numerous others mental disorders.

Resting-state networks aren't an exclusive property of the human brain. Despite their high metabolic cost (60-80% of brain's energy, Raichle and Mintun, 2006), cortical and subcortical RSNs have been observed across many mammalian species. They have been characterized among chimpanzees (Rilling et al. 2007), macaque monkeys (Vincent et al. 2007; Moeller et al. 2009; Margulies et al. 2009; Hutchison et al. 2011; Barttfeld et al. 2015), common marmosets (Belcher et al. 2013), rats (Lu et al. 2007; Pawela et al. 2008; Majeed et al. 2009; Zhang et al. 2010; Liang et al. 2011), mouse (Jonckers et al. 2011; Shah et al. 2015), et cetera. We chose the macaque brain (*Macaca mulatta*) as experimental model due to its high correspondence to the human brain concerning RSN topology (Hutchison & Everling 2012).

The relationship between intrinsic and extrinsic functional architectures in the brain is still unclear. Resting-state functional connectivity and stimulus-evoked functional connectivity are processes typically studied separately (Cole et al. 2014). Nevertheless, controversies about their equivalence have already risen. While some groups claim high correspondence of brain's functional architecture during activation and rest, sharing a common repertoire of networks in both states (Smith et al. 2009), others claim that tight

functional coupling can occur for default and task-positive regions, but it doesn't necessarily occur in the whole brain, e.g. in primary sensory and motor cortices (Mennes et al. 2013; Buckner et al. 2013). We aimed at addressing this issue by investigating the topographical correspondence between intrinsic and extrinsic functional architectures in the macaque brain exposed to different conditions of visual stimulation.

In order to study the topography of functional architectures, we made use of a mathematical analysis technique that is usually being applied in rsfMRI, namely spatial Independent Component Analysis (sICA). sICA is a blind-source separation technique used to decompose multivariate signal, ideally linearly mixed, into maximally statistical-independent spatial components (or networks). Briefly, the idea behind ICA is to individually rotate each axis of the data, until minimal Gaussianity (alternatively, mutual information) of data projection on the axes is achieved. Feasibility of this approach is based on the central limit theorem, which states that independent random variables are individually less Gaussian than any linear combinations of them. Typically, before ICA is performed, centering (subtraction of the mean to create zero-mean data), whitening (linear change of data coordinates to remove data correlations) and dimensionality reduction (reduction of the number of random variables keeping most of variance) are applied to the data. Note, that contrary to Principal Component Analysis (PCA), ICA doesn't impose orthogonality of dimensions. Importantly, if the sources aren't independent, ICA will find the space of maximal statistical independence (Herault & Ans 1984; Comon 1994; Hyvärinen et al. 2001). Applied to fMRI, sICA basically relates the time courses of each voxel with the time courses of each maximally independent component, resulting in spatial maps of similarity coefficients. As we mentioned above, overlapping of spatial maps is possible as orthogonality is not required. Advantages of sICA in comparison with alternative methodologies, i.e. seed-based analysis, are: a) non-necessity of prior spatial assumptions; b) less influence of structured confounds; c) simultaneous comparison of every voxel; and d) the fact that sICA components tend to be less noisy than estimates obtained using alternative techniques (Birn et al. 2008; Murphy et al. 2009). Disadvantages include the necessity to arbitrarily choose the dimensionality reduction parameters and model order selection, and the inherent variability associated with its stochastic nature, which can cause variability even after running it in the same dataset multiple times. We used post-hoc analysis (ICASSO) to confirm stability of our sICA decomposition.

Using sICA, we were able to consistently identify a set of intrinsic functional networks and their putative correspondents, contained within our stimulus-driven datasets. After decoupling low-frequency oscillations from stimulus-evoked components, we observed high topographical correspondence among all low-frequency networks across subjects and conditions. Our data suggests that extrinsic functional architecture is constituted of an intrinsic component and a stimulus-evoked counterpart. More details about this project are depicted in chapter 3.

2.2 Low-level audiovisual integrative processes

In our second project, we decided to focus on extrinsic functional interactions between visual and auditory systems. Specifically, we were interested in knowing how early visual and auditory cortices would be able to integrate multimodal information. For decades, it has been considered that multisensory interactions would be an exclusive property of higher-level cortical regions, e.g. frontal, prefrontal, intraparietal and superior temporal cortices (Andersen et al. 1997; Fuster et al. 2000; Beauchamp 2005). However, recently, evidence has been observed in favour of the hypothesis, that cross-modal interactions could also occur within low-level cortical areas (Ghazanfar & Schroeder 2006). Interestingly, while there is considerable evidence demonstrating visual modulations of early auditory processes (for a review, see Schroeder and Foxe, 2005), very few studies have reported auditory modulations in the primary visual cortex at a neurophysiological level. In one of those, Wang et al., utilized extracellular recordings among behaving monkeys in order to demonstrate that a simultaneous presentation of a sound during a visually guided saccade task significantly reduced neuronal onset latency of single neurons in V1 and, in parallel, increased behavioural performance (Wang et al. 2008). A year later, Lakatos et al showed that auditory stimuli were able to reset ongoing neuronal network oscillations in V1 (Lakatos et al. 2009). Additionally, behavioural studies reported auditory modulation of early visual cortices at feedforward processing time, shorter than top-down latencies (Bolognini et al. 2010; Shams et al. 2000; Watkins et al. 2006; Watkins et al. 2007). Based on this evidence, we reasoned that direct cortico-cortical projections between primary auditory and visual cortices were possibly playing a role in mediating such early integrative processes. At a cellular level, multisensory integration is defined as the process by which at least two heteromodal sensory inputs are

combined to form a distinct output (Stein et al. 2009). Anatomically, a pre-requisite for integration is that neural connections from different sensory receptors reach directly or indirectly a common individual neuron. The axonal confluence allows cross-modal postsynaptic currents to collide on the same excitable neuronal membrane, which creates potential for unimodal responses to modify processing of cross-modal information (Meredith 2002; Clemo et al. 2012). Therefore, if primary auditory (A1) and primary visual (V1) cortices were integrating information at feedforward latencies, direct A1-V1 projections were probably involved. Indeed, monosynaptic connections between A1 and V1 in the macaque brain have been reported before (Falchier et al. 2002; Rockland & Ojima 2003; Clavagnier et al. 2004). Surprisingly, more than 10 years have passed and the exact function of those projections are still undetermined.

To reconcile the aforementioned evidence with current models of multisensory integration, we proposed a new model for audiovisual interactions. Briefly, we suggest that an unexpected sound stimulus is able to trigger overt orient responses towards its source and, at the same time, increase V1 sensitivity at the cortical representations where the object is expected to appear in the field of view. In other words, auditory cues regarding spatial and object identity would enhance visual sensitivity and detectability of a possibly relevant event. This is suggested to be performed by three distinct functional pathways working in parallel. A pathway encompassing the superior colliculus would coordinate overt orienting behaviour, a monosynaptic A1-V1 pathway would enhance spatiotemporal sensitivity and a third pathway traversing higher order cognitive areas would facilitate object detectability. Particular to our model, we consider the possibility of cross-modal interactions occurring in non-overlapping regions of field of hearing and field of view. Our proposal is detailed in chapter 4.

2.3 Dual stream concept in visual and auditory systems

In our last two projects, described in chapters 5 and 6 respectively, we explored sensory processing occurring beyond early cortical stages. Specifically, we compared the hypotheses of specialized dual streams, mediating specific features of the sensory input, progressing hierarchically across visual and auditory systems, namely the “what” and “where” pathways.

In 1972, M. Mishkin proposed that two distinct anatomical pathways would be involved in the processing of two different types of visual information (Mishkin 1972). In his own words, "One, the superior longitudinal fasciculus, follows a dorsal path, traversing the posterior parietal region in its course to the frontal lobe; the other, the inferior longitudinal fasciculus, follows a ventral route into the temporal lobe. (…) the ventral or occipitotemporal pathway is specialized for object perception (identifying what an object is) whereas the dorsal or occipitoparietal pathway is specialized for spatial perception (locating where an object it)" (Ungerleider & Mishkin 1982). His proposal was based on the anatomical identification of two major neuronal fiber bundles diverging from occipital cortex and projecting rostrally in the brain (Flechsig 1896; Flechsig 1920), along with evidence available through lesion, behavioural and electrophysiological studies carried out in humans and monkeys (Mishkin 1972). Since then, the "what-and-where" proposal has been corroborated with a plethora of modern evidence, serving as a solid foundation for new hypotheses about visual processing (Goodale & Milner 1992; Milner & Goodale 2008).

Interestingly, Mishkin's idea traversed the field of visual research and inspired analogous hypotheses comprising different sensory modalities. In the late 90's, a similar dichotomic model concerning the primate auditory system was proposed. In this model, an analogous "where" stream, specialized in representing spatial positions, would originate in the caudal part of the superior temporal gyrus and reach the parietal cortex; whereas a specialized "what" stream, specialized in representing object and individuals, would encompass more anterior portions of the lateral belt (Rauschecker et al. 1997; Rauschecker 1998; Romanski et al. 1999). Subsequent neurophysiological studies in macaque monkeys confirmed that while the caudal lateral belt (area CL) is more selective to sound location, the anterior lateral belt (area AL) of auditory cortex responds preferentially to identity of sounds, including monkey vocalizations (Kusmierek & Rauschecker 2014; Tian et al. 2001). The concept of specialized dual-stream processing in the auditory cortices of primates was further supported by human neuroimaging studies showing that object localization of auditory objects are processed within a parietal-to-lateral-prefrontal pathway while object identification happens via an anterior-temporal-to-inferior-frontal (Maeder et al. 2001; Arnott et al. 2004; Ahveninen et al. 2006). Nonetheless, several studies have contested this concept, especially in what concerns the "where" pathway (Cohen & Wessinger 1999; Zatorre et al. 2002; Middlebrooks 2002;

Sumner & Krumbholz 2012; Bizley & Cohen 2013). To investigate the auditory dual-stream concept we used whole-brain fMRI in macaque monkeys to study each stream separately.

Concerning the "what" pathway, considered to be specialized for processing the identity of objects and individuals, we scanned awake animals while they were being acoustically stimulated by conspecific vocalizations (monkey calls) and environmental sounds. Monkey calls are a special category of sound stimuli because they not only convey information about representation of objects and events but also about affective states, possibly similar to human communication (Cheney & Seyfarth 1990; Ghazanfar & Hauser 1999; Yovel & Belin 2013). This characteristic is particularly interesting in the context of evolution of speech and language (Rauschecker 2012; Bornkessel-Schlesewsky et al. 2015). In our results, we observed preferential activity due to monkey vocalizations in the anterior STG and in other regions along the auditory ventral stream as well as in specific areas of the parabelt and antero-lateral belt. Our findings support the role of a ventral "what" stream, and also provide evidence of multimodal interactions happening in higher order multisensory areas, including regions related to visual processing. This project is detailed in chapter 5.

Next, we focused on the functional mechanisms underlying the "where" pathway. The existence of a dorsal auditory pathway specialized in processing spatial information including areas CL/CM of posterior superior temporal region (Rauschecker & Tian 2000; Tian et al. 2001) is supported by electrophysiological recordings and anatomically tract tracing in macaque monkeys (Romanski et al. 1999). Area CL contains neurons sharply tuned to sounds presented at different azimuth positions (Tian et al. 2001), which are significantly more selective than neurons in any other region of the auditory cortex (Woods et al. 2006; Miller & Recanzone 2009; Kusmierek & Rauschecker 2014). However, other neurophysiological studies show that spatial position of sounds is coded by neurons spread throughout the superior temporal cortex, being broadly tuned to the contralateral hemifield (Werner-Reiss & Groh 2008; Salminen et al. 2009; Magezi & Krumbholz 2010). They are in agreement with the hypothesis that acoustic space is coded by opponent neural populations selectively representing the left or right side (Stecker & Middlebrooks 2003; Stecker et al. 2005). To investigate at a voxel level if azimuth space is portrayed in the auditory cortex with local or distributed functional representations, we scanned awake and anesthetized monkeys stimulated with

a special set of spatial sounds. Our auditory stimuli were custom designed to induce differential BOLD-activity according to distinct azimuth spatial sectors. Among our findings, we report the existence of opponent patterns of positive and negative BOLD responses, which favours the distributed-coding hypothesis (Stecker & Middlebrooks 2003). We also found that hemifield tuning is dependent on interaural time differences and that right posterior superior temporal region represents space with a hemifield-code more robustly than any other auditory field. Overall, our results support the hypothesis of a dorsal stream specialized in processing spatial information, but with some particularities. For more details, see chapter 6.

2.4 Aim of projects

Overall, our aim was to study distinct operational principles of intrinsic (stimulus- and task- free) and extrinsic (stimulus- or task- evoked) functional architectures. The objective of our first project was to investigate topographical equivalence of extrinsic and intrinsic low-frequency functional networks in the macaque brain exposed to different conditions of visual processing (chapter 3). We further exploited extrinsic brain functional architecture from a multisensory perspective, taking into account both visual and auditory modalities. Since a considerable amount of evidence pointed to audiovisual interactions at early stages of visual processing but a consistent model was still missing, we tried to fill out this blank by suggesting a potential role for auditory modulations in primary visual cortex (chapter 4). Finally, we investigated the concept of a "what-and-where" dual-stream in the auditory cortex, which would be analogous to the visual "what-and-where" pathways. Each stream was studied individually (chapters 5 and 6, respectively).

3 SIMULTANEOUS RESTING-STATE AND VISUALLY-DRIVEN FUNCTIONAL NETWORKS IN THE MACAQUE BRAIN

3.1 Motivation

Initially, studies of functional connectivity in the human brain focused mainly on the extrinsic network architecture related to stimulus- or task-evoked hemodynamic responses (Friston 1994). However, a paradigm shift started in 1995, when it was firstly reported that even in the absence of external stimulation, temporal correlations in hemodynamic activity between spatially remote brain areas can be observed (Biswal et al. 1995). Those spatially constrained temporal correlations were termed resting-state networks (RSNs). Currently, they are considered to form an intrinsic functional architecture in the brain (Fox & Raichle 2007). More than a decade later, in 2007, the existence of an analogous intrinsic architecture was confirmed to exist also in the brain of anesthetized macaque monkeys (Vincent et al. 2007). Since then, numerous studies investigating resting-state and stimulus/task-evoked functional connectivity have been performed on both species and across a multitude of conditions (Hutchison & Everling 2012; Miranda-Dominguez et al. 2014). Still, how extrinsic and intrinsic functional

architectures relate to each other is yet to be determined. While some groups claim that the functional networks observed in the active brain and in the resting brain are the same (Smith et al. 2009), other studies showed that tight functional coupling might happen for default and task-positive regions, but not necessarily for primary sensory and motor cortices, limbic regions or subcortical structures (Mennes et al. 2013; Buckner et

al. 2013). With this project, we sought to shed light in this controversy by assessing topographical correspondence of intrinsic and extrinsic functional hemodynamic networks in the anesthetized macaque brain exposed to different conditions of visual stimulation.

3.2 Methods

We collected high-field (7T) whole-brain fMRI images from two anesthetized macaque monkeys stimulated with three main paradigms: a) no visual stimulation, b) visual stimulation using a one-minute block-design displaying natural movie clips alternated with gray background, and c) continuous visual stimulation using uninterrupted natural movies. As control, we additionally collected fMRI data during continuous exposition to the same gray background used in the block design. Preprocessing was done with AFNI (Cox 2012) and consisted of despiking, slice timing correction, motion correction with 6-parameters affine transformation, spatial smoothing with 3 mm full width at half maximum (FWHM) Gaussian kernel and bandpass filtering (0.01 to 0.1 Hz). Concerning the datasets where the animals were visually stimulated, we separated the estimated visual activity from the raw data before bandpass filtering by using general linear modelling (GLM). After confirming significant visual activity in the visual cortices caused by our visual paradigms ($p<0.05$, FDR corrected), we proceeded the analysis by using only the residuals of the GLM, viz. the "error" or unexplained variance. The next step consisted in estimating maximally independent spatial sources from BOLD signal for every condition (McKeown et al. 1998). For that, we used spatial independent component (sICA) as implemented in GIFT software (Calhoun et al. 2001). Data processing steps we performed with GIFT can be generally summarized in three parts: reduction of voxel time series dimensionality by means of principal component analysis (PCA, Pearson, 1901); ICA decomposition of 20 a-priori-imposed spatial components using the Infomax algorithm (Bell & Sejnowski 1995); and back-reconstruction of the data. Reliability of decomposition was post-hoc checked with ICASSO algorithm (100x ICA reiteration, Himberg et al., 2004). To exclude possible algorithmic biases, we confirmed GIFT-ICA results using FSL-MELODIC (Smith et al. 2004). For intersubject comparisons, fMRI datasets were spatially normalized to the F99 surface-based macaque atlas (Van Essen 2002) and cortical areas were defined according to the LVE00

partitioning scheme (Lewis & Van Essen 2000b), available in Caret software (Van Essen 2002). Intersession networks were grouped based on pairwise spatial correlations using a custom-written unsupervised network classifier (see appendix 10.5). Structural and functional connectivity were compared by cosine similarity of intersecting matrices. Finally, we used Eigenvector Centrality Mapping (ECM, Lohmann et al., 2010), a hypothesis-free method that attributes network properties to voxels, to calculate the functional "hubness" of distinct areas of the resting brain.

3.3 Results

ICA decomposition of resting-state data identified 8 consistent functional networks identified in both subjects: the precentral-temporal network; the medial-occipital network; the fronto-parietal network; the paracentral network; the default-mode network; the lateral-occipital network; a subcortical network encompassing the putamen, caudate and amygdala; and a cerebellar network. The first 6 aforementioned components were mostly cortical and have been previously reported (Lowe et al. 2002; Mantini et al. 2011; Hutchison et al. 2011). Components of no-interest, i.e. white matter and CSF, were also observed but excluded from further analysis. Following the identification of resting state networks, we set out to search for their putative correlates in the residuals of visually-driven datasets and in the long, continuous stimulation, movie datasets. Strikingly, all consistent resting-state networks had a correlate showing high topographical similarity in the stimulus-driven datasets, a resting-state-like network. Interestingly, we identified a consistent pattern of thalamocortical connectivity in the precentral-temporal network, which could be related to a thalamocortical pacemaker (Hughes et al. 2004; Hughes & Crunelli 2005; Lörincz et al. 2008). Additionally, we observed increased eigenvector centrality in fronto-parietal areas in our resting-state datasets, suggesting that this region works as an intrinsic functional hub. Finally, in agreement with the literature, we didn't observe high correspondence between functional and structural connectivity (Adachi et al. 2012; Shen et al. 2012; Buckner et al. 2013).

3.4 Conclusions

In this work, we showed that a resting-state-like intrinsic architecture is contained and can be recovered from fMRI datasets showing significant bottom-up visual activity. Topographical correspondence with resting-state networks was strikingly large. Our findings are in agreement with a previous human fMRI study suggesting that brain's extrinsic architecture could be composed of a primarily intrinsic component and a secondarily paradigm-evoked counterpart (Cole et al. 2014). Remarkably, we didn't observe functional interference between intrinsic networks and strong bottom-up visual activity, not even in the two visual components (the lateral-occipital and the medial-occipital networks). A possible explanation is that lower frequency oscillations would be happening in deeper layers while stimulus-induced oscillations would be simultaneously occurring in superficial layers (Maier et al. 2010; Buffalo et al. 2011). Consequently, our BOLD signal would have captured the combined hemodynamic activity related to both laminar domains. In general, it's possible that no modulation of whole-brain intrinsic network architecture occurred because anaesthesia inhibited most of top-down influences (Rainer et al. 2001); and top-down modulation is considered to be an essential factor in shaping intrinsic functional networks (Engel et al. 2001; Capotosto et al. 2014). An important source of top-down projections are the fronto-parietal regions (Engel et al. 2001). It has been suggested that these regions are composed of flexible hubs capable of regulating task-evoked functional connectivity (Cole et al. 2013). Our resting-state datasets support this hypothesis by showing increased eigenvector centrality in voxels contained in fronto-parietal regions. An additional interesting finding was a consistent pattern of thalamocortical functional connectivity in the precentral-temporal network, which could be related to a specialized pacemaker mechanism. It has been previously proposed that such a thalamocortical pacemaker could work as a modulator/generator of spontaneous oscillations of neural activity, being directly related to brain's intrinsic functional architecture (Hughes et al. 2004; Hughes & Crunelli 2005; Lörincz et al. 2008). Finally, from a practical perspective, since we showed that there's important information contained in the normally discarded stimuli-driven residuals, our study stimulates the reinterpretation of a large existing neuroimaging database, potentially providing substantial gain of knowledge with minimal additional effort. Nevertheless, to which extent and under which alternative paradigms our results are generalizable are a subject for future studies.

4 A Potential Role of Auditory Induced Modulations in Primary Visual Cortex

4.1 Motivation

In the absence of external stimulation, resting-state networks can be observed in the brain (Biswal 2012). However, nature is seldom quiescent. Throughout the day, animals are constantly confronted with isolated events which are often critical to their survival. Normally, each of those events emanate different types of information. In order to optimize detection of such event-related signals, specialized sensory channels were selected through evolution. Photoreceptors were developed to detect photons; mechanoreceptors to recognize mechanical pressure or distortion; chemoreceptors to distinguish specific chemical substances; and thermoreceptors to code changes in temperature. In this study, we focused on the interactions of auditory and visual modalities that have a primary importance for primates (Kajikawa et al. 2012).

Audiovisual processing takes place at multiple stages. As soon as auditory and visual stimuli are translated by their specialized receptors, a cascade of hierarchical processing starts. Initially, basic sensory processing is high specialized and defined into early cortical regions (Macaluso & Driver 2005; Kanwisher 2010). For instance, low-order aspects of visual inputs are decomposed in primary visual cortices, while basic sound features are computed in primary auditory cortices. Generally, resulting outputs converge through a hierarchical albeit highly recurrent network onto higher-order multisensory areas, being combined into a coherent percept (Felleman & Van Essen 1991; Ghazanfar & Schroeder 2006; Wei et al. 2012).

From the perspective of the brain as a "Bayesian" estimator of the environment (Ernst & Banks 2002; Knill & Pouget 2004; Fetsch et al. 2013), such a combination of multiple, independent sensory measurements is highly efficient because it minimizes the uncertainty of sensory estimation. In other words, by integrating information from all available senses, the brain maximizes use of available data at any moment and enhances physiological salience of potentially relevant events. As a consequence, adequate reactions are facilitated and the chances of survival boosted (Stein et al. 2014). The ability of the brain to use its auditory and visual senses synergistically, powerful enough to compensate for a complementary sense when necessary, is referred to as audiovisual integration.

For a long time, it was considered that audiovisual interactions would happen exclusively in higher-order cortical regions, i.e. in the frontal, temporal and parietal association areas. However, recent studies showed that cross-modal interactions can be observed also at low-level stages of sensory processing (Ghazanfar & Schroeder 2006). Reports about visual modulation of auditory processing in early cortical stages are becoming increasingly common (Schroeder & Foxe 2005). Nevertheless, despite behavioural evidence for auditory modulation of visual perception (Shams & Kim 2010) and the existence of direct projections from the primary auditory cortex to the primary visual cortex (Falchier et al. 2002; Rockland & Ojima 2003; Clavagnier et al. 2004), few studies have reported neurophysiological evidence for auditory modulations in V1. Here we try to reconcile multimodal evidence for auditory induced modulations in primate V1 by proposing a new model for such interactions.

4.2 Model

Most models of audiovisual integration take into account that both visual and auditory information are available at their specific channels at approximately the same time. In other words, it's normally assumed that visual and auditory stimuli derived from a particular event are simultaneously enclosed by the field of view and the field of hearing. Our model overcomes such limitation by generalizing to situations where the event happens in non-overlapping regions of audiovisual sensory fields. Specifically, we suggest that the auditory component of an event happening outside the field of view would be able to prepare the visual system to detect the expected event by modulating

low-level visual areas using specialized parallel processing streams. Our model was inspired by behavioural (Shams & Kim 2010), anatomical (Falchier et al. 2002; Rockland & Ojima 2003; Clavagnier et al. 2004) and neurophysiological studies (Lakatos et al. 2008; Wang et al. 2008; Lakatos et al. 2009).

In our model, we propose that an auditory spatial cue conveying object identity is able to modulate overt orienting responses, visual spatial sensitivity and visual object selectivity at approximately the same time. For each function, there would be a specialized processing stream operating through distinct neural pathways. According to our hypothesis, after such an auditory cue stimulates the cochlea, auditory information is projected to the cochlear nuclei and sent to the olivary nucleus (ON). In the ON, spatial information such as azimuthal distance is calculated. From there, evoked outputs are directed the inferior colliculus (IC), where the first bifurcation in signal flow happens. While one stream is sent to the superior colliculus (SC), the other progresses through the medial geniculate nucleus and reaches the auditory cortices. The SC stream would coordinate overt orient responses towards the expected location of the cued event, for instance, gaze direction (Sparks 1999). Since SC contains overlapping auditory, visual, somatosensory and motor receptive fields, cross-modal interactions and adequate motor responses are facilitated (Stein et al. 1975). In parallel, the stream sent to the auditory cortices would bifurcate once again in the primary auditory cortex (A1). While one part of it would be monosynaptically projected to the primary visual cortex (V1), the other share would polysynaptically transverse higher level audiovisual areas, eventually converging on V1. The function of the A1-V1 stream would be to enhance in visual spatial sensitivity in a bottom-up fashion. Complementarily, the higher-level stream would be responsible to recover previously stored audiovisual memories of similar experiences, to create a visual expectation of the event to be detected and to modulate visual receptive fields all the way down to V1, based on this expectation. By doing so, visual identification of the related event would be promoted. Of most importance, our model generates predictions that can be experimentally tested, i.e. specific increases in neural activity in V1 due to errors in predictions between expected and incoming audiovisual signals.

5 FUNCTIONAL MRI OF THE VOCALIZATION-PROCESSING NETWORK IN THE MACAQUE BRAIN

5.1 Motivation

Among all categories of auditory stimuli, species-specific vocalizations are of a special kind. It conveys semantic information not just about objects and events but also about affective states, being crucial for social interactions, reproductive success and survival (Cheney & Seyfarth 1990; Ghazanfar & Hauser 1999; Yovel & Belin 2013). Not surprisingly, the identification of common neural networks for vocalization processing in monkeys and speech processing in humans are of particular interest for understanding the evolution of speech and language (Rauschecker 2012; Bornkessel-Schlesewsky et al. 2015). In this study, we sought to investigate how auditory-related areas represent conspecific vocalizations in the awake behaving macaque brain. We made use of the high spatial resolution of whole-brain fMRI to have a global overview of areas involved in the processing of complex sounds, relating them to their putative anatomical counterparts. Our purely auditory paradigm was also able to activate cortical areas known to be involved in visual processing.

5.2 Methods

Two male rhesus monkeys (*Macaca mulatta*) were trained to lie motionless in sphinx position inside a MRI-compatible primate chair while performing a behavioural task. The task consisted of a go/no-go auditory discrimination paradigm adapted to sparse-sampling fMRI acquisition. Sparse-sampling design allows the acquisition of

auditory-evoked BOLD response without contamination of scanner noise, caused mainly by the frequent gradient-switching noise typical of continuous GE-EPI sequences. During the behavioural task, the animals had to fixate at a central red spot while hearing 6 s of auditory stimulation (80 dB). After this period, a brain volume would be acquired for approximately 2 s. A trial ended when a white-noise target sound, delivered at a random delay (0.5 – 1.5 s), cued the macaques to perform a saccade to the left or to the right side of the screen. Each trial was alternated with a similar but silent condition. Data for each monkey was individually collected using a horizontal Siemens MAGNETOM Trio 3T scanner and a custom-made saddle radiofrequency coil covering the whole brain. Behavioural performance was assessed to ensure that the animals were attending to each stimulus. Auditory stimuli were presented with Presentation software (Neurobehavioural Systems) through modified electrostatic in-ear headphones. Three sound categories were played: environmental sounds, monkey vocalizations (calls) and scrambled monkey calls. Eye movements were recorded with an infrared eye-tracking system. Stimulus specific predictors were created by convolving square wave stimulus functions with a one-parameter gamma variate hemodynamic response function (HRF). Statistically significant activation was determined with general linear modelling (GLM). A bootstrapping procedure applied to the resulting statistical t-maps calculated a mean weighted laterality index. Shortly, the algorithmic steps are: a) to choose 20 thresholds ranging from 0 until the maximum t-value present in a symmetrically defined region of interest for each contrast; b) To select 100 samples with 25% of the original size were in a uniformly random manner for each threshold; c) To calculate 10.000 laterality indexes (LI's) corresponding to every left and right sample combinations; d) To find a trimmed mean based on the middle 50% of LI's; e) to calculate the mean weighted laterality index (LIwm) using the formula:

$$LIwm = \sum_{i=1}^{n} Wi * Xi \,/\, \sum_{i=1}^{n} Wi$$

where n is the number of thresholds, X is the trimmed mean and W is the threshold at which X was calculated. A value of -1 represents complete right lateralization while a

value of +1 represents complete left lateralization (Wilke & Schmithorst 2006; Wilke & Lidzba 2007).

5.3 Results

Irrespective of stimulus category, our auditory paradigm elicited significant BOLD responses in subcortical auditory pathways, auditory areas of the superior temporal gyrus and also regions in inferior temporal, parietal and prefrontal cortices. Specifically, we observed significant activation in the cochlear nuclei, inferior colliculi, medial geniculate bodies, A1 and STG. After contrasting monkey vocalizations with environmental sounds, we found vocalization-sensitive regions in the anterolateral area (AL), lateral rostrotemporal area (RTL), rostrotemporal pole (RTp), ventrolateral prefrontal cortex (vlPFC) and inferior parietal areas (PF and PFG). Additionally, to verify if the activations we observed were due to specific spectrotemporal differences of vocalizations and environmental sounds, we contrasted monkey calls with their scrambled versions. We found that RTL/RTp areas were significantly more activated by the undistorted condition. Besides that, we observed significant activation in higher visual areas, such as IT and MT. A right hemispheric bias was observed for every contrast in every animal.

5.4 Conclusions

Here we studied fMRI responses evoked by complex sounds in awake behaving animals without the need of any contrast agent, i.e. MION. We showed that our sparse-sampling auditory paradigm is highly effective in mapping cortical and subcortical auditory structures (Rauschecker et al. 1995; Poremba et al. 2003). Our results confirm the existence of a bias in the right auditory cortex of macaque brains when processing complex sounds (Petkov et al. 2008; Joly, Ramus, et al. 2012) with higher sensitivity to monkeys calls in anterior superior temporal gyrus (Poremba et al. 2003; Petkov et al. 2008; Kikuchi et al. 2010; Joly, Ramus, et al. 2012; Joly, Pallier, et al. 2012; Fukushima et al. 2014). Increased local selectivity for monkey vocalizations is in full agreement with single-unit studies of the R/AL region in macaque cortex (Tian et al. 2001; Kuśmierek et al. 2012). Our findings support the hypothesis that vocalizations are cortically represented

through an auditory ventral pathway, encompassing a network of interconnected areas in anterior superior temporal gyrus and ventrolateral prefrontal cortex. A potential function for the ventral auditory stream would be to extract abstract information necessary for recognition and categorization of vocalizations (Ghazanfar & Logothetis 2003; Rauschecker 2012). Interestingly, our auditory paradigm also activated higher level visual areas, such as middle temporal (MT) and inferior temporal (IT), which are respectively known for visual motion processing (Maunsell & Van Essen 1983) and for object perception, including faces (Tsao et al. 2006; Ku et al. 2011).

6 WIDESPREAD AND OPPONENT FMRI SIGNALS REPRESENT SOUND LOCATION IN MACAQUE AUDITORY CORTEX

6.1 Motivation

Knowing the meaning of an auditory stimulus and associating it with particular emotional states or individuals are not the only critical factors for survival. It's also extremely important to know the spatial origin of the sound. As mentioned in chapter 4, a natural event is normally accompanied by coincident sounds. As an evolutionary consequence, sophisticated apparatus for sound-source localization were selected. In the mammalian brain, positioning of an acoustic target is derived from a combination of interaural time differences (ITD), interaural level differences (ILD) and spectral cues (Blauert 1997; Cohen & Knudsen 1999; Grothe et al. 2010). Concerning primates, it's known that processing of spatial information happens not only along the ascending auditory pathway (Thompson & Cortez 1983; Wise & Irvine 1985; Grothe et al. 2010) but also at the superior temporal region. Nonetheless, the underlying mechanisms of cortical sound-source localization are still unclear.

Two main hypothesis for cortical sound-source localization related to the primate brain have been proposed. One conjectures that sound location is represented in confined areas of the auditory cortex (Tian et al. 2001). Alternatively, the other suggests that sound-source processing is distributed across the superior temporal cortex (Stecker & Middlebrooks 2003). Neurophysiological evidence exists in support of both propositions. While some studies using single-unit recordings report the existence of

neurons sharply tuned to frontal azimuth position that are located mainly in the caudolateral area (Tian et al. 2001); other studies demonstrate the existence of neurons broadly tuned to the contralateral hemifield spread throughout the auditory cortices (Werner-Reiss & Groh 2008; Salminen et al. 2009; Woods et al. 2006; Miller & Recanzone 2009; Kusmierek & Rauschecker 2014). To understand whether acoustic localization is processed locally or diffusely throughout the auditory system at the population level, large scale measurements of neural activity are fundamental. Here we took advantage of high resolution fMRI, able to sample indirect neuronal activity of multiple cortical sites simultaneously with millimetre spatial precision, in order to investigate acoustic space representation in macaque auditory cortex.

6.2 Methods

In the experiments pertinent to this study, 4 rhesus monkeys (*Macaca mulatta*) were used. Two males were functionally imaged under anesthesia and two females were scanned while being awake. Before experiments, the macaques were previously implanted with an MRI compatible headpost. All experimental procedures were carefully done to ensure the well-being of the animals, were previously approved by the local authorities (Regierungspraesidium) and were in full compliance with the guidelines of the European Community (EUVD 86/609/EEC) for the care and use of animals in laboratories. The animals assigned to awake fMRI experiments were trained to sit still during scanning in a custom-made MRI chair. Eye movements were recorded with an infrared eye-tracking system. All acoustic stimuli were delivered through electrostatic in-ear headphones. Sparse sampling GE-EPI fMRI sequences were used to avoid contaminations of BOLD responses due to scanner noise, similar to described in chapter 5. Images were collected with a whole-head volume coil. Experiments involving anesthesia were performed in a vertical 7T Bruker scanner while experiments with awake monkeys were done in a vertical 4.7T Bruker magnet.

To evaluate the sensitivity of our methodology and to define functionally active auditory areas in the superior temporal gyrus, we firstly mapped cortical tonotopy using phase-encoding paradigms. Tonotopy, the spatial arrangement of areas processing tones of consecutive frequencies in a topological neighbourhood, is a functional property known to be present in macaque auditory cortices (Morel et al. 1993; Kosaki et al. 1997;

Rauschecker et al. 1995; Recanzone et al. 2000). Our auditory stimuli consisted of 12 cycles of sound blocks, consisting of pure tones and bandpassed noise bursts, presented progressively from low to high frequencies. Each consecutive block was an octave higher than the previous one. Such a paradigm induced a traveling wave of BOLD-response across the superior temporal gyrus. Responsive voxels were determined by using a measure of coherence:

$$C(f_0) = A(f_0)/(\sum_{f=f_0-\frac{\Delta f}{2}}^{f_0+\frac{\Delta f}{2}} A\,(f)^2)^{\frac{1}{2}}$$

where $f0$ is the frequency of the stimulus, $A(f0)$ the signal amplitude at $f0$, $A(f)$ the harmonic term amplitude at voxel temporal frequency f and Δf the bandwidth of frequencies in cycles/scan around $f0$. For our analyses, every $f0$ corresponded to 12 cycles (0.01 Hz) and Δf corresponded to the frequencies around the fundamental (except the second and third harmonics). Coherence measures the association of time-series by relating the amplitude at the fundamental frequency to signal variance. For our analysis, voxels with a coherence value greater than 0.3 were selected. The preferred sound-frequency of those voxels were assigned according to the maximal BOLD response for a specific stimulus frequency. Areal boundaries were delineated using mirror-reversals in the tonotopy maps as reference.

Coherence was additionally used to map spatial domains in the auditory cortices. However, instead of 12 cycles of sound blocks with different frequencies as auditory stimulus, we used 12 sets of spatially contained sounds covering every 30o sector of azimuth space. Subsequently, we used general linear modelling to verify the significance of BOLD responses for each spatial sector. Laterality of activity was calculated using mean weighted laterality index, as described in chapter 5. Finally, we used multivariate pattern dissimilarity analysis to verify which regions of the superior temporal cortex showed response patterns that best fitted a hemifield code model.

6.3 Results

Our tonotopic phase-mapping experiments showed narrow BOLD-responses to specific frequency ranges across the auditory cortex, with a gradual shift from low-frequency A1 to anterior and posterior regions of it. We could discern frequency-reversal boundaries of four cortical fields, namely the anterior, rostral, primary and posterior fields. In contrast, our spatiotopic phase-mapping analysis, derived from binaural auditory stimulation spanning every 30º spatial sector of azimuth space, didn't show any topographic representation at a millimetre scale. Mean BOLD responses in each hemisphere were broadly modulated and shifted between two opposite phases across the hemispheres, being tuned to the contralateral hemifield.

General linear model analysis of spatially-evoked BOLD responses showed distinct patterns of positive and negative BOLD responses within each hemisphere as a function of azimuth space. In general, spatial tuning curves showed opposite polarity between signals, with positive responses oriented approximately to ±120º of polar space and negative responses tuned to ±60º of polar space between hemispheres. We observed a contralateral bias among equidistant spatial sectors, especially in spatial sectors near the lateral axis. Such a bias was presented not only in the auditory cortex but also in the inferior colliculi, in agreement with neurophysiological evidence for subcortical hemifield tuning (Groh et al. 2003).

We further observed that interaural time difference (ITD) plays an important role in contralateral tuning. By stimulating our monkeys with a version of the original recorded sounds, in which the ITD cues were absent but with intact interaural level differences and spectral cues, we observed a loss of hemifield tuning affecting particularly the right hemisphere. Finally, our representational similarity analysis comparing sector-specific evoked BOLD responses in each cortical field showed that the right pST is the cortical field that best represents acoustic azimuth space in a hemifield code fashion.

6.4 Conclusions

Here we showed that at fMRI scale, differently to what happens with topological representation of tone frequencies, functional representation of acoustic azimuth space in

macaque auditory cortex isn't topographically organized. In contrast, our data suggest that sectors of acoustic space are contralaterally represented with opponent patterns of negative and positive BOLD responses. We found that the maximum amplitude and spread of positive BOLD responses are evoked by contralateral sectors at approximately ± 90º to 120º of polar space, which agrees with lesion (Heffner & Masterton 1975; Jenkins & Masterton 1982; Nodal et al. 2012), single-unit (Deouell et al. 2007; Woods et al. 2006; Magezi & Krumbholz 2010) and optical imaging studies (Nelken et al. 2008). Additionally, we showed that interaural time differences are essential cues to suppress functional activity in the opposite hemisphere at cortical level, which supports the opponent-channel coding hypothesis (Stecker et al. 2005). Moreover, we verified that ITD-related suppression was more evident in the right posterior region and that this region better coded full azimuth acoustic space in a hemifield fashion than any other auditory field. Supporting our findings, studies have shown that human right pST is notably sensitive to spatial auditory motion (Baumgart et al. 1999; Krumbholz et al. 2007). Our results were independent of the awareness state of the animals, being consistent among anesthetized and awake subjects. Taken together, our study provides evidence for a mixed representation of azimuth space in macaque auditory cortex, containing elements of both local and distributed hypothesis. We suggest that while acoustic space is broadly-tuned using a hemifield code (Salminen et al. 2009; Stecker et al. 2005), this form of coding generates an increased sensitivity for sound-source localization in pST (Rauschecker & Tian 2000; Tian et al. 2001; Warren et al. 2002; Griffiths et al. 1996).

7 DISCUSSION

The objective of this thesis was to investigate operational principles of intrinsic (stimulus- and task- free) and extrinsic (stimulus- or task- evoked) functional topologies of the macaque brain using high-field BOLD-fMRI. In our first project (chapter 3), we characterized intrinsic functional networks in anesthetized animals (resting-state) and, subsequently, we assessed the topographical relationship between resting-state networks (RSNs) and their putative correlates during periods of visual stimulation. We continued our investigation on extrinsic functional frameworks by focusing on the two most dominant sensory systems in the primate brain, the visual and auditory systems. While reviewing the literature, we realized that there was a limited understanding on mechanisms underlying interactions between the audio and visual modality at early cortical stages. To shed light on this, based on recent findings, we elaborated an original model for auditory induced modulations in primary visual cortices (chapter 4). Next, interested in understanding how the brain represents sources of audiovisual stimuli, which are often biologically relevant events critical to survival, we set out to investigate functional representation of objects (including individuals) and space in primate brains (chapters 5 and 6, respectively). We decided to concentrate in auditory representations of objects and space in order to complement the vast amount of studies related to visual representations. We present our last findings in the context of a dual stream concept specialized in processing object identity and spatial locations in the auditory system, analogous to the "what" and "where" streams of the visual system. Each project is thoroughly discussed in the following sections.

7.1 Intrinsic and extrinsic functional architectures in the macaque brain

Although more than two decades have passed since functional resting-state networks were firstly described (Biswal et al. 1995), there is still no consensus on the equivalence of intrinsic and extrinsic functional architectures in the human brain. While some groups claim that the "full repertoire of functional networks utilized by the brain in action is continuously and dynamically 'active' even when at 'rest'" (Smith et al. 2009),

others affirm that “the extrinsic and intrinsic functional architectures of the human brain are not equivalent” (Mennes et al. 2013). As is often the case when it comes to controversial assertions in science, there is evidence supporting both viewpoints. For instance, tight functional coupling of extrinsic and intrinsic functional architectures for default and task-positive regions, but not for primary sensory and motor cortices, limbic regions or subcortical structures have been reported (Mennes et al. 2013; Buckner et al. 2013). To address the core of the debate, we sought to investigate topographical consistency of extrinsic and intrinsic low-frequency functional networks in the macaque brain stimulated with different visual paradigms. Unique to our approach, we aimed at disentangling intrinsic from stimulus-evoked networks embedded in exactly the same datasets (chapter 3).

For this purpose, we used high field fMRI (7T) to scan the brain of two anesthetized macaque monkeys exposed to three different stimulus conditions: visual stimulation with a one-minute ON one-minute OFF block design (in which natural movie clips were alternated with gray background); visual stimulation using uninterrupted long versions of the same natural movies; and a condition without any kind of explicit stimulation (pure resting-state condition). Convenient to our purposes, anaesthesia avoided heterogeneity of brain states that could dynamically change functional network architecture (Tagliazucchi & Laufs 2014) in a run by run basis. At the same time, it allowed us to examine modulation of neural activity due to mainly bottom-up visual processing, mostly without top-down cognitive modulations (Rainer et al. 2001).

Independent component analysis (ICA) with a-priori-imposed 20 components (Hutchison et al. 2011) in our resting-state datasets resulted in 8 consistent resting-state networks (RSNs) across subjects and sessions. Namely, we observed the precentral-temporal network, the paracentral network, the fronto-parietal network (all three previously described in Hutchison et al., 2011), the default-mode network (DMN, Mantini et al., 2011), the lateral-occipital network, and the medial-occipital network (the last two firstly reported in Vincent et al., 2007). Each one of the 6 aforementioned networks encompassed mainly cortical areas. In addition to those, we also observed a cerebellar network; and a network encompassing the caudate, putamen and amygdala (CPA). Due to the brain areas involved, the CPA network might be related to multiple memory systems (Packard & Teather 1998). Additional components of no-interest, i.e. white matter and CSF, were observed but excluded from further analysis.

Subsequently, we set out to find putative correlates of the previously observed resting-state networks in the datasets showing significant visually-driven activity, i.e. in the alternated block-design datasets and in the long-movie datasets. Our objective was to investigate to which extent extrinsic bottom-up visual processing evoked by our paradigms could modulate intrinsic functional network architecture. ICA decomposition of data residuals derived from the block-design condition (obtained after GLM analysis decoupled explained from unexplained variance) and of the long-movie datasets revealed that for each consistent RSN component, there existed a remarkably topographically similar component contained in every type of stimuli-driven dataset. Interestingly, extrinsic bottom-up visual processing had very little influence, if any, on the underlying intrinsic functional architecture. This remained true even for the two visual resting-state networks, where intrinsic and extrinsic activity were occurring at the same time and at the same place.

At this point, we can think of a couple of hypothesis to explain why our observed hemodynamic resting-state-like networks were contained in datasets showing extrinsic stimulus-driven activity. Specifically to the early visual cortices, where intrinsic and stimulus-driven components were observed concomitantly, it is possible that low-frequency oscillations were happening in deeper layers while high-frequency, stimulus-induced activity were occurring in superficial layers (Maier et al. 2010; Buffalo et al. 2011). Since our voxels were relatively large (1.5 mm3) and thus encompassed multiple cortical layers, it is possible that BOLD time-courses captured combined hemodynamic activity derived from granular and non-granular layers. Concerning whole-brain activity, it's possible that no modulation of intrinsic architecture was verified because anaesthesia might have played an influential role in the stability of hemodynamic temporal correlations, making the brain less susceptible to extrinsic modulations. In order to explore this hypothesis, datasets obtained from awake monkeys probed with very similar paradigms have already been collected and are subject of future studies. Another possibility is that top-down influences might be more influential in modulating low-frequency oscillations than bottom-up, stimulus driven effects. In fact, it has been suggested that the fronto-parietal control system, an important source of top-down projections (Engel et al. 2001), is composed of flexible hubs of activity, potentially capable of regulating evoked functional connectivity across tasks (Cole et al. 2013). Modulation would be possibly exerted through short-term plasticity (Zucker & Regehr

2002; Yao et al. 2007) or by regulating synchrony of oscillations in neuronal populations (Buzsáki & Draguhn 2004; Fries 2005). To investigate which regions of the brain have increased intrinsic "hubness", we applied eigenvector centrality mapping (ECM, Lohmann et al., 2010) to our resting-state datasets. We observed increased centrality in fronto-parietal regions, which suggests a crucial role of this region in controlling network architecture. Overall, our findings indicate that extrinsic functional architecture in macaque monkeys is composed by two distinct components, an intrinsic component and another stimulus-evoked (or task-evoked component), as previously suggested for humans (Cole et al. 2014). It's possible that bottom-up and top-down modulations would be exerted through different frequency channels (Bastos et al. 2015; Michalareas et al. 2016).

To come up with a concrete hypothesis regarding the neural correlates of low-frequency hemodynamic networks would be a speculation. This is because, neither the neurophysiological basis, nor the function of resting-state networks are fully understood (Raichle & Mintun 2006). For example, it has been shown that the best correlate of BOLD-fMRI signal is the LFP (local-field potential, Logothetis et al., 2001); therefore, it would be natural to think that functional networks would be closely related to coherent oscillations in LFP activity. However, a well-designed study about the neural basis of global resting-state fMRI activity found that LFP oscillations could explain, at best, 10% of fMRI variance in their datasets (maximum mean cross-correlation between LFP and fMRI signal of 0.3, Schölvinck et al., 2010). Notwithstanding, theoretical models trying to explain such complex relationship have been put forward. One particularly interesting proposal associates resting-state networks with an oscillatory model presenting narrow-band limited power dynamics (Cabral, Kringelbach, et al. 2014; Cabral, Luckhoo, et al. 2014; Li et al. 2015) that could use ensembles of thalamocortical neurons, connected through gap-junctions, as a specialized pacemaker complex (Hughes et al. 2004; Hughes & Crunelli 2005; Lörincz et al. 2008; Li et al. 2015). Interestingly, we observe consistent thalamocortical connectivity in our precentral-temporal, which could be related to such a pacemaker complex. We intend to explore such thalamocortical connectivity in upcoming projects, possibly combining our BOLD-datasets with additional electrophysiological data.

Taken together, our data support that the "full repertoire of functional networks utilized by the brain in action is continuously and dynamically 'active' even when at

'rest'" (Smith et al. 2009) but at the same time, we showed that intrinsic and extrinsic components aren't necessarily equivalent, being linearly contained and recoverable from stimulus-driven datasets. To which extent and under which circumstances mutual modulatory effects could occur are subject to future investigations, ideally including invasive and non-invasive multimodal techniques.

We foresee two immediate practical consequences of our results. First of all, they stimulate the reinterpretation of a large existing neuroimaging database, but now taking into account residuals of hypothesis-driven analysis, normally discarded. This will potentially provide substantial gain of knowledge with minimal additional effort. The second application is regarding the design and analysis of neuroimaging studies. Since stimulus-driven fMRI datasets might get contaminated by spontaneous BOLD fluctuations (Arfanakis et al. 2000; Fox et al. 2006), it may be a good idea to avoid stimulus configurations in which responses are expected to happen in the frequency range of resting-state-like networks. Besides that, we think that it's perhaps useful to include ICA decomposition as a pre-processing step in the analysis of stimulus-driven neuroimaging data, in order to identify resting-state-like components in specific brain regions, and to use their time courses as regressors of no-interest in standard GLM analysis. Statistical power of analyses could be potentially increased if stimulus-unrelated oscillations are excluded from raw datasets.

7.2 A role for extrinsic audiovisual interactions in primary visual cortex

Although evidence for auditory influences in low-level areas of visual cortex have been brought forward, no functional framework explaining possible mechanisms for such an interaction existed. To bridge this gap, we proposed a model for auditory induced modulations in primary visual cortex of primates inspired by recent anatomical, behavioral and physiological data (chapter 4). Unique to our model, we consider crossmodal modulations even when field of view and field of hearing aren't overlapping. Specifically, we advocated that an unexpected auditory signal is able to trigger a reflexive overt orienting response towards sound source and, at the same time, to increase sensitivity in the striate cortex at the locations where the object is expected to enter visual field. Functionally, this would be achieved with parallel processing of three major pathways: a route headed by the superior colliculus (SC) would deal with overt orienting

behavior; direct projections from primary auditory cortex to primary visual cortex (A1-V1) would enhance spatiotemporal sensitivity; and indirect A1-V1 projections traversing higher-level areas would facilitate object detectability. Our model is based on multiple experimental evidence.

In agreement with the functional role proposed for the first stream (or pathway), there is a considerable number of studies showing close association between orienting behavior in primates and superior colliculi (Kustov & Robinson 1996; Sparks 1999; Klier et al. 2003; Krauzlis et al. 2004; Stein et al. 2014). For instance, it has been demonstrated that SC sends projections to the brainstem premotor circuitry and is able to modulate pupil dilation, saccade generation, and head and body movements (Corneil & Munoz 2014). Additionally, other studies have shown that SC has overlapping representations of visual, auditory and motor receptive field maps, facilitating overt orienting responses (Stein et al. 2014). Lastly, reversible inactivation of SC can impair typical orienting behaviors, such as saccade target selection (McPeek & Keller 2004). It's still unknown how modality-specific spatial representation is performed in SC but when it comes to object recognition, this structure doesn't seem to take part in it (Sprague 1996).

In line with the proposed role for the second stream, it has been shown that A1 sends monosynaptic projections to V1 (Falchier et al. 2002; Rockland & Ojima 2003; Clavagnier et al. 2004), but no specific function for it has been clearly determined. We hypothesize that direct A1-V1 projections would preempt visual cortex with short latency inputs (faster than feedback from higher cognitive areas) to help spatiotemporal localization of objects. In consonance with our hypothesis, behavioral evidence has shown that visual temporal search can be modulated by auditory stimulation at an early perceptual level (Vroomen & de Gelder 2000). Sound modulation of certain visual illusions can be accompanied by an increase or a decrease of V1 activity (e.g. of BOLD responses, Shams et al., 2000; Watkins et al., 2006, 2007). Additionally, it has been reported that an auditory cue can cause a focal increase in occipito-cortical excitability at the expected retinotopic location where an object should appear and at feedforward latencies (Bolognini et al. 2010).

Finally, we suggest that the third stream carries top-down feedback information about object identity to primary visual areas and can modulate visual processing of object-specific features at early processing stages. In accordance with our hypothesis, some studies reported that object expectation can enhance its visual detectability at low-level

cortical processing (Summerfield & Egner 2009; McManus et al. 2011; Chennu et al. 2013; Kok et al. 2014). Also, it has been shown that previous auditory labeling of an object can modulate its visibility during flash suppression experiments (Lupyan & Ward 2013). Lastly, an elegant study demonstrated that object expectation is able to sharpen visual representation in V1 (Kok et al. 2012).

Multisensory integration is an effective way to generate a coherent percept, powerful enough even to compensate for absent or unreliable sensory information (Stein & Meredith 1993; Knill & Pouget 2004; Stein et al. 2014). Traditionally considered a property of high-level sensory areas, this concept has been challenged by an increasing amount of evidence reporting its occurrence at early stages of sensory processing (Felleman & Van Essen 1991; Ghazanfar & Schroeder 2006; Wei et al. 2012; Wang et al. 2008; Lakatos et al. 2009; Giard & Peronnet 1999; Fort et al. 2002; Molholm et al. 2002; Mishra et al. 2007; Naue et al. 2011; Watkins et al. 2006; Watkins et al. 2007). Here we proposed a novel model that attempts to reconcile recent scientific findings related to extrinsic low-level modulation of primary visual cortex due to auditory stimulation. However, direct experimentation is still required to validate it. One interesting approach would be to design audiovisual experiments where behavioural and neural activity are concomitantly recorded in freely behaving animals (Roy & Wang 2012; Schwarz et al. 2014).

7.3 Object/individual representation in macaque auditory system

For this project, we used whole-brain coverage fMRI in awake behaving monkeys to investigate how sounds belonging to different categories of objects/individuals are represented in the auditory cortices. We tested the animals with three categories of complex sounds: monkey vocalizations, scrambled monkey vocalizations and environmental sounds. Conspecific vocalizations are of particular interest because they contain information about objects and individuals, as well as affective/emotional states (Ghazanfar & Hauser 1999). In addition to that, the fact that spectrotemporal phonetic structure of human speech sounds and monkey vocalizations are very similar (Rauschecker 1998), the study of vocalizations is very useful to understand evolution of language and speech (Bornkessel-Schlesewsky et al. 2015) and its neural substrates (Gil-da-Costa et al. 2004; Joly, Pallier, et al. 2012).

We observed positive BOLD responses for all three sound categories along the ascending auditory pathway but increased sensitivity to vocalizations in the superior temporal gyrus (STG). Specifically, combined categories showed robust activation in the cochlear nuclei, inferior colliculi, medial geniculate bodies and auditory cortices, with a slight right-hemispheric bias, in agreement with previously reported MION-fMRI experiments (Joly, Ramus, et al. 2012). However, contrasting the monkey calls with the other two categories resulted in consistent activity in specific regions of STG, particularly in areas AL, RTL and RTp, and in the ventrolateral prefrontal cortex. Our results extend previous findings (Poremba et al. 2003; Petkov et al. 2008; Kikuchi et al. 2010; Joly, Ramus, et al. 2012; Joly, Pallier, et al. 2012; Fukushima et al. 2014) and support the hypothesis of a functionally specialized auditory ventral pathway working as an analogue to the visual "what stream", preferentially processing object/individual identity (Rauschecker & Tian 2000). A possible explanation for the different spatial location observed for vocalization processing in monkey STG (anterior STG) when compared to humans Wernicke's area (posterior STG) is that, during evolution, the anterior part of human temporal lobe may have grown disproportionally, analogous to what happened to human prefrontal cortex. This could have relocated some brain regions in relation to others (Rauschecker & Tian 2000).

Interestingly, purely auditory conspecific vocalizations were able to increase BOLD activity in higher-level visual areas, such as middle temporal (MT) and inferior temporal (IT) cortices. As widely known, MT and IT are brain areas involved in visual motion processing (Maunsell & Van Essen 1983; Born & Bradley 2005; Czuba et al. 2014) and object perception, including faces (Dubner & Zeki 1971; Desimone et al. 1984; Logothetis & Sheinberg 1996; Tsao et al. 2006; Ku et al. 2011). Evidence for auditory modulation in both low-level (Wang et al. 2008; Lakatos et al. 2009; Azevedo et al. 2015) and high-level visual areas (You & Yeh 2010), and the fact that vocalizations are naturally associated with facial expressions and body movement (Furl et al. 2012; Polosecki et al. 2013; Perrodin et al. 2014) are in agreement with our results. Nonetheless, additional experiments are certainly necessary to explain specific details about the neuronal mechanisms underlying such multisensory communication.

7.4 Azimuth space representation in macaque auditory system

In our last study, we sought to scrutinize how macaque auditory system represents spatial locations in the azimuth plane. Specifically, we used high-resolution fMRI and state-of-the-art multivariate analysis to define cortical auditory fields based on tonotopic mapping, and to characterize BOLD responses in these fields with respect to distinct polar sectors of azimuth space. Experiments were carried out in both anesthetized and awake monkeys. Our results show that, at a millimetre scale, instead of a topographical organization, representation of auditory space is distributed throughout superior temporal cortices. Further, we demonstrated that such representation is accomplished using contralateral hemifield tuning, which is depicted by an opponent pattern of positive and negative BOLD responses across hemispheres. Finally, we showed that the observed hemifield tuning is heavily dependent on suppression caused by interaural time differences (ITD). Overall, our results support studies showing that ITD coding in several mammalian brains is performed using an opponent hemifield code based on neuronal inhibition (McAlpine et al. 2001; Grothe 2003), and not using topographically organized coincidence detectors, as has been reported to occur in the brain stem of barn owls (Jeffress 1948; Knudsen & Konishi 1978).

Additionally, we observed maximum amplitude and spatial spread of positive BOLD responses for contralateral sectors of azimuth space, which is congruent with electrophysiological recordings (Deouell et al. 2007; Woods et al. 2006; Magezi & Krumbholz 2010), optical imaging reports (Nelken et al. 2008) and lesion studies (Jenkins & Masterton 1982; Nodal et al. 2012; Heffner & Masterton 1975). However, since BOLD responses are statistically calculated based on the indirect activity of populations of neurons, our results don't preclude the existence of sharply tuned neurons to spatial position, as previously reported in posterior regions of superior temporal cortex (pST, Tian et al., 2001). Robust contralateral bias in BOLD signal to laterally-symmetric spatial polar sectors have been also reported in human neuroimaging studies (Salminen et al. 2009; Palomäki et al. 2005) and monkey single-unit electrophysiological recordings (Woods et al. 2006; Miller & Recanzone 2009; Werner-Reiss & Groh 2008; Stecker & Middlebrooks 2003). Complementarily, we observed small patches of positive BOLD response surrounded by patterns of negative BOLD response in the right auditory cortex after ipsilateral acoustic stimulation. The positive patches could derive from callosal input

to EE regions (contralateral excitatory-contralateral excitatory regions, Hackett et al., 1998; Imig and Brugge, 1978; Pandya and Rosene, 1993; Reser, 2000), while the negative patterns could correspond to subcortical inhibition (Grothe 2003) or to lateral inhibition of EE cells in regions sensitive to ITD (Brugge & Merzenich 1973).

As briefly mentioned, we demonstrated that ITD-cues are fundamental for interhemispheric hemifield tuning. We concluded this by testing our animals with a similar set of spatial sounds but with ITD cues removed from it (No-ITD). No-ITD stimuli evoked constant positive BOLD in the right hemisphere but no significant patterns of negative BOLD. We hypothesize that the positive-BOLD response is due to a lack of ITD-suppression effects. We confirmed the necessity of ITD to hemispherical shifts, a characteristic of hemifield tuning, by finding lateralization indices with extremely low values for No-ITD sounds played around the midline. Previous human studies showing that lesions in the right auditory hemisphere results in serious deficits in sound localization (Bisiach et al. 1984; Spierer et al. 2009) and motion detection (Griffiths et al. 1996) corroborate our findings.

Finally, representation similarity analysis (RSA) between theoretical and observed BOLD response patterns showed that right pST, at a voxel level, is the auditory field that best represents full azimuth space using hemifield coding. This last result is in line with evidence for population rate coding in humans (Werner-Reiss & Groh 2008; Salminen et al. 2009) and supports the idea of a specialized posterior region in the auditory cortex for spatial representation. Taken together, we showed that azimuth space in the macaque brain is represented using hemifield coding with increased posterior sensitivity. Results were similar for anesthetized and awake macaques. Our results support the proposal of a specialized "where" pathway in the auditory system; however, to which degree analogy with the visual "where" stream holds is still a matter of intense debate (Cohen & Wessinger 1999; Belin & Zatorre 2000; Zatorre et al. 2002; Middlebrooks 2002; Sumner & Krumbholz 2012; Bizley & Cohen 2013).

7.5 Summary

The general aim of this thesis was to explore, at a millimetre scale, how intrinsic (stimulus- and task- free) and extrinsic (stimulus- or task- evoked) functional architectures in the macaque brain operate. In our first project, we assessed topographical

correspondence of intrinsic and extrinsic frameworks under different conditions of bottom-up visual processing. In agreement with human results (Smith et al. 2009), our results showed that a whole set of consistent resting-state networks was also present in stimulus-driven conditions. In addition to that, we showed that, at least in visual cortices, intrinsic and extrinsic components aren't equivalent. We hypothesized that while the intrinsic component would be operating in deeper cortical layers, the stimulus-driven component would be occurring in superficial layers. In general, our findings are in agreement with previous human evidence, suggesting that the extrinsic architecture is composed of a primarily intrinsic component and a secondarily stimulus-evoked counterpart (Cole et al. 2014). Next, we exploited different aspects of extrinsic functional architectures. Specifically, we investigated multisensory interactions between the visual and auditory systems at early cortical stages. To reconcile evidence suggesting auditory modulations happening in early visual cortices, we proposed a new model for auditory induced modulations in V1. According to our model, three functional streams would be employed in parallel with specific purposes. A functional stream coordinated by the superior colliculi would be associated with overt-orienting responses; whereas monosynaptic and polysynaptic (traversing higher-level regions) projections from A1 to V1 would increase visual sensitivity and visually detectability of events. Finally, we confirmed the existence, in the auditory system, of a ventral stream specialized in processing sound identity; and of a dorsal stream specialized in processing spatial locations. Concerning spatial representations in the auditory cortices, we demonstrated that azimuth space is represented using a hemifield code with larger posterior sensitivity. To which extent the auditory "what-and-where" dual concept is analogous to the visual "what-and-where" hypothesis is subject of future studies.

8 REFERENCES

Adachi, Y. et al., 2012. Functional connectivity between anatomically unconnected areas is shaped by collective network-level effects in the macaque cortex. *Cerebral cortex (New York, N.Y. : 1991)*, 22(7), pp.1586–92.

Ahveninen, J. et al., 2006. Task-modulated "what" and "where" pathways in human auditory cortex. *Proceedings of the National Academy of Sciences of the United States of America*, 103(39), pp.14608–13.

Allen, G. et al., 2007. Reduced hippocampal functional connectivity in Alzheimer disease. *Archives of neurology*, 64(10), pp.1482–7.

Andersen, R.A. et al., 1997. Multimodal representation of space in the posterior parietal cortex and its use in planning movements. *Annual review of neuroscience*, 20, pp.303–30.

Arfanakis, K. et al., 2000. Combining independent component analysis and correlation analysis to probe interregional connectivity in fMRI task activation datasets. *Magnetic resonance imaging*, 18(8), pp.921–30.

Arnott, S.R. et al., 2004. Assessing the auditory dual-pathway model in humans. *NeuroImage*, 22(1), pp.401–8.

Astle, D.E. et al., 2015. Cognitive training enhances intrinsic brain connectivity in childhood. *The Journal of neuroscience : the official journal of the Society for Neuroscience*, 35(16), pp.6277–83.

Azevedo, F.A.C. et al., 2015. A Potential Role of Auditory Induced Modulations in Primary Visual Cortex. *Multisensory research*, 28(3–4), pp.331–49.

Azevedo, F.A.C. et al., 2009. Equal numbers of neuronal and nonneuronal cells make the human brain an isometrically scaled-up primate brain. *The Journal of comparative neurology*, 513(5), pp.532–41.

Baggio, H.-C. et al., 2015. Cognitive impairment and resting-state network connectivity in Parkinson's disease. *Human brain mapping*, 36(1), pp.199–212.

Barttfeld, P. et al., 2015. Signature of consciousness in the dynamics of resting-state brain activity. *Proceedings of the National Academy of Sciences*, 112(3), p.201418031.

Bastos, A.M.A.M. et al., 2015. Visual Areas Exert Feedforward and Feedback Influences through Distinct Frequency Channels. *Neuron*, 85(2), pp.390–401.

Baumgart, F. et al., 1999. A movement-sensitive area in auditory cortex. *Nature*, 400(6746), pp.724–6.

Beauchamp, M.S., 2005. See me, hear me, touch me: multisensory integration in lateral occipital-temporal cortex. *Current opinion in neurobiology*, 15(2), pp.145–53.

Belcher, A.M. et al., 2013. Large-scale brain networks in the awake, truly resting marmoset monkey. *The Journal of neuroscience : the official journal of the Society for Neuroscience*, 33(42), pp.16796–804.

Belin, P. & Zatorre, R.J., 2000. "What", "where" and "how" in auditory cortex. *Nature neuroscience*, 3(10), pp.965–6.

Bell, A.J. & Sejnowski, T.J., 1995. An information-maximization approach to blind separation and blind deconvolution. *Neural computation*, 7(6), pp.1129–59.

Birn, R.M., Murphy, K. & Bandettini, P.A., 2008. The effect of respiration variations on independent component analysis results of resting state functional connectivity. *Human brain mapping*, 29(7), pp.740–50.

Bisiach, E. et al., 1984. Disorders of perceived auditory lateralization after lesions of the right hemisphere. *Brain : a journal of neurology*, 107 (Pt 1, pp.37–52.

Biswal, B. et al., 1995. Functional connectivity in the motor cortex of resting human brain using echo-planar MRI. *Magnetic resonance in medicine : official journal of the Society of Magnetic Resonance in Medicine / Society of Magnetic Resonance in Medicine*, 34(4), pp.537–41.

Biswal, B.B., 2012. Resting state fMRI: a personal history. *NeuroImage*, 62(2), pp.938–44.

Biswal, B.B. et al., 2010. Toward discovery science of human brain function. *Proceedings of the National Academy of Sciences of the United States of America*, 107(10), pp.4734–9.

Bizley, J.K. & Cohen, Y.E., 2013. The what, where and how of auditory-object

perception. *Nature reviews. Neuroscience*, 14(10), pp.693–707.

Blauert, J., 1997. *Spatial Hearing: The Psychophysics of Human Sound Localization*, London: MIT Press.

Bolognini, N. et al., 2010. Auditory enhancement of visual phosphene perception: the effect of temporal and spatial factors and of stimulus intensity. *Neuroscience letters*, 477(3), pp.109–14.

Born, R.T. & Bradley, D.C., 2005. Structure and function of visual area MT. *Annual review of neuroscience*, 28, pp.157–89.

Bornkessel-Schlesewsky, I. et al., 2015. Neurobiological roots of language in primate audition: common computational properties. *Trends in Cognitive Sciences*, 19(3), pp.142–50.

Brugge, J.F. & Merzenich, M.M., 1973. Responses of neurons in auditory cortex of the macaque monkey to monaural and binaural stimulation. *Journal of neurophysiology*, 36(6), pp.1138–58.

Buckner, R.L., Krienen, F.M. & Yeo, B.T.T., 2013. Opportunities and limitations of intrinsic functional connectivity MRI. *Nature neuroscience*, 16(7), pp.832–7.

Buffalo, E.A. et al., 2011. Laminar differences in gamma and alpha coherence in the ventral stream. *Proceedings of the National Academy of Sciences of the United States of America*, 108(27), pp.11262–7.

Buzsáki, G. & Draguhn, A., 2004. Neuronal oscillations in cortical networks. *Science (New York, N.Y.)*, 304(5679), pp.1926–9.

Cabral, J., Luckhoo, H., et al., 2014. Exploring mechanisms of spontaneous functional connectivity in MEG: how delayed network interactions lead to structured amplitude envelopes of band-pass filtered oscillations. *NeuroImage*, 90, pp.423–35.

Cabral, J., Kringelbach, M.L. & Deco, G., 2014. Exploring the network dynamics underlying brain activity during rest. *Progress in Neurobiology*, 114, pp.102–131.

Calhoun, V.D. et al., 2001. A method for making group inferences from functional MRI data using independent component analysis. *Human brain mapping*, 14(3), pp.140–51.

Capotosto, P. et al., 2014. Resting-state modulation of α rhythms by interference with

angular gyrus activity. *Journal of cognitive neuroscience*, 26(1), pp.107–19.

Cheney, D.L. & Seyfarth, R.M., 1990. *How Monkeys see the World.*, Chicago: University of Chicago Press.

Chennu, S. et al., 2013. Expectation and attention in hierarchical auditory prediction. *The Journal of neuroscience : the official journal of the Society for Neuroscience*, 33(27), pp.11194–205.

Cherkassky, V.L. et al., 2006. Functional connectivity in a baseline resting-state network in autism. *Neuroreport*, 17(16), pp.1687–90.

Clavagnier, S., Falchier, A. & Kennedy, H., 2004. Long-distance feedback projections to area V1: implications for multisensory integration, spatial awareness, and visual consciousness. *Cognitive, affective & behavioral neuroscience*, 4(2), pp.117–26.

Clemo, H.R., Keniston, L.P. & Meredith, M.A., 2012. Structural Basis of Multisensory Processing.

Cohen, A.L. et al., 2008. Defining functional areas in individual human brains using resting functional connectivity MRI. *NeuroImage*, 41(1), pp.45–57.

Cohen, Y.E. & Knudsen, E.I., 1999. Maps versus clusters: different representations of auditory space in the midbrain and forebrain. *Trends in neurosciences*, 22(3), pp.128–35.

Cohen, Y.E. & Wessinger, C.M., 1999. Who Goes There? *Neuron*, 24(4), pp.769–771.

Cole, M.W. et al., 2014. Intrinsic and Task-Evoked Network Architectures of the Human Brain. *Neuron*, 83(1), pp.238–251.

Cole, M.W. et al., 2013. Multi-task connectivity reveals flexible hubs for adaptive task control. *Nature neuroscience*, 16(9), pp.1348–55.

Comon, P., 1994. Independent component analysis, A new concept? *Signal Processing*, 36(3), pp.287–314.

Cordes, D. et al., 2000. Mapping functionally related regions of brain with functional connectivity MR imaging. *AJNR. American journal of neuroradiology*, 21(9), pp.1636–44.

Corneil, B.D. & Munoz, D.P., 2014. Overt responses during covert orienting. *Neuron*, 82(6), pp.1230–43.

Cox, R.W., 2012. AFNI: what a long strange trip it's been. *NeuroImage*, 62(2), pp.743–7.

Croxson, P.L. et al., 2005. Quantitative investigation of connections of the prefrontal cortex in the human and macaque using probabilistic diffusion tractography. *The Journal of neuroscience : the official journal of the Society for Neuroscience*, 25(39), pp.8854–66.

Czuba, T.B. et al., 2014. Area MT encodes three-dimensional motion. *The Journal of neuroscience : the official journal of the Society for Neuroscience*, 34(47), pp.15522–33.

Deligianni, F. et al., 2014. Relating resting-state fMRI and EEG whole-brain connectomes across frequency bands. *Frontiers in neuroscience*, 8, p.258.

Deouell, L.Y. et al., 2007. Cerebral responses to change in spatial location of unattended sounds. *Neuron*, 55(6), pp.985–96.

Desimone, R. et al., 1984. Stimulus-selective properties of inferior temporal neurons in the macaque. *The Journal of neuroscience : the official journal of the Society for Neuroscience*, 4(8), pp.2051–2062.

van Diessen, E. et al., 2015. Opportunities and methodological challenges in EEG and MEG resting state functional brain network research. *Clinical neurophysiology : official journal of the International Federation of Clinical Neurophysiology*, 126(8), pp.1468–81.

Dubner, R. & Zeki, S.M., 1971. Response properties and receptive fields of cells in an anatomically defined region of the superior temporal sulcus in the monkey. *Brain research*, 35(2), pp.528–32.

Engel, A.K., Fries, P. & Singer, W., 2001. Dynamic predictions: oscillations and synchrony in top-down processing. *Nature reviews. Neuroscience*, 2(10), pp.704–16.

Ernst, M.O. & Banks, M.S., 2002. Humans integrate visual and haptic information in a statistically optimal fashion. *Nature*, 415(6870), pp.429–33.

Van Essen, D.C., 2002. Surface-based atlases of cerebellar cortex in the human, macaque, and mouse. *Annals of the New York Academy of Sciences*, 978, pp.468–79.

Falchier, A. et al., 2002. Anatomical evidence of multimodal integration in primate striate cortex. *The Journal of neuroscience : the official journal of the Society for Neuroscience*, 22(13), pp.5749–59.

Felleman, D.J. & Van Essen, D.C., 1991. Distributed hierarchical processing in the primate cerebral cortex. *Cerebral cortex (New York, N.Y.)*, 1(1), pp.1–47.

Fetsch, C.R., DeAngelis, G.C. & Angelaki, D.E., 2013. Bridging the gap between theories of sensory cue integration and the physiology of multisensory neurons. *Nature reviews. Neuroscience*, 14(6), pp.429–42.

Flechsig, P., 1920. *Anatomie des menschlichen Gehirns und Rückenmarks auf myelogenetischer Grundlage*, Leipzig: Thieme.

Flechsig, P., 1896. *Gehirn und Seele*, Leipzig: von Veit.

Fort, A. et al., 2002. Early auditory-visual interactions in human cortex during nonredundant target identification. *Brain research. Cognitive brain research*, 14(1), pp.20–30.

Fox, M.D., 2010. Clinical applications of resting state functional connectivity. *Frontiers in Systems Neuroscience*, 4.

Fox, M.D. et al., 2006. Coherent spontaneous activity accounts for trial-to-trial variability in human evoked brain responses. *Nature neuroscience*, 9(1), pp.23–5.

Fox, M.D. & Raichle, M.E., 2007. Spontaneous fluctuations in brain activity observed with functional magnetic resonance imaging. *Nature reviews. Neuroscience*, 8(9), pp.700–11.

Fries, P., 2005. A mechanism for cognitive dynamics: neuronal communication through neuronal coherence. *Trends in cognitive sciences*, 9(10), pp.474–80.

Friston, K.J., 1994. Functional and effective connectivity in neuroimaging: a synthesis. *Human brain mapping*, 2, pp.56–78.

Fukushima, M. et al., 2014. Differential coding of conspecific vocalizations in the ventral auditory cortical stream. *The Journal of neuroscience : the official journal of the Society for Neuroscience*, 34(13), pp.4665–76.

Furl, N. et al., 2012. Dynamic and static facial expressions decoded from motion-sensitive areas in the macaque monkey. *The Journal of neuroscience : the official journal of*

the Society for Neuroscience, 32(45), pp.15952–62.

Fuster, J.M., Bodner, M. & Kroger, J.K., 2000. Cross-modal and cross-temporal association in neurons of frontal cortex. *Nature*, 405(6784), pp.347–51.

Ghazanfar, A.A. & Logothetis, N.K., 2003. Neuroperception: facial expressions linked to monkey calls. *Nature*, 423(6943), pp.937–8.

Ghazanfar, A.A. & Schroeder, C.E., 2006. Is neocortex essentially multisensory? *Trends in cognitive sciences*, 10(6), pp.278–85.

Ghazanfar, A. & Hauser, M., 1999. The neuroethology of primate vocal communication: substrates for the evolution of speech. *Trends in cognitive sciences*, 3(10), pp.377–384.

Giard, M.H. & Peronnet, F., 1999. Auditory-visual integration during multimodal object recognition in humans: a behavioral and electrophysiological study. *Journal of cognitive neuroscience*, 11(5), pp.473–90.

Gil-da-Costa, R. et al., 2004. Toward an evolutionary perspective on conceptual representation: species-specific calls activate visual and affective processing systems in the macaque. *Proceedings of the National Academy of Sciences of the United States of America*, 101(50), pp.17516–21.

Goodale, M.A. & Milner, A.D., 1992. Separate visual pathways for perception and action. *Trends in neurosciences*, 15(1), pp.20–5.

Greicius, M.D. et al., 2004. Default-mode network activity distinguishes Alzheimer's disease from healthy aging: evidence from functional MRI. *Proceedings of the National Academy of Sciences of the United States of America*, 101(13), pp.4637–42.

Greicius, M.D. et al., 2003. Functional connectivity in the resting brain: a network analysis of the default mode hypothesis. *Proceedings of the National Academy of Sciences of the United States of America*, 100(1), pp.253–8.

Griffiths, T.D. et al., 1996. Evidence for a sound movement area in the human cerebral cortex. *Nature*, 383(6599), pp.425–7.

Groh, J.M., Kelly, K.A. & Underhill, A.M., 2003. A monotonic code for sound azimuth in primate inferior colliculus. *Journal of cognitive neuroscience*, 15(8), pp.1217–31.

Grothe, B., 2003. New roles for synaptic inhibition in sound localization. *Nature reviews. Neuroscience*, 4, pp.540–550.

Grothe, B., Pecka, M. & McAlpine, D., 2010. Mechanisms of sound localization in mammals. *Physiological reviews*, 90(3), pp.983–1012.

Hackett, T.A., Stepniewska, I. & Kaas, J.H., 1998. Subdivisions of auditory cortex and ipsilateral cortical connections of the parabelt auditory cortex in macaque monkeys. *The Journal of comparative neurology*, 394(4), pp.475–95.

Hampson, M. et al., 2004. Changes in functional connectivity of human MT/V5 with visual motion input. *Neuroreport*, 15(8), pp.1315–9.

Hampson, M. et al., 2002. Detection of functional connectivity using temporal correlations in MR images. *Human brain mapping*, 15(4), pp.247–62.

Han, X., 2012. Optogenetics in the nonhuman primate. *Progress in brain research*, 196, pp.215–33.

Heffner, H. & Masterton, B., 1975. Contribution of auditory cortex to sound localization in the monkey (Macaca mulatta). *Journal of neurophysiology*, 38(6), pp.1340–58.

Herault, J. & Ans, B., 1984. Réseau de neurones à synapses modifiables: décodage de messages sensoriels composites par apprentissage non supervisé et permanent. *Comptes rendus des séances de l'Académie des sciences. Série 3, Sciences de la vie*, 299(13), pp.525–528.

Himberg, J., Hyvärinen, A. & Esposito, F., 2004. Validating the independent components of neuroimaging time series via clustering and visualization. *NeuroImage*, 22(3), pp.1214–22.

Hughes, S.W. et al., 2004. Synchronized oscillations at alpha and theta frequencies in the lateral geniculate nucleus. *Neuron*, 42(2), pp.253–68.

Hughes, S.W. & Crunelli, V., 2005. Thalamic mechanisms of EEG alpha rhythms and their pathological implications. *The Neuroscientist : a review journal bringing neurobiology, neurology and psychiatry*, 11(4), pp.357–72.

Hutchison, R.M. et al., 2011. Resting-state networks in the macaque at 7 T. *NeuroImage*, 56(3), pp.1546–55.

Hutchison, R.M. & Everling, S., 2012. Monkey in the middle: why non-human primates

are needed to bridge the gap in resting-state investigations. *Frontiers in neuroanatomy*, 6, p.29.

Hyvärinen, A., Karkunen, J. & Oja, E., 2001. *Independent Component Analysis*, Wiley.

Imig, T.J. & Brugge, J.F., 1978. Sources and terminations of callosal axons related to binaural and frequency maps in primary auditory cortex of the cat. *The Journal of comparative neurology*, 182(4), pp.637–60.

Jafri, M.J. et al., 2008. A method for functional network connectivity among spatially independent resting-state components in schizophrenia. *NeuroImage*, 39(4), pp.1666–81.

Jeffress, L.A., 1948. A place theory of sound localization. *Journal of comparative and physiological psychology*, 41(1), pp.35–39.

Jenkins, W.M. & Masterton, R.B., 1982. Sound localization: effects of unilateral lesions in central auditory system. *Journal of neurophysiology*, 47(6), pp.987–1016.

Joly, O., Ramus, F., et al., 2012. Interhemispheric differences in auditory processing revealed by fMRI in awake rhesus monkeys. *Cerebral cortex (New York, N.Y. : 1991)*, 22(4), pp.838–53.

Joly, O., Pallier, C., et al., 2012. Processing of vocalizations in humans and monkeys: a comparative fMRI study. *NeuroImage*, 62(3), pp.1376–89.

Jonckers, E. et al., 2011. Functional connectivity fMRI of the rodent brain: comparison of functional connectivity networks in rat and mouse. *PloS one*, 6(4), p.e18876.

Kajikawa, Y. et al., 2012. Audiovisual Integration in Nonhuman Primates: A Window into the Anatomy and Physiology of Cognition. *The Neural Bases of Multisensory Processes*.

Kanwisher, N., 2010. Functional specificity in the human brain: a window into the functional architecture of the mind. *Proceedings of the National Academy of Sciences of the United States of America*, 107(25), pp.11163–70.

Kelly, C. et al., 2010. Broca's region: linking human brain functional connectivity data and non-human primate tracing anatomy studies. *The European journal of neuroscience*, 32(3), pp.383–98.

Kennedy, D.P. & Courchesne, E., 2008. The intrinsic functional organization of the brain

is altered in autism. *NeuroImage*, 39(4), pp.1877–85.

Kikuchi, Y., Horwitz, B. & Mishkin, M., 2010. Hierarchical auditory processing directed rostrally along the monkey's supratemporal plane. *The Journal of neuroscience : the official journal of the Society for Neuroscience*, 30(39), pp.13021–13030.

Klier, E.M., Wang, H. & Crawford, J.D., 2003. Three-dimensional eye-head coordination is implemented downstream from the superior colliculus. *Journal of neurophysiology*, 89(5), pp.2839–53.

Knill, D.C. & Pouget, A., 2004. The Bayesian brain: the role of uncertainty in neural coding and computation. *Trends in neurosciences*, 27(12), pp.712–9.

Knudsen, E.I. & Konishi, M., 1978. A neural map of auditory space in the owl. *Science (New York, N.Y.)*, 200, pp.795–797.

Knyazev, G.G., 2007. Motivation, emotion, and their inhibitory control mirrored in brain oscillations. *Neuroscience and biobehavioral reviews*, 31(3), pp.377–95.

Kok, P., Failing, M.F. & de Lange, F.P., 2014. Prior expectations evoke stimulus templates in the primary visual cortex. *Journal of cognitive neuroscience*, 26(7), pp.1546–54.

Kok, P., Jehee, J.F.M. & de Lange, F.P., 2012. Less is more: expectation sharpens representations in the primary visual cortex. *Neuron*, 75(2), pp.265–70.

Kosaki, H. et al., 1997. Tonotopic organization of auditory cortical fields delineated by parvalbumin immunoreactivity in macaque monkeys. *The Journal of comparative neurology*, 386(2), pp.304–16.

Koyama, M. et al., 2004. Functional Magnetic Resonance Imaging of Macaque Monkeys Performing Visually Guided Saccade Tasks. *Neuron*, 41(5), pp.795–807.

Krauzlis, R.J., Liston, D. & Carello, C.D., 2004. Target selection and the superior colliculus: goals, choices and hypotheses. *Vision research*, 44(12), pp.1445–51.

Krüger, J. & Bach, M., 1981. Simultaneous recording with 30 microelectrodes in monkey visual cortex. *Experimental brain research*, 41(2), pp.191–4.

Krumbholz, K., Hewson-Stoate, N. & Schönwiesner, M., 2007. Cortical response to auditory motion suggests an asymmetry in the reliance on inter-hemispheric connections between the left and right auditory cortices. *Journal of neurophysiology*,

97(2), pp.1649–55.

Ku, S.-P. et al., 2011. fMRI of the face-processing network in the ventral temporal lobe of awake and anesthetized macaques. *Neuron*, 70(2), pp.352–62.

Kuśmierek, P., Ortiz, M. & Rauschecker, J.P., 2012. Sound-identity processing in early areas of the auditory ventral stream in the macaque. *Journal of neurophysiology*, 107(4), pp.1123–41.

Kusmierek, P. & Rauschecker, J.P., 2014. Selectivity for space and time in early areas of the auditory dorsal stream in the rhesus monkey. *Journal of neurophysiology*, 111(8), pp.1671–85.

Kustov, A.A. & Robinson, D.L., 1996. Shared neural control of attentional shifts and eye movements. *Nature*, 384(6604), pp.74–7.

Lakatos, P. et al., 2008. Entrainment of neuronal oscillations as a mechanism of attentional selection. *Science (New York, N.Y.)*, 320(5872), pp.110–3.

Lakatos, P. et al., 2009. The leading sense: supramodal control of neurophysiological context by attention. *Neuron*, 64(3), pp.419–30.

Lebedev, A. V et al., 2014. Large-scale resting state network correlates of cognitive impairment in Parkinson's disease and related dopaminergic deficits. *Frontiers in systems neuroscience*, 8, p.45.

Li, J.M. et al., 2015. Functional connectivity arises from a slow rhythmic mechanism. *Proceedings of the National Academy of Sciences of the United States of America*, 112(19), pp.E2527-35.

Li, S.-J. et al., 2002. Alzheimer Disease: evaluation of a functional MR imaging index as a marker. *Radiology*, 225(1), pp.253–9.

Liang, M. et al., 2006. Widespread functional disconnectivity in schizophrenia with resting-state functional magnetic resonance imaging. *Neuroreport*, 17(2), pp.209–13.

Liang, Z., King, J. & Zhang, N., 2011. Uncovering intrinsic connectional architecture of functional networks in awake rat brain. *The Journal of neuroscience : the official journal of the Society for Neuroscience*, 31(10), pp.3776–83.

Liu, H. et al., 2006. Decreased regional homogeneity in schizophrenia: a resting state

functional magnetic resonance imaging study. *Neuroreport*, 17(1), pp.19–22.

Liu, Y. et al., 2008. Disrupted small-world networks in schizophrenia. *Brain : a journal of neurology*, 131(Pt 4), pp.945–61.

Logothetis, N.K. et al., 1999. Functional imaging of the monkey brain. *Nature neuroscience*, 2(6), pp.555–62.

Logothetis, N.K. et al., 2012. Hippocampal-cortical interaction during periods of subcortical silence. *Nature*, 491(7425), pp.547–53.

Logothetis, N.K. et al., 2001. Neurophysiological investigation of the basis of the fMRI signal. *Nature*, 412(6843), pp.150–7.

Logothetis, N.K. et al., 2010. The effects of electrical microstimulation on cortical signal propagation. *Nature neuroscience*, 13(10), pp.1283–91.

Logothetis, N.K. & Sheinberg, D.L., 1996. Visual object recognition. *Annual review of neuroscience*, 19, pp.577–621.

Logothetis, N.K.N., 2008. What we can do and what we cannot do with fMRI. *Nature*, 453(7197), pp.869–78.

Lohmann, G. et al., 2010. Eigenvector centrality mapping for analyzing connectivity patterns in fMRI data of the human brain. *PloS one*, 5(4), p.e10232.

Lörincz, M.L., Crunelli, V. & Hughes, S.W., 2008. Cellular dynamics of cholinergically induced alpha (8-13 Hz) rhythms in sensory thalamic nuclei in vitro. *The Journal of neuroscience : the official journal of the Society for Neuroscience*, 28(3), pp.660–71.

Lowe, M.J. et al., 2002. Multiple sclerosis: low-frequency temporal blood oxygen level-dependent fluctuations indicate reduced functional connectivity initial results. *Radiology*, 224(1), pp.184–92.

Lowe, M.J., Mock, B.J. & Sorenson, J.A., 1998. Functional connectivity in single and multislice echoplanar imaging using resting-state fluctuations. *NeuroImage*, 7(2), pp.119–32.

Lu, C.-M. et al., 2010. Use of fNIRS to assess resting state functional connectivity. *Journal of neuroscience methods*, 186(2), pp.242–9.

Lu, H. et al., 2007. Synchronized delta oscillations correlate with the resting-state

functional MRI signal. *Proceedings of the National Academy of Sciences of the United States of America*, 104(46), pp.18265–9.

De Luca, M. et al., 2005. Blood oxygenation level dependent contrast resting state networks are relevant to functional activity in the neocortical sensorimotor system. *Experimental brain research*, 167(4), pp.587–94.

Lupyan, G. & Ward, E.J., 2013. Language can boost otherwise unseen objects into visual awareness. *Proceedings of the National Academy of Sciences of the United States of America*, 110(35), pp.14196–201.

Macaluso, E. & Driver, J., 2005. Multisensory spatial interactions: a window onto functional integration in the human brain. *Trends in neurosciences*, 28(5), pp.264–71.

Maeder, P.P. et al., 2001. Distinct pathways involved in sound recognition and localization: a human fMRI study. *NeuroImage*, 14(4), pp.802–816.

Magezi, D.A. & Krumbholz, K., 2010. Evidence for opponent-channel coding of interaural time differences in human auditory cortex. *Journal of neurophysiology*, 104(4), pp.1997–2007.

Maier, A. et al., 2010. Distinct superficial and deep laminar domains of activity in the visual cortex during rest and stimulation. *Frontiers in systems neuroscience*, 4.

Majeed, W., Magnuson, M. & Keilholz, S.D., 2009. Spatiotemporal dynamics of low frequency fluctuations in BOLD fMRI of the rat. *Journal of magnetic resonance imaging : JMRI*, 30(2), pp.384–93.

Mantini, D. et al., 2011. Default Mode of Brain Function in Monkeys. *Journal of Neuroscience*, 31(36), pp.12954–12962.

Mantini, D. et al., 2007. Electrophysiological signatures of resting state networks in the human brain. *Proceedings of the National Academy of Sciences of the United States of America*, 104(32), pp.13170–5.

Margulies, D.S. et al., 2009. Precuneus shares intrinsic functional architecture in humans and monkeys. *Proceedings of the National Academy of Sciences of the United States of America*, 106(47), pp.20069–74.

Maunsell, J.H. & Van Essen, D.C., 1983. Functional properties of neurons in middle

temporal visual area of the macaque monkey. I. Selectivity for stimulus direction, speed, and orientation. *Journal of neurophysiology*, 49(5), pp.1127–47.

McAlpine, D., Jiang, D. & Palmer, A.R., 2001. A neural code for low-frequency sound localization in mammals. *Nature neuroscience*, 4, pp.396–401.

McKeown, M.J. et al., 1998. Analysis of fMRI data by blind separation into independent spatial components. *Human brain mapping*, 6(3), pp.160–88.

McManus, J.N.J., Li, W. & Gilbert, C.D., 2011. Adaptive shape processing in primary visual cortex. *Proceedings of the National Academy of Sciences of the United States of America*, 108(24), pp.9739–46.

McPeek, R.M. & Keller, E.L., 2004. Deficits in saccade target selection after inactivation of superior colliculus. *Nature neuroscience*, 7(7), pp.757–63.

Mennes, M. et al., 2013. The extrinsic and intrinsic functional architectures of the human brain are not equivalent. *Cerebral cortex (New York, N.Y. : 1991)*, 23(1), pp.223–9.

Meredith, M.A., 2002. On the neuronal basis for multisensory convergence: a brief overview. *Brain research. Cognitive brain research*, 14(1), pp.31–40.

Michalareas, G. et al., 2016. Alpha-Beta and Gamma Rhythms Subserve Feedback and Feedforward Influences among Human Visual Cortical Areas. *Neuron*, 89(2), pp.384–397.

Middlebrooks, J.C., 2002. Auditory space processing: here, there or everywhere? *Nature neuroscience*, 5(9), pp.824–826.

Miller, L.M. & Recanzone, G.H., 2009. Populations of auditory cortical neurons can accurately encode acoustic space across stimulus intensity. *Proceedings of the National Academy of Sciences of the United States of America*, 106(14), pp.5931–5935.

Milner, A.D. & Goodale, M.A., 2008. Two visual systems re-viewed. *Neuropsychologia*, 46(3), pp.774–85.

Miranda-Dominguez, O. et al., 2014. Bridging the gap between the human and macaque connectome: a quantitative comparison of global interspecies structure-function relationships and network topology. *The Journal of neuroscience : the official journal of the Society for Neuroscience*, 34(16), pp.5552–63.

Mishkin, M., 1972. Cortical visual areas and their interactions. In A. G. Karczmar & J. C. Eccles, eds. *Brain and Human Behavior*. Berlin: Springer.

Mishra, J. et al., 2007. Early cross-modal interactions in auditory and visual cortex underlie a sound-induced visual illusion. *The Journal of neuroscience : the official journal of the Society for Neuroscience*, 27(15), pp.4120–31.

Moeller, S. et al., 2009. Functional Connectivity of the Macaque Brain across Stimulus and Arousal States. *Journal of Neuroscience*, 29(18), pp.5897–5909.

Mohammadi, B. et al., 2009. Changes of resting state brain networks in amyotrophic lateral sclerosis. *Experimental neurology*, 217(1), pp.147–53.

Molholm, S. et al., 2002. Multisensory auditory-visual interactions during early sensory processing in humans: a high-density electrical mapping study. *Brain research. Cognitive brain research*, 14(1), pp.115–28.

Morel, A., Garraghty, P.E. & Kaas, J.H., 1993. Tonotopic organization, architectonic fields, and connections of auditory cortex in macaque monkeys. *The Journal of comparative neurology*, 335(3), pp.437–59.

Murphy, K. et al., 2009. The impact of global signal regression on resting state correlations: are anti-correlated networks introduced? *NeuroImage*, 44(3), pp.893–905.

Nakahara, K. et al., 2007. Exploring the neural basis of cognition: multi-modal links between human fMRI and macaque neurophysiology. *Trends in cognitive sciences*, 11(2), pp.84–92.

Naue, N. et al., 2011. Auditory event-related response in visual cortex modulates subsequent visual responses in humans. *The Journal of neuroscience : the official journal of the Society for Neuroscience*, 31(21), pp.7729–36.

Nelken, I. et al., 2008. Responses of auditory cortex to complex stimuli: functional organization revealed using intrinsic optical signals. *Journal of neurophysiology*, 99(4), pp.1928–41.

Niazy, R.K. et al., 2015. Resting-State Networks. In K. Uludağ, K. Uğurbil, & L. Berliner, eds. *fMRI: From Nuclear Spins to Brain Functions*. New York: Springer, pp. 387–425.

Nodal, F.R., Bajo, V.M. & King, A.J., 2012. Plasticity of spatial hearing: behavioural effects of cortical inactivation. *The Journal of physiology*, 590(Pt 16), pp.3965–86.

Ongür, D., Ferry, A.T. & Price, J.L., 2003. Architectonic subdivision of the human orbital and medial prefrontal cortex. *The Journal of comparative neurology*, 460(3), pp.425–49.

Packard, M.G. & Teather, L.A., 1998. Amygdala modulation of multiple memory systems: hippocampus and caudate-putamen. *Neurobiology of learning and memory*, 69(2), pp.163–203.

Palomäki, K.J. et al., 2005. Spatial processing in human auditory cortex: the effects of 3D, ITD, and ILD stimulation techniques. *Brain research. Cognitive brain research*, 24(3), pp.364–79.

Pandya, D.N. & Rosene, D.L., 1993. Laminar termination patterns of thalamic, callosal, and association afferents in the primary auditory area of the rhesus monkey. *Experimental neurology*, 119(2), pp.220–34.

Passingham, R., 2009. How good is the macaque monkey model of the human brain? *Current opinion in neurobiology*, 19(1), pp.6–11.

Pawela, C.P. et al., 2008. Resting-state functional connectivity of the rat brain. *Magnetic resonance in medicine*, 59(5), pp.1021–9.

Pearson, K., 1901. On lines and planes of closest fit to systems of points in space. *Philosophical Magazine*, 2(6), pp.559–572.

Penttonen, M., 2003. Natural logarithmic relationship between brain oscillators. *Thalamus & Related Systems*, 2(2), pp.145–152.

Perrodin, C. et al., 2014. Auditory and visual modulation of temporal lobe neurons in voice-sensitive and association cortices. *The Journal of neuroscience : the official journal of the Society for Neuroscience*, 34(7), pp.2524–37.

Petkov, C.I. et al., 2008. A voice region in the monkey brain. *Nature neuroscience*, 11(3), pp.367–74.

Petrides, M., Cadoret, G. & Mackey, S., 2005. Orofacial somatomotor responses in the macaque monkey homologue of Broca's area. *Nature*, 435(7046), pp.1235–8.

Petrides, M. & Pandya, D.N., 2002. Comparative cytoarchitectonic analysis of the human

and the macaque ventrolateral prefrontal cortex and corticocortical connection patterns in the monkey. *The European journal of neuroscience*, 16(2), pp.291–310.

Petrides, M. & Pandya, D.N., 1999. Dorsolateral prefrontal cortex: comparative cytoarchitectonic analysis in the human and the macaque brain and corticocortical connection patterns. *The European journal of neuroscience*, 11(3), pp.1011–36.

Polosecki, P. et al., 2013. Faces in motion: selectivity of macaque and human face processing areas for dynamic stimuli. *The Journal of neuroscience : the official journal of the Society for Neuroscience*, 33(29), pp.11768–73.

Ponce-Alvarez, A. et al., 2015. Task-Driven Activity Reduces the Cortical Activity Space of the Brain: Experiment and Whole-Brain Modeling. *PLoS computational biology*, 11(8), p.e1004445.

Poremba, A. et al., 2003. Functional mapping of the primate auditory system. *Science (New York, N.Y.)*, 299(5606), pp.568–72.

Power, J.D., Schlaggar, B.L. & Petersen, S.E., 2014. Studying brain organization via spontaneous fMRI signal. *Neuron*, 84(4), pp.681–96.

Raichle, M.E. et al., 2001. A default mode of brain function. *Proceedings of the National Academy of Sciences of the United States of America*, 98(2), pp.676–82.

Raichle, M.E. & Mintun, M.A., 2006. Brain work and brain imaging. *Annual review of neuroscience*, 29, pp.449–76.

Rainer, G. et al., 2001. Nonmonotonic noise tuning of BOLD fMRI signal to natural images in the visual cortex of the anesthetized monkey. *Current biology : CB*, 11(11), pp.846–54.

Rauschecker, J.P., 1998. Parallel processing in the auditory cortex of primates. *Audiology and Neuro-Otology*, 3(2–3), pp.86–103.

Rauschecker, J.P. et al., 1997. Serial and parallel processing in rhesus monkey auditory cortex. *The Journal of comparative neurology*, 382(1), pp.89–103.

Rauschecker, J.P., 2012. Ventral and dorsal streams in the evolution of speech and language. *Frontiers in evolutionary neuroscience*, 4, p.7.

Rauschecker, J.P. & Tian, B., 2000. Mechanisms and streams for processing of “what” and “where” in auditory cortex. *Proceedings of the National Academy of Sciences of*

the United States of America, 97(22), pp.11800–11806.

Rauschecker, J.P., Tian, B. & Hauser, M., 1995. Processing of complex sounds in the macaque nonprimary auditory cortex. *Science (New York, N.Y.)*, 268(5207), pp.111–4.

Recanzone, G.H., Guard, D.C. & Phan, M.L., 2000. Frequency and intensity response properties of single neurons in the auditory cortex of the behaving macaque monkey. *Journal of neurophysiology*, 83(4), pp.2315–2331.

Rees, G., Friston, K. & Koch, C., 2000. A direct quantitative relationship between the functional properties of human and macaque V5. *Nature neuroscience*, 3(7), pp.716–23.

Reser, D.H., 2000. Binaural Interactions in Primary Auditory Cortex of the Awake Macaque. *Cerebral Cortex*, 10(6), pp.574–584.

Riedl, V. et al., 2014. Local activity determines functional connectivity in the resting human brain: a simultaneous FDG-PET/fMRI study. *The Journal of neuroscience : the official journal of the Society for Neuroscience*, 34(18), pp.6260–6.

Rilling, J.K. et al., 2007. A comparison of resting-state brain activity in humans and chimpanzees. *Proceedings of the National Academy of Sciences of the United States of America*, 104(43), pp.17146–51.

Rockland, K.S. & Ojima, H., 2003. Multisensory convergence in calcarine visual areas in macaque monkey. *International Journal of Psychophysiology*, 50(1–2), pp.19–26.

Romanski, L.M. et al., 1999. Dual streams of auditory afferents target multiple domains in the primate prefrontal cortex. *Nature neuroscience*, 2(12), pp.1131–1136.

Roy, S. & Wang, X., 2012. Wireless multi-channel single unit recording in freely moving and vocalizing primates. *Journal of neuroscience methods*, 203(1), pp.28–40.

Salminen, N.H. et al., 2009. A population rate code of auditory space in the human cortex. *PloS one*, 4(10), p.e7600.

Schölvinck, M.L. et al., 2010. Neural basis of global resting-state fMRI activity. *Proceedings of the National Academy of Sciences of the United States of America*, 107(22), pp.10238–43.

Schroeder, C.E. & Foxe, J., 2005. Multisensory contributions to low-level, "unisensory" processing. *Current opinion in neurobiology*, 15(4), pp.454–8.

Schwarz, D.A. et al., 2014. Chronic, wireless recordings of large-scale brain activity in freely moving rhesus monkeys. *Nature methods*, 11(6), pp.670–6.

Shah, D. et al., 2015. Cholinergic and serotonergic modulations differentially affect large-scale functional networks in the mouse brain. *Brain structure & function*.

Shams, L., Kamitani, Y. & Shimojo, S., 2000. Illusions. What you see is what you hear. *Nature*, 408(6814), p.788.

Shams, L. & Kim, R., 2010. Crossmodal influences on visual perception. *Physics of life reviews*, 7(3), pp.269–84.

Shen, K. et al., 2012. Information processing architecture of functionally defined clusters in the macaque cortex. *The Journal of neuroscience : the official journal of the Society for Neuroscience*, 32(48), pp.17465–76.

Smith, S.M. et al., 2004. Advances in functional and structural MR image analysis and implementation as FSL. *NeuroImage*, 23 Suppl 1, pp.S208-19.

Smith, S.M. et al., 2009. Correspondence of the brain's functional architecture during activation and rest. *Proceedings of the National Academy of Sciences of the United States of America*, 106(31), pp.13040–5.

Spadone, S. et al., 2015. Dynamic reorganization of human resting-state networks during visuospatial attention. *Proceedings of the National Academy of Sciences of the United States of America*, 112(26), pp.8112–7.

Sparks, D.L., 1999. Conceptual issues related to the role of the superior colliculus in the control of gaze. *Current opinion in neurobiology*, 9(6), pp.698–707.

Spierer, L. et al., 2009. Hemispheric competence for auditory spatial representation. *Brain*, 132, pp.1953–1966.

Sporns, O., 2014. Contributions and challenges for network models in cognitive neuroscience. *Nature neuroscience*, 17(5), pp.652–60.

Sprague, J.M., 1996. Neural mechanisms of visual orienting responses. *Progress in brain research*, 112, pp.1–15.

Stecker, G.C., Harrington, I.A. & Middlebrooks, J.C., 2005. Location coding by opponent

neural populations in the auditory cortex. *PLoS biology*, 3(3), p.e78.

Stecker, G.C. & Middlebrooks, J.C., 2003. Distributed coding of sound locations in the auditory cortex. *Biological Cybernetics*, 89, pp.341–349.

Stein, B.E. et al., 2009. Challenges in quantifying multisensory integration: alternative criteria, models, and inverse effectiveness. *Experimental brain research*, 198(2–3), pp.113–26.

Stein, B.E., Magalhaes-Castro, B. & Kruger, L., 1975. Superior colliculus: visuotopic-somatotopic overlap. *Science (New York, N.Y.)*, 189(4198), pp.224–6.

Stein, B.E. & Meredith, M.A., 1993. *The Merging of the Senses*, Cambridge, MA: MIT Press.

Stein, B.E., Stanford, T.R. & Rowland, B.A., 2014. Development of multisensory integration from the perspective of the individual neuron. *Nature reviews. Neuroscience*, 15(8), pp.520–35.

Summerfield, C. & Egner, T., 2009. Expectation (and attention) in visual cognition. *Trends in cognitive sciences*, 13(9), pp.403–9.

Sumner, C.J. & Krumbholz, K., 2012. Which bit of auditory cortex does "where"? *The Journal of physiology*, 590(16), p.3645.

Supekar, K. et al., 2008. Network analysis of intrinsic functional brain connectivity in Alzheimer's disease. *PLoS computational biology*, 4(6), p.e1000100.

Tagliazucchi, E. & Laufs, H., 2014. Decoding wakefulness levels from typical fMRI resting-state data reveals reliable drifts between wakefulness and sleep. *Neuron*, 82(3), pp.695–708.

Thompson, G.C. & Cortez, A.M., 1983. The inability of squirrel monkeys to localize sound after unilateral ablation of auditory cortex. *Behavioural brain research*, 8(2), pp.211–6.

Tian, B. et al., 2001. Functional specialization in rhesus monkey auditory cortex. *Science (New York, N.Y.)*, 292(5515), pp.290–293.

Tsao, D.Y. et al., 2006. A cortical region consisting entirely of face-selective cells. *Science (New York, N.Y.)*, 311(5761), pp.670–4.

Ungerleider, L.G. & Mishkin, M., 1982. Two cortical visual systems. In M. R. Ingle DJ,

Goodale MA, ed. *Analysis of Visual Behaviour*. Cambridge, MA: MIT Press, pp. 549–586.

Vincent, J.L. et al., 2007. Intrinsic functional architecture in the anaesthetized monkey brain. *Nature*, 447(7140), pp.83–6.

Vnek, N. et al., 1999. Optical imaging of functional domains in the cortex of the awake and behaving monkey. *Proceedings of the National Academy of Sciences of the United States of America*, 96(7), pp.4057–60.

Vroomen, J. & de Gelder, B., 2000. Sound enhances visual perception: cross-modal effects of auditory organization on vision. *Journal of experimental psychology. Human perception and performance*, 26(5), pp.1583–90.

Waites, A.B. et al., 2006. Functional connectivity networks are disrupted in left temporal lobe epilepsy. *Annals of neurology*, 59(2), pp.335–43.

Wang, K. et al., 2007. Altered functional connectivity in early Alzheimer's disease: a resting-state fMRI study. *Human brain mapping*, 28(10), pp.967–78.

Wang, K. et al., 2006. Discriminative analysis of early Alzheimer's disease based on two intrinsically anti-correlated networks with resting-state fMRI. *Medical image computing and computer-assisted intervention : MICCAI ... International Conference on Medical Image Computing and Computer-Assisted Intervention*, 9(Pt 2), pp.340–7.

Wang, L. et al., 2006. Changes in hippocampal connectivity in the early stages of Alzheimer's disease: evidence from resting state fMRI. *NeuroImage*, 31(2), pp.496–504.

Wang, Y. et al., 2008. Visuo-auditory interactions in the primary visual cortex of the behaving monkey: electrophysiological evidence. *BMC neuroscience*, 9, p.79.

Warren, J.D. et al., 2002. Perception of Sound-Source Motion by the Human Brain. *Neuron*, 34(1), pp.139–148.

Watkins, S. et al., 2007. Activity in human V1 follows multisensory perception. *NeuroImage*, 37(2), pp.572–8.

Watkins, S. et al., 2006. Sound alters activity in human V1 in association with illusory visual perception. *NeuroImage*, 31(3), pp.1247–56.

Wei, T. et al., 2012. Predicting conceptual processing capacity from spontaneous neuronal activity of the left middle temporal gyrus. *The Journal of neuroscience : the official journal of the Society for Neuroscience*, 32(2), pp.481–9.

Weng, S.-J. et al., 2010. Alterations of resting state functional connectivity in the default network in adolescents with autism spectrum disorders. *Brain research*, 1313, pp.202–14.

Werner-Reiss, U. & Groh, J.M., 2008. A rate code for sound azimuth in monkey auditory cortex: implications for human neuroimaging studies. *The Journal of neuroscience : the official journal of the Society for Neuroscience*, 28(14), pp.3747–58.

Whitfield-Gabrieli, S. et al., 2009. Hyperactivity and hyperconnectivity of the default network in schizophrenia and in first-degree relatives of persons with schizophrenia. *Proceedings of the National Academy of Sciences of the United States of America*, 106(4), pp.1279–84.

Wilke, M. & Lidzba, K., 2007. LI-tool: a new toolbox to assess lateralization in functional MR-data. *Journal of neuroscience methods*, 163(1), pp.128–36.

Wilke, M. & Schmithorst, V.J., 2006. A combined bootstrap/histogram analysis approach for computing a lateralization index from neuroimaging data. *NeuroImage*, 33(2), pp.522–30.

Wise, L.Z. & Irvine, D.R., 1985. Topographic organization of interaural intensity difference sensitivity in deep layers of cat superior colliculus: implications for auditory spatial representation. *Journal of neurophysiology*, 54(2), pp.185–211.

Womelsdorf, T. et al., 2014. Dynamic circuit motifs underlying rhythmic gain control, gating and integration. *Nature neuroscience*, 17(8), pp.1031–9.

Woods, T.M. et al., 2006. Effects of stimulus azimuth and intensity on the single-neuron activity in the auditory cortex of the alert macaque monkey. *Journal of neurophysiology*, 96(6), pp.3323–37.

Xiong, J. et al., 1999. Interregional connectivity to primary motor cortex revealed using MRI resting state images. *Human brain mapping*, 8(2–3), pp.151–6.

Yao, H. et al., 2007. Rapid learning in cortical coding of visual scenes. *Nature neuroscience*, 10(6), pp.772–8.

You, H.-H. & Yeh, S.-L., 2010. Auditory cues facilitate both low-level and high-level unattended visual processing. *Journal of Vision*, 7(9), pp.647–647.

Yovel, G. & Belin, P., 2013. A unified coding strategy for processing faces and voices. *Trends in cognitive sciences*, 17(6), pp.263–71.

Zatorre, R.J. et al., 2002. Where is "where" in the human auditory cortex? *Nature neuroscience*, 5, pp.905–909.

Zhang, N. et al., 2010. Mapping resting-state brain networks in conscious animals. *Journal of neuroscience methods*, 189(2), pp.186–96.

Zhang, Z. et al., 2009. Impaired perceptual networks in temporal lobe epilepsy revealed by resting fMRI. *Journal of neurology*, 256(10), pp.1705–13.

Zucker, R.S. & Regehr, W.G., 2002. Short-term synaptic plasticity. *Annual review of physiology*, 64, pp.355–405.

Zuo, X.-N. et al., 2010. The oscillating brain: complex and reliable. *NeuroImage*, 49(2), pp.1432–45.

9 LIST OF AUTHOR CONTRIBUTIONS

9.1 **Azevedo F. A. C.**, Ortiz-Rios M., Casarsa, L. A., Balla D. Z, Li, Q., Lohmann, G., Logothetis N. K., and Keliris G. A. (2017). Simultaneous resting-state and visually-driven functional networks in the macaque brain (*in preparation*).

FACA and GAK designed the study, FACA programmed stimulus delivery and event design, collected and analysed the data and wrote the manuscript. MOR, CLA, BDZ helped in data collection. LG, NKL and GAK participated in writing the manuscript.

9.2 **Azevedo F. A. C.**, Ortiz-Rios M., Li Q., Logothetis N. K., and Keliris G. A. (2015). A Potential Role of Auditory Induced Modulations in Primary Visual Cortex. *Multisensory Research*. 28 (3-4): 331-49.

FACA, MOR, GAK proposed the model, FACA wrote the manuscript. MOR, LQ, NKL and GAK contributed with fruitful discussions and in writing the manuscript.

9.3 Ortiz-Rios M., Kuśmierek P., DeWitt I., Archakov D., **Azevedo F. A. C.**, Sams M., Jääskeläinen I. P., Keliris G. A., and Rauschecker J. P. (2015). Functional MRI of the vocalization-processing network in the macaque brain. *Frontiers in Neuroscience*. 9, 113.

FACA contributed in data analyses and in writing the manuscript. MOR designed the study, trained the animals, programmed stimulus presentation, contributed with data collection and analysis, and wrote the manuscript. PK programmed the behavioural task and participated in writing the manuscript. DA trained the animals and acquired part of the data. IDW generated the scrambled stimuli and acquired part of the data. GAK, interpreted data and participated in writing the manuscript. MS, IPJ, and JPR co-designed the study and participated in writing the manuscript.

9.4 Ortiz-Rios M., **Azevedo F. A. C.**, Kuśmierek P., Balla D. Z., Munk M. H., Keliris G. A., Logothetis N. K., and Rauschecker J. P. Widespread and opponent fMRI signals represent sound location in macaque auditory cortex. *Neuron. 93(4), 971-983.*

FACA contributed with event design, behavioural training of the monkeys, data acquisition and in writing the manuscript. MOR designed the study, programmed stimulus delivery and event design, collected and analysed the data and wrote the manuscript. GAK helped with event design, data acquisition for awake-fMRI experiments and writing of the manuscript. MHM helped with anesthetized experiments and writing of the manuscript. DB optimized the data acquisition for awake-fMRI experiments. PK provided some methodologies and participated in writing the manuscript. NKL and JPR co-designed this study and participated in writing the manuscript.

10 APPENDICES

10.1: **Azevedo F. A. C.**, Ortiz-Rios M., Casarsa, L. A., Balla D. Z, Li, Q., Lohmann, G., Logothetis N. K., and Keliris G. A. (2017). Simultaneous resting-state and visually-driven functional networks in the macaque brain *(in preparation)*.

10.2: **Azevedo F. A. C.**, Ortiz-Rios M., Li Q., Logothetis N. K., and Keliris G. A. (2015). A Potential Role of Auditory Induced Modulations in Primary Visual Cortex. *Multisensory Research*. 28 (3-4): 331-49.

10.3: Ortiz-Rios M., Kuśmierek P., DeWitt I., Archakov D., **Azevedo F. A. C.**, Sams M., Jääskeläinen I. P., Keliris G. A., and Rauschecker J. P. (2015). Functional MRI of the vocalization-processing network in the macaque brain. *Frontiers in Neuroscience*. 9, 113.

10.4: Ortiz-Rios M., **Azevedo F. A. C.**, Kuśmierek P., Balla D. Z., Munk M. H., Keliris G. A., Logothetis N. K., and Rauschecker J. P. Widespread and opponent fMRI signals represent sound location in macaque auditory cortex. *Neuron*. 93(4), 971-983.

10.5: Illustrated description of the unsupervised network classifier developed for the study "Simultaneous resting-state and visually-driven functional networks in the macaque brain".

10.1 Simultaneous resting-state and visually-driven functional networks in the macaque brain (*in preparation*)

TITLE: Simultaneous resting-state and visually-driven functional networks in the macaque brain

AUTHORS: Frederico A. C. Azevedo[1,2], Michael Ortiz-Rios[1], Leonardo C. Azevedo[1], Dávid Z. Balla[1], Qinglin Li[1,2], Gabriele Lohmann[3], Nikos K. Logothetis[1,4] and Georgios A. Keliris[1,5]

AFFILIATIONS: [1]Department of Physiology of Cognitive Processes, Max Planck Institute for Biological Cybernetics, Tübingen, Germany; [2]International Max Planck Research School (IMPRS), Tübingen, Germany; [3]Magnetic Resonance Center, Max Planck Institute for Biological Cybernetics, Tübingen, Germany; [4]Division of Imaging Science and Biomedical Engineering, University of Manchester, Manchester M13 9PT, United Kingdom; [5]Department of Biomedical Sciences, University of Antwerp, 2610 Wilrijk, Belgium.

ABSTRACT

The brain is a dynamical system interconnected through long-range temporally-correlated functional networks. In the absence of external stimulation, several functional networks thought to be related to spontaneous activity have been identified. In contrast, when the brain is being challenged with sensory inputs, a different pattern of evoked activity emerges. How the brain orchestrates such distinct patterns of functional activity is still unclear. Here we address this issue by investigating the topographical correspondence between resting-state and visually-driven functional networks in the monkey brain during different states of consciousness. We show that, depending on the brain state, most resting-state networks can coexist and are linearly independent from stimulus-induced networks. Additionally, we observed a new resting-state network, which encompasses the caudate, putamen and amygdala, being thus possibly related to memory mechanisms. Our findings conceal studies of spontaneous and stimulus-induced functional architectures in the non-human primate brain, topics which are usually investigated separately.

INTRODUCTION

Brains are restless[1]. Typically, 60-80% of brain's energy consumption is spent during spontaneous activity[2]. Such activity isn't random. At a mesoscale, spontaneous large-amplitude low frequency fluctuations (<0.1 Hz) of hemodynamic activity across functionally related areas of the brain can be consistently observed. These functional networks, termed resting state networks[3], constitute an intrinsic functional architecture in the brain[4]. Their origin and specific functions are not well understood, but they could reflect neural fluctuations within anatomically connected areas[5] or even predict active mechanisms related to cognition[6]. In parallel, brain activity is constantly modulated by extrinsic sensory stimulation and cognitive states[7,8]. How both intrinsic and extrinsic functional architectures relate to each other is a question under active investigation[9].

Currently, controversies about the equivalence of extrinsic and intrinsic functional architectures in the human brain still exist. While it has been suggested that the functional architecture of the brain during spontaneous and evoked activity have close correspondence, to the point of sharing a full repertoire of functional networks in both states[10], such a tight coupling has been disputed. For instance, studies show that although a high similarity in functional network topography might occur in default and task-positive regions, it doesn't necessarily generalize to the whole brain. Specifically, regions such as primary sensory and motor cortices, limbic regions or subcortical structures would present weak correspondence in the hemodynamic patterns of spontaneous and evoked activity[7,11]. To shed light on this debate from the perspective of the non-human primate brain, we investigated the topographical correspondence of extrinsic and intrinsic low-frequency functional architectures in the macaque brain exposed to different conditions of visual stimulation and different states of consciousness, anesthetized and

awake. Unique to our approach, we aimed at disentangling intrinsic from stimulus-evoked networks embedded in same functional datasets.

For our experiments, we used high field functional magnetic resonance imaging (fMRI) to scan brain activity of two monkeys probed with three different conditions of visual stimulation. Specifically, data were collected in the absence of visual input, i.e. in a resting-state condition; during visual stimulation with a standard 1-min alternated block design showing movie clips; and throughout continuous visual stimulation. Similar paradigms were used while the animals were anesthetized or awake. Using spatial Independent Component Analysis (sICA) in the resting-state datasets of both subjects, we consistently observed a set of 11 functional networks in the anesthetized state, including a new Caudate-Putamen-Amygdala (CPA) functional network. In the awake state, we found a subset of 7 of the 11 networks present during anesthesia. Surprisingly, after analyzing the residuals of the modelled stimulus-evoked activity, the part of the data which is commonly discarded as noise, we could still uncover every resting state-network in the anesthetized state. Likewise, in the awake state all but one resting-state networks were present in the GLM-residuals of the block-design condition. Overall, we show that the vast majority of resting-state networks are linearly contained and can be recovered from the same datasets displaying significant visually induced activity in the non-human primate brain. This remains true even in cortical regions where spontaneous and induced BOLD activity happens at the same time.

MATERIAL AND METHODS

Non-human primates

Our experiments were performed on two adult female macaque monkeys, M1 and M2 (*Macaca mulatta, 8 kg each*), in both anesthetized and awake conditions. Prior to the experiments, we stereotaxically implanted a custom-made PEEK (polyetheretherketone; TecaPEEK, Ensinger, Inc., Nufringen, Germany) headpost on the cranium of each animal, precisely over the superior part of the central sulcus. The implants were secured with custom made ceramic screws (zirconium oxide Y_2O_3-TPZ 5x1, Pfannenstiel, Bad Toelz, Germany) and sealed at their junctions to the bone with bone cement (Palacos, Merck Biomaterial GmBh, Darmstadt, Germany). Every surgical procedure was performed in the animals under general anesthesia [12]. All the experimental procedures were carefully done to ensure the well-being of the animals, were previously approved by the local authorities (Regierungspraesidium) and were in full compliance with the guidelines of the European Community (EUVD 86/609/EEC) for the care and use of animals in laboratories.

Data Acquisition

Anesthesia condition: Our experimental procedures have been previously detailed elsewhere [12]. Shortly, after premedication with glyco-pyrrolate (i.m. 0.01 mg/kg) and ketamine (i.m. 15 mg/kg), we administered a cocktail of fast-acting drugs (fentanyl at 3 μg/kg, thiopental at 5 mg/kg, and the muscle relaxant succinyl-choline chloride at 3 mg/kg). Anesthesia was stabilized with remifentanil (0.5^{-2} ug/kg/min) and muscle relaxant mivacurium chloride (5 mg/kg/h). Physiological parameters such as heart rate, blood pressure and oxygenation, CO_2 and temperature were monitored and kept in normal physiological range. Measurements were performed in a 60-cm-diameter-bore Bruker 7T

vertical MRI scanner (Bruker Corporation, Ettlingen, Germany) with a custom designed 12-cm quadrature volume coil spanning the whole head. Preceding the functional experiments, T1-weighted Modified Driven Equilibrium Fourier Transform images (MDEFT, TR = 15 ms, TE = 4.5 ms, inversion time = 800 ms; number of segments = 4; flip angle = 20º, receiver bandwidth = 50 kHz, voxel matrix = 256 x 256, number of slices = 128, voxel resolution = 0.5 x 0.5 x 0.5 mm^2) were acquired as subject-specific high resolution anatomical template. These templates were used as high-resolution anatomical references for both anesthesia and awake datasets. Functional sequences consisted of single-shot interleaved gradient-echo echo-planar images (GE-EPI, TR = 1000 ms for M1 and TR = 1200 ms for M2, TE = 18 ms, flip angle = 53º, receiver bandwidth = 144 kHz, voxel matrix = 64 x 64, number of slices = 25 for M1 and 27 for M2, voxel resolution = 1.5 mm^3). TR for M2 (= 1200 ms) was slightly longer than that used with M1 (TR = 1000 ms) because an excess of adipose tissue around the neck required additional fat suppression parameters. For both animals, we collected a total of 600 volumes per run. Therefore, each run of M1 lasted 10 min while each run of M2 lasted 12 min. Volumes were acquired approximately parallel to the anterior-posterior commissures plane (AC-PC). In the end of each session, T1-weighted fast low angle shot (FLASH) images (TR = 2000 ms, TE = 15 ms, flip angle = 69º, receiver bandwidth = 50 kHz) with the same geometry as the functional scans were collected and used as low-resolution anatomical reference. FLASH images are useful because they present less pronounced spatial distortions than GE-EPI volumes.

In total, we collected 4 sessions of data for M1 and 3 sessions for M2 during the presentation of all three visual paradigms. During paradigm (i) no visual stimulation was presented. Paradigm (ii) showed a one-min "on/off" block design alternating an empty background with scenes of Star Wars or African Wildlife. Finally, paradigm (iii)

contained uninterrupted versions of the same movies presented in (ii). Concerning paradigm (i), 35 datasets for M1 (14, 10, 6, 5 datasets/session) and 21 for M2 (10, 8, 3 datasets/session) were collected. During paradigm (ii), 20 datasets for M1 (10, 10 datasets/session) and 19 for M2 (10, 9 datasets/session) were obtained. For paradigm (iii), 10 datasets for M1 (1 session) and 6 datasets for M2 (1 session) were acquired. Visual stimuli were presented through a custom-built projector and SVGA fiber-optic system (field of view = 30° x 23°, frame rate = 60 Hz, resolution = 640 × 480 pixels). During (i), optical periscopes were switched off to avoid contamination by subtle confounding factors, i.e. background flickering [13].

Awake condition: Before the awake experiments, both monkeys were trained in a mock scanner to remain headposted and motionless in a custom-made fMRI chair while two of the aforementioned visual paradigms were presented. Specifically, the monkeys were trained with paradigm (i), no visual stimulation, and paradigm (ii), one-min "on/off" block design alternating an empty background with scenes of Star Wars or African Wildlife (Fig. 2a). Optical stimulators were the same type with the ones used during anesthesia. Eye movements were recorded with an infrared eye-tracking system (iView, SensoMotoric Instruments GmbH, Teltow, Germany). Scanner noise was attenuated with ear plugs and foam pillows. Both monkeys were considered trained when the amplitude of motion detected by a custom-made body sensor[14] did not exceed amplitude of breathing in 95% of the scanning time (approximately 2 hours). Typically, the monkeys kept their eyes closed for most of the time during paradigm (i). Functional measurements were done in a 40-cm-diameter-bore vertical Bruker scanner (Bruker Corporation, Ettlingen, Germany) equipped with a 12-cm quadrature volume coil. We acquired single-shot interleaved gradient-echo echo-planar images (GE-EPI, TR = 1000 ms, TE = 18 ms, flip angle = 53°, receiver bandwidth = 144 kHz, voxel matrix = 90 x 60, number of slices =

18, voxel resolution = 1 x 1 x 2 mm^3 resampled to 1,5mm^3). Each run contained a total of 600 volumes. Since the whole brain couldn't be acquired with those parameters within a 1 s TR, we chose an oblique field of view that maximizing temporal, parietal and occipital lobes. Similar to anesthesia experiments, T1-weighted fast low angle shot (FLASH, TR = 2000 ms, TE = 15 ms, flip angle = 69º, receiver bandwidth = 50 kHz) images were used as low-resolution anatomical references for the functional images. In total, we collected 2 sessions for M1 (6, 5 datasets/session) and 3 sessions for M2 (5, 5, 2 datasets/session) concerning visual paradigm (i); and 2 sessions for M1 (5, 4 datasets/session) and 1 session for M2 (4 datasets) concerning paradigm (ii).

Data Analysis

Data preprocessing was performed with AFNI [15]. Similar steps were applied to both anesthesia and awake datasets. For datasets where no visual stimulus was presented, we performed despiking, slice timing correction, motion correction with 6-parameters affine transformation, bandpass filtering from 0.01 to 0.1 Hz, spatial smoothing with 3 mm full width at half maximum (FWHM) Gaussian kernel, removal of motion artifacts and removal of activity located in white-matter plus cerebrospinal fluid. Volumes presenting derivative values with Euclidean Norms above 0.2 were excluded of further analysis. Subsequent to preprocessing, we used GIFT software package for Matlab [16] to perform spatial independent component analysis (ICA [17]) imposing 20 independent components a priori [18]. In short, GIFT processing reduced temporal dimension of the variance-normalized voxel timecourses by means of principal component analysis (PCA [19]). Thereafter, it estimated spatial independent components with Infomax algorithm. Finally, it back-reconstructed the data. Reliability of the decomposition was assessed with ICASSO algorithm [20] (100x ICA reiteration). As a control we also used FSL-MELODIC [21] in a subset of datasets obtaining similar results. Spatial components were quantified

with empirical z-scores, a measure directly proportional to the temporal correlation between estimated component and each voxel timecourse. In the datasets containing visual stimulation conditions, preprocessing was done in a similar way, but before bandpass filtering we applied a general linear model. After preprocessing, task-evoked BOLD responses were quantified by means of a general linear model (GLM). In the next step, all the modelled variance was subtracted from the original datasets. By doing so, we could separate visually-induced BOLD effects from the unexplained variance of our model. Stimulus-specific regressors were obtained by convolving square-wave stimulus function with a standard one-parameter gamma distribution estimate of hemodynamic response function. Finally, GLM residuals were bandpass filtered (from 0.01 to 0.1 Hz) and their 20 maximally independent components estimated via spatial ICA decomposition, as previously described (Fig. 2b).

All results were spatially normalized to the F99 surface-based macaque atlas [22] in a three-step process. Firstly, we non-linearly warped the GE-EPI's to their corresponding FLASH anatomical reference using AFNI's 3dQwarp function. After that, we linearly aligned the warped images to their respective MDEFT anatomical reference using AFNI's 3dAllineate function (12 affine parameters). Finally, we once again used 3dQwarp to perform the last non-linear warping step to spatially normalize the transformed GE-EPI's to the F99 atlas (Fig. S3). All cortical areas were defined according to the LVE00 partitioning scheme [23] available in Caret software [24] (Fig. S1). Functional modality boundaries were based on the modality parcellation contained in Caret (Fig. S2). Resulting components of across subjects and conditions were grouped using a custom-written unsupervised network classifier algorithm (see Fig. S4 for an example). Briefly, the algorithm grouped independent functional networks based on a similarity index rank calculated for all possible combinations of all pairwise spatial correlations between

positively thresholded components. After unbiased clustering, group components belonging to the same condition and subject were averaged. Functional connectivity matrices were created by including all regions containing at least 15% voxels with empirical z-scores greater than 1. Our anatomical connectivity matrix was formed by combining the best estimate connectivity matrix obtained from the Cocomac database [25] (using the F99-LVE00 division) with the macaque47 functional connectivity matrix, contained in the brain-connectivity-toolbox [26,27]. We further quantified hemispheric laterality and functional-to-anatomical correspondence of binary connectivity matrices using cosine similarity.

RESULTS

Intrinsic Architecture in anesthetized and awake monkeys

Controversies exist about the equivalence of extrinsic and intrinsic functional architectures in the human brain, with evidences showing tight functional coupling for default and task-positive regions, but not for primary sensory and motor cortices, limbic regions or subcortical structures [7,11]. To address those, we sought to analyze topographical consistency of extrinsic and intrinsic low-frequency functional networks in the macaque brain exposed to different conditions of visual input and cognitive state. The macaque brain is a good surrogate to the human brain due its similarity in cellular composition [28], architecture [29,30], structural connectivity [31,32], and functional organization [33–36]. Consequently, knowledge obtained with non-invasive approaches, typically performed in humans, can be confidently complemented with findings derived from multimodal approaches in the non-human primate brain, be it invasive or not.

We started our investigation by decomposing the functional network architecture of the monkey brain (*Macaca mulatta*, n = 2) devoid of any kind of experimental stimulation into their 20 maximally statistically independent components. Consistent components across subjects were classified as resting-state networks (RSNs). During the resting-state condition, the animals were kept in complete darkness and scanner noise was considerably attenuated with hearing protectors. All our anesthesia experiments were performed in a vertical 7T Bruker scanner (Bruker Corporation, Ettlingen, Germany). On the other hand, all our awake scans were done in a vertical 4.7T Bruker scanner. We chose to scan the awake animals at a lower magnetic field strength to minimize the artefactual effects of body and jaw movement in the images, more pronounced at higher magnetic fields [14]. After standard resting-state preprocessing of our gradient-echo echo-planar images (GE-EPI, TR ~ 1000 ms, 600 volumes/run, voxel resolution 1.5 mm^3), which included spatial smoothing with a 3-mm full width at half maximum (FWHM) Gaussian kernel and bandpass filtering from 0.01 to 0.1 Hz (see material and methods), we performed spatial ICA decomposition (sICA) on our datasets to estimate the 20 maximally independent components [4,18]. For every post-hoc selected component, we assured that ICASSO stability (a measure dealing with the stochasticity of different runs in ICA analysis) approached 1 (mean stability index 0.92 +/- 0.02 , 100x reiteration). Intersession and intersubject comparisons were made after each statistical map was spatially normalized to the F99 surface-based macaque atlas and parcellated according to the LVE00 partitioning scheme (Fig. S1). Independent components were clustered based on pairwise spatial correlations using a custom-written unsupervised classifier for fMRI statistical maps (Fig. S4). Our main inclusion criteria to define reliability of identified networks were topographical consistency across sessions and subjects, hemispheric bilateralism and superposition with gray matter.

We observed 11 resting-state networks in our anesthesia datasets. From those, 10 have been previously reported but one is original. The reported RSNs present in our functional images were namely the precentro-temporal, medio-occipital, fronto-parietal, superior-temporal, paracentral, default-mode (DMN), parietal, latero-occipital, thalamic and cerebellar [4,18]. In addition to that, we observed an unreported network encompassing the caudate, putamen and amygdala. We named it, therefore, the CPA network (Fig. 1a). Concerning our awake datasets, we were able to identify all previous networks except 4 of them: the parietal, superior-temporal, thalamic and CPA networks (Fig. 1b). The absence of those 4 networks in the acquired volumes could be attributed to the distinct state of alertness or to technical differences in data acquisition/quality in the awake condition, i.e. more motion artefacts or narrower field of view (Fig. 1c). All cortical networks were quantified using the F99 surface-based macaque atlas [22] and the LVE00 cortical parcellation scheme [23] as references. See supplementary figures for a detailed description of each network individually.

Comparison of intrinsic architectures across visual conditions

In a second step, after characterizing the topographical architecture of the RSNs observed in our datasets, we set out to find reminiscent low-frequency large-amplitude functional networks putatively contained in datasets displaying significant visually-evoked BOLD response. We examined datasets derived from anesthesia and awake cognitive states. To induce strong visual responses in the BOLD-fMRI data, we visually stimulated our animals with an alternated one-min block-design showing scenes of Star Wars or African savanna. As a control for the vigorous changes in stimulus intensity throughout the block-design, we additionally presented our monkeys with continuous versions of the same movie clips presented in the blocks. This control condition was just acquired during the anesthesia condition, where animal compliance wasn't required.

Resulting datasets were preprocessed with similar steps as described in the previous section, concerning resting-state analysis. The only exception was bandpass filtering, left to be performed at a later stage (Fig. 2a). After preprocessing, we performed a general linear model (GLM) analysis of the expected hemodynamic response in our data to identify runs displaying significant evoked visual responses ($p<0.05$, FDR corrected, Fig. 2b). Only runs showing significant visual processing were selected for further analysis. Next, we disentangled the variance our model could explain (betas * design matrix) from the remaining residuals of the model in every run independently.

In most traditional fMRI analysis, the residuals are discarded as uninformative data. Here, we decided to investigate the amount of intrinsic functional networks that could be recovered from those residuals. For that, we decided to bandpass them within the same frequency range as before, from 0.01 Hz to 0.1 Hz, and performed spatial ICA decomposition with exact the same parameters used in the resting state analysis (Fig. 2). To our surprise, we observed independent components with strikingly similar functional topography as the resting-state networks (Fig. 3-6, table S1). Extrinsically induced visual processing wasn't able to interfere with the intrinsic network architecture. Remarkably, significant topographical changes weren't observed not even in any of the two mainly-visual resting-state networks, encompassing areas where visual activity and spontaneous activity were occurring simultaneously. Such mutual independence in intrinsic and visually evoked functional architectures was complete during anesthesia, where every consistent component identified by our unsupervised network classifier was present across all subjects and conditions (Fig. 3). In the awake datasets, only the fronto-parietal component couldn't be observed in the residuals of the block-design.

DISCUSSION

The primate brain is a complex dynamic system comprised of temporally correlated functional networks [37,38]. It's generally accepted that the structure of this correlated activity depends on the brain's internal state and on stimulus input [4,39]. In the absence of external stimulation, spontaneous large-scale low-frequency functional networks can be observed [3,40,41]. On the other hand, when the brain is being stimulated, a stimulus-specific pattern of activity composed of extrinsic functional networks is generated [12,42,43]. Although it has been suggested that correspondence of whole-brain's functional network topography during periods of activation and rest functional frameworks is large [10], this assertion has been disputed. In fact, several studies have shown that extrinsic and intrinsic functional architectures aren't necessarily equivalent [7,11]. Here in this work, we sought to address the topographical relationship between intrinsic and extrinsic architectures by investigating the spatial correlation of functional networks present under different conditions of visual stimulation and consciousness. Importantly, we showed that most intrinsic components were contained and could be reliably recovered from datasets displaying significant visually-evoked activity.

Firstly, we showed that in the anesthetized state 11 of 20 maximally statistically independent components were consistent across sessions and subjects. From those, 8 components encompassed mainly the cerebral cortex, while 2 encircled mainly subcortical areas, and 1 corresponded to the cerebellum (Fig. 1a, S5-S11). Shortly, the precentro-temporal network encompassed ventral motor areas and is potentially involved with understanding of action, control of grasping, mouth and tongue[18]. Besides that, we also observed increased connectivity with portions of insular cortex and thalamus. The fronto-parietal component contained parts of frontal eye fields, inferior arm of the arcuate sulcus, dorsal central sulcus and intraparietal sulcus. This network is thought to be

involved in the processing of ocular movements and goal-directed top-down inputs [18,44]. The lateral-occipital network enclosed areas that represent preferentially the foveal visual field, while the medial-occipital network comprised areas related to peripheral visual field processing [4]. Thus, those two networks possibly play a role in visual processing. The superior temporal network included areas related to auditory processing areas, i.e. auditory belt and parabelt, and adjacent areas in the superior temporal gyrus [18,45]. The paracentral component included areas related to dorsal somatomotor and processing of somatosensory input [18,46,47]. The DMN, which included the medial and lateral parietal cortex, the anterior and posterior cingulate cortex, and medial prefrontal cortex, is a network known to be less pronounced during cognitive demanding tasks. Besides that, it's speculated that this network is involved with introspective cognition in humans [48,49]. The parietal network, which resembled one of the first RSNs demonstrated to exist in anesthetized monkey brains [4], encompassed parietal areas, such as MST and LIP. The thalamic network comprised mainly the thalamus, a central relay station of the brain which is connected with many associative brain areas through multi-functional pathways. The thalamus is thought to regulate brain rhythms and consciousness [50]. The cerebellar network circumscribed the cerebellum, a structure involved in motor control, learning and higher cognitive functions, such as spatial cognition and attention [51,52]. Finally, the CPA network consistently encircled the caudate, putamen and amygdala. Due to the regions involved, we speculate that this network could be involved in multiple memory systems [53]. A detailed depiction of each individual component can be found in the supplementary material.

The awake datasets contained a subset of 7 networks with similar topography to the 11 RSNs previously described (Fig. 1b). The parietal, superior-temporal, thalamic and CPA networks were the only ones which were absent. There's a couple of reasons for

that. The first reason has to do with motion artefacts. Although our monkeys were trained to sit still during the scanning sessions, the amount of movement is still unavoidably higher than in the anesthesia condition. Since body and head motion can systematically affect functional connectivity measures [54], some of the observed RSNs could have been affected. Another source of disparity could be due to the partial acquisition of brain volumes in our awake experiments. Since we wanted to keep the repetition time (TR) of our brain volumes around 1 second in all conditions, we had to sacrifice part of the field of view in our 4.7 T scanner. For our awake scans, we chose to emphasize the occipital, temporal, parietal and the inferior part of the frontal cortex (Fig. 1c). This effect is clearly seen in the awake paracentral network, in which an obvious oblique linear boundary caused by the limited field of view can be observed (Fig. 1b). Finally, the absence of those networks could genuinely reflect a different state of consciousness. According to previous studies, spontaneous functional connectivity is differentially modulated by awareness states. It can be more or less shaped differently shaped by fluctuations determined by fixed anatomical connections or by a continuous stream of ongoing cognitive processes [55], depending on the animal's degree of consciousness.

In a second stage, after mapping the individual components of the intrinsic functional architecture in the anesthetized and awake state, we investigated if the presence of intense visual activity induced by passive visual stimulation could significantly disrupt the topography of the previously described RSNs. Our working hypothesis was that acute external visual stimulation would be able to consistently disrupt correlation patterns of voxel timeseries, which would be reflected in altered RSN topography. To investigate that, we showed our animals with a one-minute interleaved block-design showing movie clips and with uninterrupted versions of the same movies. After preprocessing those datasets with standard steps commonly applied to resting-state fMRI data (but not

bandpass filtering), we modelled the evoked visual effects in the BOLD signal with a GLM design and selected only the runs that displayed significant responses. Thereafter, we subtracted the explained variance from the acquired data, bandpass-filtered them to remove extremely low (< 0.01 Hz) and high frequencies (> 0.1 Hz) and performed spatial ICA decomposition on the remaining data. To our surprise, we were able to recover every one of the 11 low-frequency large-amplitude fluctuation previously observed in the resting-state condition (Fig. 3). A similar result was obtained with the awake condition, where we could recover 6 of the 7 RSNs previously identified. The only resting-state network that couldn't be observed was the fronto-parietal network (Fig. 5). Our results showed that strong stimulus-driven visual activity wasn't able to modulate considerably intrinsic network topography. Interestingly, even in cortical regions where bottom-up activity and intrinsic oscillations were happening at the same time, i.e. in early visual cortices, we didn't observe any significant cross-interaction among intrinsic and stimulus-evoked architectures. Thus, our findings suggest that visually-induced extrinsic architecture is composed of an independent intrinsic component which is linearly superimposed to a stimulus-specific functional architecture. Future studies applying a similar methodology to a variety of other tasks and functional modalities are still necessary to show if this property is generalizable across different cognitive tasks throughout the brain. Our results are in full agreement with a human fMRI study in which the authors used large-scale graphs built from human functional connectivity data to compare intrinsic and task-evoked functional architectures in the whole brain [56]. Particular to our methodology, we used sICA to investigate the individual role of each intrinsic network in the extrinsic architecture. By doing so, direct comparison of our results with the majority of macaque resting-state literature is facilitated, since most of those studies use similar data analysis techniques.

In terms of neurophysiological correlates, we can only tentatively explain our results. The neurophysiological basis of BOLD signal is still an area of active research [57–59]. For instance, a study of global-resting state fMRI in awake monkeys showed that oscillations in neural activity were able to explain, at best, 10% of fMRI signal variance. To make things even more complex, the authors showed that correlation of fMRI and electrophysiological signals was an irregular parameter [60]. To explain our findings, we hypothesize that, at least in the early visual cortices where intrinsic and stimulus-evoked activity coexisted, the observed BOLD signal would be reflecting the sum of hemodynamic activity derived from different cortical layers. Our hypothesis is in agreement with an electrophysiological study performed in awake monkeys, in which multilaminar electrodes were implanted in V1 while the monkeys were resting or being stimulated with a visual stimulus, showing the existence istinct superficial and deep laminar domains of activity in the visual cortex during rest and stimulation [61].

We foresee two practical applications for our findings. Firstly, they stimulate the reinterpretation of a large existing neuroimaging database to study functional connectivity, but now taking into account the residuals of hypothesis-driven analysis, which are normally discarded as noise. The second application concerns the design and analysis of neuroimaging studies. In agreement with previous evidences which shows contamination of stimulus-driven fMRI activity by spontaneous BOLD fluctuations in humans [62,63], in order to easily decouple both types of signal, it may be a good idea to avoid stimulus configurations in which responses are expected to happen in similar frequency ranges of resting-state-like networks (0.01 Hz and 0.1 Hz). By doing so, it becomes straight forward to perform ICA decomposition and to regress out regional intrinsic oscillations of stimulus-driven datasets, resulting in increased statistical power for the evoked effect.

ACKNOWLEDGMENTS

We thank Vishal Kapoor for fruitful discussions and in revising the manuscript. This work was supported by the Max Planck Society.

COMPETING FINANCIAL INTERESTS

The authors declare no competing financial interests.

REFERENCES

1. Raichle, M. E. The restless brain. *Brain Connect.* **1,** 3–12 (2011).
2. Raichle, M. E. & Mintun, M. A. Brain work and brain imaging. *Annu. Rev. Neurosci.* **29,** 449–76 (2006).
3. Biswal, B., Yetkin, F. Z., Haughton, V. M. & Hyde, J. S. Functional connectivity in the motor cortex of resting human brain using echo-planar MRI. *Magn. Reson. Med.* **34,** 537–41 (1995).
4. Vincent, J. L. *et al.* Intrinsic functional architecture in the anaesthetized monkey brain. *Nature* **447,** 83–6 (2007).
5. Greicius, M. D., Supekar, K., Menon, V. & Dougherty, R. F. Resting-State Functional Connectivity Reflects Structural Connectivity in the Default Mode Network. *Cereb. Cortex* **19,** 72–78 (2009).
6. Tavor, I. *et al.* Task-free MRI predicts individual differences in brain activity during task performance. *Science* **352,** 216–20 (2016).
7. Mennes, M., Kelly, C., Colcombe, S., Castellanos, F. X. & Milham, M. P. The extrinsic and intrinsic functional architectures of the human brain are not equivalent. *Cereb. Cortex* **23,** 223–9 (2013).
8. Spadone, S. *et al.* Dynamic reorganization of human resting-state networks during visuospatial attention. *Proc. Natl. Acad. Sci. U. S. A.* **112,** 8112–7 (2015).
9. Ponce-Alvarez, A., He, B. J., Hagmann, P. & Deco, G. Task-Driven Activity Reduces the Cortical Activity Space of the Brain: Experiment and Whole-Brain Modeling. *PLoS Comput. Biol.* **11,** e1004445 (2015).

10. Smith, S. M. *et al.* Correspondence of the brain's functional architecture during activation and rest. *Proc. Natl. Acad. Sci. U. S. A.* **106,** 13040–5 (2009).

11. Buckner, R. L., Krienen, F. M. & Yeo, B. T. T. Opportunities and limitations of intrinsic functional connectivity MRI. *Nat. Neurosci.* **16,** 832–7 (2013).

12. Logothetis, N. K., Guggenberger, H., Peled, S. & Pauls, J. Functional imaging of the monkey brain. *Nat. Neurosci.* **2,** 555–62 (1999).

13. Logothetis, N. K. *et al.* How not to study spontaneous activity. *Neuroimage* **45,** 1080–9 (2009).

14. Keliris, G. A. *et al.* Robust controlled functional MRI in alert monkeys at high magnetic field: effects of jaw and body movements. *Neuroimage* **36,** 550–70 (2007).

15. Cox, R. W. AFNI: software for analysis and visualization of functional magnetic resonance neuroimages. *Comput. Biomed. Res.* **29,** 162–73 (1996).

16. Calhoun, V. D., Adali, T., Pearlson, G. D. & Pekar, J. J. A method for making group inferences from functional MRI data using independent component analysis. *Hum. Brain Mapp.* **14,** 140–51 (2001).

17. McKeown, M. J. *et al.* Analysis of fMRI data by blind separation into independent spatial components. *Hum. Brain Mapp.* **6,** 160–88 (1998).

18. Hutchison, R. M. *et al.* Resting-state networks in the macaque at 7 T. *Neuroimage* **56,** 1546–55 (2011).

19. Pearson, K. On lines and planes of closest fit to systems of points in space. *Philos. Mag.* **2,** 559–572 (1901).

20. Himberg, J., Hyvärinen, A. & Esposito, F. Validating the independent components of neuroimaging time series via clustering and visualization. *Neuroimage* **22,** 1214–22 (2004).

21. Beckmann, C. F. & Smith, S. M. Probabilistic independent component analysis for functional magnetic resonance imaging. *IEEE Trans. Med. Imaging* **23,** 137–52 (2004).

22. Van Essen, D. C. Surface-based atlases of cerebellar cortex in the human, macaque,

and mouse. *Ann. N. Y. Acad. Sci.* **978,** 468–79 (2002).

23. Lewis, J. W. & Van Essen, D. C. Mapping of architectonic subdivisions in the macaque monkey, with emphasis on parieto-occipital cortex. *J. Comp. Neurol.* **428,** 79–111 (2000).

24. Van Essen, D. C. Cortical cartography and Caret software. *Neuroimage* **62,** 757–64 (2012).

25. Stephan, K. E. The history of CoCoMac. *Neuroimage* **80,** 46–52 (2013).

26. Sporns, O., Honey, C. J. & Kötter, R. Identification and classification of hubs in brain networks. *PLoS One* **2,** e1049 (2007).

27. Honey, C. J., Kötter, R., Breakspear, M. & Sporns, O. Network structure of cerebral cortex shapes functional connectivity on multiple time scales. *Proc. Natl. Acad. Sci. U. S. A.* **104,** 10240–5 (2007).

28. Azevedo, F. A. C. *et al.* Equal numbers of neuronal and nonneuronal cells make the human brain an isometrically scaled-up primate brain. *J. Comp. Neurol.* **513,** 532–41 (2009).

29. Petrides, M. & Pandya, D. N. Dorsolateral prefrontal cortex: comparative cytoarchitectonic analysis in the human and the macaque brain and corticocortical connection patterns. *Eur. J. Neurosci.* **11,** 1011–36 (1999).

30. Petrides, M. & Pandya, D. N. Comparative cytoarchitectonic analysis of the human and the macaque ventrolateral prefrontal cortex and corticocortical connection patterns in the monkey. *Eur. J. Neurosci.* **16,** 291–310 (2002).

31. Croxson, P. L. *et al.* Quantitative investigation of connections of the prefrontal cortex in the human and macaque using probabilistic diffusion tractography. *J. Neurosci.* **25,** 8854–66 (2005).

32. Kelly, C. *et al.* Broca's region: linking human brain functional connectivity data and non-human primate tracing anatomy studies. *Eur. J. Neurosci.* **32,** 383–98 (2010).

33. Rees, G., Friston, K. & Koch, C. A direct quantitative relationship between the functional properties of human and macaque V5. *Nat. Neurosci.* **3,** 716–23 (2000).

34. Koyama, M. *et al.* Functional Magnetic Resonance Imaging of Macaque Monkeys Performing Visually Guided Saccade Tasks. *Neuron* **41,** 795–807 (2004).

35. Petrides, M., Cadoret, G. & Mackey, S. Orofacial somatomotor responses in the macaque monkey homologue of Broca's area. *Nature* **435,** 1235–8 (2005).

36. Nakahara, K., Adachi, Y., Osada, T. & Miyashita, Y. Exploring the neural basis of cognition: multi-modal links between human fMRI and macaque neurophysiology. *Trends Cogn. Sci.* **11,** 84–92 (2007).

37. Friston, K. J., Frith, C. D. & Frackowiak, R. S. J. Time-dependent changes in effective connectivity measured with PET. *Hum. Brain Mapp.* **1,** 69–79 (1993).

38. Lee, L., Harrison, L. M. & Mechelli, A. A report of the functional connectivity workshop, Dusseldorf 2002. *Neuroimage* **19,** 457–65 (2003).

39. Fox, M. D. & Raichle, M. E. Spontaneous fluctuations in brain activity observed with functional magnetic resonance imaging. *Nat. Rev. Neurosci.* **8,** 700–11 (2007).

40. Biswal, B. B. Resting state fMRI: a personal history. *Neuroimage* **62,** 938–44 (2012).

41. Hipp, J. F., Hawellek, D. J., Corbetta, M., Siegel, M. & Engel, A. K. Large-scale cortical correlation structure of spontaneous oscillatory activity. *Nat. Neurosci.* **15,** 884–90 (2012).

42. Ogawa, S. *et al.* Intrinsic signal changes accompanying sensory stimulation: functional brain mapping with magnetic resonance imaging. *Proc. Natl. Acad. Sci. U. S. A.* **89,** 5951–5 (1992).

43. Raichle, M. E. A paradigm shift in functional brain imaging. *J. Neurosci.* **29,** 12729–34 (2009).

44. Noudoost, B., Chang, M. H., Steinmetz, N. A. & Moore, T. Top-down control of visual attention. *Curr. Opin. Neurobiol.* **20,** 183–90 (2010).

45. Petkov, C. I. *et al.* A voice region in the monkey brain. *Nat. Neurosci.* **11,** 367–74 (2008).

46. Kaas, J. H. The functional organization of somatosensory cortex in primates. *Ann.*

Anat. **175,** 509–18 (1993).

47. Dum, R. P. & Strick, P. L. Motor areas in the frontal lobe of the primate. *Physiol. Behav.* **77,** 677–82 (2002).

48. Raichle, M. E. *et al.* A default mode of brain function. *Proc. Natl. Acad. Sci. U. S. A.* **98,** 676–82 (2001).

49. Mantini, D. *et al.* Default Mode of Brain Function in Monkeys. *J. Neurosci.* **31,** 12954–12962 (2011).

50. Kumar, V. J., van Oort, E., Scheffler, K., Beckmann, C. F. & Grodd, W. Functional anatomy of the human thalamus at rest. *Neuroimage* **147,** 678–691 (2017).

51. Timmann, D. & Daum, I. Cerebellar contributions to cognitive functions: A progress report after two decades of research. *The Cerebellum* **6,** 159–162 (2007).

52. Bernard, J. A. *et al.* Resting state cortico-cerebellar functional connectivity networks: a comparison of anatomical and self-organizing map approaches. *Front. Neuroanat.* **6,** 31 (2012).

53. Packard, M. G. & Teather, L. A. Amygdala modulation of multiple memory systems: hippocampus and caudate-putamen. *Neurobiol. Learn. Mem.* **69,** 163–203 (1998).

54. Van Dijk, K. R. A., Sabuncu, M. R. & Buckner, R. L. The influence of head motion on intrinsic functional connectivity MRI. *Neuroimage* **59,** 431–438 (2012).

55. Barttfeld, P. *et al.* Signature of consciousness in the dynamics of resting-state brain activity. *Proc. Natl. Acad. Sci.* **112,** 201418031 (2015).

56. Cole, M. W., Bassett, D. S., Power, J. D., Braver, T. S. & Petersen, S. E. Intrinsic and Task-Evoked Network Architectures of the Human Brain. *Neuron* **83,** 238–251 (2014).

57. Logothetis, N. K. The neural basis of the blood-oxygen-level-dependent functional magnetic resonance imaging signal. *Philos. Trans. R. Soc. B Biol. Sci.* **357,** 1003–1037 (2002).

58. Moon, C.-H., Fukuda, M., Park, S.-H. & Kim, S.-G. Neural interpretation of blood oxygenation level-dependent fMRI maps at submillimeter columnar resolution. *J.*

Neurosci. **27,** 6892–902 (2007).

59. Kim, J. & Horwitz, B. Investigating the neural basis for fMRI-based functional connectivity in a blocked design: application to interregional correlations and psycho-physiological interactions. *Magn. Reson. Imaging* **26,** 583–93 (2008).

60. Schölvinck, M. L., Maier, A., Ye, F. Q., Duyn, J. H. & Leopold, D. A. Neural basis of global resting-state fMRI activity. *Proc. Natl. Acad. Sci. U. S. A.* **107,** 10238–43 (2010).

61. Maier, A., Adams, G. K., Aura, C. & Leopold, D. A. Distinct superficial and deep laminar domains of activity in the visual cortex during rest and stimulation. *Front. Syst. Neurosci.* **4,** (2010).

62. Arfanakis, K. *et al.* Combining independent component analysis and correlation analysis to probe interregional connectivity in fMRI task activation datasets. *Magn. Reson. Imaging* **18,** 921–30 (2000).

63. Fox, M. D., Snyder, A. Z., Zacks, J. M. & Raichle, M. E. Coherent spontaneous activity accounts for trial-to-trial variability in human evoked brain responses. *Nat. Neurosci.* **9,** 23–5 (2006).

64. Cole, M. W. *et al.* Multi-task connectivity reveals flexible hubs for adaptive task control. *Nat. Neurosci.* **16,** 1348–55 (2013).

65. Adachi, Y. *et al.* Functional connectivity between anatomically unconnected areas is shaped by collective network-level effects in the macaque cortex. *Cereb. Cortex* **22,** 1586–92 (2012).

66. Shen, K. *et al.* Information processing architecture of functionally defined clusters in the macaque cortex. *J. Neurosci.* **32,** 17465–76 (2012).

67. Barbas, H. & Pandya, D. N. Architecture and frontal cortical connections of the premotor cortex (area 6) in the rhesus monkey. *J. Comp. Neurol.* **256,** 211–28 (1987).

68. Preuss, T. M. & Goldman-Rakic, P. S. Myelo- and cytoarchitecture of the granular frontal cortex and surrounding regions in the strepsirhine primateGalago and the anthropoid primateMacaca. *J. Comp. Neurol.* **310,** 429–474 (1991).

69. Carmichael, S. T. & Price, J. L. Architectonic subdivision of the orbital and medial prefrontal cortex in the macaque monkey. *J. Comp. Neurol.* **346,** 366–402 (1994).

70. Hughes, S. W. *et al.* Synchronized oscillations at alpha and theta frequencies in the lateral geniculate nucleus. *Neuron* **42,** 253–68 (2004).

71. Hughes, S. W. & Crunelli, V. Thalamic mechanisms of EEG alpha rhythms and their pathological implications. *Neuroscientist* **11,** 357–72 (2005).

72. Lörincz, M. L., Crunelli, V. & Hughes, S. W. Cellular dynamics of cholinergically induced alpha (8-13 Hz) rhythms in sensory thalamic nuclei in vitro. *J. Neurosci.* **28,** 660–71 (2008).

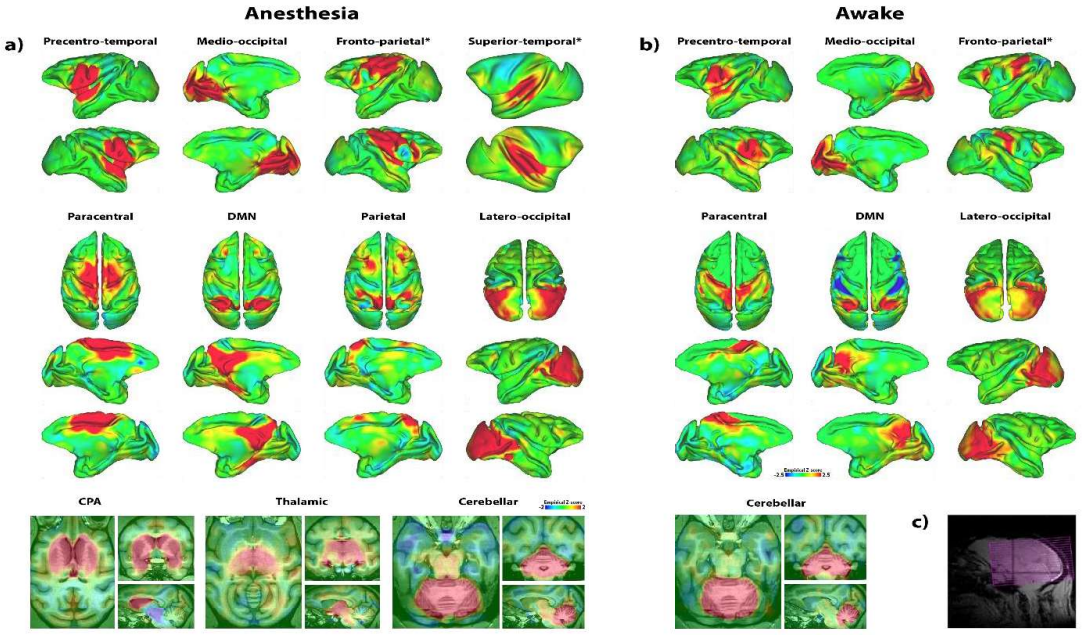

Figure 1. Resting-state networks. We collected BOLD-fMRI data of two macaque monkey brains (*Macaca mulatta*) while they were anesthetized or awake. The animals were scanned in complete darkness, devoid of any kind of experimental stimulation. Scanner noise was attenuated with earplugs and foam pillows. Anesthesia experiments were performed at a 7 T vertical Bruker scanner while awake datasets were collected at a 4.7 T vertical Bruker scanner. Data preprocessing consisted of despiking, slice timing correction, motion correction (6 parameters affine transformation), spatial smoothing (3 mm FWHM Gaussian kernel), bandpass filtering within 0.01 and 0.1 Hz, removal of motion artifacts and removal of white matter and CSF activity. Thereafter, RSNs were isolated using spatial ICA with 20 components imposed a priori. Resulting RSNs were clustered session by session based on similar spatial correlations. For that, we used a custom-written unsupervised network classifier. Finally, clusters containing similar networks were averaged. Color scale represents empirical Z-scores, a measure of similarity between the timecourse of each voxel with the timecourse of the related independent component. A) In the anesthetized condition, we consistently observed 11 networks, namely the precentro-temporal, medio-occipital, fronto-parietal, superior-temporal, paracentral, default-mode (DMN), parietal, latero-occipital, CPA, thalamic and cerebellar networks. The CPA network is reported here for the first time. It encompasses mainly the caudate, putamen and amygdala. B) In the awake condition, we identified all the aforementioned networks but 4 of them: the parietal, superior-temporal thalamic and CPA networks. C) Partial brain acquisition in our awake experiments could be one of the reasons for the decreased amount of networks observed in this condition.

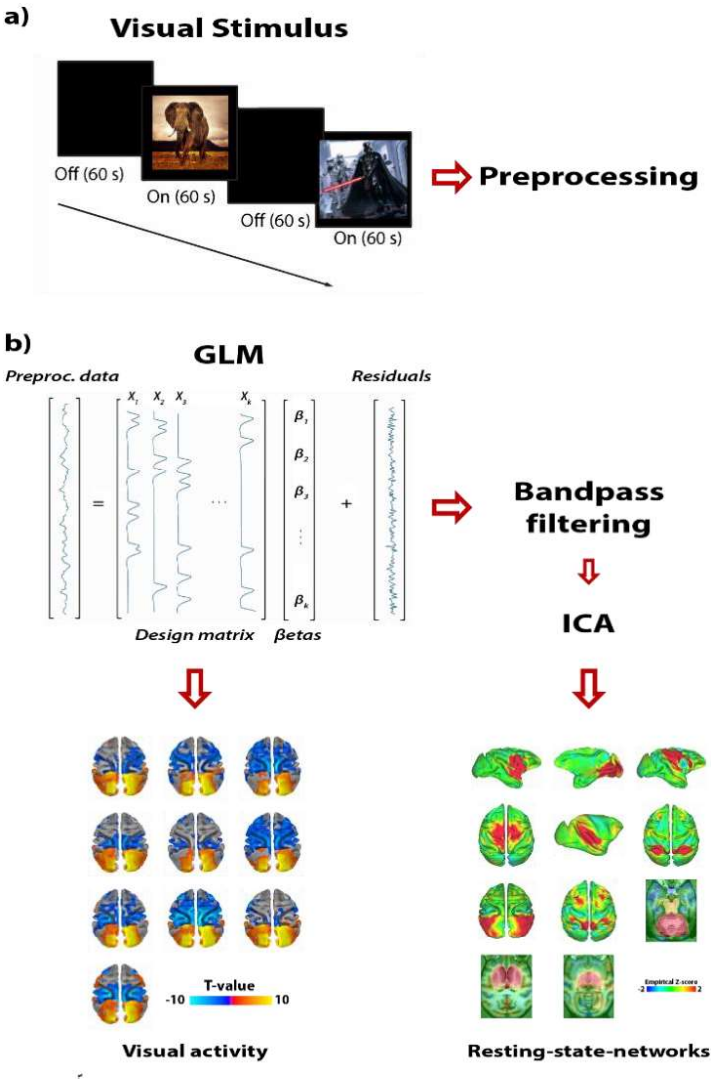

Figure 2. Intrinsic and visually-evoked functional architectures during visual stimulation. A) In addition to our resting-state condition, we scanned the same animals while presenting a 1-min block design of visual stimuli. In this paradigm, naturalistic movie clips (Star Wars or African Savanna) were interleaved with a blank background for periods of 60 seconds. Preprocessing was done in a similar way to the resting-sate pipeline, except for bandpass filtering, left to a later stage. B) Only runs showing significant visual activity according to a GLM analysis were selected for further processing. After regressing out the variance in the BOLD signal which was explained the GLM, the residual data were bandpass-filtered within 0.01 and 0.1 Hz, and decomposed with spatial ICA in 20 maximally independent networks. Resulting networks were clustered and averaged.

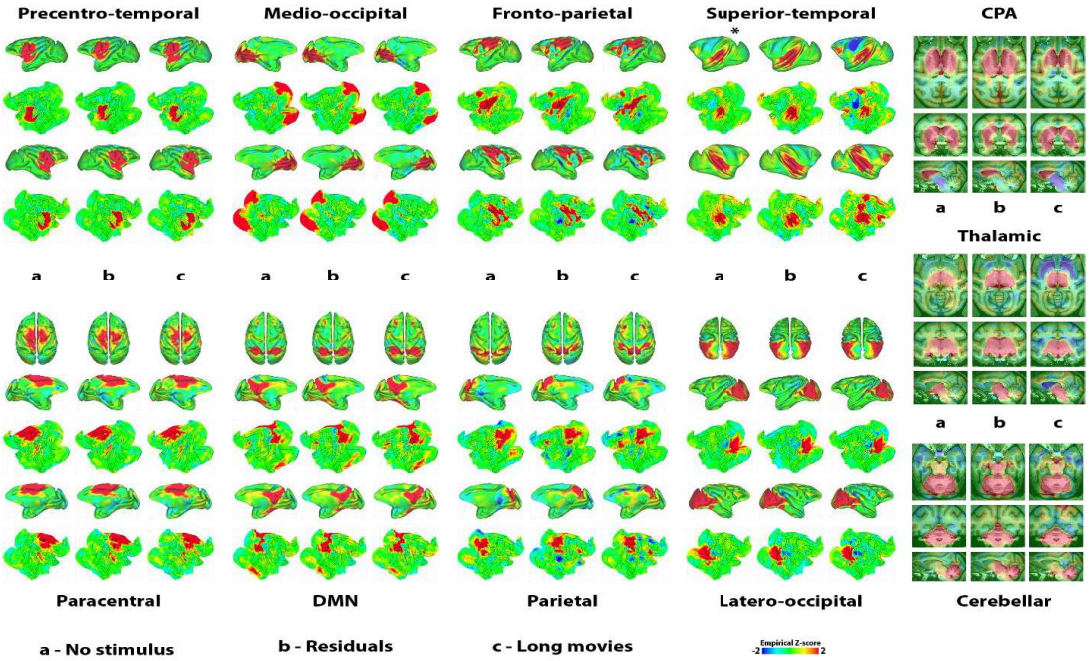

Figure 3. Intrinsic networks across conditions in the anesthesia datasets. Session-averaged RSNs obtained during anesthesia for all conditions of visual stimulation. a) no visual stimulation, b) Residuals of the visual block-design, c) continuous movies. In the anesthesia datasets, all 11 RSNs (precentro-temporal, medio-occipital, fronto-parietal, superior-temporal, paracentral, DMN, parietal, latero-occipital, CPA, thalamic and cerebellar networks) could be observed also in the residuals of the extrinsic architecture.

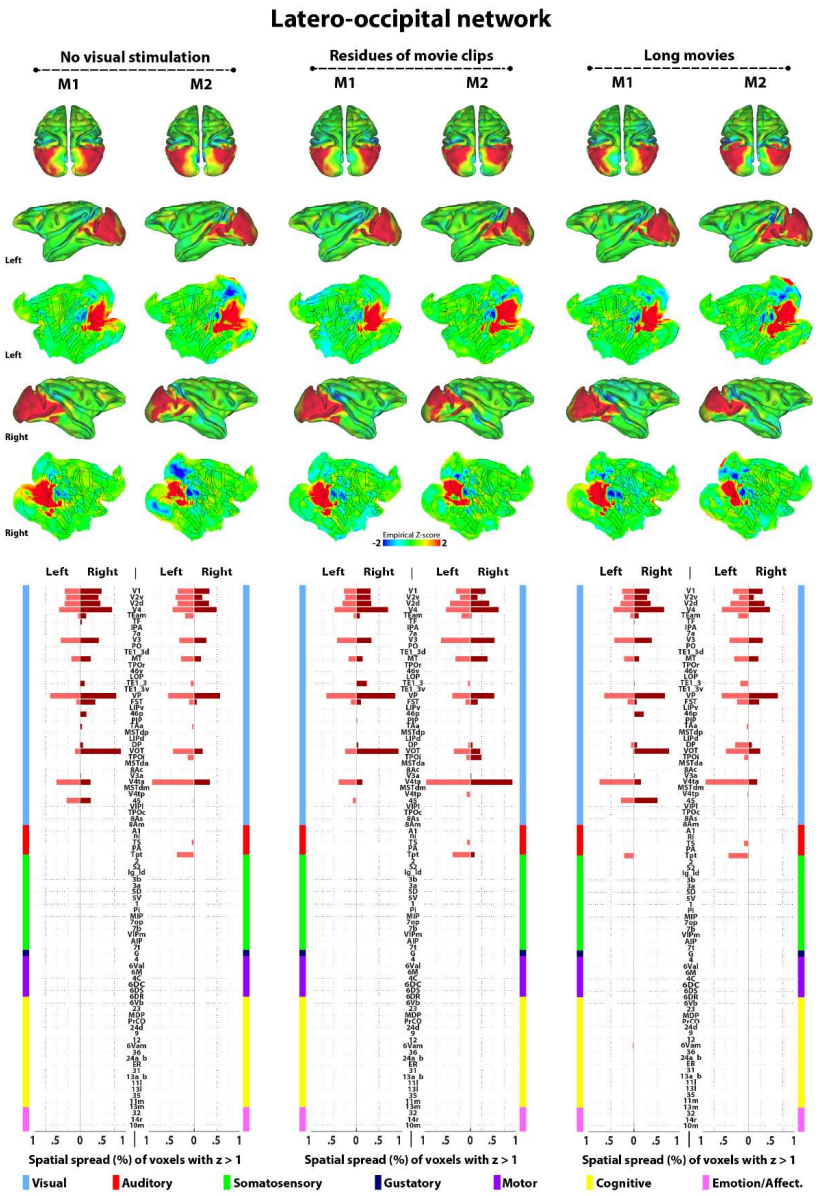

Figure 4. Detailed quantification of latero-occipital network obtained in the anesthesia condition. Here we display a thorough analysis of the latero-occipital network acquired in anesthetized experiments across-subjects and experimental conditions. In the left pair of columns, the data corresponds to the condition where no visual stimulation was performed. The middle pair of columns shows the results extracted from the residues of the alternated block-design. Finally, the last two pair of columns display the results obtained for the continuous visual stimulation. M1 = monkey 1 and M2 = monkey 2. As in figure 1, Color scale represents empirical Z-scores. Every cortical network was quantified based on the Lewis and Van Essen cortical parcellation scheme (LVE00, Fig. S1) and grouped according to functional modalities (color coded, Fig. S2). After statistical analyses session-specific BOLD data was spatially normalized to the F99 atlas using a three-step spatial normalization pipeline (Fig. S3). The bar graphs display the percentage of each ROI occupied by voxels containing an average empirical z-score greater than 1. Light red corresponds to the left hemisphere and dark red refers to the right hemisphere. Similar quantifications done for each cortical network can be found in the supplementary material.

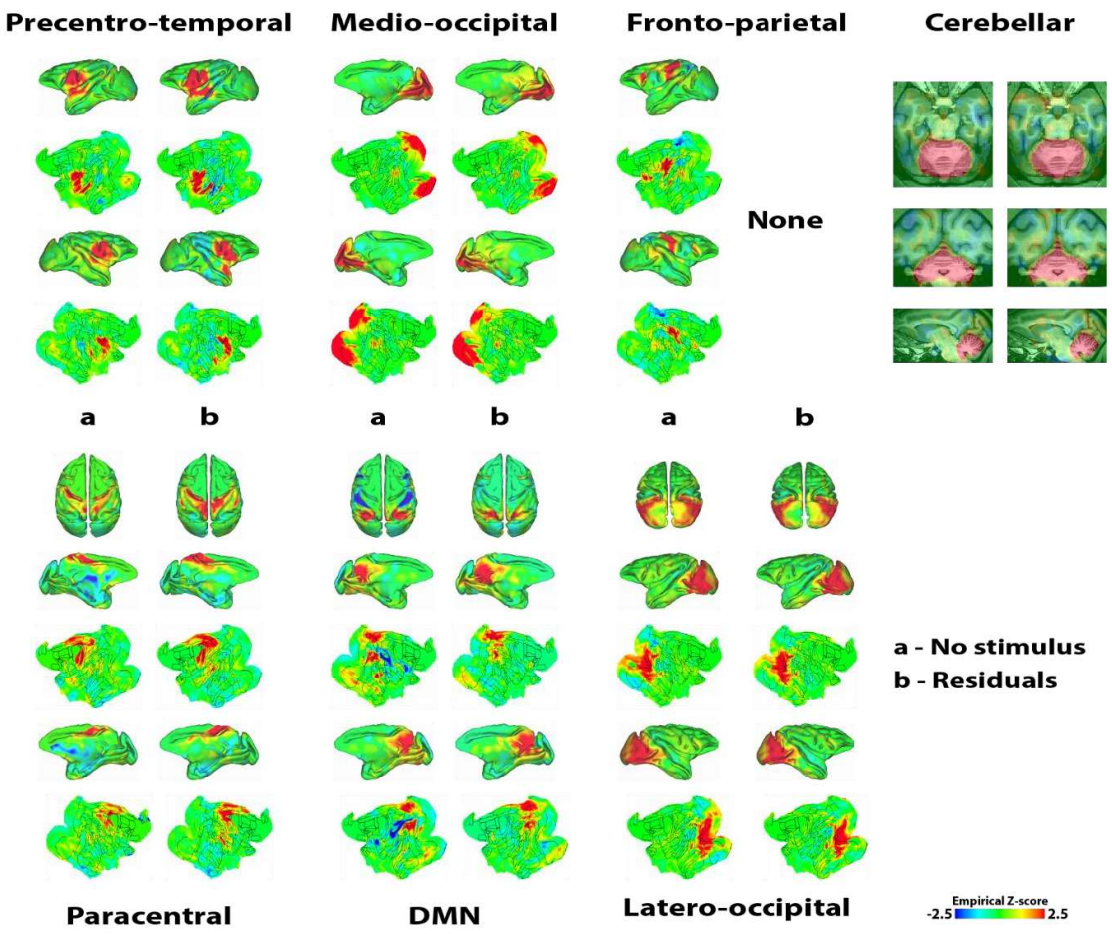

Figure 5. Intrinsic networks across conditions in awake datasets. Session-averaged RSNs obtained during the awake state for all conditions of visual stimulation. a) no visual stimulation, b) Residuals of the visual block-design. In our findings, the only network that couldn't be observed in the residuals of the block design for the awake state was the fronto-parietal network. Since this network is thought to be composed of flexible hubs that dynamically update their pattern of functional connectivity according to task/stimulus demands [64], region-specific shifts of functionality due to the rich visual stimulus could have disrupted the global coherence of this network.

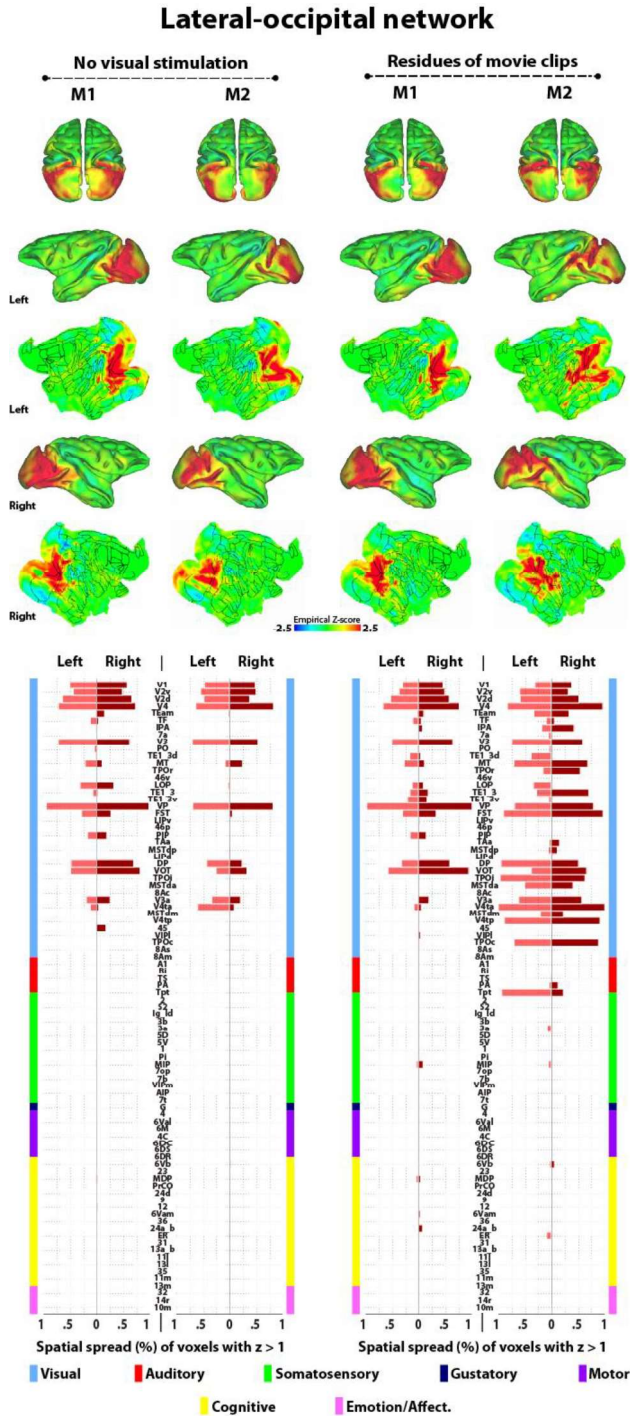

Figure 6. Latero-occipital network in awake experiments. We used the same parameters described in fig. 4 to quantify networks in the alert state. The left pair of columns corresponds to latero-occipital network in the absence of any stimulus, while the right pair of columns displays the same network contained in the residues of the alternated block-design. A similar description of the other networks can be found in the supplementary material.

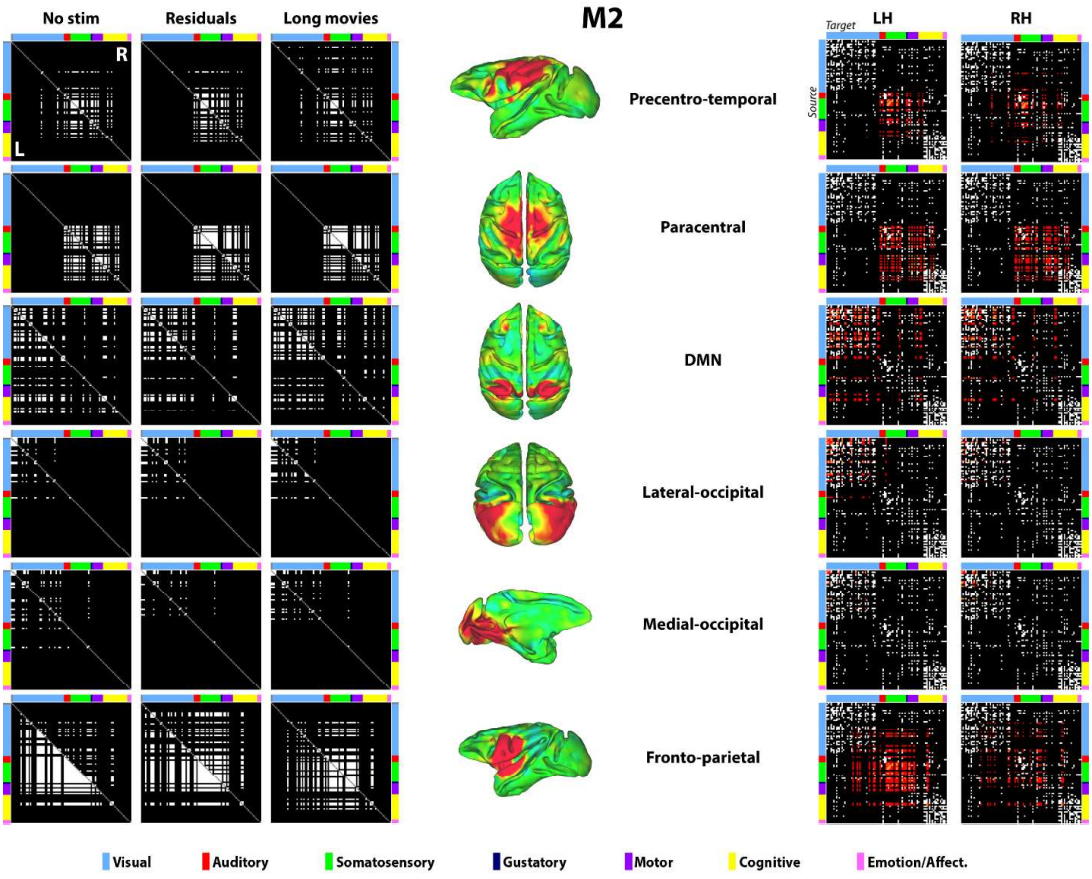

Figure 7. Left) Laterality of the functional networks in the anesthesia. Binarized functional connectivity matrices for each cortical functional network across conditions for monkey 2 (M2). Inclusion criteria was regions where at least 15% of voxels presented empirical z-score equal or above 1 (Figs. S5-S11). Lower triangular matrix represents the left hemisphere (L) while upper triangular matrix represents right hemisphere. White color means existence of interareal functional connectivity. In order to preserve the diagonals of both hemispheres separated, both matrices were shifted laterally and are separated by a diagonal gray line. In general, networks tended to be bilaterally symmetric. **Right) Structural vs functional connectivity.** Comparison between structural and functional connectivity per hemisphere for M2. White represent known monosynaptic connectivity and red represent functional connectivity of each cortical network common across conditions. Notice that the red color inside the matrices represent across-

SUPPLEMENTARY FIGURES

LVE00 cortical parcellation scheme

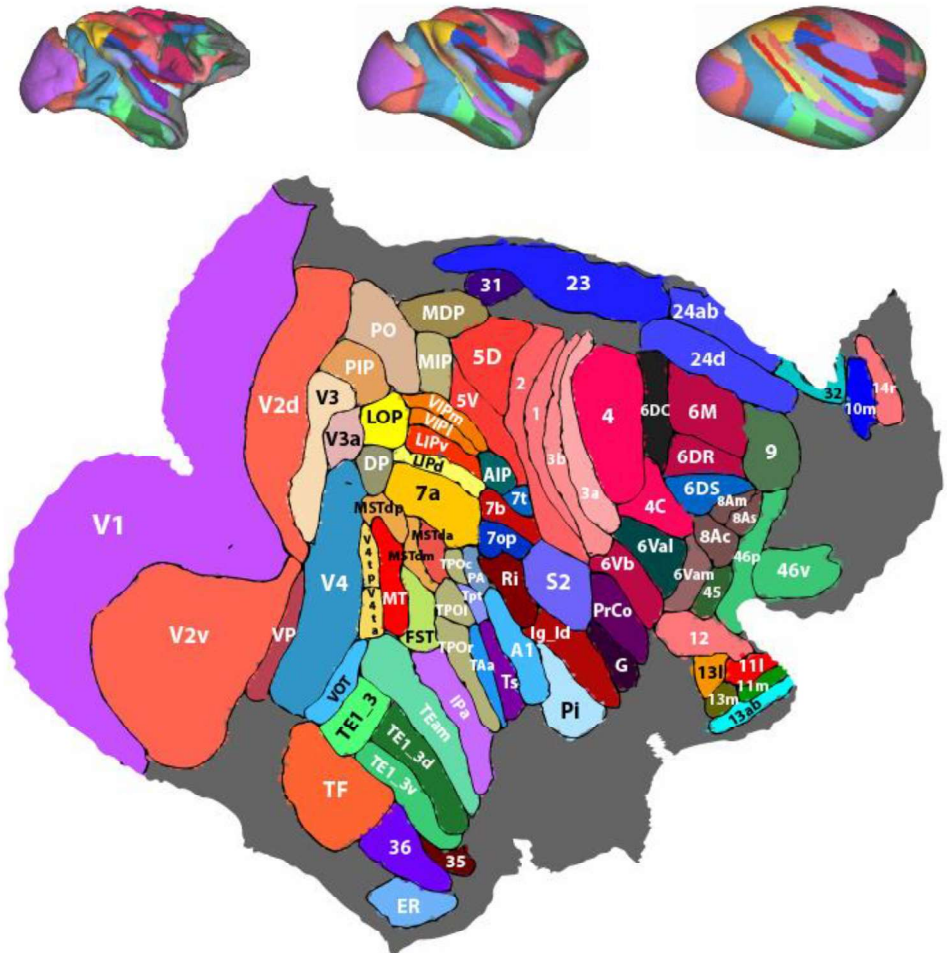

Figure S1. Right hemisphere of the F99 macaque atlas overlaid with the LVE00 cortical parcellation scheme [24] shown in four different configurations: fiducial, inflated, very inflated and flat surfaces (clockwise, starting at top-left surface). A total of 88 cortical areas are mapped. Abbreviations: **1, 2** somatosensory areas 1 and 2; **3a, 3b** subdivisions of somatosensory area 3; **4** primary motor cortex; **4C** area 4C [67]; **5D, 5V** subdivisions of somatosensory area 5 (dorsal, ventral); **6DC, 6DR, 6DS** subdivisions of area 6D; 6M area 6M; **6Val, 6Vam** subdivisions of area 6Va (lateral, medial); **6Vb** subdivision of area 6V; **7a** visual area 7a; **7b** somatosensory area 7b; **7op** operculator area 7; 7t subdivision of area 7 (near tip of IPS); 8Ac, 8Am, 8As subdivisions of Walker area 8A [68]; **9, 12** areas 9 and 12 [69]; **10m, 11l, 11m, 13ab, 13l, 13m, 14r** subdivisions of area 10, 11, 13 and 14 [69]; **23, 32** cingulate areas 23 and 32; **24ab, 24d** subdivisions of cingulate area 24; **31** intraparietal area 31; **35, 36** perirhinal areas 35 and 36; **45** Walker area 45; **46p, 46v** subdivisions of area 46 (posterior, ventral); **A1** primary auditory cortex; **AIP** anterior intraparietal area; **DP** dorsal prelunate area; **ER** entorhinal cortex; **FST** floor of superior temporal area; **G** gustatory cortex**; Ig_Id** granular plus dysgranular insular cortex; **IPa** area Ipa (Cusick et al. 1995); **LIPd, LIPv** subdivisions of lateral intraparietal area (dorsal, ventral); **LOP** lateral occipital parietal; **MDP** medial dorsal parietal area; **MIP** medial intraparietal area; **MSTda, MSTdm, MSTdp** subdivisions of dorsomedial superior temporal area (anterior, medial, posterior); **MT** middle temporal area; **PA** posterior area of superior temporal gyrus; **Pi** parainsular area; **PIP** posterior intraparietal area; **PO** parietal-occipital area; **PrCO** precentral opercular cortex; **Ri** retroinsula; **S2** somatosensory area 2 (ventral); **TAa** area TAa (Cusick et al. 1995); **TE1_3** subdivisions TE1, TE2, and TE3 (Seltzer & Pandya 1978); **TE1_3d, TE1_3v** subdivisions of TE1, TE2, plus TE3 (dorsal, ventral); **TEam** area TEa plus TEm (Seltzer & Pandya 1978); **TF** temporal area F; **TPOc, TPOi, TPOr** subdivisions of temporal parietal occipital (caudal, intermediate, rostral); **Tpt** temporoparietal area; **Ts** superior temporal gyrus (anterior); **V1, V2d, V2v, V3, V3A, V4, V4ta, V4tp** visual areas 1, 2 (dorsal), 2 (ventral), 3, V3A, 4, 4 (anterior transitional area) and 4 (posterior transitional area); **VIPl, VIPm** subdivisions of ventral intraparietal (lateral, medial); **VOT** ventral occipitotemporal area; **VP** ventral posterior area. Unless otherwise cited, ROIs are based on this cortical parcellation scheme.

Parcellation of functional modalities

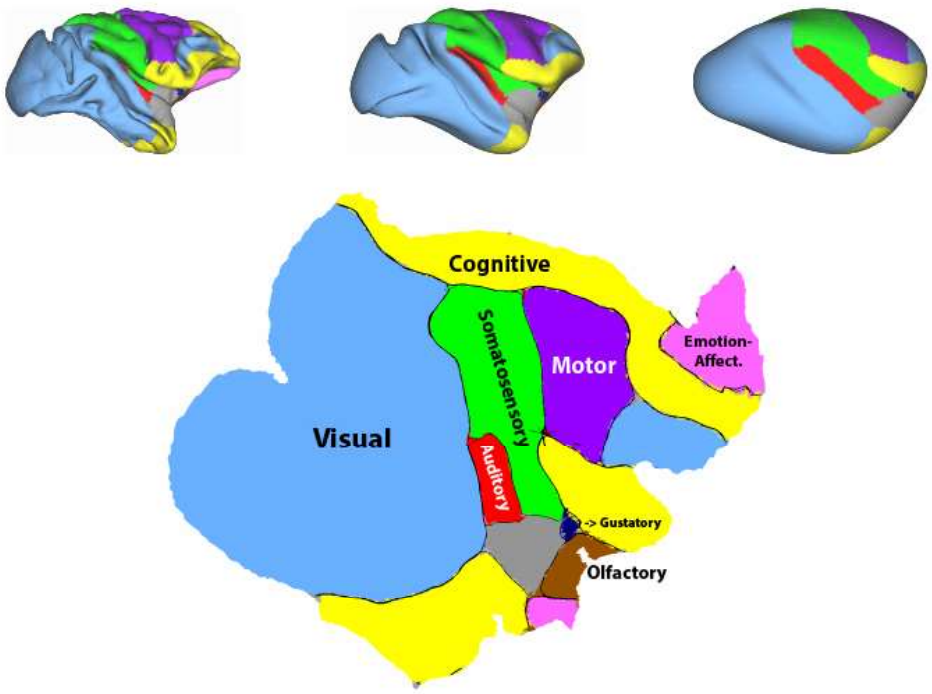

	Modality	ROIs	# ROIs
	Visual	V1, V2v, V2d, V3, V3a, V4, V4ta, V4tp, MT, MSTdm, MSTdp, MSTda, FST, PO, PIP, LOP, LIPv, LIPd, TPOI, TPOc, TPOr, TAa, IPA, VP, VIPl, VOT, TEam, TE1_3, TE1_3d, TE1_3V, TF, DP, 7a, 8Am, 8As, 8Ac, 45, 46p, 46v	39
	Auditory	PA, Ts, A1, RI, Tpt	5
	Somatosensory	1, 2, 3a, 3b, 5V, 5D, 7b, 7op, 7t, MIP, VIPm, AIP, Ig_Id, PI, S2	15
	Gustatory	G	1
	Motor	4, 4C, 6M, 6DR, 6DS, 6DC, 6Val	7
	Cognitive	6Vam, 6Vb, 9, 11l, 11m, 12, 13ab, 13l, 13m, 23, 24ab, 24d, 31, 35, 36, MDP, ER, PrCO	18
	Emotion/Affect.	10m, 14r, 32	3

Figure S2. Fiducial, inflated, very inflated and flat configurations for the right hemisphere of the F99 macaque atlas parcellated into 7 distinct functional modalities [24]. Corresponding cortical areas are listed in the table at the bottom. Functional modalities are accordingly color-coded throughout the figure.

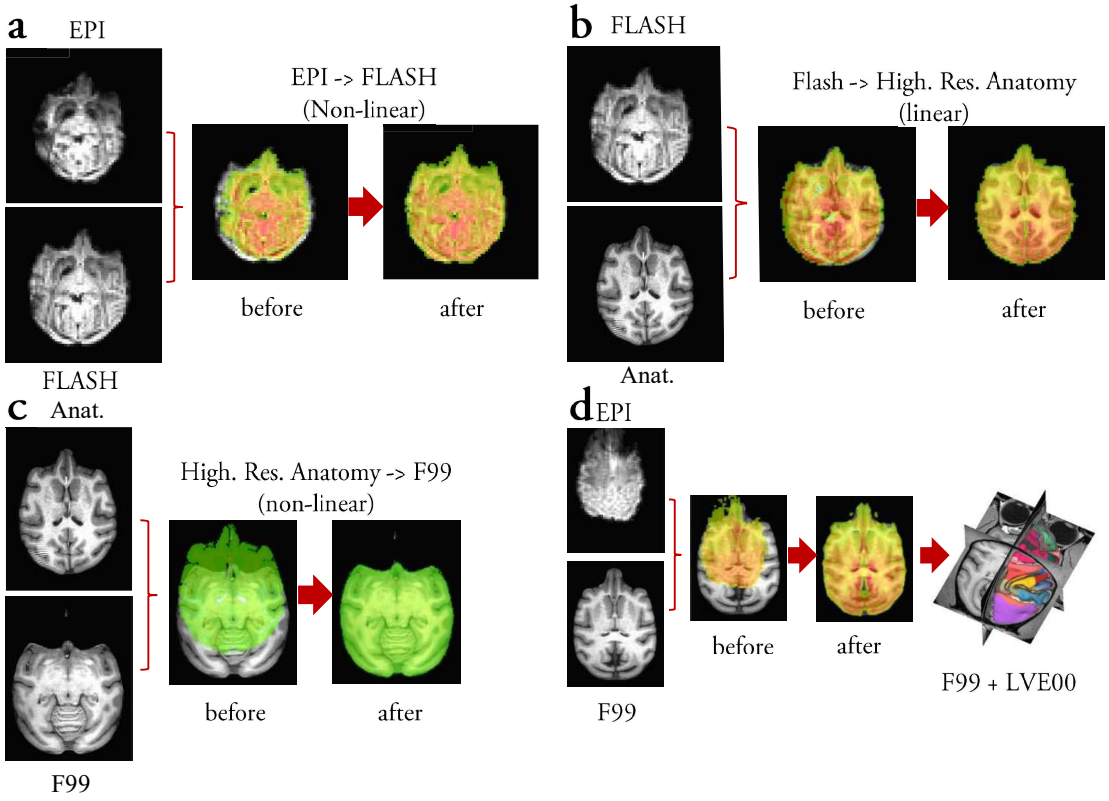

Figure S3. Three-steps spatial normalization of GE-EPI's to F99 atlas. A) Non-linear alignment of an average GE-EPI to the FLASH image. The FLASH image was collected in every session using the same resolution and field of view of the GE-EPI. Since the FLASH scan presents less distortions than the GE-EPI sequence, it's used as a low-resolution anatomical reference for the first spatial normalization of functional images. In the right side, the superposition of both images before and after alignment are portrayed. B) Linear alignment of the FLASH image to the MDEFT, a high resolution anatomical reference of our monkeys' brains. The MDEFT of each monkey was collected before the functional experiments started. C) Non-linear alignment of our MDEFT's with the F99 atlas. Since the MRI sequence parameters of the MDEFT's of our monkeys and F99's MDEFT were similar, non-linear transformation performed by AFNI was very accurate. D) For each of the previous procedures, we obtained a transformation or warp matrix separately. After our statistical analysis were performed in the non-normalized data, we applied those 3 normalization matrices to our results accordingly. By doing so, we were able to align the results obtained across sessions and subjects onto the F99 atlas and to compare them directly.

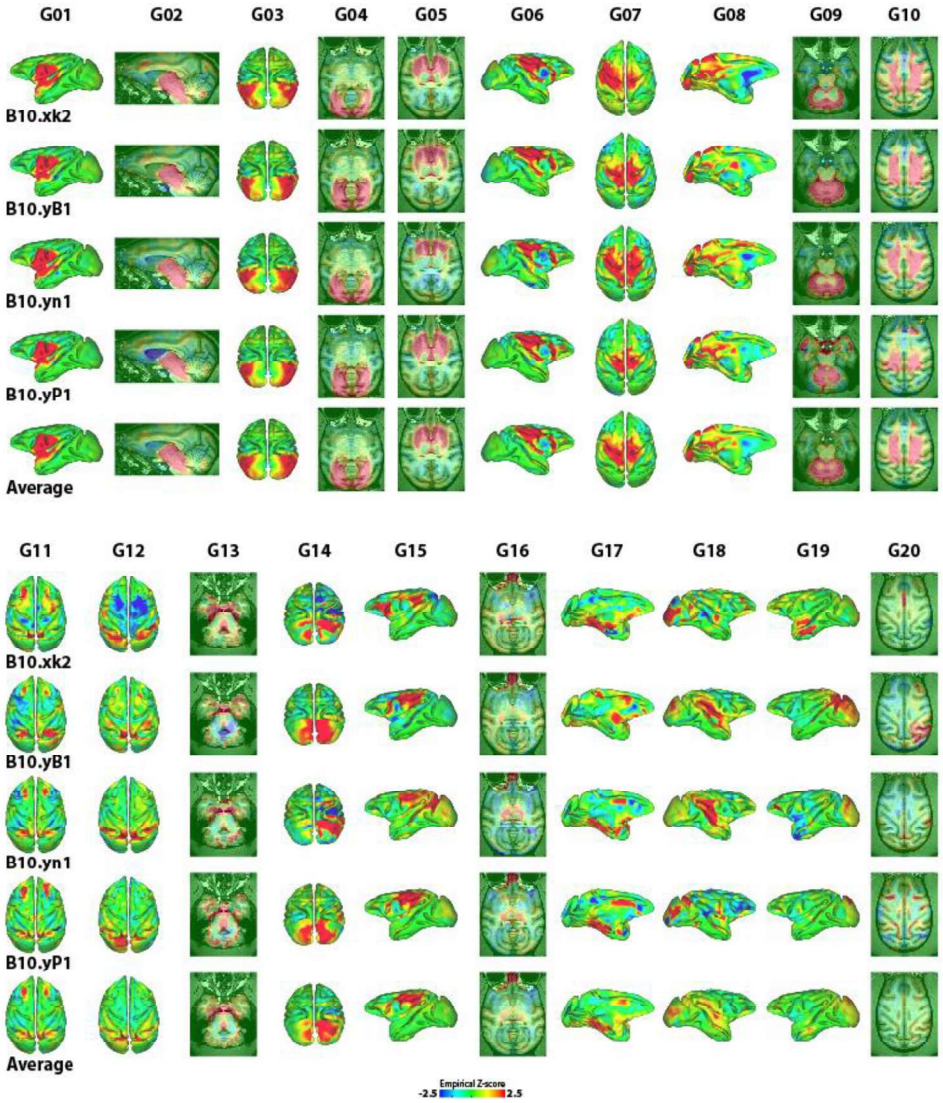

Figure S4. Groups of independent components automatically clustered by our custom-written unsupervised network classifier. In this example, four different resting-state sessions of monkey 1 (M1) were analyzed. Groups are displayed column-wise and are numbered from G01 to G20. Sessions are displayed row-wise (B10.xk2, B10.yB1, B10.yn1, and B10.yP1). Last rows of top and bottom groups show the averages of all four individual components portrayed above them. Note that in this example, functional correlations located in the white-matter and CSF weren't previously removed from the datasets. Color scale represents empirical Z-scores outputted by GIFT software, which is a measure of similarity between the timecourse of each voxel with the timecourse of the related independent component.

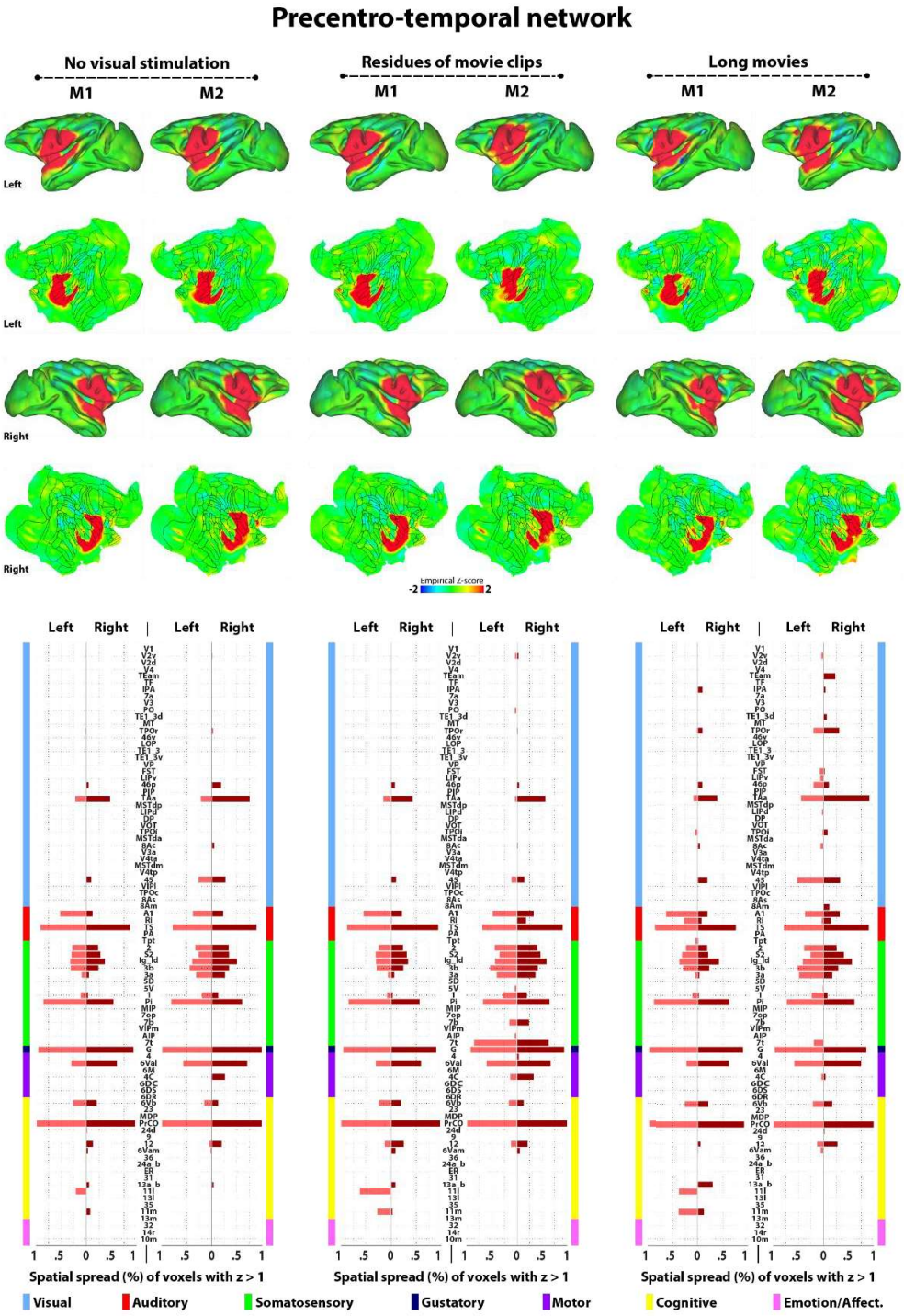

Figure S5. Precentro-temporal network (anesthesia).

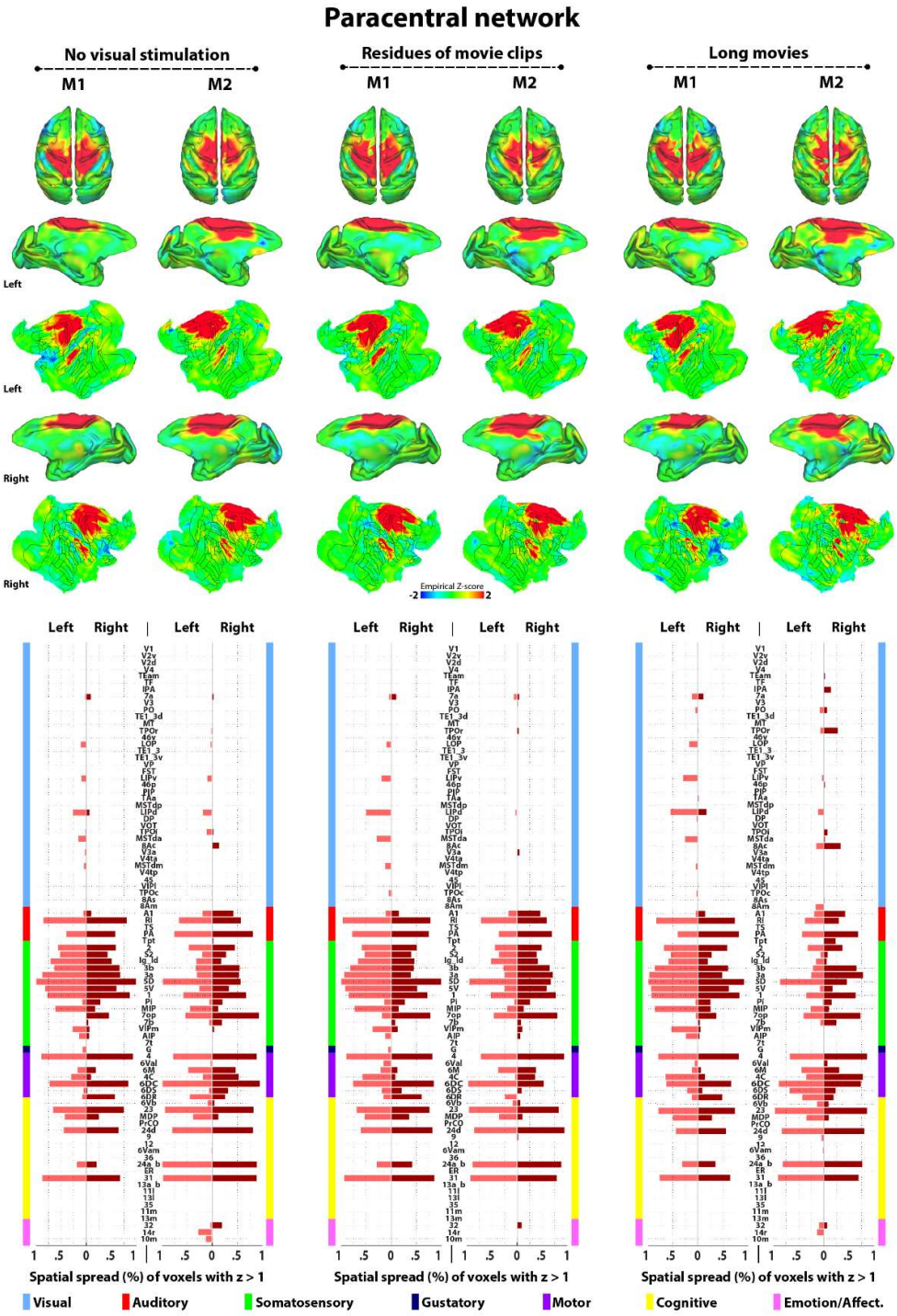

Figure S6. Paracentral network (anesthesia).

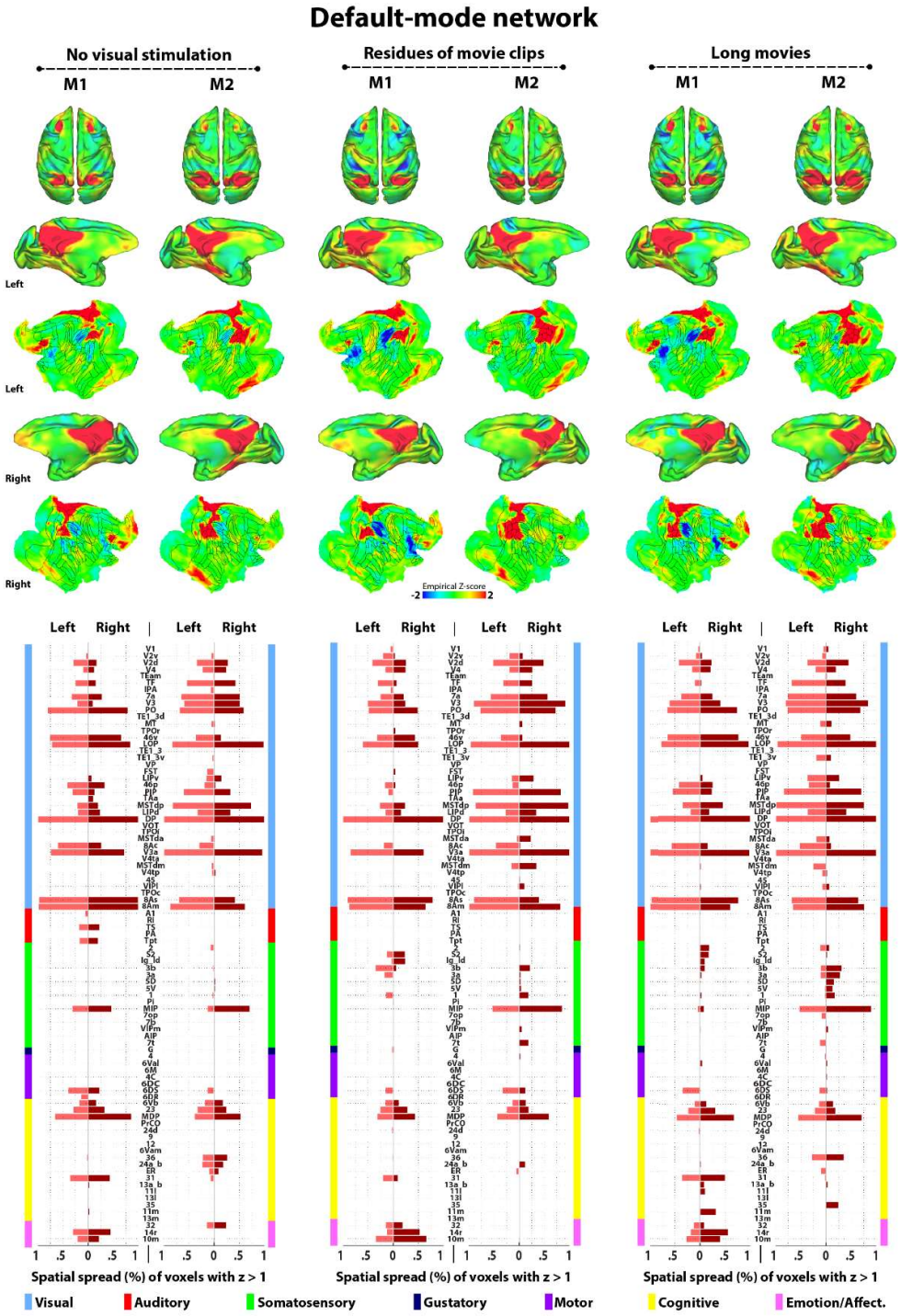

Figure S7. Default-mode network (anesthesia).

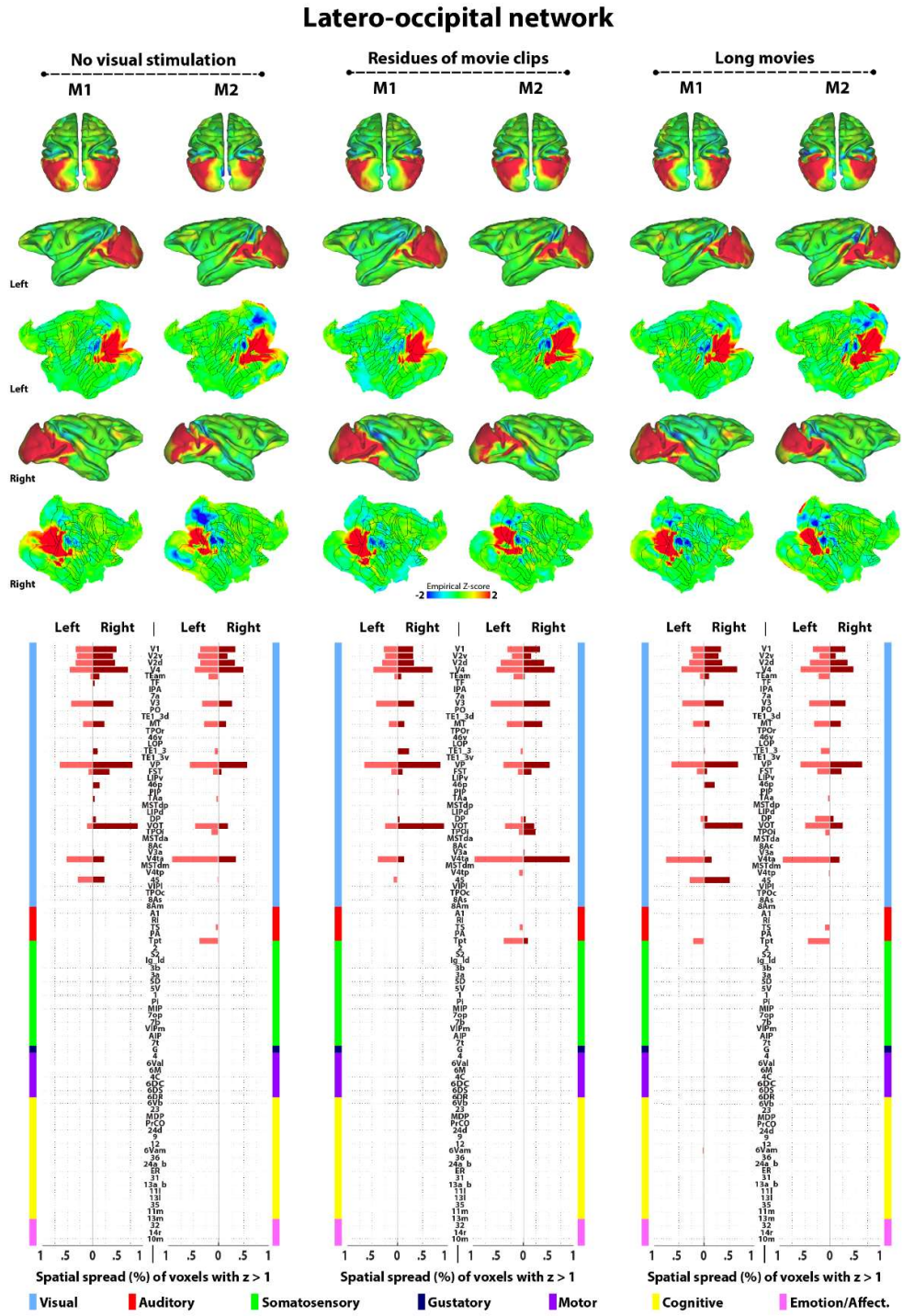

Figure S8. Latero-occipital network (anesthesia).

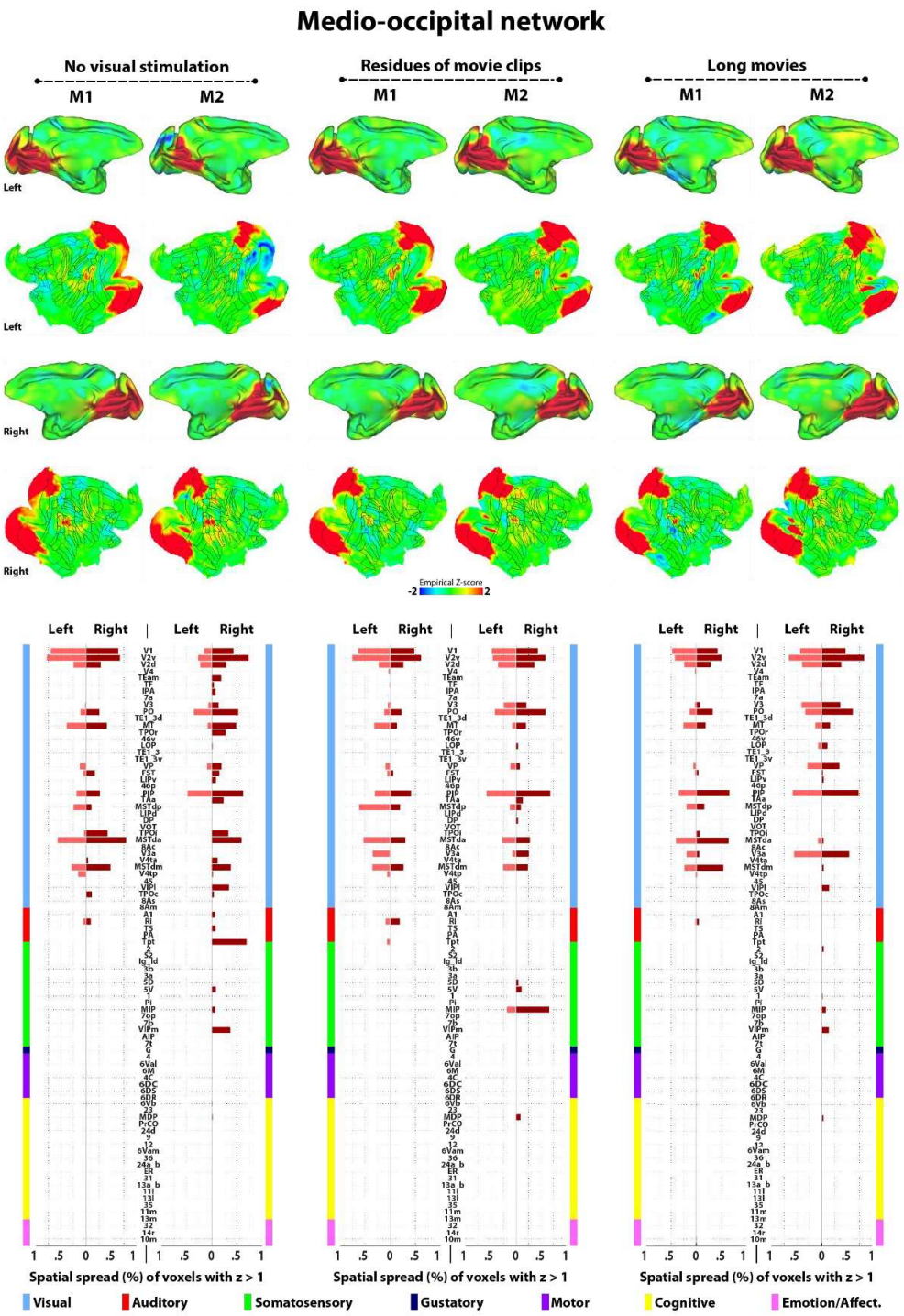

Figure S9. Medio-occipital network (anesthesia).

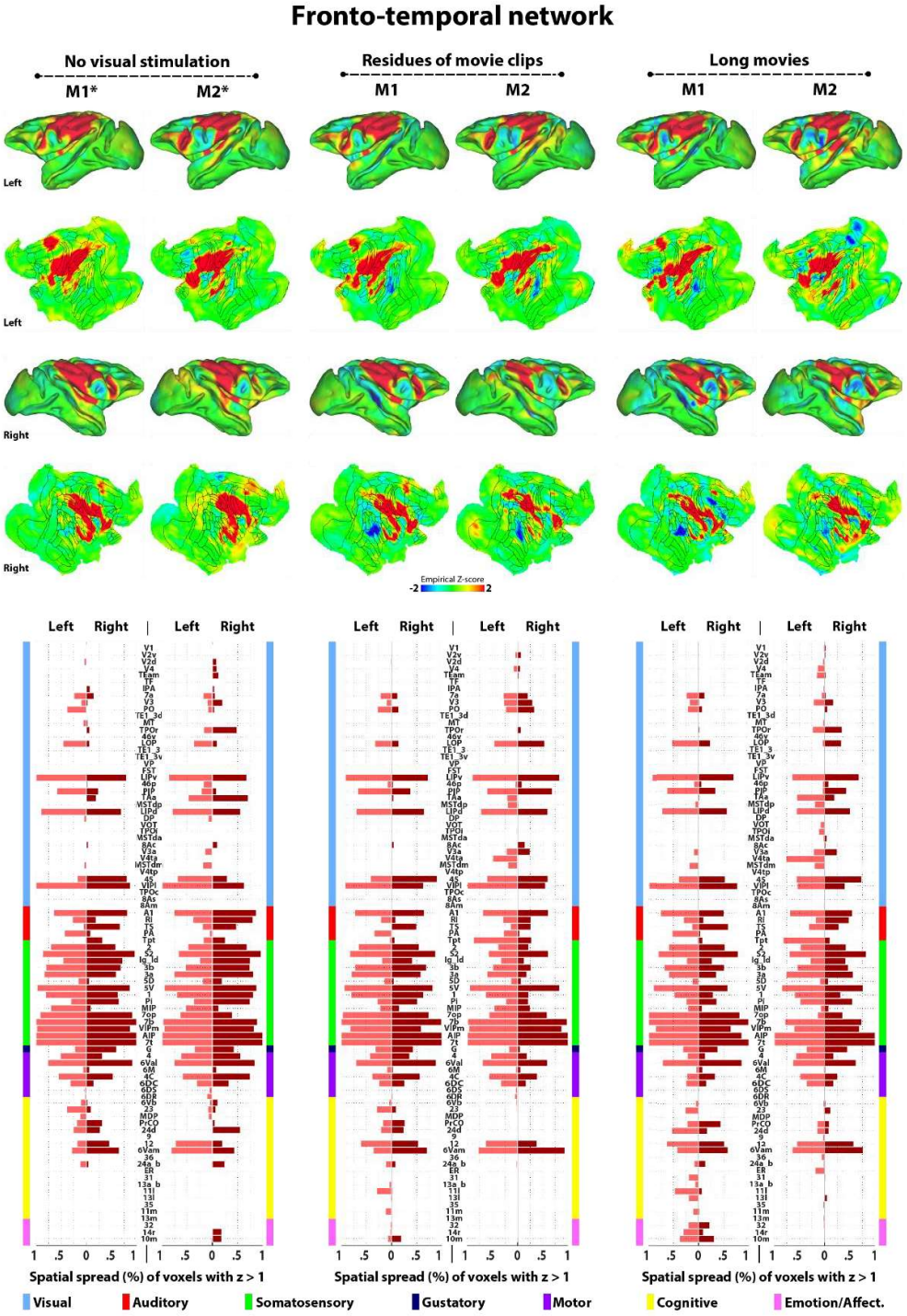

Figure S10. Fronto-temporal network (anesthesia).

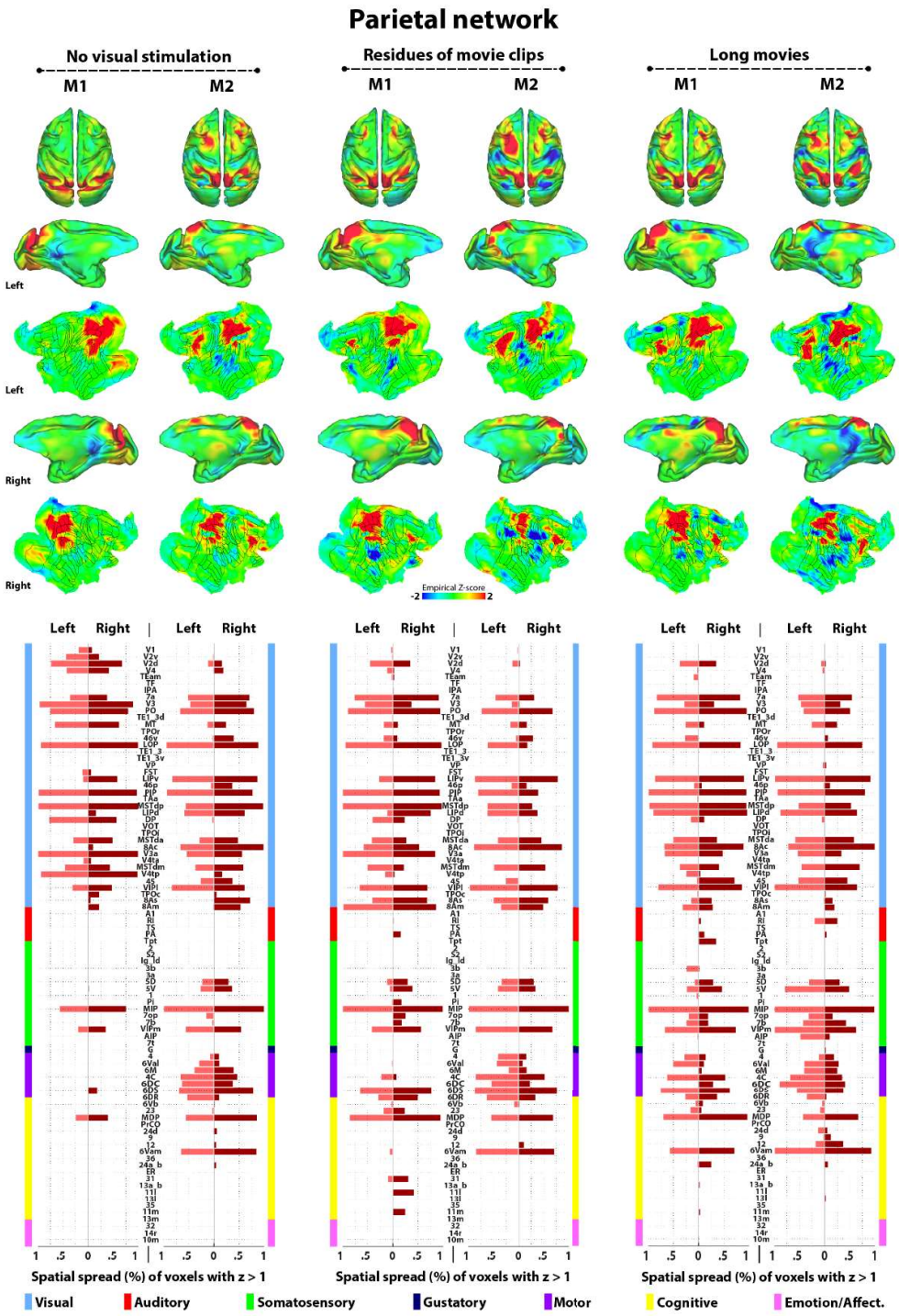

Figure S11. Parietal network (anesthesia).

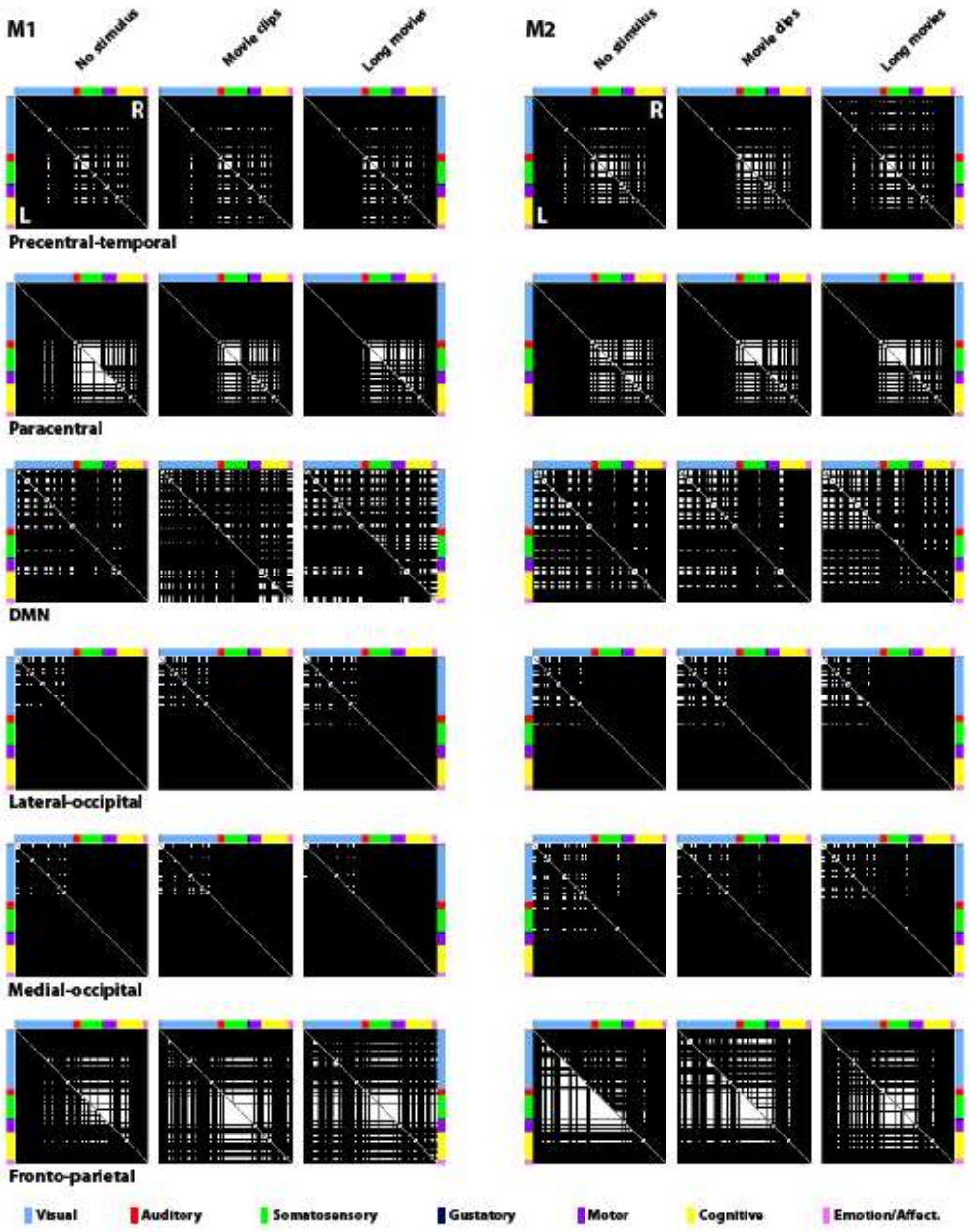

Figure S12. Anesthesia datasets. Binarized functional connectivity matrices for each cortical functional network across subjects and conditions. Inclusion criteria was regions where at least 15% of voxels presented empirical z-score equal or above 1 (Figs. S5-S11). Lower triangular matrix represents the left hemisphere (L) while upper triangular matrix represents right hemisphere. White color means existence of interareal functional connectivity. In order to preserve the diagonals of both hemispheres separated, both matrices were shifted laterally and are separated by a diagonal gray line.

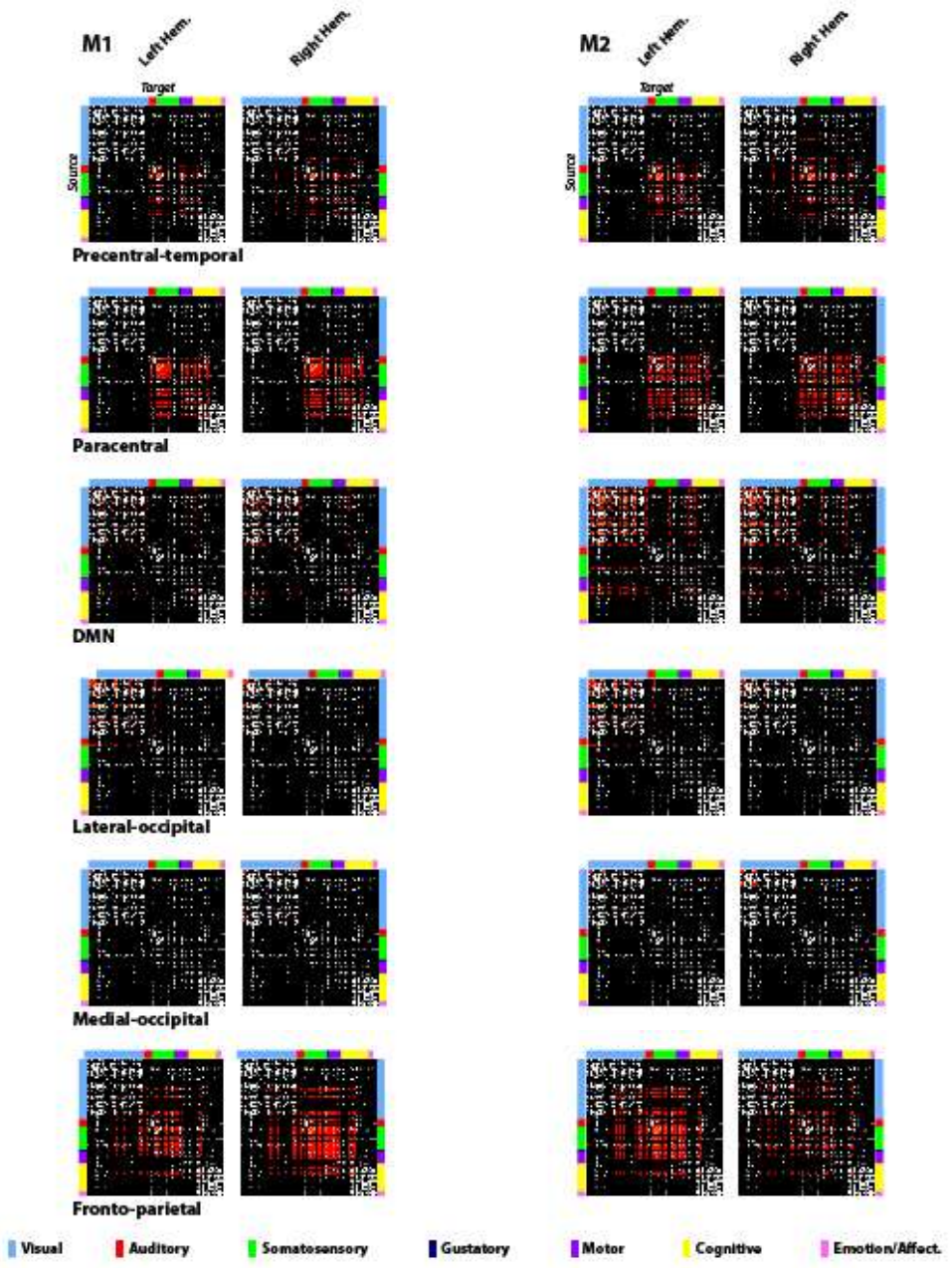

Figure S13. Anesthesia datasets. Comparison between structural and functional connectivity per hemisphere for both monkeys. White represent known monosynaptic connectivity and red represent functional connectivity of each cortical network common across conditions. Notice that the red color inside the matrices represent across-condition functional connectivity derived from fig. S10 and isn't related to the red component of the colorbars representing auditory modality. Cosine similarities of the intersection of structural and functional matrices can be found in table S2.

Table S1: Anesthesia datasets. ***Pairwise spatial correlations among consistent components (rows) across conditions. SI is a similarity index based in root-mean-square of row-wise spatial correlations outputted by our custom-written unsupervised network classifier.***

M1	**Resting-state vs Block design**	**Resting-state vs Long movies**	**Block design vs Long movies**	**SI**
Precentral-temporal	0.91	0.86	0.82	0.8630
Medial-occipital	0.79	0.78	0.81	0.7951
Fronto-parietal	0.71	0.70	0.68	0.6966
Paracentral	0.82	0.65	0.65	0.7117
DMN	0.5	0.68	0.54	0.5759
Lateral-occipital	0.89	0.88	0.86	0.8750
CPA	0.77	0.82	0.8	0.7959
Cerebellar	0.79	0.35	0.47	0.5694
M2				**SI**
Precentral-temporal	0.89	0.81	0.75	0.8187
Medial-occipital	0.81	0.71	0.8	0.7736
Fronto-parietal	0.74	0.65	0.61	0.6703
Paracentral	0.85	0.81	0.74	0.7997
DMN	0.82	0.74	0.79	0.7835
Lateral-occipital	0.8	0.75	0.74	0.7649
CPA	0.38	0.72	0.36	0.5125
Cerebellar	0.79	0.82	0.72	0.7775

Table S2: Anesthesia datasets. ***Cosine similarity values of the intersection of functional and structural connectivity matrices for each hemisphere of each monkey. Functional connectivity partially follows monosynaptic connectivity [65,66]. Visually related functional networks, namely medial-occipital and lateral-occipital, present greatest correspondence with underlying direct anatomical connectivity.***

M1	**Left Hemisphere**	**Right Hemisphere**
Precentral-temporal	0.34	0.32
Medial-occipital	0.47	0.47
Fronto-parietal	0.34	0.32
Paracentral	0.38	0.39
DMN	0.44	0.39
Lateral-occipital	0.65	0.57
M2		
Precentral-temporal	0.36	0.38
Medial-occipital	0.60	0.74
Fronto-parietal	0.33	0.30
Paracentral	0.38	0.37
DMN	0.42	0.46
Lateral-occipital	0.54	0.61

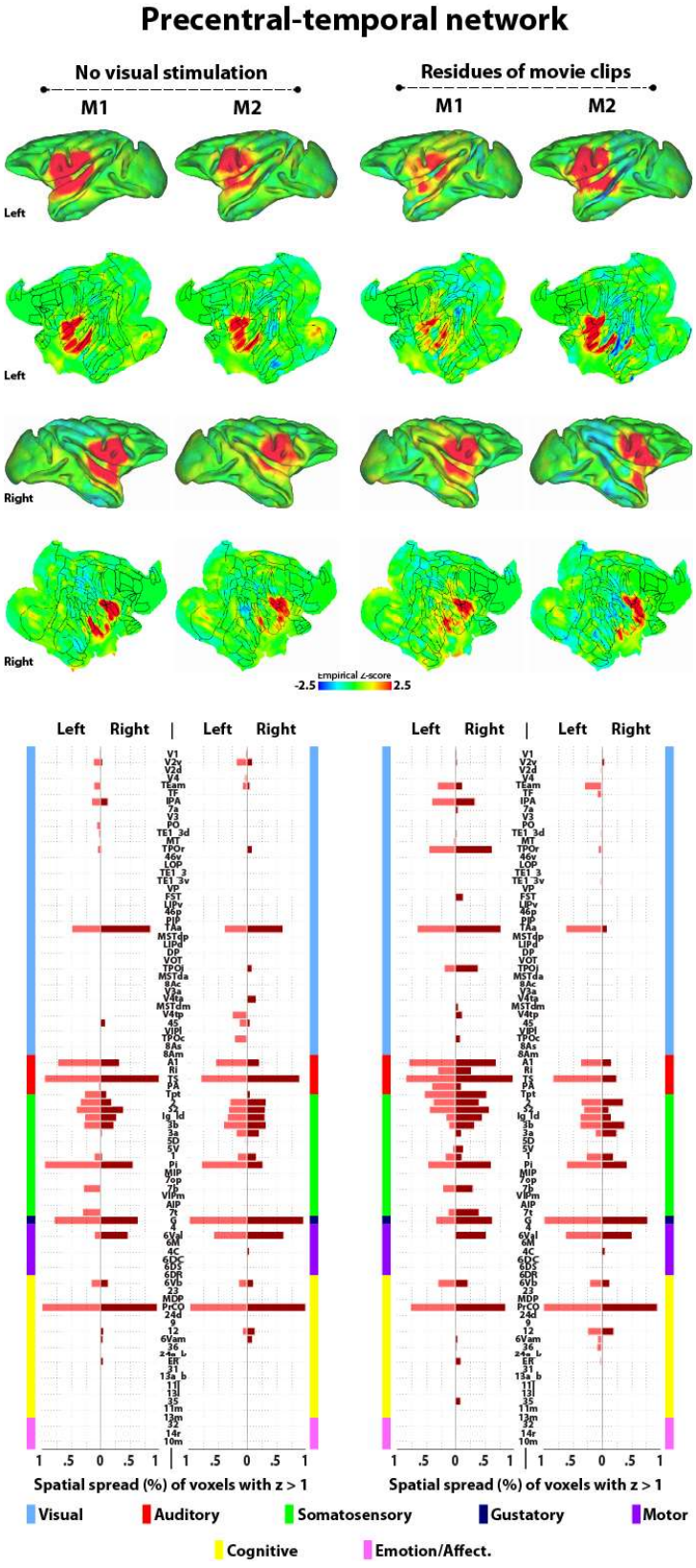

Figure S14. Precentro-temporal network (awake).

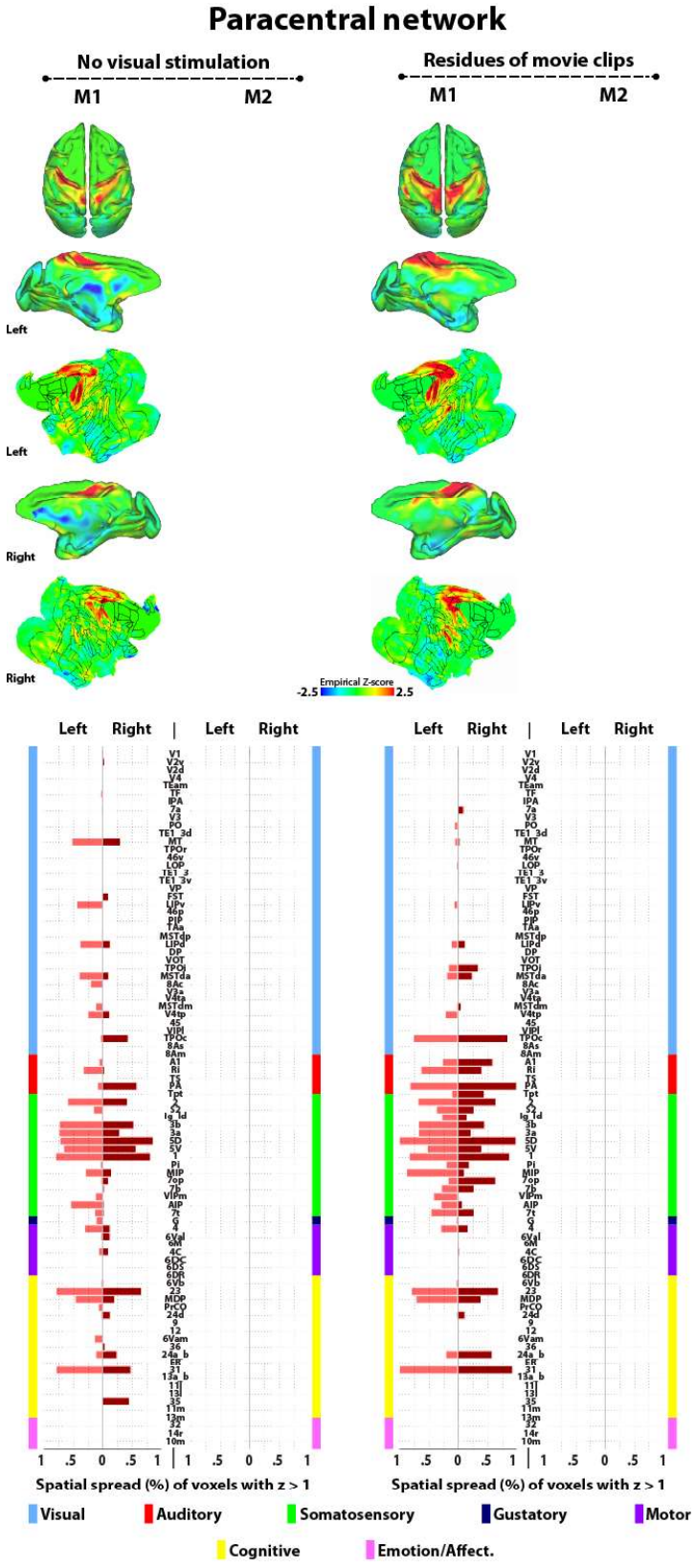

Figure S15. Precentral-temporal network (awake).

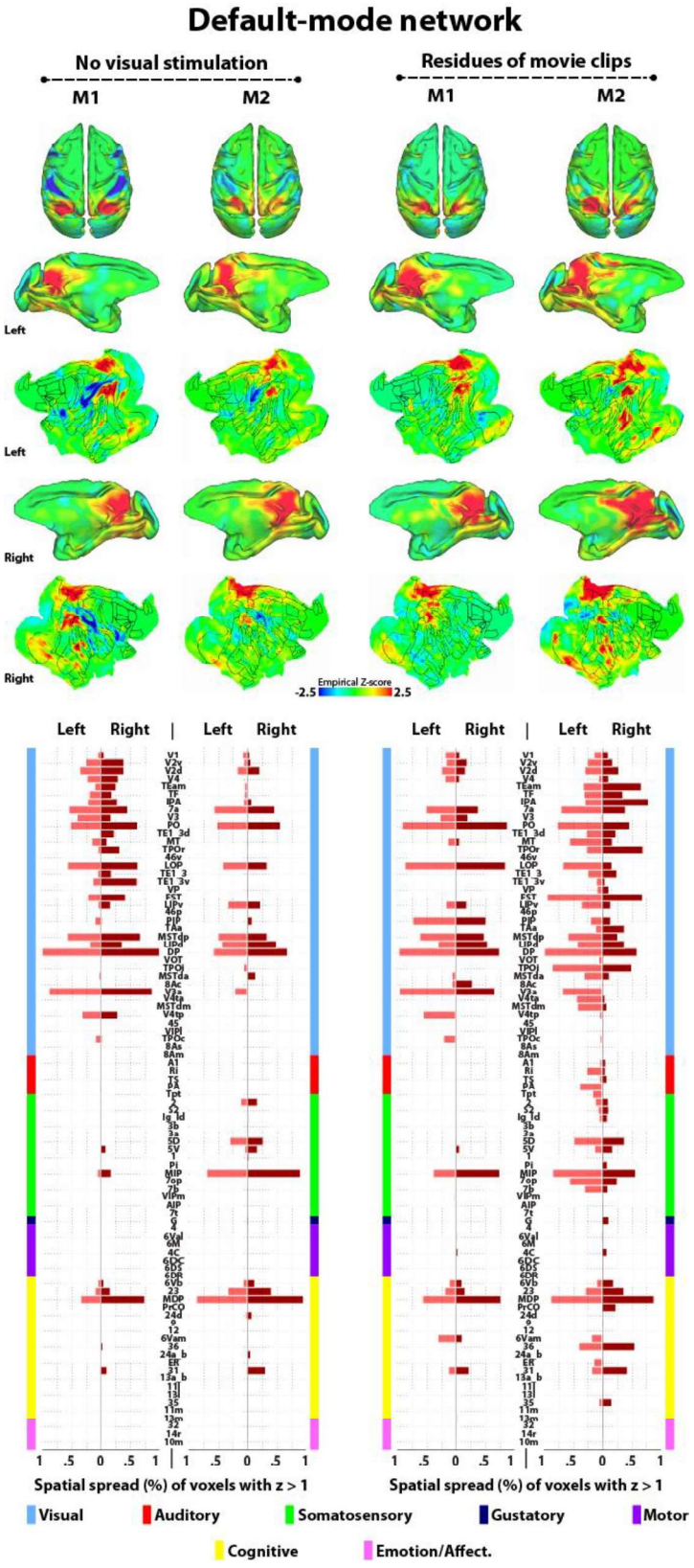

Figure S16. Precentral-temporal network (awake).

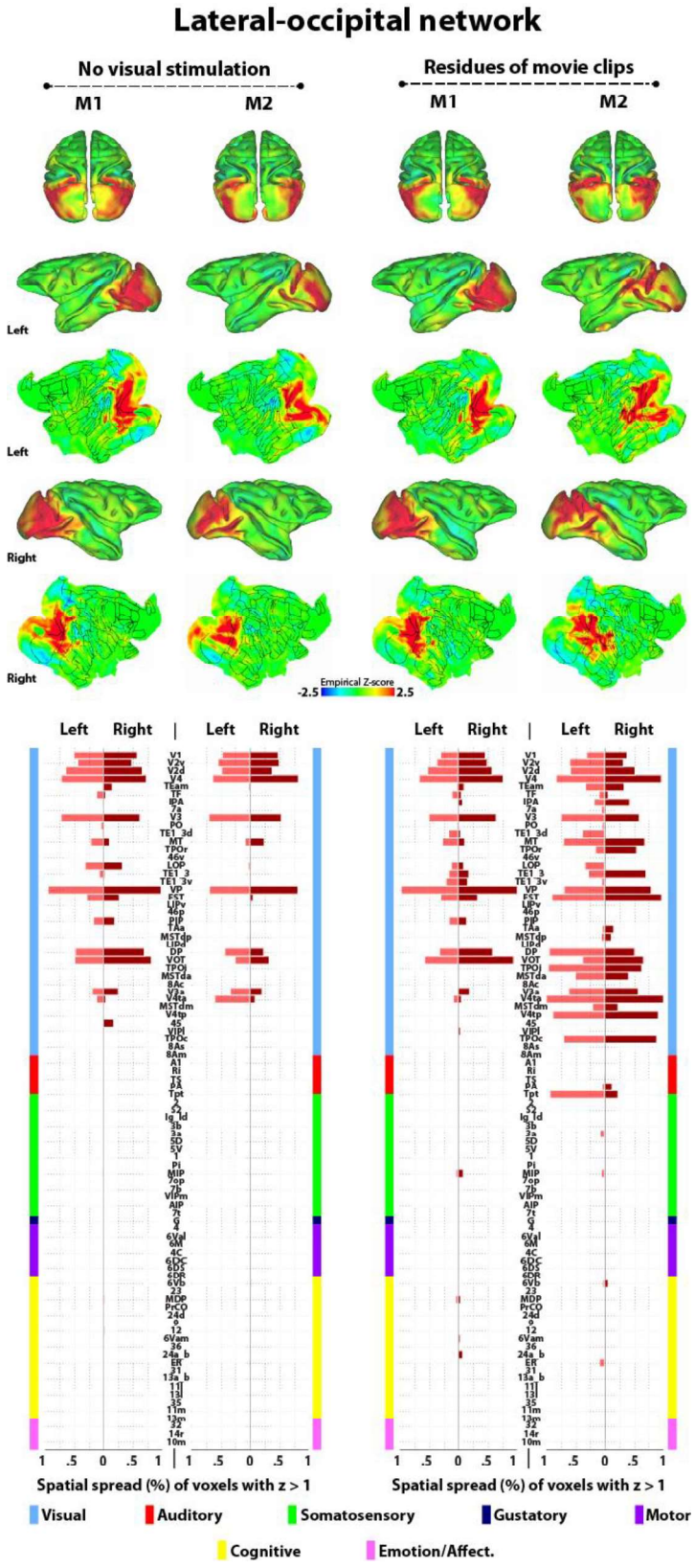

Figure S17. Lateral occipital network (awake).

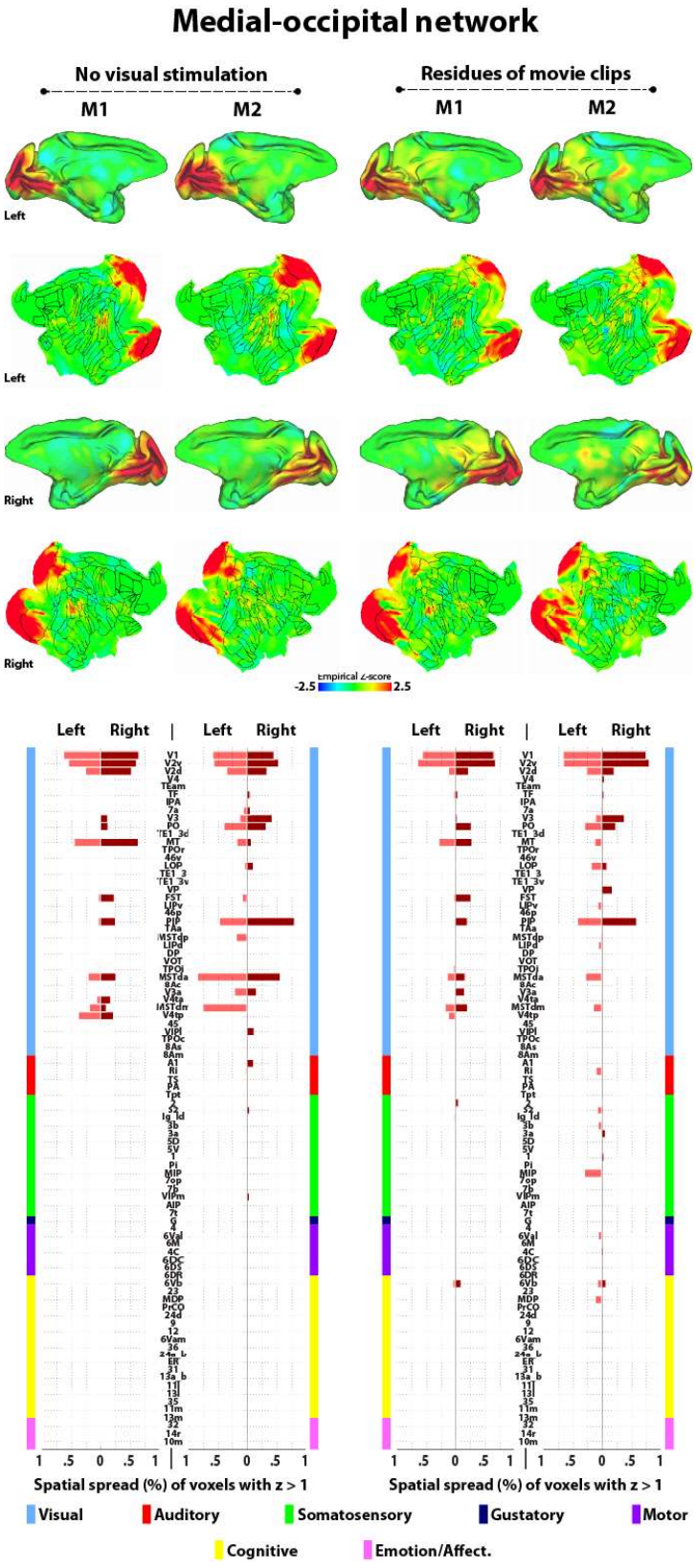

Figure S18. Medial-occipital network (awake).

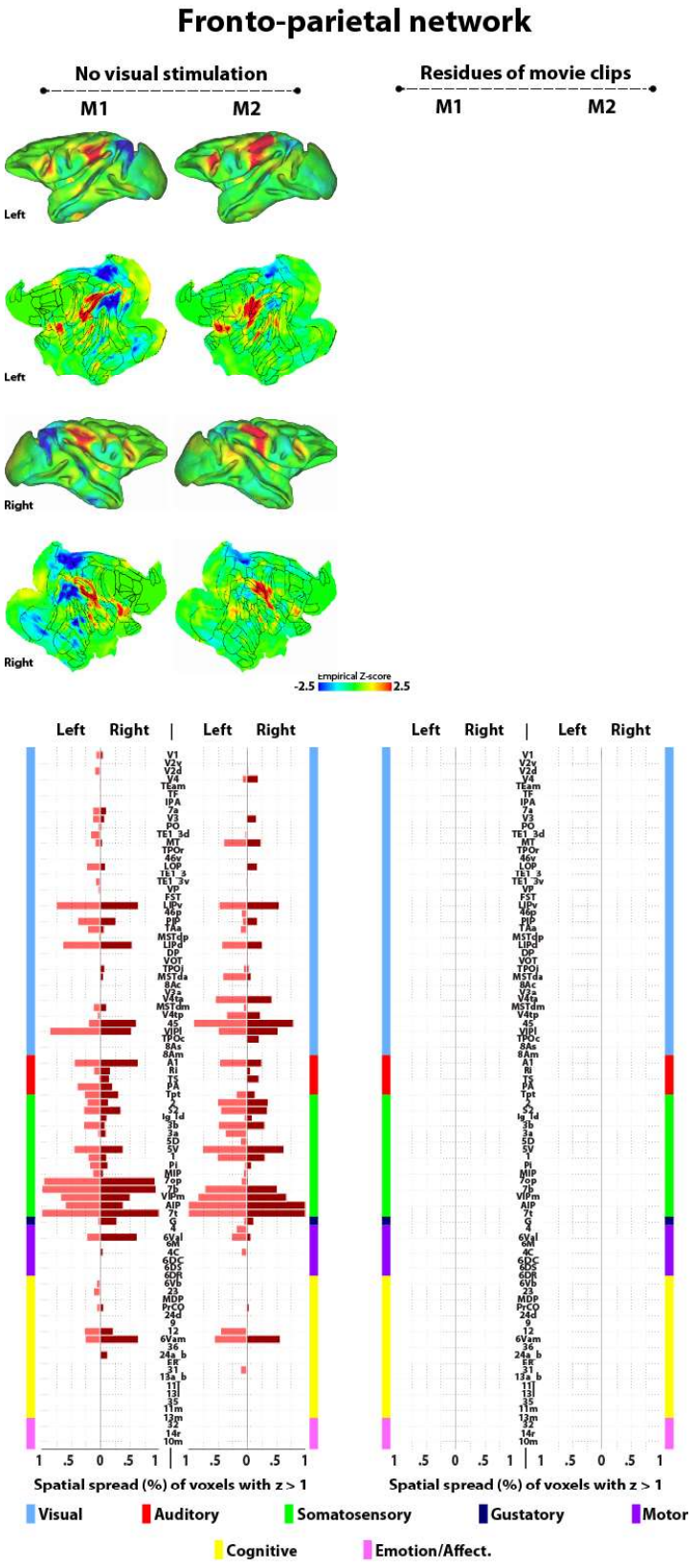

Figure S19. Fronto-parietal network (awake).

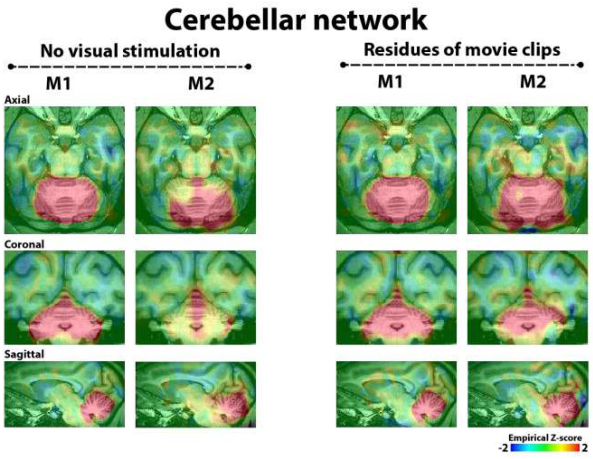

Figure S20. Cerebellar network (awake).

10.2 A Potential Role of Auditory Induced Modulations in Primary Visual Cortex

BRILL

Multisensory Research 28 (2015) 331–349

MULTISENSORY RESEARCH

brill.com/msr

A Potential Role of Auditory Induced Modulations in Primary Visual Cortex

Frederico A. C. Azevedo [1,2,*], **Michael Ortiz-Rios** [1,2], **Qinglin Li** [1,2], **Nikos K. Logothetis** [1,3] **and Georgios A. Keliris** [1,4,*]

[1] Department of Physiology of Cognitive Processes, Max Planck Institute for Biological Cybernetics, 72076 Tübingen, Germany

[2] IMPRS for Cognitive and Systems Neuroscience, Universität Tübingen, 72074 Tübingen, Germany

[3] Division of Imaging Science and Biomedical Engineering, University of Manchester, Manchester M13 9PT, United Kingdom

[4] Department of Biomedical Sciences, University of Antwerp, 2610 Wilrijk, Belgium

Received 30 January 2015; accepted 12 March 2015

Abstract

A biologically relevant event is normally the source of multiple, typically correlated, sensory inputs. To optimize perception of the outer world, our brain combines the independent sensory measurements into a coherent estimate. However, if sensory information is not readily available for every pertinent sense, the brain tries to acquire additional information *via* covert/overt orienting behaviors or uses internal knowledge to modulate sensory sensitivity based on prior expectations. Cross-modal functional modulation of low-level auditory areas due to visual input has been often described; however, less is known about auditory modulations of primary visual cortex. Here, based on some recent evidence, we propose that an unexpected auditory signal could trigger a reflexive overt orienting response towards its source and concomitantly increase the primary visual cortex sensitivity at the locations where the object is expected to enter the visual field. To this end, we propose that three major functionally specific pathways are employed in parallel. A stream orchestrated by the superior colliculus is responsible for the overt orienting behavior, while direct and indirect (*via* higher-level areas) projections from A1 to V1 respectively enhance spatiotemporal sensitivity and facilitate object detectability.

* To whom correspondence should be addressed. E-mail: frederico.azevedo@tuebingen.mpg.de; georgios.keliris@tuebingen.mpg.de

DOI:10.1163/22134808-00002494

Keywords
Superior colliculus, auditory cortex, visual cortex, A1, V1, object selectivity, spatial sensitivity, overt orienting

1. Introduction

Biologically relevant events impinge different signatures of information on the sensory channels creating the necessity of integration into a unified stream of consciousness. If we look upon the brain as an optimal Bayesian estimator of the environment (Ernst and Banks, 2002; Fetsch *et al.*, 2013; Knill and Pouget, 2004), a combination of multiple, independent sensory measurements minimizes the uncertainty of a sensory estimate. By integrating information from all available senses, the brain maximizes the usage of the available information at any moment, enhances the physiological salience of such events and facilitates behavioral reactions resulting in increased probability of survival (Stein *et al.*, 2014).

Initially, sensory processing is highly specialized into low-level primarily unisensory cortical regions (Kanwisher, 2010; Macaluso and Driver, 2005). For instance, basic visual and auditory features are extracted and processed in the primary visual and auditory cortices respectively (see Note 1). Subsequently, the outputs of these and other primary sensory areas converge through a hierarchical albeit highly recurrent network onto higher-order multisensory areas (Felleman and Van Essen, 1991), where information from different modalities is combined to form a coherent percept (Ghazanfar and Schroeder, 2006; Wei *et al.*, 2012).

Classically, the capacity of multisensory interactions was considered an exclusive property of higher-level cortical regions, i.e., the superior temporal, intraparietal, frontal and prefrontal cortex. However, an increasing amount of evidence showed that cross-modal interactions occur not only in higher order cognitive areas but also at low-level stages of sensory processing (Ghazanfar and Schroeder, 2006). While studies reporting visual modulation of early auditory processing are common (Schroeder and Foxe, 2005), reports showing auditory induced modulation in primary visual cortex are scarce, although behavioral evidence on auditory influences of visual perception (Shams and Kim, 2010) and direct anatomical projections from A1 to V1 have been demonstrated (Clavagnier *et al.*, 2004; Falchier *et al.*, 2002; Rockland and Ojima, 2003).

Here, based on the current evidence of low-level auditory modulations in visual cortex, we propose that short-latency auditory information arising beyond the visual field could convey spatiotemporal information that directs and prepares upcoming visual cortical responses in parallel with a reorienting response towards an object. Furthermore, parallel processing of auditory

features in higher-level areas can preempt visual cortex on the identity of an object in a framework consistent with predictive coding.

2. Audiovisual Interactions in Low-Level Sensory Cortices

Cross-modal interactions in low-level sensory areas could be a widespread feature of cortical processing (Ghazanfar and Schroeder, 2006). For example, several studies have demonstrated visually induced modulations in low-level auditory cortices of humans and monkeys (for a review see Schroeder and Foxe, 2005). In a neurophysiological experiment in monkeys Ghazanfar *et al.* showed that auditory cortex integrates audiovisual information contained in facial gestures and vocalization stimuli through the enhancement or suppression of local field potentials (Ghazanfar *et al.*, 2005). Similarly, Kayser *et al.* reported visual modulation of local field potentials and single unit activity of neurons located in the primary and secondary auditory fields (Kayser *et al.*, 2008). The same authors, by using fMRI in non-human primates, found visually induced activation in several auditory fields including A1 (Kayser *et al.*, 2007). Human fMRI studies by Calvert *et al.* found that the substantial improvement of auditory speech perception when the speaker's face was visible was accompanied by a significant response enhancement in auditory cortex (Calvert *et al.*, 1999). More recently, Werner and Noppeney showed that a simultaneous visual input could enhance the stimulus salience by amplifying the auditory response in the human primary auditory cortex while the subjects performed an audiovisual object categorization task (Werner and Noppeney, 2010). In support of these findings, Romei *et al.* reported facilitation in auditory detection caused by single-pulse transcranial magnetic stimulation (TMS) of the occipital lobe of human subjects shortly after stimulus onset (60–75 ms). Interestingly, this was equivalent to the magnitude of the effect observed after audiovisual stimulation alone (Romei *et al.*, 2007).

On the other hand, despite evidence for feedback projections to area V1 not only from multisensory (STP) cortices but also from area A1 (Clavagnier *et al.*, 2004; Falchier *et al.*, 2002; Rockland and Ojima, 2003), few studies have directly demonstrated neurophysiological evidence for auditory modulation in primary visual cortex of primates. This asymmetry could be purely a sampling bias since A1, located in proximity to many associative areas that are often studied for crossmodal interactions, has been more frequently assessed in this context in comparison to V1. Alternatively, the asymmetry could represent a real difference stemming from their functional role such as the higher spatial reliability of visual cortex (Witten and Knudsen, 2005) being more often (in a Bayesian sense) required for integration (Knill and Pouget, 2004).

In one study, Wang *et al.* recorded single-unit spiking activity in area V1 of monkeys while they performed a visually guided saccadic task with or without

a simultaneous presentation of a sound. According to this report, audiovisual integration could significantly reduce the neuronal onset latency of single neurons as well as the saccade latency, resulting in an improved behavioral performance (Wang *et al.*, 2008). However, they did not observe any integration effect when the monkeys fixated passively indicating that the behavioral context was a crucial factor for multisensory modulation. As a possible mechanism, the authors suggested that the auditory response, being faster than visual responses, could depolarize the membrane potential and consequently induce an earlier increase in the firing rate of V1 neurons. Based on the short latencies found in this study, they hypothesized that the auditory modulation of V1 activity probably happened through STP afferents in addition to direct auditory projections to V1.

In an elegant study by Lakatos *et al.*, monkeys were trained to perform an intermodal selection task in which the animals had to attend to a stream of tones or lights while intracortical field potentials and multiunit activity were recorded in primary visual and auditory cortices. The authors showed that modality-specific stimuli, be it visual or auditory, could reset ongoing neuronal network oscillations in both V1 and A1, under the condition that the monkeys were attending to the specific stimulus modality presented (Lakatos *et al.*, 2009). In addition, they demonstrated that the increased phase-locking caused by the non-preferred stimulus, namely the auditory stimulus in V1 or the visual stimulus in A1, was not accompanied by significant MUA changes. In this study, cross-modal integration in primary cortices led to subthreshold modulations with cross-modal phase resetting as the main mechanism consistent with previous studies (Ghazanfar *et al.*, 2008; Kayser *et al.*, 2008; Lakatos *et al.*, 2007, 2008). Based on the short timing of gamma phase locking in both primary cortices, the authors suggested that the observed multimodal interactions could have occurred through a feed-forward nonspecific thalamic projection to both A1 and V1.

Complementary to the neurophysiological evidence in non-human primates, human TMS research also reported evidence of auditory modulation of low-level visual cortices. In a series of successive studies, Romei *et al.* demonstrated that auditory stimulation can decrease the threshold of perceived phosphene induced by a single pulse TMS applied over the occipital pole (Romei *et al.*, 2007); that the early excitability of low-level visual cortices is pre-perceptual and stimulus-selective (Romei *et al.*, 2009) and that it can provoke phase-locking of occipital alpha-oscillations (Romei *et al.*, 2012). Further, Bolognini *et al.* showed that early cross-modal enhancement of occipital cortical excitability is not just temporally but also spatially specific. A subthreshold TMS pulse induced a phosphene percept if applied at the expected retinotopic location cued by a peripheral auditory stimulus (Bolognini *et al.*, 2010).

3. Auditory Spatial Localization and Identity Information Could Enhance Visual Sensitivity and Detectability

Bringing together some of the aforementioned evidence and considering current models of multisensory integration, we put forward a new proposition. Spatial and temporal non-semantic auditory information of an unexpected multisensory event can potentially increase the visual sensitivity and thus the subsequent visual detection of the event. According to our hypothesis, an unattended audiovisual event triggers three parallel processing streams in charge of specific functions: reflexive overt orienting, increase in spatiotemporal sensitivity and increase in object detectability. We suggest that these three processes are separate but interdependent, interacting with recurrent connections. In this scheme, reflexive overt orienting happening subcortically has a minimal processing time leading to the initiation of a motor response towards the target event. Fast auditory spatiotemporal localization of the target is expected to be critical for this process. Further, we conjecture that a copy of this signal is sent to primary visual cortex together with a reference of the upcoming motor response. In this way, primary visual cortex can predict through re-referencing the upcoming location of the target in the visual field and enhance its sensitivity at this location. In parallel, auditory processing in higher cortical regions is able to extract information about target identity and influence primary visual processing *via* feedback projections enhancing object selectivity.

Most proposed models of multisensory integration have the assumption that sensory information is readily available on each modality-specific sense. In other words, a model of audiovisual interactions normally takes into account that the visual information of a relevant event is inside the field of view of a subject and the auditory information is simultaneously inside his field of hearing. Importantly, however, the field of view and the field of hearing do not always overlap. While the field of hearing covers space essentially completely, the field of vision is much more focal and limited. It consists of approximately 95° away from the nose and 60° towards the nose in the azimuthal plane as well as 75° downward and 60° upward for each eye (Henson, 1993; Fig. 1). Since the field of hearing under normal conditions is global, comprehending every spatial angle around the head, an auditory cue will be most certainly available at any time. On the contrary, an event happening outside the field of view will not convey visual spatial information.

We discuss our proposition in the context of an example. Imagine being distracted walking in a street when suddenly an unfriendly dog barks his attacking intentions towards you. First, the only thing you realize is that there's an imminent danger, say behind, very near and slightly to your right. Immediately, an alertness signal is sent to the brain and the sympathetic system prepares the body for an extreme fight-or-flight behavior. Notwithstanding, for a successful

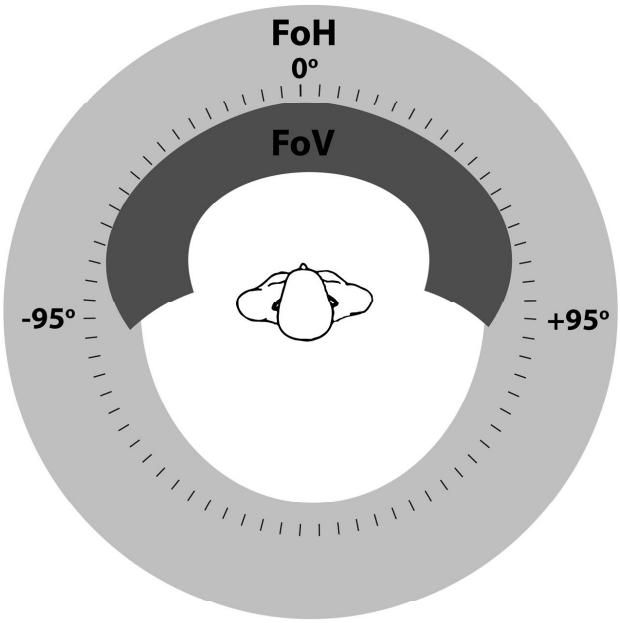

Figure 1. Schematic representation of the field of hearing (FoH, light gray) and of the field of view (FoV, dark grey) of humans. While the normal FoH has a global scope, encompassing every angle around the head, the FoH is focal, covering a wedge of approximately 95° away from the nose and 60° towards the nose in the azimuthal plane and 75° downward and 60° upward for each eye. Outside the visual wedge, the two sensory fields do not overlap.

reaction, two types of external information are still crucial, where and what the imminent danger is.

The fastest processing pathway, the reflexive overt orienting (Fig. 2a), is responsible for alerting the body and aligning its most spatially precise sense, normally vision, to the relevant event. A large amount of evidence suggests that this function is performed by the cochlea → superior colliculus (SC, Note 1) → motor pathways (Sparks, 1999; Wurtz and Albano, 1980). Under normal conditions, when a sound reaches the ear, the auditory information flows from the cochlea to the cochlear nuclei in the medulla, then spatial features like azimuthal distance are calculated in the superior olivary nuclei (Oliver *et al.*, 2003) and the processed auditory inputs then reach the inferior colliculus. In this midbrain nucleus, the auditory neural pathways bifurcate. One stream is projected to the superior colliculi and the other reaches the primary auditory cortex.

In the superior colliculi, auditory information is thought to converge to neurons whose receptive fields represent the approximate location of the sound source. As in the SC the auditory, visual and somatosensory receptive fields of overlapping sensory fields are aligned, if multiple cross-modal excitatory stimulus input arrive at approximately the same location (spatial rule) and the same time (temporal rule), they will have a higher probability of multisensory enhancement. In addition, if the event is happening in the periphery of

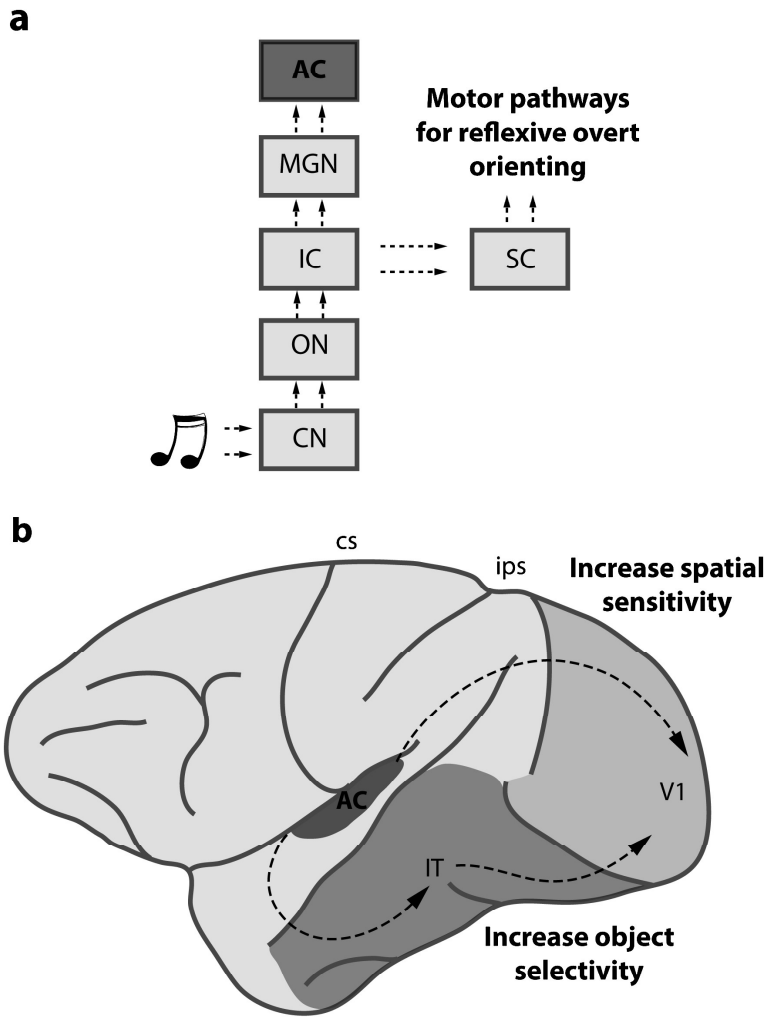

Figure 2. Simplified plots for the main suggested anatomical pathways involved in our proposal. An auditory spatial cue conveying object identity would be able to trigger three functional streams of processing to facilitate the overt orienting response, spatial sensitivity and object selectivity. (a) After the cue reaches the cochlea, the auditory information is sent to the cochlear nuclei (CN) in the medulla, subsequently projected to the olivary nuclei (ON), where spatial features such azimuthal distance are calculated and the outputs are forwarded to the inferior colliculus (IC). At this point, one stream is sent to the superior colliculus (SC), where the overlapping cross-modal sensory and motor receptive fields promote sensory reflexive orientation to the expected location of the event. In parallel to that, auditory information flows through the medial geniculate nucleus (MGN) to the auditory cortex (AC). (b) In the primary auditory cortices, the partially processed auditory information would be once more split to play distinct but complementary functional roles: bottom-up enhancement of visual spatial sensitivity and top-down facilitation of visual detectability of an expected object, eventually converging to low-level visual areas, such as the primary visual cortex (V1). Monosynaptic A1–V1 projections would be responsible for the former function, while top-down processing pathways involving the inferior temporal cortex (IT) would associate the identity of the object conveyed by the sound with the visual memory of the same object, creating a visual expectation for it. The object-specific expectation would then be able to modulate the receptive fields of the visual cortices including V1, optimizing its visual identification. Cs: central sulcus; ips: intraparietal sulcus.

the visual field, a related sound would considerably increase the multisensory response gain (principle of inverse effectiveness, Meredith and Stein, 1986), enhancing the saliency of that event. Since in the SC the multisensory and motor maps are also aligned, a reflexive overt orienting reaction toward the event is significantly facilitated. As a result, the body, head and eyes turn to foveate the important event. Such a reflexive overt orienting behavior is well explained for multisensory events happening in the intersection of sensory fields. However, the exact details of how the SC, auditory and visual cortices represent all spatial positions in the primate brain, including the regions not covered by the visual field, is still a subject of debate.

A second stream, in our scheme thought to be involved in enhancing spatial sensitivity (Fig. 2), bifurcates in the inferior colliculus and follows the ascending pathway to the medial geniculate body and then primary auditory cortices. According to our hypothesis, the partially processed auditory information is divided again in A1. One of those streams is monosynaptically projected to V1 while the other is sent to higher-cognitive regions. As the majority of the direct projections from the auditory cortex are thought to be reaching peripheral retinotopic locations in V1 (Falchier *et al*., 2002; Rockland and Ojima, 2003), a sound coming from a peripheral region would be able to enhance the visual detectability of events. In addition, a sound coming from a region not covered by the visual field can prepare the visual system by enhancing the visual detectability of events predicted to enter the visual field of view because of stimulus motion or by the execution of a motor response. This enhancement could be done by subthreshold modulations such as depolarization of the membrane potential as described by Wang *et al*. (2008) or by phase-resetting of ongoing gamma oscillations, similarly with the modulation reported by Lakatos *et al*. (2009). An additional aid in the multisensory representation of space comes from corticofugal projections from V1 and from other extrastriate areas to SC such as BAs 18 and 19 that have been demonstrated to respond to localized sounds (Corneil and Munoz, 2014; Morrell, 1972).

Finally the third stream, important for the detection of the identity of objects (Fig. 2b), is distributed to higher-order auditory processing areas, to the hippocampus, amygdala, entorhinal cortex, parahippocampal gyrus and to associative areas, where the identity of the auditory percept can be matched with its visual and other modality counterparts. In the context of our example, the bark of the dog would be associated to the semantic category of a dog including potential visual images. If instead of a bark, the auditory stimulus were a human voice to be matched to a person, more specific areas and pathways could be involved like for example direct connections of the voice areas in STS and the face area FFA (Blank *et al*., 2011). In summary, after the recollection of the expected visual percept, a target-template representation is

maintained in the visual working memory (Carlisle *et al.*, 2011) and feedback projections are sent down to the thalamus and to low-level visual cortices. As a consequence, feature specific neurons of V1 can be fine-tuned to facilitate the processing of low-level features corresponding to the expected visual memory of the object, enhancing object detectability.

As soon as the object gets inside the field of view due to the overt orienting, multisensory processing can occur in a way similar to the ones proposed by other models of multisensory integration. For instance, Talsma *et al.* proposed a framework in which the degree of competition among stimuli determines the type of multisensory interaction performed (Talsma *et al.*, 2010). The authors suggest that the preattentive brain tries to automatically realign spatiotemporally a salient stimulus to another stimulus with lesser salience, following a bottom up strategy. For example, a sudden sound cue improves the detectability of a spatially congruent visual event (McDonald *et al.*, 2000). If the matching is congruent, the subsequent neural responsiveness in higher-order cortical areas is increased and the likelihood of processing the multisensory stimulus is enhanced. Talsma *et al.* further propose that complementarily to the default stimulus driven processing, top-down attentional modulation influences multiple stages of bottom up processing.

According to our hypothesis, auditory information together with the reorienting motor reference create an expectation of a visual stimulus at a certain spatial position, increasing the chance of the event to be detected. If the observed object meets the expected object, the reaction to the stimuli can be decided and executed. If not, the mismatch in the perceived and expected event generates a measurable anticipation error in the visual cortices, consistent with predictive coding (Friston, 2005; Rao and Ballard, 1999).

4. Discussion

Multisensory integration is an efficient way to generate perceptual estimates of the environment based on the not always reliable sensory information (Knill and Pouget, 2004). Classical views have highlighted the importance of associative multisensory areas in this process. However, recent evidence suggested that interactions happen also at low-level 'unisensory' stages. Most obviously, such modulations could be taking place very early in time before information processing proceeds in higher areas and could thus offer a faster channel for reflexive action. In addition, cross-modal inputs to low-level cortical areas are able to modulate primary saliency filters, which can generate benefits for perceptual processing, such as an improved resolvability of competing multiple stimuli (Van der Burg *et al.*, 2011). If congruent multimodal inputs are not simultaneously available for each sensory modality, the preceding unimodal stimulation is able to create prior expectations on low-level representations

of the other modality, potentially improving the quality (Kok *et al.*, 2012) and content (Kok *et al.*, 2013) of its early sensorial representation. On the other hand, invalid or uncertain predictions can degrade perceptual processing (Posner *et al.*, 1978; Rolke and Hofmann, 2007). In general terms, by combining cross-modal inputs, the brain amplifies minimal signals and reduces their ambiguity, which results in improved orienting towards, detection and identification of relevant events (Calvert, 2001; Stein and Meredith, 1993).

In this opinion article, we propose a mechanism by which cross-modal expectation generated by an object-specific auditory spatial cue is able to tune the visual system and facilitate the detection of an object. In summary, we conjecture that three streams distributed in parallel throughout the brain subserve specific functions: reflexive overt orienting, enhancement of spatiotemporal sensitivity and facilitation of object detectability. Evidence suggests that these functions are closely linked to key brain structures, such as the superior colliculus, primary auditory and visual cortices, and through specific neural pathways, such as direct A1–V1 projections and top-down modulatory feedback projections to V1.

For example, the superior colliculus has been unequivocally implicated in the primate visual orienting circuit (Klier *et al.*, 2003; Krauzlis *et al.*, 2004; Kustov and Robinson, 1996; Sparks, 1999). By sending projections to the brainstem premotor circuitry, it modulates pupil control, saccade generation and head and body movements (Corneil and Munoz, 2014). Due to the overlap of visual, auditory and motor receptive fields, a sensorimotor overt orienting response is facilitated (Stein *et al.*, 2014). On the other hand, a reversible inactivation of the region in the SC representing the target cue is able to impair orienting behaviors, such as gaze orienting (McPeek and Keller, 2004). Nevertheless, how exactly the SC represents space for each sense is not completely understood. For instance, some evidence show that auditory signals could evolve to a reference frame similar to that used by vision, an eye-centered coordinate (Lee and Groh, 2012) and that the visual and auditory space can dynamically change due to anticipatory shifts in receptive field position (Leung *et al.*, 2008). Concerning object recognition, even though the SC plays a critical role in the ability to direct motor responses towards objects, behavioral studies have indicated that the SC is not actually needed for extracting object identity *per se* (Sprague, 1996).

Moreover, evidence clearly indicates a role of top-down feedback projections in carrying auditory information related to object identity. Several studies indicate that expectation can enhance low-level visual detectability (Chennu *et al.*, 2013; Kok *et al.*, 2014; McManus *et al.*, 2011; Sharma *et al.*, in press; Summerfield and Egner, 2009). For instance, Lupyan and Ward showed that an object image made invisible by continuous flash suppression became visible if the subjects heard the name of the expected object shortly before its

suppressed presentation. Further, they showed that an invalid semantic label weakens object detection. In addition, they demonstrated that expectation could facilitate visual discriminability of objects containing even small differences in low-level geometric features, such as squares and circles (Lupyan and Ward, 2013). In another example, Kok *et al*. designed a Multivoxel Pattern Analysis (MVPA)–fMRI study in which human subjects had to discriminate the orientation or contrast of two consecutively presented grating stimuli after an auditory cue predicted the overall orientation of the gratings. They found that gratings with expected orientation evoked less activity in V1 than unexpected gratings, independently of the relevance of the orientation for the discrimination task. However, the MVPA orientation classification accuracy increased suggesting that expectation is able to sharpen visual representations in V1 (Kok *et al*., 2012).

The neural mechanisms behind the facilitation of perception caused by top-down expectations are not completely understood. Lupyan and Ward suggested that the processing of the object name could have initiated a feedback activity to object-selective regions, such as IT, generating a predictive signal to the visual system that would reach low-level visual areas and aid the detection of objects belonging to an expected category (Lupyan and Ward, 2013). According to the predictive coding models (Friston, 2005; Rao and Ballard, 1999), populations of neurons would be able to estimate the sensory inputs as well as the mismatch (prediction error) between the expected and incoming sensory signals. In line with it, Kok *et al*. proposes that top-down expectations would increase the gain of prediction error neurons encoding the expected feature. If top-down expectation matches bottom-up inputs, the prediction error is rapidly resolved. However, if expectation differs from reality, a large prediction error is generated, which is reflected by an increase in neural activity (Kok *et al*., 2012).

Albeit the existence of direct projections from A1 to V1 has been already demonstrated (Clavagnier *et al*., 2004; Falchier *et al*., 2002; Rockland and Ojima, 2003), direct evidence for the role of such projections is still missing. A study implicated these projections in cross-modal selective attention, functional cortical reorganization after sensory deprivation and/or spatial awareness (Clavagnier *et al*., 2004). Here, we suggest that these projections can preempt visual cortex with shorter latency than feedback from higher areas and help spatial and temporal localization of objects independent of their identity. Some evidence supports this hypothesis. For example, Vroomen and De Gelder (2000) demonstrated that specific sounds can enhance visual temporal search. In this study, participants had to detect a visual target in a rapidly changing sequence of visual distracters. Normally the visual stimuli were presented concomitantly with a low tone beep; however, when a high tone was synchronously presented with the visual target, the detectability of the target

increased significantly. The subjects reported the sensation of a briefly freezing of the target image. Furthermore, Watkins *et al.* showed that the perceptual illusion of a single flash being misperceived as two distinct flashes due to the presentation of two consecutive auditory beeps (Shams *et al.*, 2000) accompanies an enhancement of visual activity in V1 (Watkins *et al.*, 2006) and that the opposite illusion, a double flash being misperceived as a single flash due to a single beep relates to a decrease in V1 activity (Watkins *et al.*, 2007). Finally, the focal increase in occipito-cortical excitability at feedforward processing time and at the expected retinotopic location cued by a congruent peripheral sound strongly support our hypothesis for the role of the monosynaptic projections from A1 to V1 (Bolognini *et al.*, 2010).

Importantly in our view, these projections could also participate in a foveation mechanism that enhances selectivity toward a peripheral event, especially when this is beyond the coverage of the visual field. Previous studies of cross-modal interactions and multi-sensory integration have focused in experiments where both sensory modalities (e.g., vision and audition) are stimulated within their respective field of input. However, as we note here (see Fig. 1), this is often not the case during naturalistic behavior. Thus, it will be important to design studies in the future where a cross-modal event is presented outside the field of view. In addition, the subjects should be given the chance to freely act upon such events in order to bring them to the field of view by body, head and eye-movements. Recent advances in wireless, chronic recordings from multiple areas simultaneously (Schwarz *et al.*, 2014) are an ideal way to perform these experiments in behaving freely moving primates providing a great promise for future studies.

5. Conclusion

How an auditory stimulus can influence low-level visual processing of a relevant event is still an open question. Evidence points mainly towards subthreshold modulation of the primary cortex that happens in a bottom-up fashion, for example through projections from the STP and core/belt areas to V1, or in a top-down manner, originating in higher-order cognitive areas and finishing at low-level visual cortices. Based on evidence for auditory modulation of V1 in the literature, we proposed a model of cross-modal interaction in which the spatial, temporal and object-related auditory informational content are distributed and processed in three parallel streams, each one interdependently responsible for a reflexive overt orienting, an increase in spatial sensitivity and an increase in object detectability. In our proposal, the auditory information related to an audiovisual event happening even outside of the field of view would prepare the visual cortex for the detection of a specific object at a specific spatial location. If the object is successfully detected, a reaction can be

initiated; however, if the expected object is different from the perceived object, a measurable predictive error is generated.

Acknowledgement

This work has been supported by the Max Planck Society.

Note 1. The Superior Colliculus, the Primary Visual Cortex and the Primary Auditory Cortex

SC: The superior colliculus (SC), also called tectum, is a paired seven-layered sensorimotor structure located in the vertebrate midbrain, superior to the brainstem and inferior to the thalamus. It can be functionally divided in two regions, a superficial visual unisensory part (layers I–III) and a deeper multisensory part (layers I–VII). The former part contains exclusive unimodal visual neurons while the latter contains a mixture of unimodal visual, auditory and somatosensory neurons as well as multisensory neurons (Stein *et al.*, 2009). The receptive fields of each sensorial representation in the SC are spatiotopically well-organized and in register with each other (Jay and Sparks, 1984; Meredith *et al.*, 1991; Middlebrooks and Knudsen, 1984; Stein *et al.*, 1993). The neurons located in a vertical tissue column represent approximately the same spatial location in the environment. The SCs receives direct visual projections from the retina and indirect visual projections from the retino-reticulo-cortical pathway (White and Munoz, 2011).

V1: The primary visual cortex (V1), also known as striate cortex, is a six-layered cortical structure located bilaterally in and around the calcarine fissure, extending rostrally almost to the lunate sulcus and posterolaterally almost to the inferior occipital sulcus (Callaway, 1998). It corresponds to the Brodmann area 17. Possibly to minimize the costs of neural wiring connectivity (Chklovskii and Koulakov, 2004), V1 is functionally organized into multiple visual maps. Each lateral V1 contains a retinotopic map, with a continuous and locally undistorted representation of the entire contralateral visual hemifield with segregated upper and lower quadrants (Adams and Horton, 2003; Vanduffel *et al.*, 2014); an ocular dominance map, with alternating columnar stripes representing segregated input coming from the ipsi- or contra-lateral retina (Hubel and Wiesel, 1968); an orientation selectivity map, where neurons with similar orientation response preference are located next to each other (Hubel and Wiesel, 1968); a direction selectivity map, with a mosaic distribution of neuronal populations displaying preferential response to image motion in a particular direction (Ohki *et al.*, 2005; Vaney *et al.*, 2012), and a color selectivity map, where clusters or blobs with poor-orientation-but-strong-color preference are regularly segregated (Landisman and Ts'o, 2002; Lu and Roe,

2008). In addition to that, evidence in the cat visual cortex suggest the existence of a spatial frequency selectivity map (Issa *et al.*, 2000) and a binocular disparity selectivity map (Kara and Boyd, 2009). Each topic map is tuned to extract a specific primary feature of a visual stimulus. The primary visual cortex receives direct input from the LGN, V2, V3, V3A, V4, MT, PO, PIP (Felleman and Van Essen, 1991), FST, LIP, TE, TEO, TH–TF, FEF (Barone *et al.*, 2000), inferior pulvinar (Benevento and Rezak, 1976), amygdala (Freese and Amaral, 2005), claustrum (Baizer *et al.*, 1997) and its periphery receives inputs from A1 (Falchier *et al.*, 2002; Rockland and Ojima, 2003).

A1: The primary auditory cortex (A1) is a six-layered cortical structure located bilaterally in the temporal lobes, specifically in the caudal part of the superior temporal gyrus, folding across the rostral Heschl's gyrus. It corresponds to Brodmann areas 41 and 42 and it is part of the auditory core, which comprises RT, R and A1 anterior caudally and is surrounded by the auditory belt (Kaas and Hackett, 2000). A1 is functionally organized along the posterior-to-anterior axis in a high-to-low gradient tonotopic (or cochleotopic) map (Saenz and Langers, 2014). This means that the neurons located caudally are preferentially activated by high frequency sounds and the neurons in the rostral A1 respond preferentially to low frequency sounds. The existence in primates of an additional binaural dominance map containing an orthogonal representation of independently mapped binaural interaction columns along the isofrequency strips in A1 is still disputed (Reser, 2000). To the moment, no spatial auditory maps were reported concerning the mammalian cortices. The primary auditory cortex of primates receives direct cortical projections from the core (R and RT) and from the belt (MM, ML, CM, CL, RM, AL) (Kaas and Hackett, 2000) and subcortical input from the thalamic nuclei, which includes PO (posterior), PM (postero-medial), LIM (Limitans) and SG (suprageniculate); from the MGm (magnocellular division) and AD (anterior dorsal division) of the medial geniculate nuclei and from the VP (ventral posterior complex) (Schroeder and Foxe, 2005).

References

Adams, D. L. and Horton, J. C. (2003). A precise retinotopic map of primate striate cortex generated from the representation of angioscotomas, *J. Neurosci.* **23**, 3771–3789.

Baizer, J. S., Lock, T. M. and Youakim, M. (1997). Projections from the claustrum to the prelunate gyrus in the monkey, *Exp. Brain Res.* **113**, 564–568.

Barone, P., Batardiere, A., Knoblauch, K. and Kennedy, H. (2000). Laminar distribution of neurons in extrastriate areas projecting to visual areas V1 and V4 correlates with the hierarchical rank and indicates the operation of a distance rule, *J. Neurosci.* **20**, 3263–3281.

Benevento, L. A. and Rezak, M. (1976). The cortical projections of the inferior pulvinar and adjacent lateral pulvinar in the rhesus monkey (*Macaca mulatta*): an autoradiographic study, *Brain Res.* **108**, 1–24.

Blank, H., Anwander, A. and von Kriegstein, K. (2011). Direct structural connections between voice- and face-recognition areas, *J. Neurosci.* **31**, 12906–12915.

Bolognini, N., Senna, I., Maravita, A., Pascual-Leone, A. and Merabet, L. B. (2010). Auditory enhancement of visual phosphene perception: the effect of temporal and spatial factors and of stimulus intensity, *Neurosci. Lett.* **477**, 109–114.

Callaway, E. M. (1998). Local circuits in primary visual cortex of the macaque monkey, *Annu. Rev. Neurosci.* **21**, 47–74.

Calvert, G. A. (2001). Crossmodal processing in the human brain: insights from functional neuroimaging studies, *Cereb. Cortex* **11**, 1110–1123.

Calvert, G. A., Brammer, M. J., Bullmore, E. T., Campbell, R., Iversen, S. D. and David, A. S. (1999). Response amplification in sensory-specific cortices during crossmodal binding, *NeuroReport* **10**, 2619–2623.

Carlisle, N. B., Arita, J. T., Pardo, D. and Woodman, G. F. (2011). Attentional templates in visual working memory, *J. Neurosci.* **31**, 9315–9322.

Chennu, S., Noreika, V., Gueorguiev, D., Blenkmann, A., Kochen, S., Ibáñez, A., Owen, A. M. and Bekinschtein, T. A. (2013). Expectation and attention in hierarchical auditory prediction, *J. Neurosci.* **33**, 11194–11205.

Chklovskii, D. B. and Koulakov, A. A. (2004). Maps in the brain: what can we learn from them? *Annu. Rev. Neurosci.* **27**, 369–392.

Clavagnier, S., Falchier, A. and Kennedy, H. (2004). Long-distance feedback projections to area V1: implications for multisensory integration, spatial awareness, and visual consciousness, *Cogn. Affect. Behav. Neurosci.* **4**, 117–126.

Corneil, B. D. and Munoz, D. P. (2014). Overt responses during covert orienting, *Neuron* **82**, 1230–1243.

Ernst, M. O. and Banks, M. S. (2002). Humans integrate visual and haptic information in a statistically optimal fashion, *Nature* **415**(6870), 429–433.

Falchier, A., Clavagnier, S., Barone, P. and Kennedy, H. (2002). Anatomical evidence of multimodal integration in primate striate cortex, *J. Neurosci.* **22**, 5749–5759.

Felleman, D. J. and Van Essen, D. C. (1991). Distributed hierarchical processing in the primate cerebral cortex, *Cereb. Cortex* **1**, 1–47.

Fetsch, C. R., DeAngelis, G. C. and Angelaki, D. E. (2013). Bridging the gap between theories of sensory cue integration and the physiology of multisensory neurons, *Nat. Rev. Neurosci.* **14**, 429–442.

Freese, J. L. and Amaral, D. G. (2005). The organization of projections from the amygdala to visual cortical areas TE and V1 in the macaque monkey, *J. Comp. Neurol.* **486**, 295–317.

Friston, K. (2005). A theory of cortical responses, *Philos. Trans. R. Soc. Lond. B Biol. Sci.* **360**(1456), 815–836.

Ghazanfar, A. A. and Schroeder, C. E. (2006). Is neocortex essentially multisensory? *Trends Cogn. Sci.* **10**, 278–285.

Ghazanfar, A. A., Maier, J. X., Hoffman, K. L. and Logothetis, N. K. (2005). Multisensory integration of dynamic faces and voices in rhesus monkey auditory cortex, *J. Neurosci.* **25**, 5004–5012.

Ghazanfar, A. A., Chandrasekaran, C. and Logothetis, N. K. (2008). Interactions between the superior temporal sulcus and auditory cortex mediate dynamic face/voice integration in rhesus monkeys, *J. Neurosci.* **28**, 4457–4469.

Henson, D. B. (1993). *Visual Fields*, 1st edn. Oxford Medical Publications, Oxford, UK.

Hubel, D. H. and Wiesel, T. N. (1968). Receptive fields and functional architecture of monkey striate cortex, *J. Physiol.* **195**, 215–243.

Issa, N. P., Trepel, C. and Stryker, M. P. (2000). Spatial frequency maps in cat visual cortex, *J. Neurosci.* **20**, 8504–8514.

Jay, M. F. and Sparks, D. L. (1984). Auditory receptive fields in primate superior colliculus shift with changes in eye position, *Nature* **309**(5966), 345–347.

Kaas, J. H. and Hackett, T. A. (2000). Subdivisions of auditory cortex and processing streams in primates, *Proc. Natl Acad. Sci. USA* **97**, 11793–11799.

Kanwisher, N. (2010). Functional specificity in the human brain: a window into the functional architecture of the mind, *Proc. Natl Acad. Sci. USA* **107**, 11163–11170.

Kara, P. and Boyd, J. D. (2009). A micro-architecture for binocular disparity and ocular dominance in visual cortex, *Nature* **458**(7238), 627–631.

Kayser, C., Petkov, C. I., Augath, M. and Logothetis, N. K. (2007). Functional imaging reveals visual modulation of specific fields in auditory cortex, *J. Neurosci.* **27**, 1824–1835.

Kayser, C., Petkov, C. I. and Logothetis, N. K. (2008). Visual modulation of neurons in auditory cortex, *Cereb. Cortex* **18**, 1560–1574.

Klier, E. M., Wang, H. and Crawford, J. D. (2003). Three-dimensional eye-head coordination is implemented downstream from the superior colliculus, *J. Neurophysiol.* **89**, 2839–2853.

Knill, D. C. and Pouget, A. (2004). The Bayesian brain: the role of uncertainty in neural coding and computation, *Trends Neurosci.* **27**, 712–719.

Kok, P., Jehee, J. F. M. and De Lange, F. P. (2012). Less is more: expectation sharpens representations in the primary visual cortex, *Neuron* **75**, 265–270.

Kok, P., Brouwer, G. J., Van Gerven, M. A. and De Lange, F. P. (2013). Prior expectations bias sensory representations in visual cortex, *J. Neurosci.* **33**, 16275–16284.

Kok, P., Failing, M. F. and De Lange, F. P. (2014). Prior expectations evoke stimulus templates in the primary visual cortex, *J. Cogn. Neurosci.* **26**, 1546–1554.

Krauzlis, R. J., Liston, D. and Carello, C. D. (2004). Target selection and the superior colliculus: goals, choices and hypotheses, *Vis. Res.* **44**, 1445–1451.

Kustov, A. A. and Robinson, D. L. (1996). Shared neural control of attentional shifts and eye movements, *Nature* **384**(6604), 74–77.

Lakatos, P., Chen, C. M., O'Connell, M. N., Mills, A. and Schroeder, C. E. (2007). Neuronal oscillations and multisensory interaction in primary auditory cortex, *Neuron* **53**, 279–292.

Lakatos, P., Karmos, G., Mehta, A. D., Ulbert, I. and Schroeder, C. E. (2008). Entrainment of neuronal oscillations as a mechanism of attentional selection, *Science* **320**(5872), 110–113.

Lakatos, P., O'Connell, M. N., Barczak, A., Mills, A., Javitt, D. C. and Schroeder, C. E. (2009). The leading sense: supramodal control of neurophysiological context by attention, *Neuron* **64**, 419–430.

Landisman, C. E. and Ts'o, D. Y. (2002). Color processing in macaque striate cortex: relationships to ocular dominance, cytochrome oxidase, and orientation, *J. Neurophysiol.* **87**, 3126–3137.

Lee, J. and Groh, J. M. (2012). Auditory signals evolve from hybrid- to eye-centered coordinates in the primate superior colliculus, *J. Neurophysiol.* **108**, 227–242.

Leung, J., Alais, D. and Carlile, S. (2008). Compression of auditory space during rapid head turns, *Proc. Natl Acad. Sci. USA* **105**, 6492–6497.

Lu, H. D. and Roe, A. W. (2008). Functional organization of color domains in V1 and V2 of macaque monkey revealed by optical imaging, *Cereb. Cortex* **18**, 516–533.

Lupyan, G. and Ward, E. J. (2013). Language can boost otherwise unseen objects into visual awareness, *Proc. Natl Acad. Sci. USA* **110**, 14196–14201.

Macaluso, E. and Driver, J. (2005). Multisensory spatial interactions: a window onto functional integration in the human brain, *Trends Neurosci.* **28**, 264–271.

McDonald, J. J., Teder-Sälejärvi, W. A. and Hillyard, S. A. (2000). Involuntary orienting to sound improves visual perception, *Nature* **407**(6806), 906–908.

McManus, J. N. J., Li, W. and Gilbert, C. D. (2011). Adaptive shape processing in primary visual cortex, *Proc. Natl Acad. Sci. USA* **108**, 9739–9746.

McPeek, R. M. and Keller, E. L. (2004). Deficits in saccade target selection after inactivation of superior colliculus, *Nat. Neurosci.* **7**, 757–763.

Meredith, M. A. and Stein, B. E. (1986). Visual, auditory, and somatosensory convergence on cells in superior colliculus results in multisensory integration, *J. Neurophysiol.* **56**, 640–662.

Meredith, M. A., Clemo, H. R. and Stein, B. E. (1991). Somatotopic component of the multisensory map in the deep laminae of the cat superior colliculus, *J. Comp. Neurol.* **312**, 353–370.

Middlebrooks, J. C. and Knudsen, E. I. (1984). A neural code for auditory space in the cat's superior colliculus, *J. Neurosci.* **4**, 2621–2634.

Morrell, F. (1972). Visual system's view of acoustic space, *Nature* **238**(5358), 44–46.

Ohki, K., Chung, S., Ch'ng, Y. H., Kara, P. and Reid, R. C. (2005). Functional imaging with cellular resolution reveals precise micro-architecture in visual cortex, *Nature* **433**(7026), 597–603.

Oliver, D. L., Beckius, G. E., Bishop, D. C., Loftus, W. C. and Batra, R. (2003). Topography of interaural temporal disparity coding in projections of medial superior olive to inferior colliculus, *J. Neurosci.* **23**, 7438–7449.

Posner, M. I., Nissen, M. J. and Ogden, W. C. (1978). Attended and unattended processing modes: the role of set for spatial location, in: *Modes of Perceiving and Processing Information*, H. Pick and E. Saltzmann (Eds), pp. 137–157. John Wiley and Sons Inc., Hillsdale, NJ, USA.

Rao, R. P. and Ballard, D. H. (1999). Predictive coding in the visual cortex: a functional interpretation of some extra-classical receptive-field effects, *Nat. Neurosci.* **2**, 79–87.

Reser, D. H. (2000). Binaural interactions in primary auditory cortex of the awake macaque, *Cereb. Cortex* **10**, 574–584.

Rockland, K. S. and Ojima, H. (2003). Multisensory convergence in calcarine visual areas in macaque monkey, *Int. J. Psychophysiol.* **50**, 19–26.

Rolke, B. and Hofmann, P. (2007). Temporal uncertainty degrades perceptual processing, *Psychonom. Bull. Rev.* **14**, 522–526.

Romei, V., Murray, M. M., Merabet, L. B. and Thut, G. (2007). Occipital transcranial magnetic stimulation has opposing effects on visual and auditory stimulus detection: implications for multisensory interactions, *J. Neurosci.* **27**, 11465–11472.

Romei, V., Murray, M. M., Cappe, C. and Thut, G. (2009). Preperceptual and stimulus-selective enhancement of low-level human visual cortex excitability by sounds, *Curr. Biol.* **19**, 1799–1805.

Romei, V., Gross, J. and Thut, G. (2012). Sounds reset rhythms of visual cortex and corresponding human visual perception, *Curr. Biol.* **22**, 807–813.

Saenz, M. and Langers, D. R. M. (2014). Tonotopic mapping of human auditory cortex, *Hearing Res.* **307**, 42–52.

Schroeder, C. E. and Foxe, J. (2005). Multisensory contributions to low-level, 'unisensory' processing, *Curr. Opin. Neurobiol.* **15**, 454–458.

Schwarz, D. A., Lebedev, M. A., Hanson, T. L., Dimitrov, D. F., Lehew, G., Meloy, J., Rajangam, S., Subramanian, V., Ifft, P. J., Li, Z., Ramakrishnan, A., Tate, A., Zhuang, K. Z. and Nicolelis, M. A. (2014). Chronic, wireless recordings of large-scale brain activity in freely moving rhesus monkeys, *Nat. Meth.* **11**, 670–676.

Shams, L. and Kim, R. (2010). Crossmodal influences on visual perception, *Phys. Life Rev.* **7**, 269–284.

Shams, L., Kamitani, Y. and Shimojo, S. (2000). Illusions. What you see is what you hear, *Nature* **408**(6814), 788.

Sharma, J., Sugihara, H., Katz, Y., Schummers, J., Tenenbaum, J. and Sur, M. (in press). Spatial attention and temporal expectation under timed uncertainty predictably modulate neuronal responses in monkey V1, *Cereb. Cortex.*

Sparks, D. L. (1999). Conceptual issues related to the role of the superior colliculus in the control of gaze, *Curr. Opin. Neurobiol.* **9**, 698–707.

Sprague, J. M. (1996). Neural mechanisms of visual orienting responses, *Prog. Brain Res.* **112**, 1–15.

Stein, B. E. and Meredith, M. A. (1993). *The Merging of the Senses*. MIT Press, Cambridge, MA, USA.

Stein, B. E., Meredith, M. A. and Wallace, M. T. (1993). The visually responsive neuron and beyond: multisensory integration in cat and monkey, *Prog. Brain Res.* **95**, 79–90.

Stein, B. E., Stanford, T. R. and Rowland, B. A. (2009). The neural basis of multisensory integration in the midbrain: its organization and maturation, *Hearing Res.* **258**, 4–15.

Stein, B. E., Stanford, T. R. and Rowland, B. A. (2014). Development of multisensory integration from the perspective of the individual neuron, *Nat. Rev. Neurosci.* **15**, 520–535.

Summerfield, C. and Egner, T. (2009). Expectation (and attention) in visual cognition, *Trends Cogn. Sci.* **13**, 403–409.

Talsma, D., Senkowski, D., Soto-Faraco, S. and Woldorff, M. G. (2010). The multifaceted interplay between attention and multisensory integration, *Trends Cogn. Sci.* **14**, 400–410.

Van der Burg, E., Talsma, D., Olivers, C. N., Hickey, C. and Theeuwes, J. (2011). Early multisensory interactions affect the competition among multiple visual objects, *NeuroImage* **55**, 1208–1218.

Vanduffel, W., Zhu, Q. and Orban, G. A. (2014). Monkey cortex through fMRI glasses, *Neuron* **83**, 533–550.

Vaney, D. I., Sivyer, B. and Taylor, W. R. (2012). Direction selectivity in the retina: symmetry and asymmetry in structure and function, *Nat. Rev. Neurosci.* **13**, 194–208.

Vroomen, J. and De Gelder, B. (2000). Sound enhances visual perception: cross-modal effects of auditory organization on vision, *J. Exp. Psychol. Hum. Percept. Perform.* **26**, 1583–1590.

Wang, Y., Celebrini, S., Trotter, Y. and Barone, P. (2008). Visuo-auditory interactions in the primary visual cortex of the behaving monkey: electrophysiological evidence, *BMC Neurosci.* **9**, 79.

Watkins, S., Shams, L., Tanaka, S., Haynes, J. D. and Rees, G. (2006). Sound alters activity in human V1 in association with illusory visual perception, *NeuroImage* **31**, 1247–1256.

Watkins, S., Shams, L., Josephs, O. and Rees, G. (2007). Activity in human V1 follows multisensory perception, *NeuroImage* **37**, 572–578.

Wei, T., Liang, X., He, Y., Zang, Y., Han, Z., Caramazza, A. and Bi, Y. (2012). Predicting conceptual processing capacity from spontaneous neuronal activity of the left middle temporal gyrus, *J. Neurosci.* **32**, 481–489.

Werner, S. and Noppeney, U. (2010). Distinct functional contributions of primary sensory and association areas to audiovisual integration in object categorization, *J. Neurosci.* **30**, 2662–2675.

White, B. J. and Munoz, D. P. (2011). The superior colliculus, in: *The Oxford Handbook of Eye Movements*, S. P. Liversedge, I. D. Gilchrist and S. Everling (Eds), pp. 195–214. Oxford University Press, Oxford, UK.

Witten, I. B. and Knudsen, E. I. (2005). Why seeing is believing: merging auditory and visual worlds, *Neuron* **48**, 489–496.

Wurtz, R. H. and Albano, J. E. (1980). Visual-motor function of the primate superior colliculus, *Annu. Rev. Neurosci.* **3**, 189–226.

10.3 Functional MRI of the vocalization-processing networks in the macaque brain

frontiers in Neuroscience

ORIGINAL RESEARCH
published: 01 April 2015
doi: 10.3389/fnins.2015.00113

Functional MRI of the vocalization-processing network in the macaque brain

Michael Ortiz-Rios[1,2,3]*, *Paweł Kuśmierek*[1], *Iain DeWitt*[1], *Denis Archakov*[1,4], *Frederico A. C. Azevedo*[2,3], *Mikko Sams*[4], *Iiro P. Jääskeläinen*[4], *Georgios A. Keliris*[2,5,6] and *Josef P. Rauschecker*[1,4,7]*

[1] Department of Neuroscience, Georgetown University Medical Center, Washington, DC, USA, [2] Department of Physiology of Cognitive Processes, Max Planck Institute for Biological Cybernetics, Tübingen, Germany, [3] IMPRS for Cognitive and Systems Neuroscience, Tübingen, Germany, [4] Brain and Mind Laboratory, Department of Neuroscience and Biomedical Engineering, Aalto University School of Science, Aalto, Finland, [5] Bernstein Centre for Computational Neuroscience, Tübingen, Germany, [6] Department of Biomedical Sciences, University of Antwerp, Wilrijk, Belgium, [7] Institute for Advanced Study and Department of Neurology, Klinikum Rechts der Isar, Technische Universität München, München, Germany

OPEN ACCESS

Edited by:
Monica Munoz-Lopez, University of Castilla-La Mancha, Spain

Reviewed by:
Simon Baumann, Newcastle University, UK
Huan Luo, Chinese Academy of Sciences, China
Olivier Joly, MRC Cognition and Brain Sciences Unit, UK

***Correspondence:**
Michael Ortiz-Rios and Josef P. Rauschecker, Department of Neuroscience, Georgetown University Medical Center, NRB WP19, 3970 Reservoir Rd. NW, Washington, DC 20057, USA
michael.ortiz@tuebingen.mpg.de; rauschej@georgetown.edu

Specialty section:
This article was submitted to Auditory Cognitive Neuroscience, a section of the journal Frontiers in Neuroscience

Received: *30 December 2014*
Accepted: *17 March 2015*
Published: *01 April 2015*

Citation:
Ortiz-Rios M, Kuśmierek P, DeWitt I, Archakov D, Azevedo FAC, Sams M, Jääskeläinen IP, Keliris GA and Rauschecker JP (2015) Functional MRI of the vocalization-processing network in the macaque brain. Front. Neurosci. 9:113. doi: 10.3389/fnins.2015.00113

Using functional magnetic resonance imaging in awake behaving monkeys we investigated how species-specific vocalizations are represented in auditory and auditory-related regions of the macaque brain. We found clusters of active voxels along the ascending auditory pathway that responded to various types of complex sounds: inferior colliculus (IC), medial geniculate nucleus (MGN), auditory core, belt, and parabelt cortex, and other parts of the superior temporal gyrus (STG) and sulcus (STS). Regions sensitive to monkey calls were most prevalent in the anterior STG, but some clusters were also found in frontal and parietal cortex on the basis of comparisons between responses to calls and environmental sounds. Surprisingly, we found that spectrotemporal control sounds derived from the monkey calls ("scrambled calls") also activated the parietal and frontal regions. Taken together, our results demonstrate that species-specific vocalizations in rhesus monkeys activate preferentially the auditory ventral stream, and in particular areas of the antero-lateral belt and parabelt.

Keywords: auditory cortex, monkey, species-specific calls, spectrotemporal features, higher-level representations

Introduction

The concept of two streams in auditory cortical processing, analogous to that in visual cortex (Mishkin et al., 1983), was proposed more than a decade ago (Rauschecker, 1998a; Rauschecker and Tian, 2000). The concept was supported by contrasting patterns of anatomical connections in the macaque from anterior/ventral and posterior/dorsal belt regions of auditory cortex to segregated domains of lateral prefrontal cortex (Romanski et al., 1999) and by different physiological properties of these belt regions. In particular, the anterior lateral belt (area AL) in the macaque exhibited enhanced selectivity for the identity of sounds (monkey vocalizations), whereas the caudal lateral belt (area CL) was particularly selective to sound location (Tian et al., 2001; see also Kuśmierek and Rauschecker, 2014). Evidence for segregated streams of auditory cortical processing has also been provided in human studies (Maeder et al., 2001; Arnott et al., 2004; Ahveninen et al., 2006).

Use of species-specific vocalizations for auditory stimulation in the macaque is of particular interest in the context of the ongoing debate about the evolution of speech and language (Rauschecker, 2012; Bornkessel-Schlesewsky et al., 2015). Comparative approaches have focused

on identifying the common neural networks involved in the processing of speech in humans and of vocalizations in non-human primates (Gil-da-Costa et al., 2004; Frey et al., 2008, 2014; Petrides and Pandya, 2009; Joly et al., 2012b). Monkey calls convey semantic information about objects and events in the environment as well as about affective states of individuals, similar to information contained in human communication sounds and speech (Cheney and Seyfarth, 1990; Ghazanfar and Hauser, 1999; Yovel and Belin, 2013). An open question regarding the vocalization-processing network in the macaque brain is whether it also carries information about the motor actions necessary to produce the vocalizations, as has been shown in humans listening to speech and music (Wilson et al., 2004; Leaver et al., 2009).

Several studies have examined the representation of complex sounds, including vocalizations, in the macaque brain using neuroimaging techniques (Poremba et al., 2003; Petkov et al., 2008; Joly et al., 2012b). In particular, the first fMRI study by Petkov et al. (2008) found activation specific to monkey vocalizations in the anterior STG region. One of the aims in later studies has been to characterize the physiological properties of the anterior superior temporal (aSTG) region that shows sensitivity to higher-level spectrotemporal features in vocalizations (Russ et al., 2008; Kikuchi et al., 2010, 2014; Perrodin et al., 2011; Fukushima et al., 2014). A recent comparative study by Joly et al. (2012b) replicated and extended these results by analyzing fMRI images of the entire brain and found an involvement of orbitofrontal cortex in the processing of monkey vocalizations. Given that the ventral pathway continues into orbitofrontal and ventrolateral prefrontal cortex (vlPFC) (Barbas, 1993; Romanski et al., 1999; Cohen et al., 2007; Petkov et al., 2015), this finding is of particular interest.

In humans, the ventral auditory pathway is thought to be particularly involved in the recognition and identification of vocalizations as well as speech (Binder et al., 2000; DeWitt and Rauschecker, 2012). By contrast, the dorsal pathway is involved primarily in processing sound source location and motion in both humans and animals (Maeder et al., 2001; Tian et al., 2001; Arnott et al., 2004). However, a recent proposal, derived from both human and non-human primate studies, suggests that the dorsal stream may also play a role in sensorimotor integration and control of complex sounds, including speech (Rauschecker and Scott, 2009; Rauschecker, 2011). Thus, activation of frontal and parietal regions might also be expected when monkeys are presented with conspecific vocalization sounds.

Here we identified which brain regions of the macaque monkey are sensitive to conspecific vocalizations using whole-brain functional magnetic resonance imaging (fMRI). We found the most distinct activation in the anterior STG and along the auditory ventral stream, but some clusters of activation were also found in prefrontal, premotor, and parietal cortex when comparing monkey vocalizations to environmental sounds. These findings are discussed in terms of their functional significance.

Materials and Methods

Subjects

Two male rhesus monkeys *(Macaca mulatta)* weighing 10–12 kg participated in our awake-fMRI experiments. Each animal was implanted with an MRI-compatible headpost (Applied Prototype) secured to the skull with ceramic screws (Thomas Recording), plastic strips, and bone cement (Osteobond, Zimmer). All surgical procedures were performed under general anesthesia with isoflurane (1–2%) following pre-anesthetic medication with ketamine (13 mg/kg) and midazolam (0.12 mg/kg). The experiments were approved by the Georgetown University Animal Care and Use Committee and conducted in accordance with standard NIH guidelines.

Behavioral Training

To ensure the monkeys attended to each stimulus for which a brain volume was acquired, we adapted a go/no-go auditory discrimination task (Kuśmierek and Rauschecker, 2009; Kikuchi et al., 2010) for sparse-sampling functional MRI.

First, each monkey was trained to lie in sphinx position in an MRI-compatible primate chair (Applied Prototype) placed inside a double-walled acoustic chamber simulating the scanner environment. Inside the chamber, the animals were trained to be accustomed to wearing headphone equipment and hearing (simulated) scanner noise, presented by a loudspeaker. Eye movements were monitored using an infrared eye-tracking system (ISCAN). Analog output of the tracker was sampled with an analog-to-digital conversion device (National Instruments). A PC running Presentation software (Neurobehavioral Systems) was used to present visual and auditory stimuli, control the reward system, and trigger imaging data acquisition (see below).

After the animal completed the fixation training, a go/no-go auditory discrimination task was introduced, in which the monkeys could initiate a trial by holding fixation on a central red spot while a block of auditory stimuli would be simultaneously presented. After the first 6 s of auditory stimulation, a trigger was sent to the scanner, starting the acquisition of an image volume (**Figure 1B**). Following acquisition and a random delay, the target sound (white noise) was presented, cueing a saccade to the left or to the right side as signaled at the beginning of each experimental session (**Figure 1A**). To provide feedback, after the response window, a yellow spot was shown indicating the correct target location. Finally, contingent on performance, the animal received a juice reward. An inter-trial interval of at least 2 s was enforced before the next trial could be initiated by fixation. Every sound presentation trial was followed by a "silence" trial, allowing for measurement of baseline blood oxygen level dependent (BOLD) signal. Monkey 1 (M1) performed the task correctly for over 90% of the trials. Monkey 2 (M2) was not able to perform the saccadic go/no-go discrimination task with high accuracy and was therefore scanned while passively listening to the acoustic stimuli. To ensure stable attention, M2 was rewarded for successfully holding fixation throughout the trial.

Auditory Stimuli

Three sound categories were used in the experiments: environmental sounds (Env), monkey vocalizations or calls (MC), and scrambled monkey calls (SMC). Spectrograms of example clips from each of these three categories are illustrated in **Figure 1C.** Environmental sounds were obtained from multiple

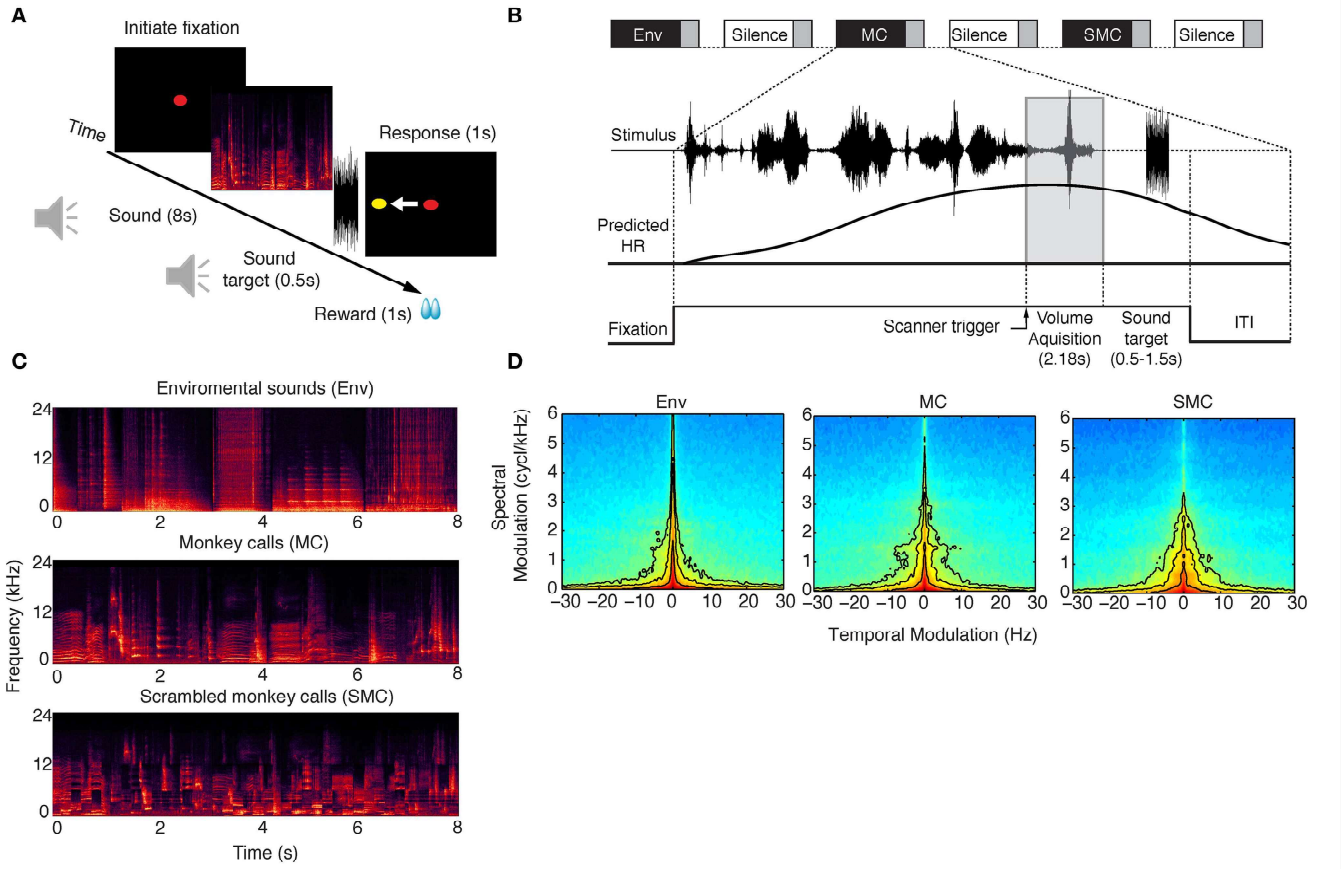

FIGURE 1 | Behavioral paradigm and example stimuli for each sound category. (A) The monkey had to keep fixation on a central spot while stimuli were presented from one of three sound categories: environmental sounds (Env), monkey calls (MC) and scrambled monkey calls (SMC). Next, a target sound (white noise, 500 ms) was played after a random delay of 0.5–1.5 s at the end of each stimulus period, and the animals were required to make a saccade to an imaginary cue position (yellow cue). The imaginary target was chosen to be either on the left or the right side of the screen, and the animal was instructed at the beginning of each session where the target was going to appear (see Materials and Methods). **(B)** All conditions were presented in a sparse-sampling design to avoid interference between the hemodynamic response (HR) generated by the scanner noise and by the stimuli. The inter-trial interval (ITI) lasted for 2 s, and the monkey was then allowed to start a new trial by initiating fixation once again. **(C)** Eight-second series of spectrograms from the three sound categories presented. **(D)** Average modulation spectra for each stimulus category. Pearson correlations between average modulation spectra were: MC vs. SMC = 0.92, MC vs. Env = 0.86.

online sources and from recordings made in our laboratory facilities (Kuśmierek and Rauschecker, 2009). They included the sounds of vehicles, cages, water, food containers, clocks, cameras, applause, coins, footsteps, chewing, heartbeats, horns, and telephones ($n = 56$). The mean duration of the Env stimuli was 1.14 s (range: 0.96–2.6 s). Monkey calls were obtained from recordings made outside our colony [M. Hauser and/or Laboratory of Neuropsychology (LN) library]. Monkey vocalizations ($n = 63$) consisted of grunts, barks, warbles, coos, and screams, as used in prior studies (Rauschecker et al., 1995; Tian et al., 2001; Kuśmierek et al., 2012). The mean duration of the vocalization stimuli was 0.67 s (range: 0.13–2.34 s). SMC were generated by randomly rearranging 200 ms by 1-octave tiles of the constant-Q spectrogram (Brown, 1991) for each monkey call and reconstructing a time-domain waveform with an inverse transform (Schörkhuber and Klapuri, 2010). Transposition along the time axis was not constrained while transposition along the frequency axis was restricted to displacement by a single octave. For each trial, a random selection of stimuli from one class (MC, Env, or SMC) was arranged sequentially into a smooth auditory clip that lasted for the duration of the trial (8 s).

Sounds were presented through modified electrostatic in-ear headphones (SRS-005S + SRM-252S, STAX), mounted on ear-mold impressions of each animal's pinna (Sarkey Eden Prairie) and covered with a custom-made earmuff system for sound attenuation. To match loudness, the stimuli were played through the sound presentation system and re-recorded with a probe microphone (Brüel and Kjær, type 4182 SPL meter) inserted in the ear-mold of an anesthetized monkey. The recordings were then filtered with an inverted macaque audiogram (Jackson et al., 1999) to simulate the effect of different ear sensitivity at different frequencies, analogous to the dB(A) scale for humans. The stimuli were finally equalized so that they produced equal maximum root mean square (RMS) amplitude (using

a 200-ms sliding window) in filtered recordings (Kuśmierek and Rauschecker, 2009). During experiments, all stimuli were amplified (Yamaha AX-496) and delivered at a calibrated RMS amplitude of ∼80 dB SPL.

Analyses of Sound Categories

A modulation spectrum analysis (Singh and Theunissen, 2003) was performed for each sound with the STRFpak Matlab toolbox (http://strfpak.berkeley.edu). We obtained a spectrogram of each sound by decomposing it into frequency bands using a bank of Gaussian filters (244 bands, filter width = 125 Hz). The filters were evenly spaced on the frequency axis (64–48,000 Hz) and separated from each other by one standard deviation. The decomposition resulted in a set of narrow-band signals, which were then cross-correlated with each other and themselves to yield a cross-correlation matrix. This matrix was calculated for time delays of ±150 ms, and the two-dimensional Fourier transform of this matrix was calculated to obtain the modulation spectrum of each sound (**Figure 1D**).

Data Acquisition

Images were acquired with a horizontal MAGNETOM Trio 3-T scanner (Siemens) with a 60-cm bore diameter. A 12-cm custom-made saddle shape radiofrequency coil (Windmiller Kolster Scientific) covered the entire brain and was optimized for imaging the temporal lobe. The time series consisted of gradient-echo echo-planar (GE-EPI) whole-brain images obtained in a sparse acquisition design. Sparse sampling allows single volumes to be recorded coincidentally with the predicted peak of the evoked hemodynamic response (Hall et al., 1999). This helps to avoid contamination of the measured stimulus-specific BOLD response by the scanner-noise-evoked BOLD response. Further, by triggering acquisition 6 s after stimulus onset, the auditory stimulus was presented without acoustic interference from gradient-switching noise, typical of a continuous fMRI design. For the functional data, individual volumes with 25 ordinal slices were acquired with an interleaved single-shot GE-EPI sequence (TE = 34 ms, TA = 2.18 s, flip angle = 90°, field of view (FOV) = 100 × 100 mm^2, matrix size = 66 × 66 voxels, slice thickness = 1.9 mm, voxel size = 1.5 × 1.5 × 1.9 mm^3). On each experiment day, a low-resolution FLASH anatomical scan was acquired with the same geometry as the functional images (TE = 14 ms, TR = 3 s, TA = 2.18 s, FOV = 100 × 100 mm^2, matrix = 512 × 512 voxels, slice thickness = 1.9 mm, number of averages = 2, flip angle = 150°). For overlaying our functional images, we created a high-resolution anatomical template (0.5 × 0.5 × 0.5 mm^3 isotropic voxels) by averaging five high-resolution anatomical scans acquired under general anesthesia with an MP-RAGE sequence (TE = 3.0 ms, TR = 2.5 s, flip angle = 8°, FOV = 116 × 96 × 128 mm^3; matrix = 232 × 192 × 256 voxels).

Data Analysis

For M1, nine EPI runs (180 time points each) were acquired over six sessions. For M2, seven runs were acquired over four sessions. All data analyses were performed using AFNI (Cox, 1996) (http://afni.nimh.nih.gov/afni), FreeSurfer (Dale et al., 1999; Fischl et al., 1999) (http://surfer.nmr.mgh.harvard.edu/), SUMA (http://afni.nimh.nih.gov/) and custom code written in Matlab (MathWorks). Preprocessing involved slice timing correction, motion correction (relative to the run-specific mean GE-EPI), spatial smoothing with a 3.0 mm full width at half-maximum Gaussian kernel, and normalization of the time series at each voxel by its mean. All volumes that had motion values with shifts >0.5 mm and/or rotations >0.5° were excluded from further analyses. Lastly, we performed linear least-squares detrending to remove non-specific variations (i.e., scanner drift). Following preprocessing, data were submitted to generalized linear model analyses. The model included three stimulus-specific regressors and six estimated motion regressors of no interest. For each stimulus category (Env, MC, SMC) we estimated a regressor by convolving a one-parameter gamma distribution estimate of the hemodynamic response function with the square-wave stimulus function. We performed *t*-tests contrasting all sounds vs. baseline ("silence" trials), MC vs. Env, and MC vs. SMC. Finally we co-registered and normalized our functional data to the population-average MRI-based template for rhesus monkeys 112RM-SL (McLaren et al., 2009) and then displayed the results on a semi-inflated cortical surface of the template extracted with Freesurfer and displayed with SUMA to facilitate visualization and identification of cortical activations. The anatomical boundaries described here are based on the macaque brain atlas of Saleem and Logothetis (2012).

To quantify the lateralization of the BOLD response across hemispheres we measured a lateralization index [LI = (R_h - L_h)/(R_h + L_h)], where R_h and L_h are the mean responses in the right and left hemisphere, respectively. The LI curve analyses ensure that the lateralization effect is not caused by small numbers of highly activated voxels across hemispheres. The LI curves were based on the *t*-values obtained from each contrast condition and were calculated using the LI-toolbox (Wilke and Lidzba, 2007) with the following options: ±5 mm mid-sagittal exclusive mask, clustering with a minimum of 5 voxels and default bootstrapping parameters (min/max sample size 5/10,000 and bootstrapping set to 25% of data). The bootstrapping method calculates 10,000 times LIs using different thresholds ranging from zero until the maximum *t*-value for a specific contrast condition. For each threshold a cut-off mean value is obtained from which a weighted mean (LI-wm) index value can then be calculated (Wilke and Lidzba, 2007). This yields a single value between −1 and 1 indicating right- or left-sided hemisphere dominance.

Results

Our first goal was to identify brain regions involved in the processing of conspecific vocalizations by the macaque brain. To this end, we collected functional MR images of two monkeys in a horizontal 3-T scanner while stimuli from three different sound categories were presented to the animals. Complex sounds are characterized by having a wide range of spectrotemporal features. While environmental sounds typically contain sharp temporal onsets, monkey vocalizations contain greater modulations in the spectral domain because of the harmonics contained in these sounds. Environmental sounds also carry abstract information

about the identity of objects, so a comparison between BOLD responses to monkey vocalizations and environmental sounds is useful in determining brain structures involved in higher-level processing. However, specific spectrotemporal differences exist between these two types of sounds. This can be seen, for instance, in the spectral modulation of monkey vocalizations at approximately 1.5–2 cycles/kHz, which is not present for other sound categories (**Figure 1D**). Thus, scrambled versions of monkey calls (SMC) were used to further control for the local spectrotemporal features in the vocalizations (see **Figure 1C** and Material and Methods). Comparison of average modulation spectra between categories showed that SMC were acoustically better matched to MC than Env (correlation coefficient between the modulation spectra: SMC vs. MC: 0.92, Env vs. MC: 0.86; **Figure 1D**).

Overall, sound stimulation elicited significant BOLD responses compared to silent trials irrespective of auditory stimulus category [q (FDR) < 0.05, $p < 10^{-3}$, one-tailed t-test, t range: 2.3–10, cluster size > 10 voxels] in a broad network of brain regions, including subcortical auditory pathways, classical auditory areas of the superior temporal gyrus (STG), but also regions in parietal and prefrontal cortices (**Figure 2**). The clusters in **Figure 2A** highlight the main activation sites on the cortical surface of monkey M1. **Figure 2B** shows selected coronal slices for both animals (M1 and M2) showing activation

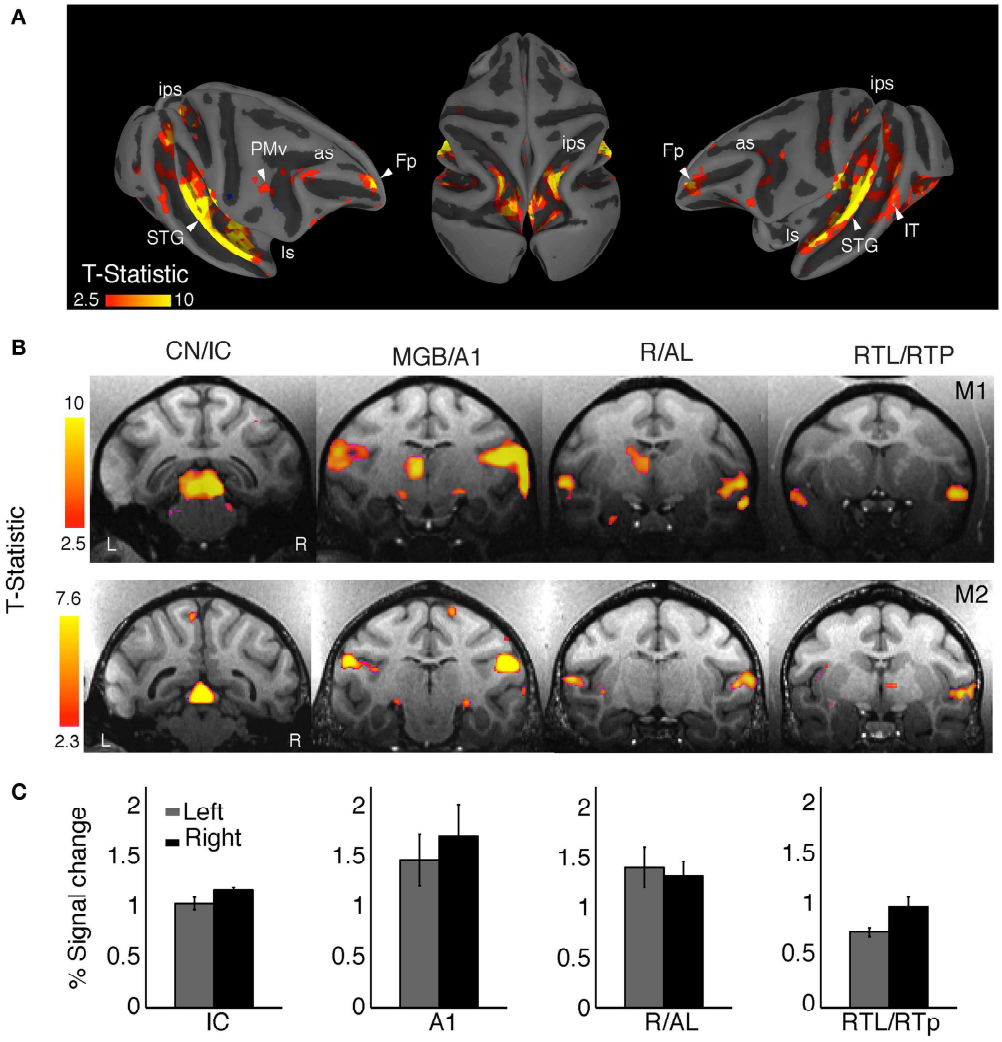

FIGURE 2 | Mapping auditory and auditory-related regions with complex sounds. (A) Representative cortical responses from monkey (M1) for all sound conditions combined (q FDR < 0.05, $p < 10^{-2}$; cluster size > 10 voxels). The projection onto the semi-inflated surface preserves sulcal and gyral landmarks while allowing visualization inside the intraparietal sulcus (ips) and lateral sulcus (ls). Activation was observed along the auditory ventral stream in the superior temporal gyrus (STG), the superior temporal sulcus (STS), ventral intraparietal area (VIP), and the frontal pole (Fp). Activated dorsal-stream regions included the ips and ventral premotor cortex (PMv). Some active clusters were also observed in the middle temporal area (MT) and the inferior temporal cortex (IT). **(B)** Activation was robust across regions in the ascending auditory pathway of the two monkeys: cochlear nuclei (CN), inferior colliculus (IC), medial geniculate nucleus (MGN), primary auditory cortex (A1), rostral area (R), anterolateral area (AL), lateral rostrotemporal area (RTL), and the rostrotemporal pole region (RTp). (**C**) The average BOLD response for the main auditory activation showed a right-hemisphere bias in both animals (M1, weighted mean $= -0.33$, M2, weighted mean $= -0.66$).

in the ascending auditory pathway. These regions include the cochlear nucleus (CN), the inferior colliculus (IC), the medial geniculate nucleus (MGN), the primary auditory cortex (A1), and areas in the anterior superior temporal cortex, including the rostral (R) and anterolateral (AL) areas, the rostrotemporolateral area (RTL), and the rostrotemporal pole (RTp) region.

Activation clusters (averaged across animals and hemispheres) taken from a normalized number of voxels (i.e., equal number of left and right voxels) were found in: IC [$N = 84$ voxels, peak coordinate = (4, −1, 12)]; A1 [$N = 198$ voxels, peak coordinate = (22, 6, 24)]; R/AL [$N = 131$ voxels, peak coordinate = (24, 17, 12)]; and RTL/RTp [$N = 165$ voxels, peak coordinate = (23, 22, 8)].

For both animals we observed a larger amplitude and spatial extent of the BOLD response in the right hemisphere as compared to the left hemisphere (**Figure 2B**). Activation (percent signal change) in selected clusters for each hemisphere is shown in **Figure 2C**. We compared the activation between the two hemispheres by calculating a laterality index (LI), with a positive index indicating a left-hemisphere bias and a negative index indicating a right-hemisphere bias. Given the fact that LIs show a threshold dependency (Nagata et al., 2001), we measured LI curves to provide a more comprehensive estimate over a whole range of thresholds (Wilke and Lidzba, 2007). Using this adaptive thresholding approach we found a right-hemisphere bias in the LI curves for general auditory activation (all sounds vs. baseline) in both monkeys (M1, weighted mean = −0.33; M2, weighted mean = −0.66). For higher thresholds, the activation was clustered in primary auditory cortex (A1) of the right hemisphere in each animal.

Vocalizations are complex naturalistic stimuli that contain behaviorally relevant information. In order to investigate if the auditory system contained representations that are sensitive to this sound category vs. other types of behaviorally relevant complex sounds, we contrasted monkey calls against environmental sounds (see Material and Methods). Environmental sounds also carry abstract information about object identity in their spectrotemporal patterns. We, therefore, also looked for areas showing elevated response to these sounds relative to monkey vocalizations. When correcting for multiple comparisons [q (FDR) < 0.05], no differences were observed for the contrast of MC vs. Env. However, at uncorrected thresholds, we found significantly higher activations by MC as compared to Env in both monkeys across regions in temporal, parietal and prefrontal cortices (M1, $p < 10^{-3}$ uncorrected, t-value range: −4.2 to 6.1, cluster size > 5 voxels; M2, $p < 10^{-2}$ uncorrected, t-value range: −3.6 to 5.9, cluster size > 5 voxels) (**Figure 3A**). Specifically, activations sensitive to MC were found in the anterior STG region, including areas AL and RTp of the rostral belt/parabelt, and further along the auditory ventral stream in ventrolateral prefrontal cortex (vlPFC). In addition, we observed activation patches in the inferior parietal lobule (areas PF/PFG) of the right parietal cortex, and bilaterally inside the inferior branch of the arcuate sulcus, possibly corresponding to Brodmann's area (BA) 44, and posterior to the arcuate sulcus, in a region that is part of ventral premotor cortex (PMv). In addition, we found regions sensitive to environmental sounds (blue) along the superior temporal sulcus (STS) and inferotemporal (IT) cortex. To investigate hemispheric lateralization in the processing of vocalizations, we measured LI curves for this contrast (Mc > Env), finding a slight right hemispheric bias in monkey M1 (weighted mean = −0.19) and a moderate right-hemisphere bias in monkey M2 (weighted mean = −0.42).

In order to determine whether spectrotemporal features alone could have driven the activation in these areas, we further

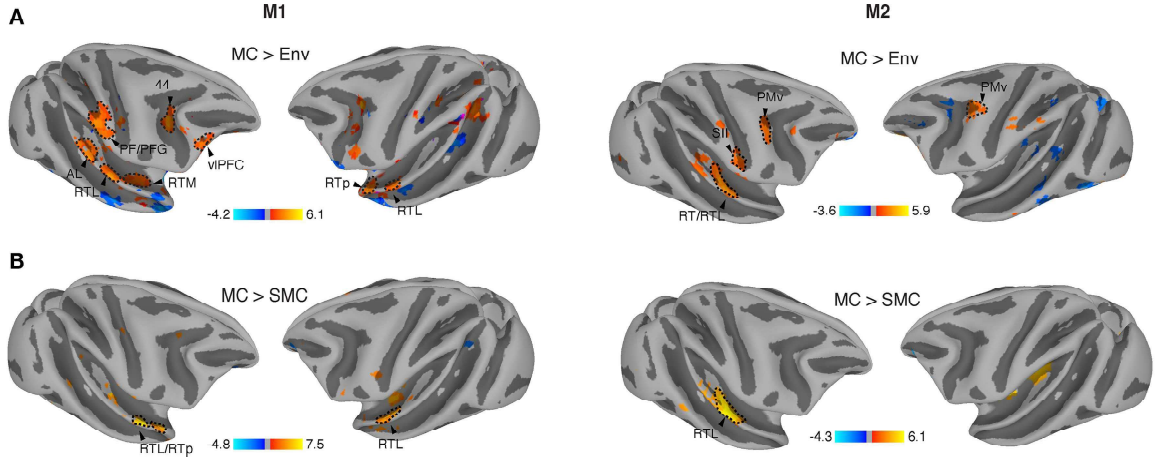

FIGURE 3 | Regions specifically activated by monkey vocalizations. (A) Vocalization-sensitive regions obtained from comparison between the effects of monkey calls and environmental sounds. All activation maps were displayed on a semi-flattened surface of the macaque monkey template. Active regions were found in the anterolateral area (AL), lateral rostrotemporal area (RTL), rostrotemporal pole (RTp), secondary somatosensory (SII) cortex, ventral premotor cortex (PMv), ventrolateral prefrontal cortex (vlPFC), and inferior parietal areas (PF and PFG). **(B)** Regions significantly more activated by monkey vocalizations than by scrambled monkey vocalizations include areas in the anterior STG, RTL/RTp. Red/orange: significantly higher activation by MC than by control sounds (SMC or Env); blue: significantly higher activation by SMC or Env than by MC.

contrasted monkey calls (MC) with scrambled monkey calls (SMC). The results showed similar patterns of MC activation in both monkeys in the RTL region of the aSTG (M1; $p < 10^{-3}$ uncorrected, t-value range > -4.8 to 7.5, cluster size > 5 voxels and for M2, $p < 10^{-2}$ uncorrected, t-value range > -4.3 to 6.1, cluster size > 5 voxels) in both monkeys specifically in the RTL region of the aSTG (**Figure 3B**). In monkey M2, a second region, the middle medial belt (MB), was also more strongly activated by monkey vocalizations than by their scrambled counterparts. The weighted-mean lateralization index (LI) for this contrast (MC > SMc) also showed higher values toward the right hemisphere (M1: weighted mean $= -0.34$; M2: weighted mean $= -0.44$). A summary is shown in **Table 1**.

Some differences in the patterns of activity were observed across the two animals. These differences might be explained either by variability across subjects or by differences in attentional state: M1 was significantly engaged in completing the task (>90% success), whereas M2 was scanned passively while holding fixation. To compensate for this variability, we calculated the minimum t-statistic ($p < 0.01$ uncorrected) across contrasts in each monkey (a conjunction test) and across monkeys in each contrast (**Figure 4**). Conjunction across contrasts (MC > Env and MC > SMC) and monkeys (M1 and M2) found a single area in the right hemisphere to be specifically involved across both conjunction analyses, area RTL/RTp (peak coordinate: 24, 17, 12).

Discussion

Species-specific vocalizations in non-human primates ("monkey calls") convey important information about affective/emotional states as well as the recognition of objects and individuals (Ghazanfar and Hauser, 1999). We used whole-brain functional magnetic resonance imaging (fMRI) in awake behaving monkeys to examine auditory responses to stimuli from three different sound categories: (a) multiple types of conspecific monkey calls, (b) environmental sounds, and (c) scrambled versions of the same monkey calls largely preserving their local spectrotemporal features.

For all three sound categories combined we found robust BOLD responses along various regions in the ascending auditory pathways (CN, IC, MGB, and A1, **Figures 2A,B**). These results, using a 3-T scanner without contrast agent, corroborate previous fMRI findings obtained on a 1.5-T magnet with the contrast agent MION, showing activation by complex sounds along the auditory pathway (Joly et al., 2012a). The results further attest to the fact that complex sounds are highly effective for mapping subcortical and cortical auditory structures (Rauschecker et al., 1995; Rauschecker, 1998b; Poremba et al., 2003). Furthermore, our results confirm the general trend of a slight right-hemisphere bias (**Table 1**) in the processing of complex sounds in the macaque auditory cortex, as measured with fMRI (Petkov et al., 2008; Joly et al., 2012a). Similar results have been found in humans for non-speech voice sounds (Belin et al., 2000).

When we compared activations produced by monkey vocalizations vs. the other two sound categories using a conjunction analysis, we found consistent activations in regions along the anterior STG, in particular in areas AL, RTL and RTp, in both animals (**Figure 4**). Our results extend previous findings of increased sensitivity to monkey vocalizations in anterior STG regions (Poremba et al., 2003; Petkov et al., 2008; Kikuchi et al., 2010; Joly et al., 2012a,b; Fukushima et al., 2014) by using control stimuli (SMC) that retained the low-level acoustic information of macaque vocalizations and whose acoustic structure was better matched to the vocalizations than the acoustic structure of other complex sounds (**Figure 1D**). Single-unit studies of the R/AL region have also found increased selectivity either to monkey calls, or to sound categories including vocalizations (Tian et al., 2001; Kuśmierek et al., 2012), consistent with the present results (**Figures 3**, **4**).

Thus, the cortical representation of vocalizations involves an auditory ventral pathway, consisting of a chain of interconnected regions in anterior STG and vlPFC that extract abstract information for the recognition and categorization of vocalizations (Rauschecker, 2012). The rostral belt, parabelt and aSTG send afferent projections into ventrolateral, polar, orbital, and medial regions of the prefrontal cortex (PFC) (Jones and Powell, 1970; Hackett et al., 1999; Romanski et al., 1999; Cavada et al., 2000; Kaas and Hackett, 2000; Hackett, 2011; Yeterian et al., 2012), and together these regions form the ventral cortical stream in audition. Vocalization-sensitive neurons are found along with face-sensitive neurons in the vlPFC (Romanski et al., 2005), allowing these regions to integrate vocalizations with the corresponding facial gestures (Romanski and Goldman-Rakic, 2002; Cohen et al., 2007; Diehl and Romanski, 2014). The PFC is involved in higher-level integrative processes for the cognitive control of vocalizations as well as in the interpretation of semantic content in vocalizations (Romanski and Averbeck, 2009). The activation patterns observed in PFC (**Figure 3A**) could represent categorical or affective information reflected in the vocalizations. Further imaging studies and multivariate analyses comparing multiple vocalization types might elucidate the differential contribution of each subregion of the PFC.

Our stimuli also activated higher-level visual areas, such as the middle temporal (MT) and inferior temporal areas (IT). These areas are known to be involved in the processing of visual motion (Maunsell and Van Essen, 1983) and in object perception (including faces), respectively (Tsao et al., 2006; Ku et al., 2011). Their activation by purely auditory stimuli raises interesting questions

TABLE 1 | LI-weighted-mean values for the overall sound activation and for each contrast condition.

	All > baseline	MC > Env	MC > SMC
M1	−0.33	−0.19	−0.34
M2	−0.66	−0.42	−0.44

Mean lateralization index values (LI-wm) are shown that were obtained from LI curves measured as a function of the statistical threshold (t-value) for the overall auditory activation (all sounds vs. baseline), for the contrast between monkey calls and environmental sounds (MC > Env) and for the contrast between monkey calls and scrambled monkey calls (MC > SMC). A positive index indicates a left-hemisphere bias, while a negative index indicates a right-hemisphere bias. LI-wm values are shown separately for monkeys M1 and M2.

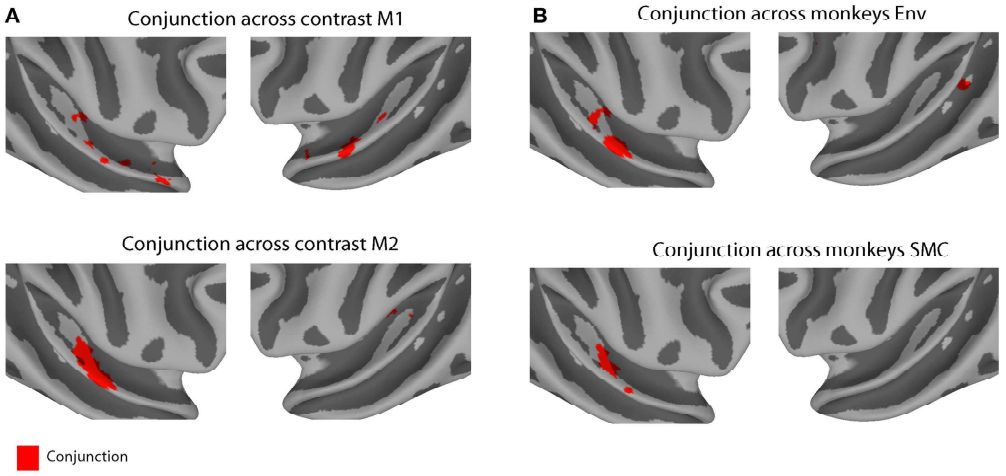

FIGURE 4 | Conjunction results across contrast conditions and across monkeys. (A) Conjunction across contrast (MC > Env and MC > SMC) for monkey M1 (n voxels = 235, top panel) and for monkey M2 (n voxels = 89, lower panel). **(B)** Conjunction across monkeys (M1 and M2) for contrast MC > Env (n voxels = 248, top panel) and for contrast MC > SMC (n voxels = 58, lower panel). Each individual contrast map was thresholded at $p < 0.01$ (uncorrected). Red region indicates conjunction voxels that were differentially activated for both contrasts in each monkey or in both monkeys for each contrast.

regarding their possible role in the multisensory processing of dynamic audio-visual stimuli, such as facial expressions that naturally occur in conjunction with vocalizations and/or motion of the face (Furl et al., 2012; Polosecki et al., 2013; Perrodin et al., 2014). However, to answer these questions more definitively, further imaging experiments utilizing dynamic audio-visual stimuli would be necessary. Such studies could enlighten us on how auditory information combines with visual information in both the ventral and dorsal pathways building multimodal representations from dynamic facial expressions combined with vocalizations (Ghazanfar and Logothetis, 2003).

When we contrasted monkey calls to environmental sounds, we also found differential activation in regions PF/PFG (area 7b) (Pandya and Seltzer, 1982; Rozzi et al., 2006) of the inferior parietal lobule (IPL), in addition to the well-known regions in the STG sensitive to monkey vocalizations. Parietal regions inside the intraparietal sulcus (IPS) have been known to receive auditory projections (Lewis and Van Essen, 2000) and to contain neurons that respond to auditory and multimodal stimuli (Stricanne et al., 1996; Bushara et al., 1999; Grunewald et al., 1999; Cohen and Andersen, 2000; Cohen, 2009), but the role of these regions has traditionally been assumed to lie in spatial processing and control of eye movements.

Similarly, we found an engagement of the ventral premotor cortex (PMv) in the processing of monkey vocalizations (**Figure 3A**). This region has previously been thought to be involved in the processing of the location (but not quality) of nearby sounds (Graziano et al., 1999). Surprisingly, when we compared the effects of vocalizations (MC) against vocalizations that were scrambled in both the spectral and temporal domains (SMC), we did not observe greater activation in parietal or prefrontal areas for MC, suggesting that the scrambled versions of the MC evoked the same amount of activity in these regions. Similar results were obtained by Joly et al. (2012b) with temporally scrambled vocalizations activating large regions of premotor and parietal cortices. Ventral premotor cortex (PMv) has also been implicated in the initiation of vocalizations in the macaque monkey (Hage and Nieder, 2013). It appears possible, therefore, that the same neurons are the source of an efference copy signal (Kauramäki et al., 2010), which is responsible for the suppression of auditory cortex during self-initiated vocalizations (Eliades and Wang, 2003). More generally, they could be part of an audio-motor network connecting perception and production of sounds (Rauschecker and Scott, 2009; Rauschecker, 2011).

Author contributions

MO co-designed the study, trained the animals, programmed stimulus presentation, acquired part of the data, conducted most analyses, and co-wrote the manuscript. PK programmed the behavioral task and participated in writing the manuscript. DA trained the animals and acquired part of the data. ID generated the scrambled stimuli and acquired part of the data. FA contributed with data analyses and participated in writing the manuscript. GK, interpreted data and participated in writing the manuscript. MS, IJ, and JR co-designed the study and participated in writing the manuscript.

Acknowledgments

Special thanks to Josie Cui for animal care and assistance with the experiments, and John VanMeter for fMRI data optimization. This work was supported by grants from the National Institutes of Health (R01-DC03489, R01-NS052494, and R56-NS052494 to JR), a PIRE Grant from the National Science Foundation (OISE-0730255 to JR), and a FiDiPro award from the Academy of Finland (JR).

References

Ahveninen, J., Jääskeläinen, I. P., Raij, T., Bonmassar, G., Devore, S., Hämäläinen, M., et al. (2006). Task-modulated "what" and "where" pathways in human auditory cortex. *Proc. Natl. Acad. Sci. U.S.A.* 103, 14608–14613. doi: 10.1073/pnas.0510480103

Arnott, S. R., Binns, M. A., Grady, C. L., and Alain, C. (2004). Assessing the auditory dual-pathway model in humans. *Neuroimage* 22, 401–408. doi: 10.1016/j.neuroimage.2004.01.014

Barbas, H. (1993). Organization of cortical afferent input to orbitofrontal areas in the rhesus monkey. *Neuroscience* 56, 841–864. doi: 10.1016/0306-4522(93)90132-Y

Belin, P., Zatorre, R. J., Lafaille, P., Ahad, P., and Pike, B. (2000). Voice-selective areas in human auditory cortex. *Nature* 403, 309–312. doi: 10.1038/35002078

Binder, J. R., Frost, J. A., Hammeke, T. A., Bellgowan, P. S., Springer, J. A., Kaufman, J. N., et al. (2000). Human temporal lobe activation by speech and nonspeech sounds. *Cereb. Cortex* 10, 512–528. doi: 10.1093/cercor/10.5.512

Bornkessel-Schlesewsky, I., Schlesewsky, M., Small, S. L., and Rauschecker, J. P. (2015). Neurobiological roots of language in primate audition: common computational properties. *Trends Cogn. Sci.* 19, 142–150. doi: 10.1016/j.tics.2014.12.008

Brown, J. C. (1991). Calculation of a constant Q spectral transform. *J. Acoust. Soc. Am.* 89, 425. doi: 10.1121/1.400476

Bushara, K. O., Weeks, R. A., Ishii, K., Catalan, M.-J., Rauschecker, J. P., and Hallett, M. (1999). Evidence for modality-specific frontal and parietal areas for auditory and visual spatial localization in humans. *Nat. Neurosci.* 2, 759–766. doi: 10.1038/11239

Cavada, C., Compañy, T., Tejedor, J., Cruz-Rizzolo, R. J., and Reinoso-Suárez, F. (2000). The anatomical connections of the macaque monkey orbitofrontal cortex. A review. *Cereb. Cortex* 10, 220–242. doi: 10.1093/cercor/10.3.220

Cheney, D. L., and Seyfarth, R. M. (1990). *How Monkeys see the World.* Chicago: University of Chicago Press.

Cohen, Y. E. (2009). Multimodal activity in the parietal cortex. *Hear. Res.* 258, 100–105. doi: 10.1016/j.heares.2009.01.011

Cohen, Y. E., and Andersen, R. A. (2000). Reaches to sounds encoded in an eye-centered reference frame. *Neuron* 27, 647–652. doi: 10.1016/S0896-6273(00)00073-8

Cohen, Y. E., Theunissen, F., Russ, B. E., and Gill, P. (2007). Acoustic features of rhesus vocalizations and their representation in the ventrolateral prefrontal cortex. *J. Neurophysiol.* 97, 1470–1484. doi: 10.1152/jn.00769.2006

Cox, R. W. (1996). AFNI: software for analysis and visualization of functional magnetic resonance neuroimages. *Comput. Biomed. Res.* 29, 162–173. doi: 10.1006/cbmr.1996.0014

Dale, A. M., Fischl, B., and Sereno, M. I. (1999). Cortical surface-based analysis. I. Segmentation and surface reconstruction. *Neuroimage* 9, 179–194. doi: 10.1006/nimg.1998.0395

DeWitt, I., and Rauschecker, J. P. (2012). Phoneme and word recognition in the auditory ventral stream. *Proc. Natl. Acad. Sci. U.S.A.* 109, E505–E514. doi: 10.1073/pnas.1113427109

Diehl, M. M., and Romanski, L. M. (2014). Responses of prefrontal multisensory neurons to mismatching faces and vocalizations. *J. Neurosci.* 34, 11233–11243. doi: 10.1523/JNEUROSCI.5168-13.2014

Eliades, S. J., and Wang, X. (2003). Sensory-motor interaction in the primate auditory cortex during self-initiated vocalizations. *J. Neurophysiol.* 89, 2194–2207. doi: 10.1152/jn.00627.2002

Fischl, B., Sereno, M. I., and Dale, A. M. (1999). Cortical surface-based analysis. II: inflation, flattening, and a surface-based coordinate system. *Neuroimage* 9, 195–207. doi: 10.1006/nimg.1998.0396

Frey, S., Campbell, J. S., Pike, G. B., and Petrides, M. (2008). Dissociating the human language pathways with high angular resolution diffusion fiber tractography. *J. Neurosci.* 5, 11435–11444. doi: 10.1523/JNEUROSCI.2388-08.2008

Frey, S., Mackey, S., and Petrides, M. (2014). Cortico-cortical connections of areas 44 and 45B in the macaque monkey. *Brain Lang.* 131, 36–55. doi: 10.1016/j.bandl.2013.05.005

Fukushima, M., Saunders, R. C., Leopold, D. A., Mishkin, M., and Averbeck, B. B. (2014). Differential coding of conspecific vocalizations in the ventral auditory cortical stream. *J. Neurosci.* 34, 4665–4676. doi: 10.1523/JNEUROSCI.3969-13.2014

Furl, N., Hadj-Bouziane, F., Liu, N., Averbeck, B. B., and Ungerleider, L. G. (2012). Dynamic and static facial expressions decoded from motion-sensitive areas in the macaque monkey. *J. Neurosci.* 32, 15952–15962. doi: 10.1523/JNEUROSCI.1992-12.2012

Ghazanfar, A. A., and Logothetis, N. K. (2003). Neuroperception: facial expressions linked to monkey calls. *Nature* 423, 937–938. doi: 10.1038/423937a

Ghazanfar, A., and Hauser, M. (1999). The neuroethology of primate vocal communication: substrates for the evolution of speech. *Trends Cogn. Sci.* 3, 377–384. doi: 10.1016/S1364-6613(99)01379-0

Gil-da-Costa, R., Braun, A., Lopes, M., Hauser, M. D., Carson, R. E., Herscovitch, P., et al. (2004). Toward an evolutionary perspective on conceptual representation: species-specific calls activate visual and affective processing systems in the macaque. *Proc. Natl. Acad. Sci. U.S.A.* 101, 17516–17521. doi: 10.1073/pnas.0408077101

Graziano, M. S., Reiss, L. A., and Gross, C. G. (1999). A neuronal representation of the location of nearby sounds. *Nature* 397, 428–430. doi: 10.1038/17115

Grunewald, A., Linden, J. F., and Andersen, R. A. (1999). Responses to auditory stimuli in macaque lateral intraparietal area. I. Effects of training. *J. Neurophysiol.* 82, 330–342.

Hackett, T. A. (2011). Information flow in the auditory cortical network. *Hear. Res.* 271, 133–146. doi: 10.1016/j.heares.2010.01.011

Hackett, T. A., Stepniewska, I., and Kaas, J. H. (1999). Prefrontal connections of the parabelt auditory cortex in macaque monkeys. *Brain Res.* 817, 45–58. doi: 10.1016/S0006-8993(98)01182-2

Hage, S. R., and Nieder, A. (2013). Single neurons in monkey prefrontal cortex encode volitional initiation of vocalizations. *Nat. Commun.* 4:2409. doi: 10.1038/ncomms3409

Hall, D. A., Haggard, M. P., Akeroyd, M. A., Palmer, A. R., Summerfield, A. Q., Elliott, M. R., et al. (1999). "Sparse" temporal sampling in auditory fMRI. *Hum. Brain Mapp.* 7, 213–223.

Jackson, L. L., Heffner, R. S., and Heffner, H. E. (1999). Free-field audiogram of the Japanese macaque (*Macaca fuscata*). *J. Acoust. Soc. Am.* 106, 3017–3023. doi: 10.1121/1.428121

Joly, O., Pallier, C., Ramus, F., Pressnitzer, D., Vanduffel, W., and Orban, G. A. (2012b). Processing of vocalizations in humans and monkeys: a comparative fMRI study. *Neuroimage* 62, 1376–1389. doi: 10.1016/j.neuroimage.2012.05.070

Joly, O., Ramus, F., Pressnitzer, D., Vanduffel, W., and Orban, G. A. (2012a). Interhemispheric differences in auditory processing revealed by fMRI in awake rhesus monkeys. *Cereb. Cortex* 22, 838–853. doi: 10.1093/cercor/bhr150

Jones, E. G., and Powell, T. P. (1970). An anatomical study of converging sensory pathways within the cerebral cortex of the monkey. *Brain* 93, 793–820. doi: 10.1093/brain/93.4.793

Kaas, J. H., and Hackett, T. A. (2000). Subdivisions of auditory cortex and processing streams in primates. *Proc. Natl. Acad. Sci. U.S.A.* 97, 11793–11799. doi: 10.1073/pnas.97.22.11793

Kauramäki, J., Jääskeläinen, I. P., Hari, R., Möttönen, R., Rauschecker, J. P., and Sams, M. (2010). Transient adaptation of auditory cortex organization by lipreading and own speech production. *J. Neurosci.* 30, 1314–1321. doi: 10.1523/JNEUROSCI.1950-09.2010

Kikuchi, Y., Horwitz, B., and Mishkin, M. (2010). Hierarchical auditory processing directed rostrally along the monkey's supratemporal plane. *J. Neurosci.* 30, 13021–13030. doi: 10.1523/JNEUROSCI.2267-10.2010

Kikuchi, Y., Horwitz, B., Mishkin, M., and Rauschecker, J. P. (2014). Processing of harmonics in the lateral belt of macaque auditory cortex. *Front. Neurosci.* 8:204. doi: 10.3389/fnins.2014.00204

Ku, S.-P., Tolias, A. S., Logothetis, N. K., and Goense, J. (2011). fMRI of the face-processing network in the ventral temporal lobe of awake and anesthetized macaques. *Neuron* 70, 352–362. doi: 10.1016/j.neuron.2011.02.048

Kuśmierek, P., Ortiz, M., and Rauschecker, J. P. (2012). Sound-identity processing in early areas of the auditory ventral stream in the macaque. *J. Neurophysiol.* 107, 1123–1141. doi: 10.1152/jn.00793.2011

Kuśmierek, P., and Rauschecker, J. P. (2009). Functional specialization of medial auditory belt cortex in the alert rhesus monkey. *J. Neurophysiol.* 102, 1606–1622. doi: 10.1152/jn.00167.2009

Kuśmierek, P., and Rauschecker, J. P. (2014). Selectivity for space and time in early areas of the auditory dorsal stream in the rhesus monkey. *J. Neurophysiol.* 111, 1671–1685. doi: 10.1152/jn.00436.2013

Leaver, A. M., Van Lare, J., Zielinski, B., Halpern, A. R., and Rauschecker, J. P. (2009). Brain activation during anticipation of sound sequences. *J. Neurosci.* 29, 2477–2485. doi: 10.1523/JNEUROSCI.4921-08.2009

Lewis, J. W., and Van Essen, D. C. (2000). Corticocortical connections of visual, sensorimotor, and multimodal processing areas in the parietal lobe of the macaque monkey. *J. Comp. Neurol.* 428, 112–137. doi: 10.1002/1096-9861(20001204)428:1<112::AID-CNE8>3.0.CO;2-9

Maeder, P. P., Meuli, R. A., Adriani, M., Bellmann, A., Fornari, E., Thiran, J. P., et al. (2001). Distinct pathways involved in sound recognition and localization: a human fMRI study. *Neuroimage* 14, 802–816. doi: 10.1006/nimg.2001.0888

Maunsell, J. H., and Van Essen, D. C. (1983). Functional properties of neurons in middle temporal visual area of the macaque monkey. I. Selectivity for stimulus direction, speed, and orientation. *J. Neurophysiol.* 49, 1127–1147.

McLaren, D. G., Kosmatka, K. J., Oakes, T. R., Kroenke, C. D., Kohama, S. G., Matochik, J. A., et al. (2009). A population-average MRI-based atlas collection of the rhesus macaque. *Neuroimage* 45, 52–59. doi: 10.1016/j.neuroimage.2008.10.058

Mishkin, M., Ungerleider, L. G., and Macko, K. A. (1983). Object vision and spatial vision: two cortical pathways. *Trends Neurosci.* 6, 414–417. doi: 10.1016/0166-2236(83)90190-X

Nagata, S. I., Uchimura, K., Hirakawa, W., and Kuratsu, J. I. (2001). Method for quantitatively evaluating the lateralization of linguistic function using functional MR imaging. *AJNR. Am. J. Neuroradiol.* 22, 985–991. Available online at: http://www.ajnr.org/content/22/5/985.long

Pandya, D. N., and Seltzer, B. (1982). Intrinsic connections and architectonics of posterior parietal cortex in the rhesus monkey. *J. Comp. Neurol.* 204, 196–210. doi: 10.1002/cne.902040208

Perrodin, C., Kayser, C., Logothetis, N. K., and Petkov, C. I. (2011). Voice cells in the primate temporal lobe. *Curr. Biol.* 21, 1408–1415. doi: 10.1016/j.cub.2011.07.028

Perrodin, C., Kayser, C., Logothetis, N. K., and Petkov, C. I. (2014). Auditory and visual modulation of temporal lobe neurons in voice-sensitive and association cortices. *J. Neurosci.* 34, 2524–2537. doi: 10.1523/JNEUROSCI.2805-13.2014

Petkov, C. I., Kayser, C., Steudel, T., Whittingstall, K., Augath, M., and Logothetis, N. K. (2008). A voice region in the monkey brain. *Nat. Neurosci.* 11, 367–374. doi: 10.1038/nn2043

Petkov, C. I., Kikuchi, Y., Milne, A., Mishkin, M., Rauschecker, J. P., and Logothetis, N. K. (2015). Different forms of effective connectivity in primate frontotemporal pathways. *Nat. Commun.* 6:6000. doi: 10.1038/ncomms7000

Petrides, M., and Pandya, D. N. (2009). Distinct parietal and temporal pathways to the homologues of Broca's area in the monkey. *PLoS Biol.* 7:e1000170. doi: 10.1371/journal.pbio.1000170

Polosecki, P., Moeller, S., Schweers, N., Romanski, L. M., Tsao, D. Y., and Freiwald, W. A. (2013). Faces in motion: selectivity of macaque and human face processing areas for dynamic stimuli. *J. Neurosci.* 33, 11768–11773. doi: 10.1523/JNEUROSCI.5402-11.2013

Poremba, A., Saunders, R. C., Crane, A. M., Cook, M., Sokoloff, L., and Mishkin, M. (2003). Functional mapping of the primate auditory system. *Science* 299, 568–572. doi: 10.1126/science.1078900

Rauschecker, J. P. (1998a). Parallel processing in the auditory cortex of primates. *Audiol. Neurootol.* 3, 86–103. doi: 10.1159/000013784

Rauschecker, J. P. (1998b). Cortical processing of complex sounds. *Curr. Opin. Neurobiol.* 8, 516–521. doi: 10.1016/S0959-4388(98)80040-8

Rauschecker, J. P. (2011). An expanded role for the dorsal auditory pathway in sensorimotor control and integration. *Hear. Res.* 271, 16–25. doi: 10.1016/j.heares.2010.09.001

Rauschecker, J. P. (2012). Ventral and dorsal streams in the evolution of speech and language. *Front. Evol. Neurosci.* 4:7. doi: 10.3389/fnevo.2012.00007

Rauschecker, J. P., and Scott, S. K. (2009). Maps and streams in the auditory cortex: nonhuman primates illuminate human speech processing. *Nat. Neurosci.* 12, 718–724. doi: 10.1038/nn.2331

Rauschecker, J. P., and Tian, B. (2000). Mechanisms and streams for processing of "what" and "where" in auditory cortex. *Proc. Natl. Acad. Sci. U.S.A.* 97, 11800–11806. doi: 10.1073/pnas.97.22.11800

Rauschecker, J. P., Tian, B., and Hauser, M. (1995). Processing of complex sounds in the macaque nonprimary auditory cortex. *Science* 268, 111–114. doi: 10.1126/science.7701330

Romanski, L. M., and Averbeck, B. B. (2009). The primate cortical auditory system and neural representation of conspecific vocalizations. *Annu. Rev. Neurosci.* 32, 315–346. doi: 10.1146/annurev.neuro.051508.135431

Romanski, L. M., Averbeck, B. B., and Diltz, M. (2005). Neural representation of vocalizations in the primate ventrolateral prefrontal cortex. *J. Neurophysiol.* 93, 734–747. doi: 10.1152/jn.00675.2004

Romanski, L. M., and Goldman-Rakic, P. S. (2002). An auditory domain in primate prefrontal cortex. *Nat. Neurosci.* 5, 15–16. doi: 10.1038/nn781

Romanski, L. M., Tian, B., Fritz, J., Mishkin, M., Goldman-Rakic, P. S., and Rauschecker, J. P. (1999). Dual streams of auditory afferents target multiple domains in the primate prefrontal cortex. *Nat. Neurosci.* 2, 1131–1136. doi: 10.1038/16056

Rozzi, S., Calzavara, R., Belmalih, A., Borra, E., Gregoriou, G. G., Matelli, M., et al. (2006). Cortical connections of the inferior parietal cortical convexity of the macaque monkey. *Cereb. Cortex* 16, 1389–1417. doi: 10.1093/cercor/bhj076

Russ, B. E., Ackelson, A. L., Baker, A. E., and Cohen, Y. E. (2008). Coding of auditory-stimulus identity in the auditory non-spatial processing stream. *J. Neurophysiol.* 99, 87–95. doi: 10.1152/jn.01069.2007

Saleem, K. S., and Logothetis, N. K. (2012). *A Combined MRI and Histology Atlas of the Rhesus Monkey Brain in Stereotaxic Coordinates, 2nd Edn., Horizontal, Coronal and Sagittal Series*. San Diego, CA: Elsevier/Academic Press.

Schörkhuber, C., and Klapuri, A. (2010). "Constant-Q transform toolbox for music processing," in *7th Sound and Music Computing Conference* (Barcelona). Available online at: http://www.iem.at/~schoerkhuber/cqt2010/

Singh, N. C., and Theunissen, F. E. (2003). Modulation spectra of natural sounds and ethological theories of auditory processing. *J. Acoust. Soc. Am.* 114, 3394–3411. doi: 10.1121/1.1624067

Stricanne, B., Andersen, R. A., and Mazzoni, P. (1996). Eye-centered, head-centered, and intermediate coding of remembered sound locations in area LIP. *J. Neurophysiol.* 76, 2071–2076.

Tian, B., Reser, D., Durham, A., Kustov, A., and Rauschecker, J. P. (2001). Functional specialization in rhesus monkey auditory cortex. *Science* 292, 290–293. doi: 10.1126/science.1058911

Tsao, D. Y., Freiwald, W. A., Tootell, R. B. H., and Livingstone, M. S. (2006). A cortical region consisting entirely of face-selective cells. *Science* 311, 670–674. doi: 10.1126/science.1119983

Wilke, M., and Lidzba, K. (2007). LI-tool: a new toolbox to assess lateralization in functional MR-data. *J. Neurosci. Methods* 163, 128–136. doi: 10.1016/j.jneumeth.2007.01.026

Wilson, S. M., Saygin, A. P., Sereno, M. I., and Iacoboni, M. (2004). Listening to speech activates motor areas involved in speech production. *Nat. Neurosci.* 7, 701–702. doi: 10.1038/nn1263

Yeterian, E. H., Pandya, D. N., Tomaiuolo, F., and Petrides, M. (2012). The cortical connectivity of the prefrontal cortex in the monkey brain. *Cortex* 48, 58–81. doi: 10.1016/j.cortex.2011.03.004

Yovel, G., and Belin, P. (2013). A unified coding strategy for processing faces and voices. *Trends Cogn. Sci.* 17, 263–271. doi: 10.1016/j.tics.2013.04.004

Conflict of Interest Statement: The authors declare that the research was conducted in the absence of any commercial or financial relationships that could be construed as a potential conflict of interest.

10.4 Widespread and opponent fMRI signals represent sound location in macaque auditory cortex

Article

Neuron

Widespread and Opponent fMRI Signals Represent Sound Location in Macaque Auditory Cortex

Highlights

- Auditory cortex lacks a topographical representation of space
- Each cortical field of the same hemisphere is tuned to the contralateral hemifield
- Hemifield tuning depends on the availability of interaural delay cues
- Posterior-dorsal sensitivity emerges from hemifield tuning

Authors

Michael Ortiz-Rios,
Frederico A.C. Azevedo,
Paweł Kuśmierek, ...,
Georgios A. Keliris,
Nikos K. Logothetis,
Josef P. Rauschecker

Correspondence

michael.ortiz-rios@newcastle.ac.uk

In Brief

Ortiz-Rios et al. use functional MRI in awake and anesthetized macaque monkeys to study the cortical representation of acoustic space and provide new neuroimaging evidence indicating that auditory cortex implements a hemifield code representation. In addition, to identifying the dependency of hemifield tuning with the availability of ITD cues, this study suggests that posterior-dorsal sensitivity for space in cortex of primates might emerge from the opponent signals across hemispheres.

Ortiz-Rios et al., 2017, Neuron *93*, 971–983
February 22, 2017
http://dx.doi.org/10.1016/j.neuron.2017.01.013

CellPress

Neuron
Article

Widespread and Opponent fMRI Signals Represent Sound Location in Macaque Auditory Cortex

Michael Ortiz-Rios,[1,2,3,4,9,*] Frederico A.C. Azevedo,[1,2] Paweł Kuśmierek,[3] Dávid Z. Balla,[1] Matthias H. Munk,[1,5] Georgios A. Keliris,[1,6] Nikos K. Logothetis,[1,7] and Josef P. Rauschecker[3,8]

[1]Department Physiology of Cognitive Processes, Max Planck Institute for Biological Cybernetics, Spemannstraße 36, 72072 Tübingen, Germany
[2]Graduate School of Neural & Behavioural Sciences, International Max Planck Research School (IMPRS), University of Tübingen, Österbergstraße 3, 72074 Tübingen, Germany
[3]Department of Neuroscience, Georgetown University Medical Center, 3970 Reservoir Road, N.W. Washington, D.C., 20057, USA
[4]Institute of Neuroscience, Henry Welcome Building, Medical School, Framlington Place, Newcastle upon Tyne, NE2 4HH, UK
[5]Department of Systems Neurophysiology, Fachbereich Biologie, Technische Universität Darmstadt, Schnittspahnstraße 10, 64287, Darmstadt, Germany
[6]Bio-Imaging Lab, Department of Biomedical Sciences, University of Antwerp, Wilrijk, 2610, Belgium
[7]Division of Imaging Science and Biomedical Engineering, University of Manchester, Manchester, M13 9PL, UK
[8]Institute for Advanced Study of Technische Universität München, Lichtenbergstraße 2 a, 85748 Garching, Germany
[9]Lead Contact
*Correspondence: michael.ortiz-rios@newcastle.ac.uk
http://dx.doi.org/10.1016/j.neuron.2017.01.013

SUMMARY

In primates, posterior auditory cortical areas are thought to be part of a dorsal auditory pathway that processes spatial information. But how posterior (and other) auditory areas represent acoustic space remains a matter of debate. Here we provide new evidence based on functional magnetic resonance imaging (fMRI) of the macaque indicating that space is predominantly represented by a distributed hemifield code rather than by a local spatial topography. Hemifield tuning in cortical and subcortical regions emerges from an opponent hemispheric pattern of activation and deactivation that depends on the availability of interaural delay cues. Importantly, these opponent signals allow responses in posterior regions to segregate space similarly to a hemifield code representation. Taken together, our results reconcile seemingly contradictory views by showing that the representation of space follows closely a hemifield code and suggest that enhanced posterior-dorsal spatial specificity in primates might emerge from this form of coding.

INTRODUCTION

The ability to localize sounds is essential for an animal's survival. In primates, auditory spatial information is thought to be processed along a dorsal auditory pathway (Romanski et al., 1999), a hierarchical system with reciprocal connections that includes caudal belt areas CL/CM of the posterior superior temporal (pST) region (Rauschecker and Tian, 2000; Tian et al., 2001). A central question regarding sound localization in primates is whether sound source location is represented in localized areas of the pST region or distributed throughout auditory cortex (AC).

Original results suggesting regional specificity for sound source localization in posterior regions of AC came independently from neuroimaging studies in humans (Griffiths et al., 1996; Baumgart et al., 1999) and from single-unit recordings in macaque monkeys (Rauschecker and Tian, 2000; Tian et al., 2001). In the macaque, neurons in area CL were found to be sharply tuned to azimuth position in the frontal hemifield and were significantly more selective than in other fields (Tian et al., 2001; Woods et al., 2006). However, recent data in both monkeys (Werner-Reiss and Groh, 2008) and humans (Salminen et al., 2009; Magezi and Krumbholz, 2010; Młynarski, 2015; Derey et al., 2016) suggest that acoustic space is also represented by broadly tuned neurons distributed more widely across AC.

Such evidence is consistent with a different perspective suggesting that acoustic space in AC is coded by opponent neural populations tuned to either side of space (Stecker et al., 2005; Stecker and Middlebrooks, 2003) as similarly found in subcortical structures (Grothe, 2003; McAlpine et al., 2001). Lesion studies in cats (Jenkins and Masterton, 1982; Malhotra et al., 2004), ferrets (Nodal et al., 2012), and monkeys (Heffner and Masterton, 1975) demonstrate that unilateral lesions of AC result in severe localization deficits for sound sources contralateral to the lesion. Similarly, previous single-unit studies in cats (Middlebrooks et al., 1994) and optical imaging experiments in ferrets (Nelken et al., 2008) have provided evidence supporting a more distributed code for sound location in the AC by showing neurons responding maximally and broadly to sound sources near the contralateral ear.

Up to date, it still remains a challenge to record simultaneously and in parallel across multiple and distal cortical regions using

single-unit and optical imaging methodology. Functional magnetic resonance imaging (fMRI) based on blood-oxygen-level-dependent (BOLD) signals provides an alternative and complementary method to study the functional representation of acoustic space across cortical regions (CRs) of each hemisphere.

In the present study, we mapped the frequency organization of AC (Formisano et al., 2003; Petkov et al., 2006) and then measured the BOLD response to spatial sounds obtained from virtual acoustic space. We further analyzed the BOLD responses to spatial sounds with and without interaural time difference (ITD) cues and found a dependency between the presence of ITD cues and contralateral tuning. Finally, we compared the representations of space across CRs with a hemifield code model using representational similarity analyses (RSA).

RESULTS

Our first aim was to identify auditory CRs based on their frequency organization and then map the spatial domain using the same phase-encoding techniques (Barton et al., 2012; Wandell et al., 2007). Auditory stimulation elicited significant BOLD responses along the auditory pathway in both anesthetized and awake monkeys (Figure S1). After optimization, we conducted tonotopic-mapping experiments utilizing tones and narrowband noise stimuli (Figure 1B) that were presented in blocks of one-octave steps in ascending frequency order and repeated in cycles 12 times (Figure S2A). The resulting average BOLD response to each frequency range was narrow and gradually shifted from low-frequency A1 to anterior and posterior regions of AC with a distinct wave pattern of positive BOLD responses (PBRs) and negative BOLD responses (NBRs) (Figure 1C). The PBR/NBR pattern reversed drastically around 2 kHz indicating a shift toward high-frequency regions. Voxels with significant (coherence > 0.3) BOLD modulation (Figures 1D and 1E) to the stimulation rate (0.01 Hz, 12 cycles/1,200 s) were mapped by their scaled phase values to the frequency range of the presented stimuli (0.125–16 kHz) (Figure 1F). Subsequently, we defined four CRs based on their frequency-reversal boundaries with the same population response mediolaterally: Posterior, Primary, Rostral, and Anterior. Each region included core fields and adjacent medial and lateral belt fields (which were not separately delineated) as follows: Posterior (including fields CL, CM), Primary (ML, A1, MM), Rostral (AL, R, RM), and Anterior (RTL, RT, RTM).

We then aimed to map the spatial domain utilizing the same analytical methods but at a stimulation rate of 0.0067 Hz (12 cycles/1,800 s). Prior to these experiments, virtual spatial sounds (broad-band noise bursts, 0.125–16 kHz, 80 dB SPL, 100 ms in duration) were created via binaural sound recordings from each individual monkey (see STAR Methods section binaural recordings). The recorded stimuli contained all individual spatial cues (ITDs, interaural level differences [ILDs], and spectral cues, Figures S3A and S3B). In addition, the virtual noise bursts changed in azimuth direction (leftward, rightward) and in distance within a 30° sector over time (Figure 1G). This innovative design allowed us to keep space partitioned while we estimated the response to spatial sounds within a constrained sector and additionally avoided repetition suppression in the BOLD response. A total of 12 sectors (spanning 30° each) around a virtual plane surrounding the head of the monkey were used to image the BOLD signal.

Compared to sound frequency responses, the mean BOLD responses to spatial sounds were broad and shifted between two opposite phases across the cerebral hemispheres (Figure 1H). Overall, the resulting maps showed no clear topographic organization, but instead reflected the broad peak response across sounds in the contralateral hemifield (Figure 1I). While M2 showed a trend toward a "space map" in the left hemisphere, this result was less clear in the other seven hemispheres. Thus, we investigated phase-peak response across cortical space spanning 10 mm by plotting regions-of-interest (ROI) in voxels crossing along trajectories parallel and orthogonal to the primary field and evidently confirmed a lack of topography in the flat-peak responses (Figure S3C, compared to Figure S3D).

In summary, our mapping experiments corroborated previous electrophysiological (Rauschecker et al., 1995) and imaging studies (Formisano et al., 2003; Petkov et al., 2006) of primate AC showing mirror-symmetric tonotopic maps and provided new evidence indicating that the functional representation of auditory space (in the azimuth plane), as measured with fMRI, lacks a clear spatial topography.

Positive and Negative BOLD Responses across Auditory Regions

How is azimuth space represented in each auditory CR? We investigated our data further by analyzing each time series with a general linear model (GLM) of the BOLD signal. We tested the significance of the model from the measured BOLD responses to each spatial condition (n = 12) as compared to the baseline/silence periods (q FDR < 0.05, $p < 10^{-6}$, cluster size > 10 voxels). Surprisingly, we found distinct patterns of PBRs and NBRs within each hemisphere that changed as a function of each spatial sector (Figure 2A and Figure S4). Spatial tuning curves calculated from the spatial spread of PBRs and NBRs in each AC showed that the overall tuning was of opposite polarity between signals, with PBRs oriented approximately at ±120° and NBRs at ±60° between hemispheres. Similarly, average hemispheric differences in PBRs and NBRs showed opposite polarity between signals, with NBRs showing a peak around frontal right sectors (Figure 2D). The peak for PBRs was observed for sectors near the contralateral ear (e.g., ±90°/120°), with a cluster size extending across much of AC. By contrast, the ipsilateral PBRs were greatly reduced in size and were accompanied by an NBR pattern in anterior and posterior regions of AC. In the primary field, the responses exhibited a concentric pattern (e.g., at +30°–60°) with positive voxels expanding the overall anterior-posterior frequency axis and negative voxels mostly lying anteriorly and posteriorly (Figures 2A and 2B).

The average BOLD signal in CRs of each monkey (mean and ± SEM, including both PBRs and NBRs) showed a marked shift in amplitude around the midline, which further indicated hemifield tuning across all CRs (Figure 2C). Similarly, spatial tuning curves obtained from PBRs showed highly significant deviations from circular uniformity (Rayleigh test, p < 0.001) with angular means oriented in opposite polarity (~ ±120°) between hemispheres

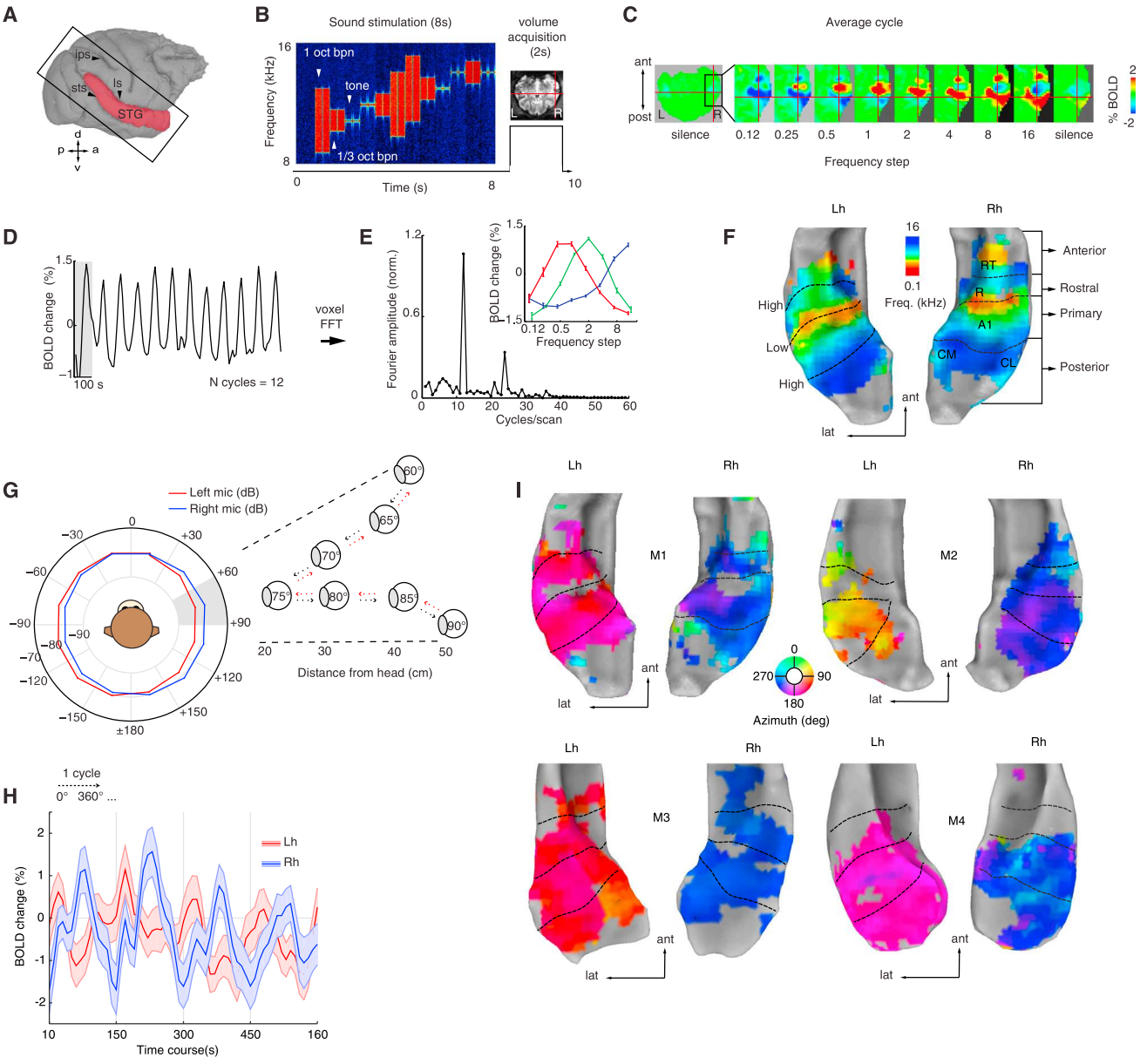

Figure 1. Phase-Mapping for Frequency and Space

(A) Image acquisition plane and extracted surface (red).

(B) Sparse imaging and stimulation design (e.g., high-frequency stimuli, 8–16 kHz).

(C) Average BOLD response to each frequency step in octaves (labeled frequency refers to the upper range of the frequency presented).

(D) Time course of an A1 voxel's BOLD response (crosshair in C) tuned to high frequency. Gray shading represents one presentation cycle.

(E) Fourier transform of the same voxel's BOLD response shows a peak at the stimulation rate (0.01 Hz = 12 cycles/1,200 s). Inset panel, mean ± SEM of 3 voxels in A1 at the peak stimulation rate. Response peaks were used to calculate the preferred phase that translates to preferred sound frequency independently at each voxel.

(F) Resulting tonotopic maps rendered into STG surfaces of each hemisphere. Black dotted lines indicate frequency-reversal boundaries of preferred sound frequency between mirror-symmetric regions. For the awake monkeys (M3 and M4), reversal boundaries were obtained from anatomical reference (Saleem and Logothetis, 2012).

(G) Binaural sound recordings and stimulation design. Mean amplitude of sounds (broad-band noise 0.125–16 kHz) recorded at each ear (red and blue) plotted in hemifield polar angles. Outset panel illustrates a virtual sector of speaker orientations and distances from the head. Sound bursts (100 ms) were played every 5° in a leftward, rightward and distance sequence oscillating pattern (dashed red and black arrows) within a 30°-wide spatial sector (shaded gray, n sectors = 12) for 7.2 s.

(H) Mean ± SEM of BOLD signal in all significant voxels (coherence > 0.3) in AC shown for four cycles of the time course to illustrate the overall broad amplitude modulation across hemispheres.

(I) Space maps highlight two phases across hemispheres in all four monkeys. STG, superior temporal gyrus; ls, lateral sulcus; ips, intraparietal sulcus; sts, superior temporal sulcus; Lh, left hemisphere; Rh, right hemisphere; ant, anterior; lat, lateral; post, posterior.

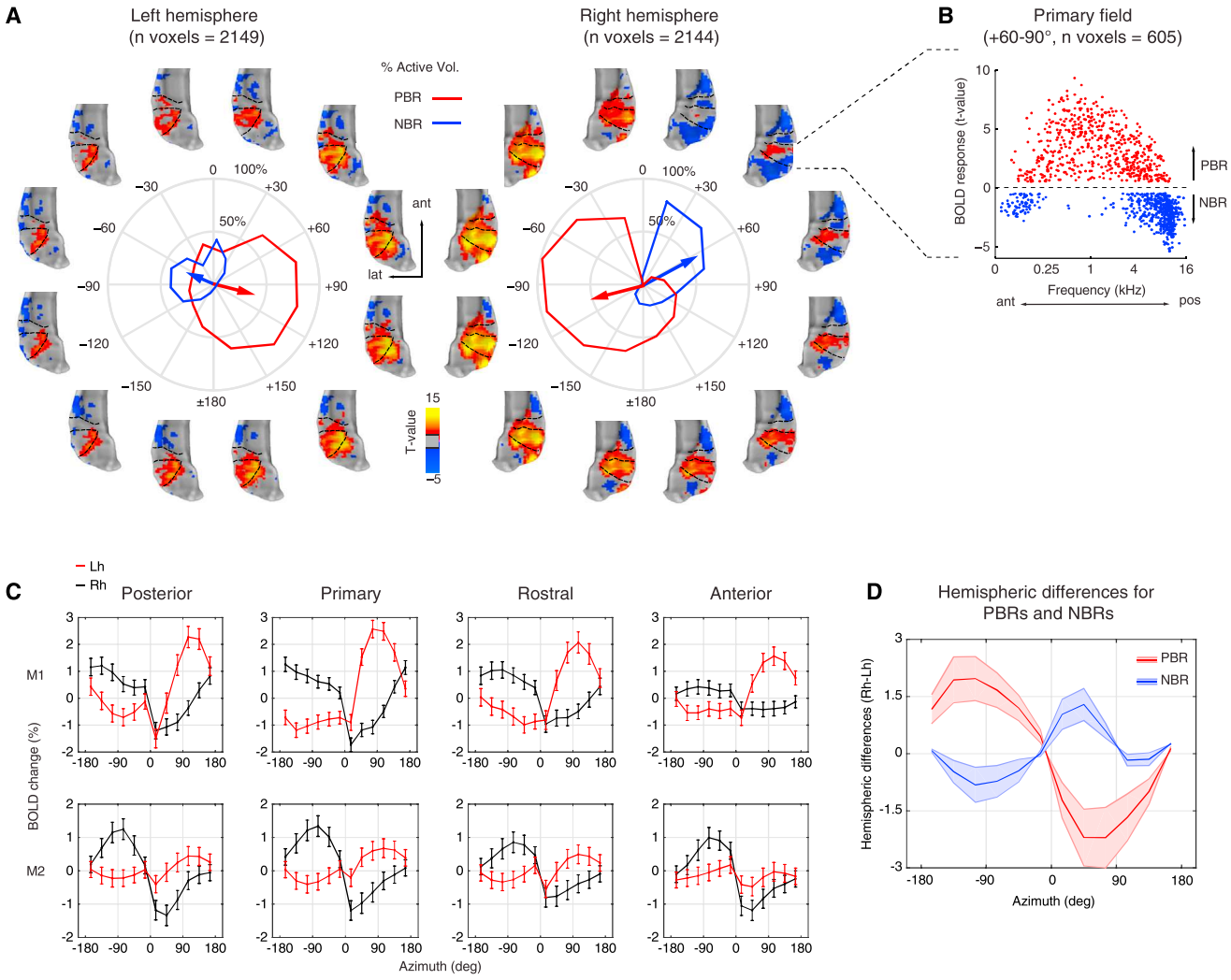

Figure 2. Positive and Negative BOLD Responses Represent Opposite Hemifields

(A) Activation t-maps with significant positive (red/yellow) and negative (blue) BOLD responses (q FDR < 0.05, $p < 10^{-6}$, cluster size > 10 voxels). Each map is shown around the corresponding spatial sector in polar plots of each hemisphere of monkey M2 (see Figure S4 for a similar plot in monkey M1). The polar plot shows spatial tuning curves obtained from the spatial spread of the positive (red) and negative (blue) BOLD responses (PBRs and NBRs, respectively). Mean resultant vectors (arrows) point toward the preferred angular direction. The length represents the percentage of active voxels around the mean direction. Negative angles (−180°–0°) in polar plot represent the left hemifield and positive angles (+180°–0°) represent the right hemifield.

(B) Scatterplot of voxels in primary field showing PBRs and NBRs to an exemplar spatial sector (+60°–90°) plotted as function of the frequency tuning of each voxel.

(C) Mean ± SEM of BOLD responses (including both PBRs and NBRs) for cortical regions of each hemisphere (Lh, red; Rh, black) of monkey M1 (top) and M2 (bottom).

(D) Average amplitude differences across hemispheres for PBRs and NBRs plotted as a function of azimuth. The differential response shows opposite polarity between hemifields with a peak in NBRs for frontal right sectors. Lh, left hemisphere; Rh, right hemisphere; ant, anterior; lat, lateral; pos, posterior.

and similarly oriented in all CRs of the same hemisphere (Figure 3). Vector length showed that more than half of the total numbers of voxels were active in response to stimulation of contralateral sectors (~ ±120°) for all CRs. The overall tuning in central regions (primary and rostral) was slightly broader than in anterior and posterior regions of the same hemisphere based on standard deviations (see Data S1 for details).

In summary, our functional analyses showed that azimuth space as measured by fMRI is represented by opponent hemifield responses of positive and negative BOLD across hemispheres. The dynamic change between PBRs and NBRs supports an opponent-channel mechanism (Stecker et al., 2005) for the representation of acoustic space in the macaque monkey.

Contralateral Bias Measured with BOLD Response Contrast

While animal studies have uniformly shown a clear contralateral bias in the firing rate of auditory cortical neurons (Tian et al., 2001; Miller and Recanzone, 2009; Stecker and Middlebrooks, 2003; Werner-Reiss and Groh, 2008; Woods et al., 2006),

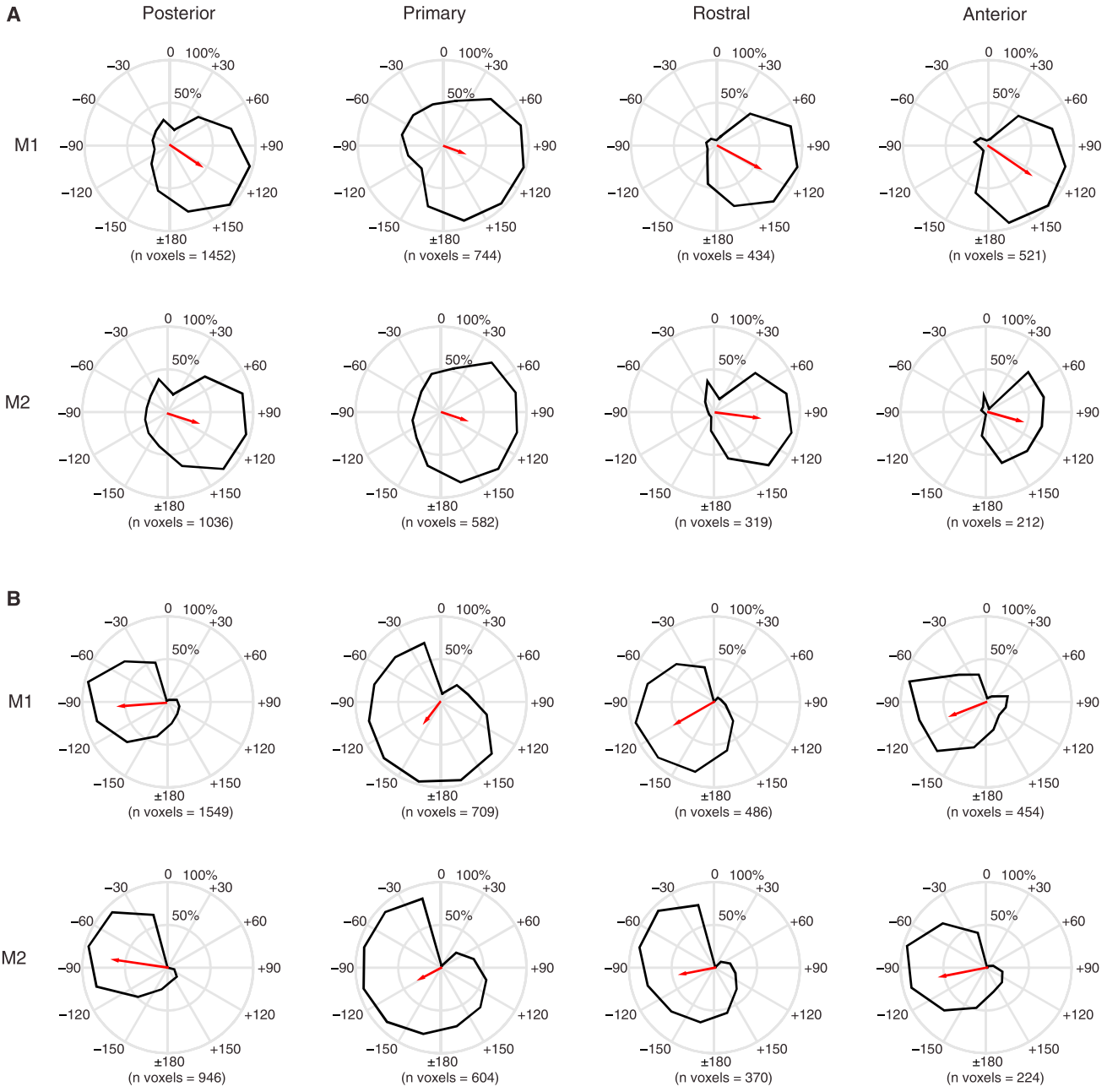

Figure 3. Cortical Fields Are Broadly Tuned to Contralateral Space

The spatial spread of the positive BOLD response was used to calculate spatial tuning curves (black curves) for each cortical field: posterior, primary, rostral, and anterior.

(A) Left hemisphere for M1 (top) and M2 (bottom).

(B) Right hemisphere for M1 (top) and M2 (bottom). The mean resultant vectors (red) point toward the preferred circular mean direction, and the length represents the percentage of active voxels concentrated around ±30° of the mean direction. All fields were approximately oriented around ± 90°–120°. Overall, cortical fields were broadly tuned, with central fields (primary and rostral) slightly broader than anterior and posterior fields (see Tables S1 and S2).

neuroimaging studies in humans have obtained mixed results in respect to the degree of contralaterality (Krumbholz et al., 2007; Werner-Reiss and Groh, 2008; Zatorre et al., 2002) in AC responses to spatial sounds. Whether these discrepancies are due to species differences in neural coding or to methodological differences (e.g., sound stimulation, single-unit, and/or fMRI) between studies in animals and humans remains a matter of debate (Werner-Reiss and Groh, 2008).

Here, we provide evidence showing a contralateral bias in the fMRI BOLD contrast between equidistant spatial sectors

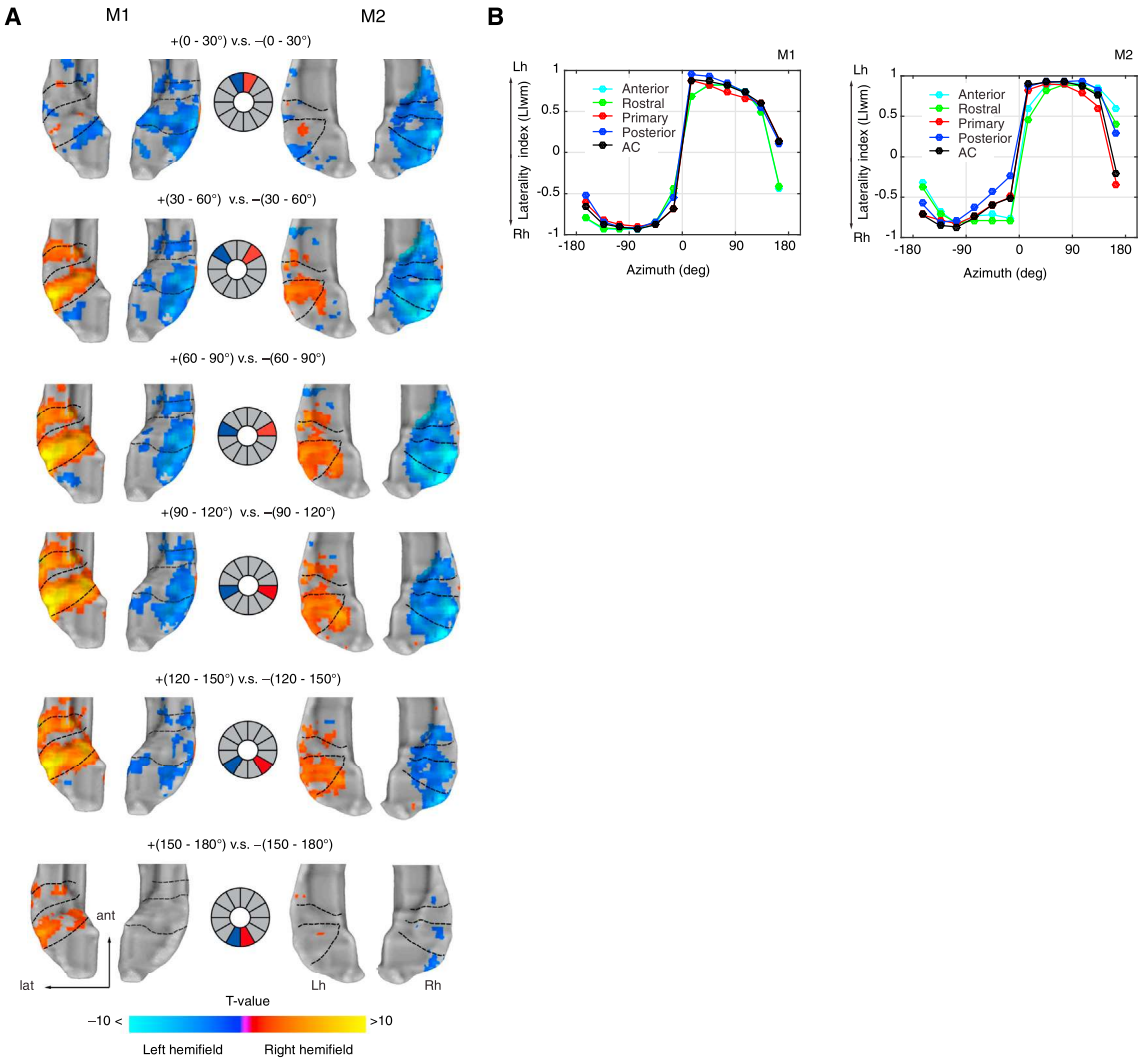

Figure 4. Auditory Cortex Represents the Contralateral Hemifield

(A) Contrast t-maps between equidistant sectors for both monkeys. Middle panel illustrates the contrast design between sectors (left hemifield in blue; right hemifield in red). Voxels preferring left hemifield sectors were mapped as negative (blue-to-cyan), while voxels preferring right hemifield sectors were mapped as positive (red-to-yellow). The range of t values (q FDR < 0.05, $p < 10^{-3}$, cluster size > 10 voxels) in the color bar was scaled according to a maximum t value of 10 to illustrate the strength of the contrast across sectors and monkeys.

(B) Mean-weighted laterality index (LIwm) between hemispheres calculated from the t value threshold of each spatial sector (see STAR Methods section Laterality index). Index range between −1 and +1 with a positive value indicating Lh biases and a negative index indicating Rh biases. Index curves are shown for each monkey and for each cortical field, including auditory cortex as a whole (all fields combined). Lh, left hemisphere; Rh, right hemisphere.

(Figure 4A). The differential activation maps (q FDR < 0.05, $p < 10^{-3}$, cluster size > 10 voxels) indicated whether the responses were greater for the left (blue to cyan) or the right hemifield (red to yellow). The strength of the BOLD response showed a robust contralateral bias for spatial sectors near the lateral axis (e.g., ~ ±90°–120°). The contrast in frontal sectors (±0°–30°) displayed greater differential response only in the right hemisphere, while contrast for backward sectors (±150–180°) showed almost no differential activation at equal threshold values (q FDR < 0.05).

We quantified these results further by calculating a hemispheric laterality index (LI = L-R/|L+R|) between corresponding CRs of the opposite hemisphere, including AC as a whole (all CRs included). Since laterality indices in fMRI typically show a threshold dependency (Wilke and Lidzba, 2007), we measured LI curves by bootstrapping LI values as a function of the t value threshold and then calculated a mean weighted laterality index (LIwm) (see STAR Methods section Laterality index). The LIwm ranges between −1 and 1 with a positive index assigned to left-hemisphere bias and a negative index to a right-hemisphere bias. The resulting indices for all CRs showed a very strong right-hemisphere bias (LIwm < −0.5) for sectors in the left hemifield and a left-hemisphere bias (LIwm > 0.5) for sectors in the right hemifield, except for a backward sector (±150°–180°) were LIwm was found to be asymmetrical toward the right hemisphere

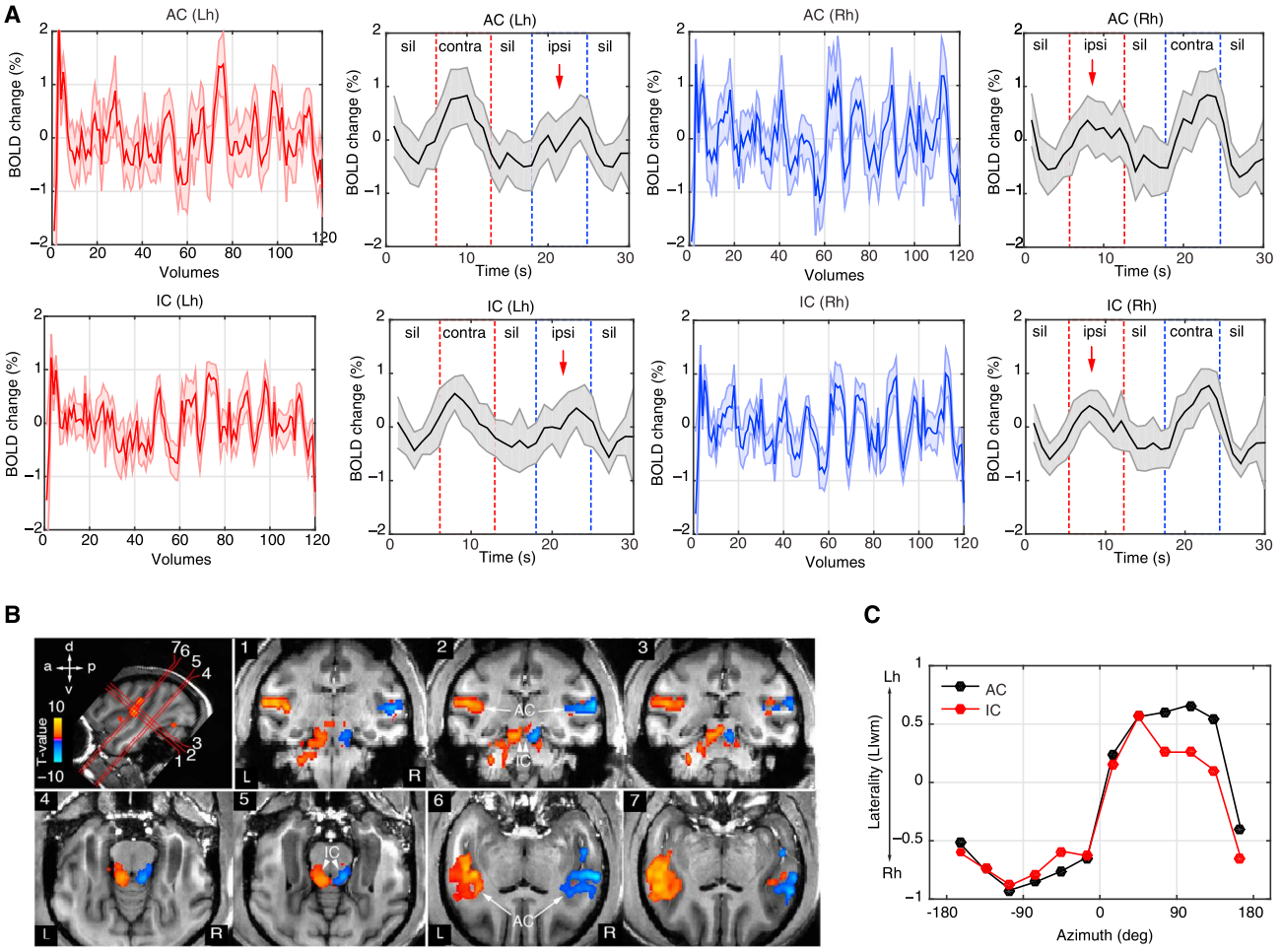

Figure 5. Cortical and Subcortical Hemifield Tuning in the Awake Monkey

(A) Example time courses and average response (mean ± SEM) of auditory cortex (AC) and inferior colliculi (IC) in each hemisphere (red, left hemisphere; blue, right hemisphere). Red dashed lines indicate duration periods of sounds presented in the right hemifield and blue dashed duration periods of sounds presented in the left hemifield. Notice the amplitude suppression for sound sources on the ipsilateral side (red arrows).

(B) Contrast t-maps (q FDR < 0.05, $p < 10^{-3}$, cluster size > 10 voxels, t value range ± 7.8) between all left and all right spatial sectors in awake monkey M3 (see also Figure S5 for M4). Top left image illustrates oblique slice orientations and planes (numbered 1–7) cutting through AC and IC. Voxels preferring the left hemifield sectors were mapped as negative (blue-to-cyan) while voxels preferring the right hemifield sectors were mapped as positive (red-to-yellow).

(C) Laterality index (LIwm) curves for AC and IC of monkey M3. Lh, left hemisphere; Rh, right hemisphere; contra, contralateral; ipsi, ipsilateral; sil, silence.

in three monkeys (Figures 4B and 5C). The LIwm changes around the midline were drastic, as observed in the steep slope between frontal sectors, compared to shallower slopes for sectors within each hemifield.

Similar contralateral representations were found in AC of the awake monkey (Figures 5 and S5). Additionally, however, we obtained reliable BOLD signals from inferior colliculli (IC) of the awake monkey. Similar to the anesthetized monkey, the average time courses showed an overall suppression effect to sound sources on the ipsilateral side. For contrast between spatial sectors of the awake monkey, we collapsed across all left and all right hemifield sectors (q FDR < 0.05, $p < 10^{-3}$, cluster size > 10) and confirmed a robust contralateral bias (Figures 5B and S5B). The LIwm values in the awake monkey resembled those in the anesthetized animal showing contralateral biases (Figure 5C).

Overall, our analyses showed a robust contralateral bias in both anesthetized and awake monkeys, as measured with fMRI. Moreover, our finding in IC further supports the neurophysiological evidence showing hemifield tuning below the cortical level (Groh et al., 2003) and attests to the feasibility of fMRI as a tool for imaging auditory spatial representations in cortical and subcortical structures of primates.

Removing ITD Cues from Spatial Sounds

Previous work has suggested that NBRs are related to decreases in neuronal activity (Shmuel et al., 2006). Given the strong inhibitory roles involved in ITD coding at subcortical levels (Brand et al., 2002; Pecka et al., 2008), we explored the effects of removing ITD cues from the original recorded sounds in the PBR/NBR pattern in AC.

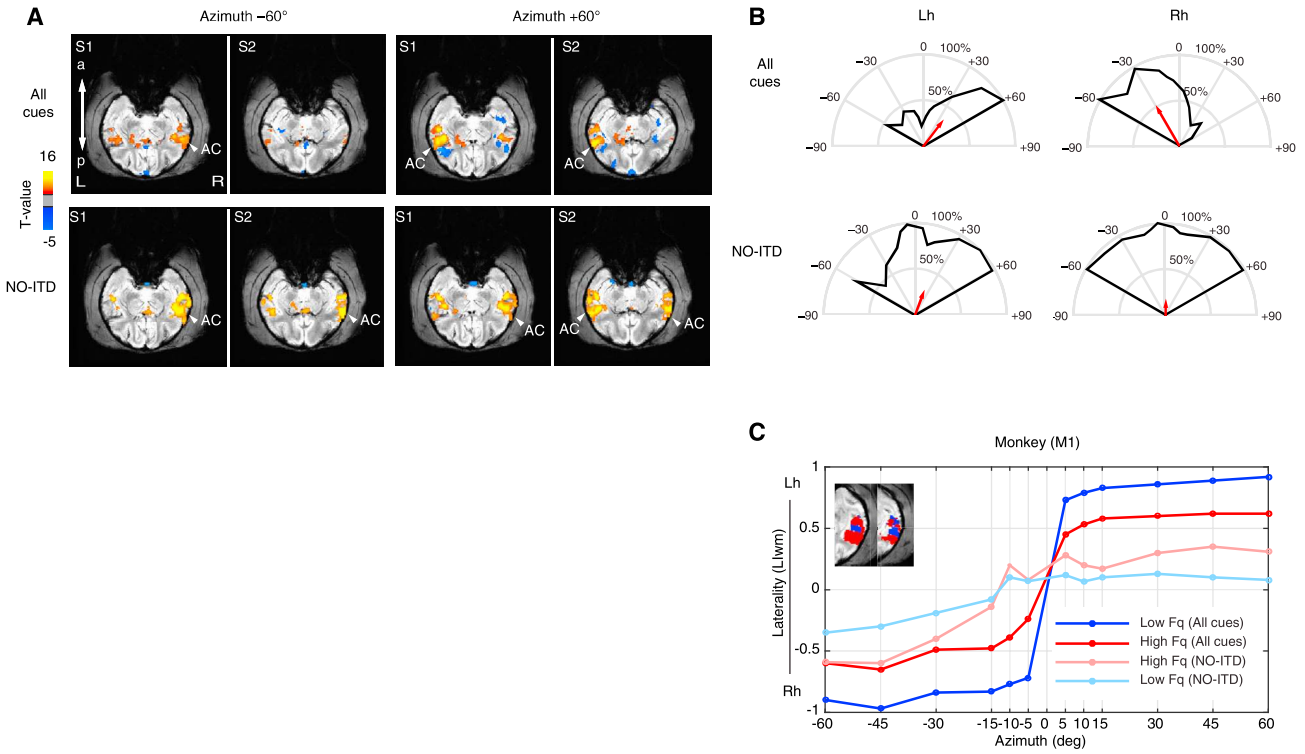

Figure 6. ITD Cues Are Essential for Contralateral Tuning in Auditory Cortex

(A) Example t-maps with significant BOLD responses (q FDR < 0.05) to spatial sounds presented in left (+60°) and right (−60°) hemifields. "All cues" condition (top) and "NO-ITD" condition (bottom) in which ITD cues were removed from the original recorded sounds, leaving ILD and spectral cues. Maps are shown for two pairs of oblique slices (S1 ventral and S2 dorsal) cutting through the superior temporal gyrus. The response to rightward +60° in the NO-ITD condition was observed in both auditory cortices (i.e., no contralateral tuning).

(B) Spatial tuning curves for frontal field show a loss of hemifield tuning in the right hemisphere for the NO-ITD condition.

(C) Laterality index (LIwm) as a function of frontal azimuth plotted for low- and high-frequency voxels shows a lack of laterality (LIwm near zero) for sounds without ITD at the midline (±15°) with only a slight increase in laterality for high frequency (LIwm < 0.5) as compared to low frequency. Compare to Figures 3, 4, and 5.

First, we replicated our previous findings (Figure 6A) showing PBRs and NBRs in AC for spatial sounds carrying all spatial cues in frontal azimuth (±0°–60°) of the anesthetized monkey (All-cues condition, q FDR < 0.01, $p < 10^{-6}$, cluster size > 10 voxels, t value range −6.4 to 8.7). Second, we measured the BOLD responses to the same sounds but without ITD cues, i.e., sounds carrying the remaining ILD and spectral cues (NO-ITD condition, q FDR < 0.01, $p < 10^{-3}$, cluster size > 10 voxels, t value range −6 to 18.8). The BOLD response to leftward sounds (e.g., NO-ITD at −60°) showed greater activation in the right hemisphere as compared to the left hemisphere (Figure 6A). However, the BOLD response to rightward sounds (e.g., NO-ITD at +60°) showed a bilateral activation in both left and right AC.

Moreover, while spatial tuning curves for the All-cues condition showed contralateral tuning (~ ±30°), the ITD-control condition showed hardly any contralateral tuning (Figure 6B). LIwm values near the midline (−15° to 15°) shifted drastically toward zero and just increased slightly (LIwm < 0.5) for more rightward sounds as compared to the All-cues condition. In addition, we investigated the effect of frequency by analyzing LIwm values from both the All-cues and NO-ITD conditions in voxels identified to belong to either low- (0.125–1 kHz) or high- (2–16 kHz) frequency regions (Figure 6C). These findings showed similar decreases in laterality around the midline for both low- and high-frequency (NO-ITD) conditions with an increase in contralaterality (LIwm > 0.25) for more lateral positions in high-frequency regions as compared to an overall decrease in LIwm values for low- (LIwm < 0.25) frequency regions. Thus, removal of ITD cues facilitated the responses of the right hemisphere across frequency regions, and consequently the difference in BOLD activity between both hemispheres plateaued near the midline (Figure 6C).

Taken together, our results suggest that the suppression effects (either in the form of smaller positive clusters and/or negative BOLD responses) are likely due to inhibitory inter-hemispheric processes provided by ITD cues. In addition, our results show that the lack of suppression caused by the removal of ITD cues particularly affected the right-hemisphere response necessary for contralateral tuning. Overall, we provide new evidence for the role of ITD mechanisms in the representation of azimuth space at the cortical level in the macaque.

Relating Cortical Representations to the Hemifield Model

Previous work has suggested that the representation of azimuth space in AC follows a hemifield rate code (Salminen et al., 2009;

Stecker et al., 2005; Werner-Reiss and Groh, 2008). Here, we use representational similarity analyses (RSA) (Kriegeskorte et al., 2008) to measure the dissimilarity between the BOLD response patterns to each spatial sector and to then compare the resultant spatial representations across CRs and hemifield model.

For each stimulus condition (i.e., each sector of space; n = 12), the beta coefficients (β) obtained from the fitted GLM were subjected to pairwise Pearson's correlation (*R*), and the distance (1 − *R*) between responses to all possible pairs of conditions was ordered into a 12 × 12 representational dissimilarity matrix (RDM). The RDM characterizes the BOLD response patterns to each spatial sector and captures distinctions within and between hemifield responses (Figure 7A).

This analysis was repeated for each CR, AC (all CRs combined), and hemifield model, providing a total of 11 RDMs. Visual inspection of each RDM from the left hemisphere revealed a small dissimilarity (blue) distance between spatial sectors within the right hemifield, while RDMs from the right hemisphere showed a small dissimilarity distance between spatial sectors within the left hemifield (Figure S6). These results largely confirm our previous results showing contralateral preference (Figures 4 and 5). More importantly, however, these analyses revealed that while most regions showed variability within ipsilateral sectors, the pST region of the right hemisphere showed a small dissimilarity within hemifields and a graded dissimilarity distance (red) across hemifields (Figure 7B and Figure S6), indicating that the right pST region carried spatial information in the NBRs to ipsilateral sound sources. By subjecting the right pST RDM to clustering analyses and multidimensional scaling (MDS), we were able to show that the response patterns segregated in an orderly manner largely replicating the spatial arrangement of stimuli that evoked them (Figures 7C and 7D). Interestingly, the elicited response patterns to frontal sectors (±30°) were very dissimilar, generating a larger distance between them, which further indicated drastic changes of responses around the midline.

We also examined the dissimilarity between spatial representations obtained from individual CR, AC, and the hemifield model by computing Spearman's rank-order correlations between RDMs (1 − Spearman's *R*). This analysis resulted in a second-order RDM (see STAR Methods fMRI dissimilarity analyses and Figure S6E). The second-order RDM when subjected to MDS showed how the right pST clustered at a closer distance to the hemifield code than the other CRs (Figure 7E). The correlation coefficient between the right pST region's RDM and the hemifield code model, averaged across individual runs and monkeys, was numerically higher than between any other CR and the hemifield model (Figure S7A). This result was replicated in most individual fMRI runs of individual animals: 17/23 runs (74%) in M1; 13/14 (93%) in M2; 14/14 (100%) in M3, and 10/14 (71%) in M4 (Figure S7B). The lower 95%-confidence boundaries for these proportions are 53%, 66%, 75%, and 45%, respectively, and are well above the expected chance level of 12.5% (1 in 8 CRs). Using a sign-rank permutation test (FDR $p < 0.01$, 95% confidence intervals by bootstrap), we determined that the right pST RDM was significantly more similar to the hemifield model RDM than any other cortical RDM (Figure S6F). Overall, our dissimilarity analyses show that representation of space in the right pST region follows closely a hemifield code.

DISCUSSION

Using fMRI and multivariate analytical methods, we mapped auditory cortical fields (CRs) in the macaque on the basis of their tonotopic organization and then measured BOLD responses to spatial auditory stimuli. We showed that the functional representation of azimuth in AC, as measured by the BOLD signal, is not organized topographically but distributed with a strong contralateral bias. We further demonstrated that the opponent pattern of positive and negative BOLD responses across the cerebral hemispheres is dependent on the presence of ITD cues. Taken together, our main findings support the existence of an opponent-channel mechanism (Stecker et al., 2005) that is based on contralateral inhibition (Grothe, 2003) for coding auditory space in primates.

ITD Cues Modulate the BOLD Response across Hemispheres

While it was originally thought that ITDs (the most salient spatial cues) were coded exclusively by a topographic arrangement of coincidence detectors in the auditory brainstem as in the case of the barn owl (Jeffress, 1948; Knudsen and Konishi, 1978); research in multiple mammalian species has revealed an additional mechanism (McAlpine et al., 2001), one in which ITDs are coded by an opponent hemifield code based on neuronal inhibition (Brand et al., 2002; Pecka et al., 2008).

Given the profound role that inhibition plays in the coding of spatial cues in the auditory brainstem (Grothe, 2003), we investigated the effect of removing ITD cues from the original spatial sounds on BOLD responses in the AC. The lack of ipsilateral suppression caused by the removal of ITD cues particularly affected the right-hemisphere response necessary for a contralateral representation. Spatial measures and laterality indices further indicated that contralateral tuning was lost after removal of ITD cues (Figure 6). Thus, removing ITD cues from the original spatial sounds facilitated the response of the right hemisphere to ipsilateral sounds, generating an overall net activation for both ipsilateral and contralateral sounds and consequently no shifts in hemifield tuning around the midline. The lack of contralaterality was more pronounced in low-frequency as compared to high-frequency regions, suggesting a similar hemifield-tuned representation for ILD cues driven by high-frequency regions (Magezi and Krumbholz, 2010). Overall, our findings indicate that ITD cues are necessary to preserve the drastic shift in hemifield representations across auditory cortices and that ILD cues might provide additional contralateral tuning information for spatial localization in the high-frequency range.

Response Tuning: Effects of Anesthesia, Attention, and Stimulus History

Functional analyses of the positive BOLD response, in both anesthetized and awake monkeys, showed a maximum amplitude and spatial spread for contralateral sectors, in agreement with previous lesion (Heffner and Masterton, 1975; Jenkins and Masterton, 1982; Nodal et al., 2012), single-unit (Middlebrooks et al., 1994; Tian et al., 2001; Miller and Recanzone, 2009; Stecker et al., 2005; Werner-Reiss and Groh, 2008; Woods

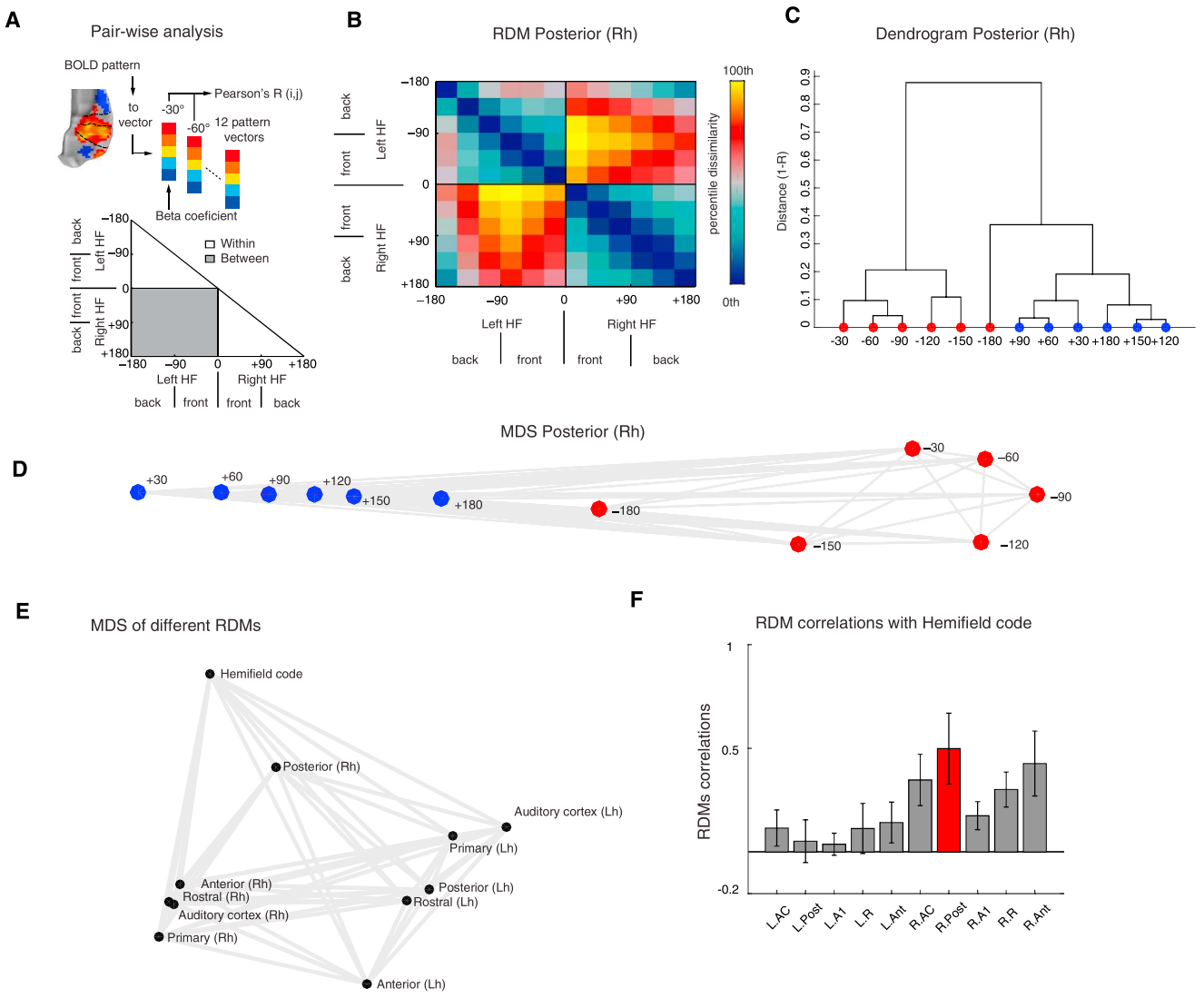

Figure 7. Posterior Superior Temporal Region Represents Space Similarly to a Hemifield Code

(A) For each field, we extracted the response patterns to each spatial sector, yielding 12 response patterns. We then calculated pairwise Pearson's correlations (R) across all spatial sectors and then assigned the dissimilarity measure ($1 - R$) to a 12 × 12 representational dissimilarity matrix (RDM). This analysis was repeated for each cortical field and the hemifield model for all runs and monkeys (see Figure S6).

(B) Mean RDM of the right posterior superior temporal region (pST) region. The color bar reflects dissimilarity in percentiles (low dissimilarity, blue; high dissimilarity, red/yellow).

(C and D) Hierarchical clustering (C) and multidimensional scaling (MDS) (D) of fMRI responses in right pST. Unsupervised hierarchical clustering (criterion: average dissimilarity) revealed a hierarchical structure dividing left and right hemifields. MDS (criterion: metric stress) resulted in apparent segregation of data derived from each hemifield (red versus blue).

(E) MDS based on dissimilarity (1 − Spearman's correlation) between RDMs (see Figure S6E and STAR Methods section fMRI dissimilarity analyses for second-order RDM). Visual inspection of the MDS structure reveals that the right pST RDM lies closer to the hemifield model than any other cortical region.

(F) Mean ± SEM of Spearman's correlation coefficients obtained from all monkeys and runs (n = 65) between CRs and hemifield code (see Figure S7 for individual runs and monkeys) RDMs. RDM from the right pST relates more to the hemifield code than any other RDM.

et al., 2006), and optical imaging data (Nelken et al., 2008). Although previous single-unit studies in mammals reported contralateral tuning centered around ±90°, our spatial tuning measures derived from the BOLD responses show a rearward shift in contralateral tuning (e.g., ± 90°–120°). While LI shifts toward more rear sound positions could potentially be due to the expectancy of subsequent sound sources (Stange et al., 2013), they are in accordance with previous population measures of neuronal tuning in awake monkey AC (Woods et al., 2006). Interestingly, shifts in amplitude tuning around the midline were drastic as compared to rear midline sectors indicating a sharp slope tuning in frontal space as compared to rear sound positions, which suggest a potential different mechanism for coding backward space.

In monkeys, single-unit studies have found neurons in posterior regions (particularly area CL) with significantly sharper tuning to spatial position (Kuśmierek and Rauschecker, 2014; Miller and Recanzone, 2009; Tian et al., 2001; Woods et al., 2006). However, we found very small differences in the spatial tuning curves between CRs. This could be due to the average activity across large neuronal populations as reflected by the BOLD signal and thus is conceivable that sharply tuned neurons can only be detected at the single-unit level. Sharply tuned neurons may also be more common in frontal auditory space, where spatial resolution at the behavioral level is highest in most species and where much of single-unit recording has taken place. One important point to keep in mind is that our experimental design does not include a spatial attention auditory task, which has been shown to sharpen cortical responses after learning (Lee and Middlebrooks, 2011). While biases in spatial attention could be detected from the average shift gaze in visual paradigms (Caspari et al., 2015), our auditory stimuli included sound sources beyond the visual field, challenging our ability to reliably decipher shifts in gaze between frontal and backward space. In addition, our data also included imaging under general anesthesia in combination with eye muscle paralysis. While anesthesia could potentially hinder the underlying cortical mechanisms involved in coding auditory space and paralytics could even obscure eye-movements modulations in auditory cortex (Werner-Reiss et al., 2003), our experimental approach allowed us to image the bottom-up driven response to cortex without—presumably—top-down attention effects. Considering the fact that fMRI indirectly measures the pooled activity of cortical neurons and that responses were similar between both awake and anesthetized conditions, we believe that eye movements and attention were not a source of response bias in our data from awake animals.

Contralateral and Asymmetrical Bias: Implications for Human and Monkey Neuroimaging Studies

While single-unit studies consistently and invariably report a contralateral bias in the firing rate of cortical neurons (Tian et al., 2001; Miller and Recanzone, 2009; Stecker and Middlebrooks, 2003; Werner-Reiss and Groh, 2008; Woods et al., 2006), neuroimaging studies in humans have obtained mixed results with respect to the degree of contralaterality (Krumbholz et al., 2007; Werner-Reiss and Groh, 2008; Zatorre et al., 2002). Here we found a robust contralateral bias in the BOLD contrast to equidistant hemifield sectors in both anesthetized and awake monkeys, suggesting that the lack of contralaterality in some previous neuroimaging studies in humans might be due to differences in sound stimulation, i.e., sounds relying on ITD (Krumbholz et al., 2007) or ILD cues alone, and might not be due to an inherent lack of functional sensitivity in fMRI (Werner-Reiss and Groh, 2008). Furthermore, our stimulation design consisted of individualized (in-ear) binaural sound recordings and the bias we obtained in our contralaterality measures is in accordance with human neuroimaging studies utilizing individualized spatial sounds (Derey et al., 2016; Młynarski, 2015; Palomäki et al., 2005; Salminen et al., 2009).

One interesting observation relates to laterality indices to right-backward sounds (e.g., +150°–180°) that were asymmetrically shifted to the right hemisphere for three of the animals. These results could be due to greater spectral and motion sensitivity in the right hemisphere (Zatorre and Belin, 2001), especially for backward space. In humans, the right hemisphere is generally more involved in spatial auditory processing (Baumgart et al., 1999; Krumbholz et al., 2007) and motion detection (Warren et al., 2002; Griffiths et al., 1996). Furthermore, lesions to the right hemisphere in humans can result in spatial hemi-neglect (Bisiach et al., 1984). In monkeys, previous neuroimaging work has focused on hemispheric biases for vocal sounds (Gil-da-Costa et al., 2006; Ortiz-Rios et al., 2015; Petkov et al., 2008; Poremba et al., 2004); however, until now, no functional MRI study in monkeys utilizing spatial sounds had been performed. In our present study, we found a dynamic BOLD modulation in both hemispheres for spatial (non-vocal) broad-band noise sounds. Interestingly, the right-hemisphere response was strongly modulated across hemifield sectors, particularly in the pST region, as shown in the small activation surrounded by deactivation in posterior and anterior regions of AC (Figures 2A and 2B). These small ipsilateral patches could correspond to EE regions (Imig and Brugge, 1978; Reser et al., 2000) receiving callosal input (Hackett et al., 1998; Pandya and Rosene, 1993), while NBRs could be due to subcortical inhibition (Grothe, 2003) or cortico-cortical lateral inhibition (Shmuel et al., 2006) from EE cells in low-frequency ITD sensitive regions (Brugge and Merzenich, 1973). In humans, the ability to localize sounds based on ITD cues alone has been found to depend on an intact right hemisphere (Bisiach et al., 1984; Spierer et al., 2009). Our results here are in accordance with the role of ITD cues in the right hemisphere of humans and support these findings by showing that the pST region could segregate the response patterns in an orderly manner similar to a hemifield rate code (Salminen et al., 2009; Werner-Reiss and Groh, 2008). Our dissimilarity analyses also provide support for the notion of a posterior region particularly sensitive to spatial sounds (Rauschecker and Tian, 2000; Tian et al., 2001) and coincides with previous single-unit and behavioral studies in cats (Stecker et al., 2005; Lomber and Malhotra, 2008) and single-unit studies in monkeys (Kuśmierek and Rauschecker, 2014; Miller and Recanzone, 2009; Tian et al., 2001; Woods et al., 2006), showing that posterior regions carry more spatial information than primary cortical regions in agreement with a posterior-dorsal auditory "where" pathway (Rauschecker and Tian, 2000; Romanski et al., 1999).

Conclusion

Taken together, our results reconcile seemingly contradictory views of auditory space coding by showing that the representation of space follows closely a hemifield code (Salminen et al., 2009; Stecker et al., 2005; Werner-Reiss and Groh, 2008) and that such representation depends on the availability of ITD cues. Moreover, our data also suggest that the cortical activation pattern across each AC, as a result of the hemifield tune response, generates the right-posterior dorsal sensitivity for space commonly seen in spatial studies (Baumgart et al., 1999; Krumbholz et al., 2007; Rauschecker and Tian, 2000; Tian et al., 2001) of primate auditory cortex.

STAR★METHODS

Detailed methods are provided in the online version of this paper and include the following:

- KEY RESOURCES TABLE
- CONCTACT FOR REAGENT AND RESOURCE SHARING
- EXPERIMENTAL MODEL AND SUBJECT DETAILS
- METHOD DETAILS
  - Auditory stimuli
  - Binaural sound recordings
  - Behavioral training for awake-monkey fMRI
  - Anesthesia for fMRI
  - MRI data acquisition
- QUANTIFICATION AND STATISTICAL ANALYSIS
  - GLM analyses
  - FMRI phase-mapping analyses
  - Laterality index
  - Spatial tuning curves
  - FMRI dissimilarity analyses
- DATA AND SOFTWARE AVAILABILITY
- ADDITIONAL RESOURCES

SUPPLEMENTAL INFORMATION

Supplemental Information includes seven figures, one table, and neuroimaging files and can be found with this article online at http://dx.doi.org/10.1016/j.neuron.2017.01.013.

AUTHOR CONTRIBUTIONS

Conceptualization, M.O.R., N.K.L., and J.P.R.; Methodology, M.O.R., F.A.C.A., G.A.K., P.K., and D.Z.B.; Investigation, M.O.R.; Formal Analysis, M.O.R.; Writing – Original Draft, M.O.R.; Writing – Review & Editing, M.O.R., F.A.C.A., G.A.K., P.K., M.H.M., N.K.L., and J.P.R; Funding Acquisition, N.K.L. and J.P.R.; Resources, N.K.L.; Supervision, J.P.R., G.A.K., M.H.M., and N.K.L.

ACKNOWLEDGMENTS

This work was supported by the Max Planck Society and by a PIRE Grant from the National Science Foundation (OISE-0730255 to Josef P. Rauschecker). We would like to thank Xin Yu for extensive discussion on the nature of BOLD signals. We would also like to thank Thomas Steudel for help during anesthetized experiments and Mirko Lindig for animal handling and anesthesia. We thank also Vishal Kapoor and Michael C. Schmid for comments on previous versions of the manuscript.

Received: December 8, 2015
Revised: December 5, 2016
Accepted: January 15, 2017
Published: February 9, 2017

REFERENCES

Barton, B., Venezia, J.H., Saberi, K., Hickok, G., and Brewer, A.A. (2012). Orthogonal acoustic dimensions define auditory field maps in human cortex. Proc. Natl. Acad. Sci. USA *109*, 20738–20743.

Baumgart, F., Gaschler-Markefski, B., Woldorff, M.G., Heinze, H.-J., and Scheich, H. (1999). A movement-sensitive area in auditory cortex. Nature *400*, 724–726.

Berens, P. (2009). CircStat: A MATLAB toolbox for circular statistics. Jstasoft *31*, i10. http://dx.doi.org/10.18637/jss.v031.i10.

Bisiach, E., Cornacchia, L., Sterzi, R., and Vallar, G. (1984). Disorders of perceived auditory lateralization after lesions of the right hemisphere. Brain *107*, 37–52.

Brand, A., Behrend, O., Marquardt, T., McAlpine, D., and Grothe, B. (2002). Precise inhibition is essential for microsecond interaural time difference coding. Nature *417*, 543–547.

Brugge, J.F., and Merzenich, M.M. (1973). Responses of neurons in auditory cortex of the macaque monkey to monaural and binaural stimulation. J. Neurophysiol. *36*, 1138–1158.

Caspari, N., Janssens, T., Mantini, D., Vandenberghe, R., and Vanduffel, W. (2015). Covert shifts of spatial attention in the macaque monkey. J. Neurosci. *35*, 7695–7714.

Cox, R.W. (1996). AFNI: software for analysis and visualization of functional magnetic resonance neuroimages. Comput. Biomed. Res. *29*, 162–173.

Dahmen, J.C., Keating, P., Nodal, F.R., Schulz, A.L., and King, A.J. (2010). Adaptation to stimulus statistics in the perception and neural representation of auditory space. Neuron *66*, 937–948.

Dale, A.M., Fischl, B., and Sereno, M.I. (1999). Cortical surface-based analysis. I. Segmentation and surface reconstruction. Neuroimage *9*, 179–194.

Derey, K., Valente, G., de Gelder, B., and Formisano, E. (2016). Opponent Coding of Sound Location (Azimuth) in Planum Temporale is Robust to Sound-Level Variations. Cereb. Cortex *26*, 450–464.

Formisano, E., Kim, D.S., Di Salle, F., van de Moortele, P.F., Ugurbil, K., and Goebel, R. (2003). Mirror-symmetric tonotopic maps in human primary auditory cortex. Neuron *40*, 859–869.

Gil-da-Costa, R., Martin, A., Lopes, M.A., Muñoz, M., Fritz, J.B., and Braun, A.R. (2006). Species-specific calls activate homologs of Broca's and Wernicke's areas in the macaque. Nat. Neurosci. *9*, 1064–1070.

Griffiths, T.D., Rees, A., Witton, C., Shakir, R.A., Henning, G.B., and Green, G.G. (1996). Evidence for a sound movement area in the human cerebral cortex. Nature *383*, 425–427.

Groh, J.M., Kelly, K.A., and Underhill, A.M. (2003). A monotonic code for sound azimuth in primate inferior colliculus. J. Cogn. Neurosci. *15*, 1217–1231.

Grothe, B. (2003). New roles for synaptic inhibition in sound localization. Nat. Rev. Neurosci. *4*, 540–550.

Hackett, T.A., Stepniewska, I., and Kaas, J.H. (1998). Subdivisions of auditory cortex and ipsilateral cortical connections of the parabelt auditory cortex in macaque monkeys. J. Comp. Neurol. *394*, 475–495.

Heffner, H., and Masterton, B. (1975). Contribution of auditory cortex to sound localization in the monkey (Macaca mulatta). J. Neurophysiol. *38*, 1340–1358.

Imig, T.J., and Brugge, J.F. (1978). Sources and terminations of callosal axons related to binaural and frequency maps in primary auditory cortex of the cat. J. Comp. Neurol. *182*, 637–660.

Jeffress, L.A. (1948). A place theory of sound localization. J. Comp. Physiol. Psychol. *41*, 35–39.

Jenkins, W.M., and Masterton, R.B. (1982). Sound localization: effects of unilateral lesions in central auditory system. J. Neurophysiol. *47*, 987–1016.

Knudsen, E.I., and Konishi, M. (1978). A neural map of auditory space in the owl. Science *200*, 795–797.

Kriegeskorte, N., Mur, M., and Bandettini, P. (2008). Representational similarity analysis - connecting the branches of systems neuroscience. Front. Syst. Neurosci. *2*, 4.

Krumbholz, K., Hewson-Stoate, N., and Schönwiesner, M. (2007). Cortical response to auditory motion suggests an asymmetry in the reliance on inter-hemispheric connections between the left and right auditory cortices. J. Neurophysiol. *97*, 1649–1655.

Kuśmierek, P., and Rauschecker, J.P. (2014). Selectivity for space and time in early areas of the auditory dorsal stream in the rhesus monkey. J. Neurophysiol. *111*, 1671–1685.

Lee, C.-C., and Middlebrooks, J.C. (2011). Auditory cortex spatial sensitivity sharpens during task performance. Nat. Neurosci. *14*, 108–114.

Logothetis, N.K., Guggenberger, H., Peled, S., and Pauls, J. (1999). Functional imaging of the monkey brain. Nat. Neurosci. *2*, 555–562.

Lomber, S.G., and Malhotra, S. (2008). Double dissociation of 'what' and 'where' processing in auditory cortex. Nat. Neurosci. *11*, 609–616.

Magezi, D.A., and Krumbholz, K. (2010). Evidence for opponent-channel coding of interaural time differences in human auditory cortex. J. Neurophysiol. *104*, 1997–2007.

Malhotra, S., Hall, A.J., and Lomber, S.G. (2004). Cortical control of sound localization in the cat: unilateral cooling deactivation of 19 cerebral areas. J. Neurophysiol. *92*, 1625–1643.

McAlpine, D., Jiang, D., and Palmer, A.R. (2001). A neural code for low-frequency sound localization in mammals. Nat. Neurosci. *4*, 396–401.

Middlebrooks, J.C., Clock, A.E., Xu, L., and Green, D.M. (1994). A panoramic code for sound location by cortical neurons. Science *264*, 842–844.

Miller, L.M., and Recanzone, G.H. (2009). Populations of auditory cortical neurons can accurately encode acoustic space across stimulus intensity. Proc. Natl. Acad. Sci. USA *106*, 5931–5935.

Młynarski, W. (2015). The opponent channel population code of sound location is an efficient representation of natural binaural sounds. PLoS Comput. Biol. *11*, e1004294.

Nelken, I., Bizley, J.K., Nodal, F.R., Ahmed, B., King, A.J., and Schnupp, J.W.H. (2008). Responses of auditory cortex to complex stimuli: functional organization revealed using intrinsic optical signals. J. Neurophysiol. *99*, 1928–1941.

Nili, H., Wingfield, C., Walther, A., Su, L., Marslen-Wilson, W., and Kriegeskorte, N. (2014). A toolbox for representational similarity analysis. PLoS Comput. Biol. *10*, e1003553.

Nodal, F.R., Bajo, V.M., and King, A.J. (2012). Plasticity of spatial hearing: behavioural effects of cortical inactivation. J. Physiol. *590*, 3965–3986.

Ortiz-Rios, M., Kuśmierek, P., DeWitt, I., Archakov, D., Azevedo, F.A.C., Sams, M., Jääskeläinen, I.P., Keliris, G.A., and Rauschecker, J.P. (2015). Functional MRI of the vocalization-processing network in the macaque brain. Front. Neurosci. *9*, 113.

Palomäki, K.J., Tiitinen, H., Mäkinen, V., May, P.J.C., and Alku, P. (2005). Spatial processing in human auditory cortex: the effects of 3D, ITD, and ILD stimulation techniques. Brain Res. Cogn. Brain Res. *24*, 364–379.

Pandya, D.N., and Rosene, D.L. (1993). Laminar termination patterns of thalamic, callosal, and association afferents in the primary auditory area of the rhesus monkey. Exp. Neurol. *119*, 220–234.

Pecka, M., Brand, A., Behrend, O., and Grothe, B. (2008). Interaural time difference processing in the mammalian medial superior olive: the role of glycinergic inhibition. J. Neurosci. *28*, 6914–6925.

Petkov, C.I., Kayser, C., Augath, M., and Logothetis, N.K. (2006). Functional imaging reveals numerous fields in the monkey auditory cortex. PLoS Biol. *4*, e215.

Petkov, C.I., Kayser, C., Steudel, T., Whittingstall, K., Augath, M., and Logothetis, N.K. (2008). A voice region in the monkey brain. Nat. Neurosci. *11*, 367–374.

Poremba, A., Malloy, M., Saunders, R.C., Carson, R.E., Herscovitch, P., and Mishkin, M. (2004). Species-specific calls evoke asymmetric activity in the monkey's temporal poles. Nature *427*, 448–451.

Rauschecker, J.P., and Tian, B. (2000). Mechanisms and streams for processing of "what" and "where" in auditory cortex. Proc. Natl. Acad. Sci. USA *97*, 11800–11806.

Rauschecker, J.P., Tian, B., and Hauser, M. (1995). Processing of complex sounds in the macaque nonprimary auditory cortex. Science *268*, 111–114.

Reser, D.H., Fishman, Y.I., Arezzo, J.C., and Steinschneider, M. (2000). Binaural interactions in primary auditory cortex of the awake macaque. Cereb. Cortex *10*, 574–584.

Romanski, L.M., Tian, B., Fritz, J., Mishkin, M., Goldman-Rakic, P.S., and Rauschecker, J.P. (1999). Dual streams of auditory afferents target multiple domains in the primate prefrontal cortex. Nat. Neurosci. *2*, 1131–1136.

Saad, Z.S., Reynolds, R.C., Cox, R.J., Argall, B., and Japee, S. (2004). SUMA: An Interface for Surface-Based Intra- and Inter-Subject Analysis with AFNI (ISBI). http://dx.doi.org/10.1109/ISBI.2004.1398837.

Saleem, K.S., and Logothetis, N.K. (2012). A Combined MRI and Histology Atlas of the Rhesus Monkey Brain in Stereotaxic Coordinates, 2nd Edn., Horizontal, Coronal and Sagittal Series (Elsevier/Academic Press).

Salminen, N.H., May, P.J.C., Alku, P., and Tiitinen, H. (2009). A population rate code of auditory space in the human cortex. PLoS ONE *4*, e7600.

Shmuel, A., Augath, M., Oeltermann, A., and Logothetis, N.K. (2006). Negative functional MRI response correlates with decreases in neuronal activity in monkey visual area V1. Nat. Neurosci. *9*, 569–577.

Spierer, L., Bellmann-Thiran, A., Maeder, P., Murray, M.M., and Clarke, S. (2009). Hemispheric competence for auditory spatial representation. Brain *132*, 1953–1966.

Stange, A., Myoga, M.H., Lingner, A., Ford, M.C., Alexandrova, O., Felmy, F., Pecka, M., Siveke, I., and Grothe, B. (2013). Adaptation in sound localization: from GABA(B) receptor-mediated synaptic modulation to perception. Nat. Neurosci. *16*, 1840–1847.

Stecker, G.C., and Middlebrooks, J.C. (2003). Distributed coding of sound locations in the auditory cortex. Biol. Cybern. *89*, 341–349.

Stecker, G.C., Harrington, I.A., and Middlebrooks, J.C. (2005). Location coding by opponent neural populations in the auditory cortex. PLoS Biol. *3*, e78.

Tian, B., Reser, D., Durham, A., Kustov, A., and Rauschecker, J.P. (2001). Functional specialization in rhesus monkey auditory cortex. Science *292*, 290–293.

Wandell, B.A., Dumoulin, S.O., and Brewer, A.A. (2007). Visual field maps in human cortex. Neuron *56*, 366–383.

Warren, J.D., Zielinski, B.A., Green, G.G.R., Rauschecker, J.P., and Griffiths, T.D. (2002). Perception of sound-source motion by the human brain. Neuron *34*, 139–148.

Werner-Reiss, U., and Groh, J.M. (2008). A rate code for sound azimuth in monkey auditory cortex: implications for human neuroimaging studies. J. Neurosci. *28*, 3747–3758.

Werner-Reiss, U., Kelly, K.A., Trause, A.S., Underhill, A.M., and Groh, J.M. (2003). Eye position affects activity in primary auditory cortex of primates. Curr. Biol. *13*, 554–562.

Wilke, M., and Lidzba, K. (2007). LI-tool: a new toolbox to assess lateralization in functional MR-data. J. Neurosci. Methods *163*, 128–136.

Woods, T.M., Lopez, S.E., Long, J.H., Rahman, J.E., and Recanzone, G.H. (2006). Effects of stimulus azimuth and intensity on the single-neuron activity in the auditory cortex of the alert macaque monkey. J. Neurophysiol. *96*, 3323–3337.

Zatorre, R.J., and Belin, P. (2001). Spectral and temporal processing in human auditory cortex. Cereb. Cortex *11*, 946–953.

Zatorre, R.J., Bouffard, M., Ahad, P., and Belin, P. (2002). Where is 'where' in the human auditory cortex? Nat. Neurosci. *5*, 905–909.

STAR★METHODS

KEY RESOURCES TABLE

REAGENT or RESOURCE	SOURCE	IDENTIFIER
Deposited Data		
Auditory-Space/data	Echo Planar Imaging datasets, https://dx.doi.org/10.6084/m9.figshare.4508576.v4	https://figshare.com/articles/Auditory_Space_data/4508576
Software and Algorithms		
AFNI/SUMA	Cox, 1996	RRID: SCR_005927
FreeSurfer	Dale et al., 1999	RRID: SCR_001847
ParaVision 4	Bruker, BioSpin GmbH, Ettlingen, Germany	RRID: SCR_001964
(MATLAB) Circular Statistis Toolbox	Berens, 2009	https://philippberens.wordpress.com/code/circstats/
(MATLAB) LI-toolbox	Wilke and Lidzba, 2007	http://www.medizin.uni-tuebingen.de/kinder/en/research/neuroimaging/software/
(MATLAB) toolbox for RSA	Nili et al., 2014	http://www.mrc-cbu.cam.ac.uk/methods-and-resources/toolboxes/
Custom scripts	This paper	https://github.com/ortizriosm/Auditory-space

CONCTACT FOR REAGENT AND RESOURCE SHARING

Further information and requests for resources and reagents should be directed, to and will be fulfilled by the Lead Contact, Dr. Michael Ortiz Rios (michael.ortiz-rios@newcastle.ac.uk).

EXPERIMENTAL MODEL AND SUBJECT DETAILS

All neuroimaging data was obtained from four rhesus monkeys *(Macaca mulatta)*; two males and two females paired in groups of two or more. Experiments under anesthesia were performed in the two male monkeys (M1 and M2, 6-7 years of age, weighing 6-8 kg) while experiments in awake-fMRI were performed in the two female monkeys (M3 and M4, 7-8 years of age, weighing 8 kg each). Monkeys designated for awake experiments were implanted with head-holder under general anesthesia with isoflurane (1%–2%) following pre-anesthetic medication with glycopyrrolate (i.m. 0.01 mg/kg) and ketamine (13 mg/kg). All surgical procedures under anesthesia were approved by the local authorities (Regierungspräsidium Tübingen) and were handled in accordance with the German law for the protection of animals and guidelines of the European Community (EUVD 86/609/EEC) for the care and use of laboratory animals.

METHOD DETAILS

Auditory stimuli

Stimuli for tonotopic mapping consisted of 250 ms pure tones (PT), 1/3-octave and 1-octave band-pass noise bursts with center frequency every octave from 0.125 to 16 kHz. These sounds were further filtered with an inverted macaque audiogram to simulate the effect of different ear sensitivity at multiple frequencies. The stimuli were equalized so that they produced equal maximum root mean square (RMS) amplitude (using a 200-ms sliding window) in filtered recordings. During experiments, all stimuli were played using a QNX real-time operating system (QNX Software Systems, Ottawa, Canada), amplified (Yamaha, AX-496) and delivered at a calibrated RMS amplitude of ~80 dB SPL through electrostatic in-ear headphones (SRS-005S +SRM-252S, STAX, Ltd., Japan) attach to a customize silicon earmold.

Binaural sound recordings

Monkeys were anesthetized (ketamine 0.2 mL + medetomidine 0.4 ml) inside an MRI-chair placed inside a sound-insulated acoustic chamber (Illtec, Illbruck Acoustic GmbH, Germany). In-ear miniature microphones (Danish Pro Audio 4060) were placed at the entrance of the ear canals of the animal. A broadband noise signal (0.125-16 kHz, 100 ms in duration) was generated in MATLAB (MATLAB 7.10) at a sampling rate and resolution of 48 kHz/16-bit and played through a loudspeaker (Apple Pro M653170, 2.2 cm

radius) mounted on a circular frame around the MRI-chair. The recorded signals from the microphones were pre-amplified (Saffire Pro 40, Focusrite) and recorded using Adobe Audition CS6 (Adobe, San Jose, CA).

The noise bursts were played every 5° (72 horizontal angle steps) from −180° to +180° at 0° elevations from the interaural plane. A full horizontal plane was recorded at four distances (20, 30, 40 and 50 cm) from head-center for a total of 72 recordings per distance. The signals measured ~82 dB SPL at 20 cm and ~70 dB SPL at 50 cm from the center of the monkey's head (Brüel and Kjær 2238 Mediator SPL meter with the 4188 microphone). Recorded sounds contained all individual spatial cues (ITDs, interaural level differences [ILDs], and spectral cues, Figures S3A and S3B).

Offline, the recorded noise bursts were concatenated every 5° to form 12 spatial sectors (Figure 2G). For example, for positions referring to the 0° to 30° sector the stimuli were concatenated in the following way: From 0° at a distance of 50 cm to 15° at a distance of 20 cm every 5° to form a looming pattern and from 15° at a distance of 20 cm to 30° at a distance of 50 cm to form a receding pattern; total duration = 1200 ms). The same pattern was applied inversely (30°/50 cm to 15°/20 and from 15°/20 to 30°/50). This pattern shifts in directionality (2400 ms) was repeated 3 times (total time = 7200 ms). Such patterns were used to avoid adaptation in the BOLD responses (Dahmen et al., 2010), to control for directionality (e.g., toward ear/away from ear) and to introduce dynamic and amplitude modulation into the perception of horizontal positions. For the stimulus manipulation of ITD we calculated interaural delay between left and right microphone signals using cross-correlation and subtracted the computed lag from either the left or the right microphone signal.

Behavioral training for awake-monkey fMRI

Monkeys assigned to awake-fMRI experiments (M3 and M4) were trained to sit still in an MRI-compatible primate chair placed inside an acoustically shielded box simulating the scanner environment. Inside the box, the animals were trained to be accustomed to wear headphone equipment and to hear simulated scanner noise, presented by a loudspeaker. Eye movements were monitored using an infrared eye-tracking system (iView, SensoMotoric Instruments GmbH, Teltow, Germany). Typically, while being trained or scanned in the absence of any visual stimulation in darkness, the monkeys kept their eyes closed resembling a light sleep condition.

Anesthesia for fMRI

Anesthesia procedures have been described elsewhere (Logothetis et al., 1999). In brief, anesthesia was induced with a cocktail of short-acting drugs (fentanyl at 3 μg/kg, thiopental at 5 mg/kg, and the muscle relaxant succinyl-choline chloride at 3 mg/kg) after premedication with glyco-pyrrolate (i.m. 0.01 mg/kg) and ketamine (i.m. 15 mg/kg). Anesthesia was then maintained with remifentanil (0.5^{-2} ug/kg/min) and the muscle relaxant mivacurium chloride (5 mg/kg/h). Physiological parameters (heart rate, blood pressure, blood oxygenation, expiratory CO_2 and temperature) were monitored and kept in desired ranges with fluid supplements. Data acquisition started approximately ~2 hr after the start of animal sedation.

MRI data acquisition

Images for anesthetized experiments were acquired with a vertical 7T magnet running ParaVision 4 (Bruker, BioSpin GmbH, Ettlingen, Germany) and equipped with a 12-cm quadrature volume coil covering the whole head. All images were acquired using sparse acquisition design with an in-plane resolution of 0.75 × 0.75 mm^2 with a 2 mm axial slice aligned parallel to the superior temporal gyrus (STG) (Figures 1A and 1B).

For functional data, gradient-echo echo planar images (GE-EPI) were acquired with 4-segments shots (TR = 500 ms, TE = 18 ms, flip angle = 40°, FOV = 96 × 96 mm^2, matrix = 128 × 128 voxels, slices = 9 - 11, slice thickness = 2 mm, resolution = 0.75 × 0.75 × 2 mm^3 voxel size) with slices aligned to the STG. Followed by the functional scans, two in-session volumes (FLASH and RARE) were acquired with the following parameters: for RARE (TE = 48 ms, TA = 24 ms, TR = 4000 ms, flip angle = 180°, FOV = 96 × 96, matrix = 256 × 256 voxels, resolution = 0.375 × 0.375 mm^2, slice thickness = 2 mm, slices = 9-11); for FLASH (TE = 15 ms, TA = 24 ms, TR = 2000 ms, flip angle = 69°, FOV = 96 × 96, matrix = 256 × 256 voxels, resolution = 0.375 × 0.375 mm^2, slice thickness = 2 mm, slices = 9-11). For tonotopic mapping experiments with anesthetized animals, 14 EPI runs (120 volumes) were acquired for M1 over one experimental session (day) and 16 runs (120 volumes) for M2 over one session; while for azimuth space experiments, 14 runs (150 time points each) were acquired for M1 over two sessions and 23 runs for M2 over two sessions.

Anatomical images, we acquired with high-resolution scan using a T1-weighted three-dimensional (3D) MDEFT pulse sequence (4 segments, TR = 15 ms, TE = 5.5 ms, flip angle = 16.7 ms, FOV = 112 × 112 × 60.2 mm^3; matrix = 320 × 320 × 172 voxels, number of slices = 172, resolution = 0.35 × 0.35 × 0.35 mm^3 voxel size). A total of 6 scans were acquired to form an average MDEFT high-resolution volume.

Measurements for awake-experiments were made on a vertical 4.7T magnet (Bruker, BioSpin GmbH, Ettlingen, Germany) equipped with a 12-cm quadrature volume coil. We acquired functional images with 360 volumes per run for each monkey (GE-EPI sequence: TR = 1000 ms, TE = 18 ms, flip angle = 53°, FOV = 96 × 96 mm^2, matrix = 96 × 96 voxels, number of slices = 18, slice thickness = 2 mm, resolution = 1.0 × 1.0 × 2 mm^3). For azimuth space experiments in awake-monkeys, 5 runs (360 volumes) were acquired for M3 over one session. Given that 3 volumes were acquired in sparse sampling and the emitted power at any given sequential volume was different but comparable across sparse blocks we separated first, second and third volumes and created 3 separate time courses (120 volumes each) per run. Thus a total of 15 runs per monkey were analyzed.

Anatomical images were acquired with an MDEFT sequence customized for awake-experiments (TE = 15 ms, TA = 840 ms, TR = 2320 ms, flip angle = 20°, FOV = 96 × 96 × 80 mm^3, matrix = 192 × 192 × 80 voxels, slice thickness = 1 mm, resolution = 0.5 × 0. 5 × 1 mm^3).

QUANTIFICATION AND STATISTICAL ANALYSIS

GLM analyses

FMRI data analyses were performed using AFNI (Cox, 1996), FreeSurfer (Dale et al., 1999), SUMA (Saad et al., 2004) and MATLAB (*MathWorks*). Preprocessing included slice-timing (3dTshift) correction, spatial-smoothing (3dmerge, 1.5 mm full width at half-maximum Gaussian kernel) and scaling of the time series at each voxel by its mean. Subsequent analyses were performed on both smooth and un-smooth data.

Smooth data was used mainly for visualization purposes while most second order analyses (e.g., dissimilarity analyses) were performed on unsmooth data. For awake-fMRI data, motion correction (3dvolreg) was used to exclude volumes that contained motion shifts > 0.5 mm and/or rotations > 0.5 degrees from further analyses. Lastly, we used 3dDeconvolve for linear least-squares detrending to remove nonspecific variations (i.e., scanner drift) and regression. Following preprocessing, data were submitted to general linear modeling analyses which included 12 spatial-condition-specific regressors and six estimated motion regressors of no interest for awake-fMRI data. For each stimulus condition (sectors 1 to 12) we estimated a regressor by convolving a one-parameter gamma distribution estimate of the hemodynamic response function with the square-wave stimulus function. We then performed t tests contrasting each azimuth sector condition with baseline ("silent" trials). To obtain auditory modulated voxels we first contrast all sounds versus silent conditions to select voxels for further analyses (see also Figure S1). Subsequently, contrast analyses between equidistant spatial sectors were performed to quantify hemifield biases.

The average anatomical scans (n = 6) were spatially normalized (3dAllineate), the head and skull removed (3dSkullStrip), and extracted brains were corrected for intensity non-uniformities from the radiofrequency coil (3dUniformize). After intensity corrections, the volumes were segmented to obtain white and gray matter. Whole-brain surfaces were then rendered along with the extracted surfaces of the STG using Freesurfer (Figure 1B). Finally, we illustrated the results on a semi-inflated cortical surface extracted with SUMA to facilitate visualization and identification of cortical regions and boundaries.

FMRI phase-mapping analyses

3dRetinoPhase scripts from AFNI were used for phase-mapping analyses. The coherence of the fMRI time series at the stimulus presentation cycle was used to measure the strength of the BOLD response amplitude in each voxel. Coherence measures the ratio of the amplitude at the fundamental frequency to the signal variance, ranging between 0 and 1 (Barton et al., 2012; Wandell et al., 2007). The measure of coherence is

$$C(f_0) = A(f_0) \Big/ \left(\sum_{f = f_0 - \frac{\Delta f}{2}}^{f_0 + \frac{\Delta f}{2}} A\ (f)^2 \right)^{\frac{1}{2}}$$

where f_0 is the stimulus frequency, $A(f_0)$ the amplitude of the signal at that frequency, $A(f)$ the amplitude of the harmonic term at the voxel temporal frequency f and Δf the bandwidth of frequencies in cycles/scan around the fundamental frequency f_0. For all tonotopy stimuli f_0 corresponds to twelve cycles (12/1200 s = 0.01 Hz) and Δf corresponds to the frequencies around the fundamental excluding the second and third harmonics (see Figure 2A for an example of voxel harmonics). In the case of spatial mapping, f_0 corresponds to twelve cycles (12/1800 s = 0.0067 Hz). Each voxel was given a coherence threshold value of 0.3. The phase response at f_0 encodes the sound frequency (or azimuth in degrees in case of the spatial domain) (see Figure 1E for an example of three voxels in A1). Phase peaks were plotted across cortical space for qualitatively comparison between sound frequency and space maps (see Figure S3). Volumes acquire during silent periods were excluded from this analysis.

Laterality index

Significant activations (q FDR > 0.05) from the two hemispheres were used to calculate a laterality index (LI). Given that LIs show a threshold dependency we measured LI curves to provide a more comprehensive estimate over a whole range of thresholds and to ensure that lateralization effects were not caused by small numbers of highly activated voxels across hemispheres. The LI curves were based on t-values obtained from each condition and were calculated using the LI-toolbox (Wilke and Lidzba, 2007) with the following options: +5 mm mid-sagittal exclusive mask, clustering with a minimum of 5 voxels and default bootstrapping parameters (min/max sample size 5/10000 and bootstrapping set to 25% of data). The bootstrapping method calculates 10,000 times LIs using different thresholds ranging from 0 until the maximum t-value for each condition. For each threshold a cut-off mean value is obtained from which a weighted mean (LIwm) index is calculated (Wilke and Lidzba, 2007). This analysis returns a single value between −1 and 1 referring to a right- or left-sided hemispheric bias. Indices between −0.25 and +0.25 were used to exclude a lateralization bias. Indices higher than +0.5 or below −0.5 were designated strongly lateralized.

Spatial tuning curves

Circular statistics and spatial tuning curves were performed using the CircStat toolbox for MATLAB (Berens, 2009). The spatial spread of the BOLD response to each azimuth sector was used to calculate spatial tuning curves. The total number of voxels per CR was used to calculate the percentage of significantly active voxels (q FDR < 0.05), either positive or negative, per azimuth sector. Descriptive statistics, mean, resultant vector length, variance, standard deviation and confidence intervals (see Table S1) were calculated using the following functions: *circ_mean*, *circ_r*, *circ_var*, *stats* and *circ_confmean* respectively. A Rayleigh test was applied to all circular data with the function *circ_rtest*, to test whether data was uniformly distributed around the circle or had a common mean direction. All deviations from circular uniformity were highly significant (Rayleigh test, $p < 0.001$) for all CRs, accepting the alternative hypothesis of a non-uniform distribution.

FMRI dissimilarity analyses

Representational similarity analyses (RSA) were performed using the MATLAB toolbox for RSA (Nili et al., 2014). The beta coefficients (β) obtained from the fitted GLM to each stimulus condition ($n = 12$) were subjected to pairwise Pearson's correlation (R) and the distance ($1 - R$) to each spatial sector was ordered into a 12×12 representational dissimilarity matrix (RDM) (Figure 7). This analysis was repeated for each CR, AC and hemifield model, providing a total of 11 RDMs (Figures S6A and S6B). For further analyses, we averaged the RDMs for each session and monkey, resulting in one RDM for each CR or hemisphere and model. To visualize the geometry of the responses without assuming any categorical structure we used multidimensional scaling (MDS). MDS arranges the spatial position of sound sources in two dimensions such that the distance between them reflects the dissimilarities between the response patterns they elicited. Similar hierarchical clustering was used to visualize the subdivisions in responses patterns. However, unlike MDS, this method assumes the existence of some structure, but not a particular arrangement.

For the hemifield code RDM we used the ITD delay functions for pairwise correlations (Figure S6C) and linearly combined noisy estimates of the ITD RDM with a categorical-model RDM (Figure S6D). We then measured the relationships between the matrices by calculating the dissimilarity distance ($1 -$ Spearman's R) obtaining a second-order dissimilarity matrix (Figure S6E). We used Spearman's correlation coefficient as to not assume a linear match between RDMs from CRs and the hemifield model (Kriegeskorte et al., 2008). Multidimensional scaling (MDS) was then performed on the second-order RDM to visualize the similarity distances between cortical representations and the hemifield model (Figure 7E).

DATA AND SOFTWARE AVAILABILITY

The accession number for the imaging data reported in this paper is http://dx.doi.org/10.6084/m9.figshare.4508576. Custom scripts had been deposited under https://github.com/ortizriosm/Auditory-space.

ADDITIONAL RESOURCES

Additional information about brain research on non-human primates could be found on http://hirnforschung.kyb.mpg.de/en/homepage.html.

10.5 Illustrated description of the unsupervised network classifier developed for the study “Simultaneous resting-state and visually-driven functional networks in the macaque brain”.

Unsupervised Network Classifier

Objective: To group volumes of fMRI data based on spatial similarity using an unsupervised algorithm.

Inputs: fMRI spatial maps and a spatial similarity threshold. Currently, the threshold has to be decided a priori but alternative criteria, such as bootstrapping, can be straightforwardly implemented in potential future releases.

Algorithm: The code is matlab-based and works with different kinds of fMRI images; however, one of its function requires AFNI (http://afni.nimh.nih.gov/afni/). This algorithm can be easily expanded, taking into account additional features, such as temporal similarity or graph metrics factors. The description of the algorithm is illustrated with a real application to one of my datasets. The goal was to group 80 resting state networks, 20 from each of 4 sessions, in groups of four elements.

Step 1. To find all *n*-tuples permutations with repetition for all the components of each session for all *n*-sessions. Here, every possibility is referred to as a group candidate. In my example, the permutation of the four sessions resulted in 160.000 group candidates (20*20*20*20 components).

Step 2. To combine every two components of every group candidate and to calculate the pairwise spatial similarity coefficients for every combination. By default, spatial similarity coefficients are calculated with with AFNI's "3ddot" function. However, alternative similarity indexes, such as unscaled dot products, least square fit coefficients, eta-squared coefficients (Cohen et al. 2008) or Sorensen-Dice coefficients, can be selected instead. Concerning the example, six pairwise spatial correlation coefficients were calculated for each of all 160.000 group candidates (tables 1 and 2).

Table 1: All possible group candidates for a dataset containing 4 experimental sessions, namely B10.xK2, B10.yB1, B10.yn1 and B10.yP1. In this case, each element of the 4-tuple group represents 1 of the 20 components, numbered from 0 to 19, of each session.

Group candidate	B10.xk2 (components)	B10.yB1 (components)	B10.yn1 (components)	B10.yP1 (components)
01	0	0	0	0
02	0	0	0	1
…				
160.000	19	19	19	19

Table 2: A summary of every possible pairwise spatial similarity coefficient and related similarity indices (SI). SI was based on spatial correlation of voxels above an a priori chosen threshold (z > 1, rightmost column). Particularly to this case, SI is the root-mean-square level (rms) of all pairwise spatial similarity coefficients present in the corresponding row.

Group candidate	B10xk2 & B10yB1	B10xk2 & B10yn1	B10xk2 & B10yP1	B10yB1 & B10yn1	B10yB1 & B10yP1	B10yn1 & B10yP1	SI
01	0.78	0.79	0.80	0.76	0.84	0.78	0.7933
02	0.79	0.79	0	0.76	0	0	0.5499
…							
160.000	0.01	0.01	0.46	0.04	0.01	0	0.1887

Step 3: To calculate the similarity index (SI) for every group candidate. By default, SI is calculated as the root-mean square (rms) of all spatial similarity coefficients in each group candidate. The advantage of rms is pairwise proximity have a greater weight, facilitating the exclusion of outlier components in post hoc analysis (Fig. 1). Nonetheless, any other desired SI function can be passed as an argument to change the default SI calculation.

Case	A & B (PSS)	A & C (PSS)	A & D (PSS)	B & C (PSS)	B & D (PSS)	C & D (PSS)	SI (arithmetic mean)	SI (rms)
1	0.5	0.5	0.5	0.5	0.5	0.5	0.5000	0.5000
2	1	1	0	1	0	0	0.5000	0.6124

Fig. 1: Schematic representation of differences in the calculation of similarity indices using arithmetic mean and with root mean square (rms). Case 1 illustrates an instance where networks A, B, C and D partially overlap with each other with a correlation of 0.5. Alternatively, case B represents an occurrence where A, B and C perfectly overlap with each other but not at all with D. While arithmetic mean of pairwise spatial correlations can't differentiate both cases, rms provides a greater value in case B (attached table). In a post-hoc analysis, outliers present in case B can be easily identified and removed of the group. Note that in this illustration, each component is illustrated in 2D space; however, real fMRI components are volumetric objects and evaluated accordingly.

Table 3: Remaining groups with respective pairwise spatial similarity coefficients and spatial similarity indices.

Final group	B10xk2 B10yB1	B10xk2 B10yn1	B10xk2 B10yP1	B10yB1 B10yn1	B10yB1 B10yP1	B10yn1 B10yP1	SI
01	0.78	0.79	0.80	0.76	0.84	0.78	0.7933
02	0.79	0.75	0.84	0.67	0.77	0.77	0.7689
03	0.73	0.80	0.75	0.71	0.79	0.74	0.7521
04	0.61	0.86	0.69	0.64	0.81	0.71	0.7257
05	0.68	0.68	0.74	0.70	0.55	0.52	0.6493
06	0.68	0.53	0.72	0.43	0.64	0.64	0.6141
07	0.46	0.52	0.42	0.68	0.70	0.54	0.5624
08	0.49	0.56	0.63	0.52	0.55	0.58	0.5567
09	0.73	0.74	0.15	0.75	0.35	0.22	0.5537
10	0.68	0.53	0.52	0.61	0.54	0.36	0.5499
11	0.17	0.30	0.44	0.67	0.53	0.69	0.5048
12	0.14	0.34	0.46	0.56	0.41	0.54	0.4327
13	0.37	0.41	0.46	0.32	0.41	0.37	0.3917
14	0.31	0.44	0.24	0.21	0.68	0.19	0.3853
15	0.29	0.08	0.23	0.31	0.57	0.31	0.3329
16	0.33	0.26	0.30	0.32	0.39	0.35	0.3276
17	0.11	0.51	0.42	0.10	0.05	0.43	0.3271
18	0.03	0.01	0.24	0.49	0.08	0.02	0.2260
19	0.00	0.08	0.05	0.02	0.03	0.40	0.1674
20	0.00	0.02	0.00	0.00	0.00	0.02	0.0111

Step 4: To rank all group candidates in descending order of similarity indices.

Step 5: To exclude repeated components in less ranked groups. In this example, as the highest rank group candidate was composed of network components “0, 0, 0, 0”, all other group candidates containing component 0 were excluded. In the next step, the next highest rank group was chosen and the same process was exhaustively repeated (Tables 3 and 4).

Step 6: To average all components of each group.

Table 4: Final selected groups and respective components.

Final group	B10.xk2	B10.yB1	B10.yn1	B10.yP1
01	0	0	0	0
02	10	2	8	6
03	1	4	5	1
04	4	17	14	11
05	3	14	2	9
06	5	6	16	5
07	17	1	12	10
08	12	15	18	12
09	11	3	11	15
10	9	12	6	4
11	16	13	15	18
12	19	18	9	19
13	2	5	7	8
14	6	16	13	16
15	18	11	17	2
16	7	10	1	7
17	14	19	3	14
18	13	7	19	13
19	8	9	10	3
20	15	8	4	17

Results: Final groups clustered by our unsupervised network classifier.

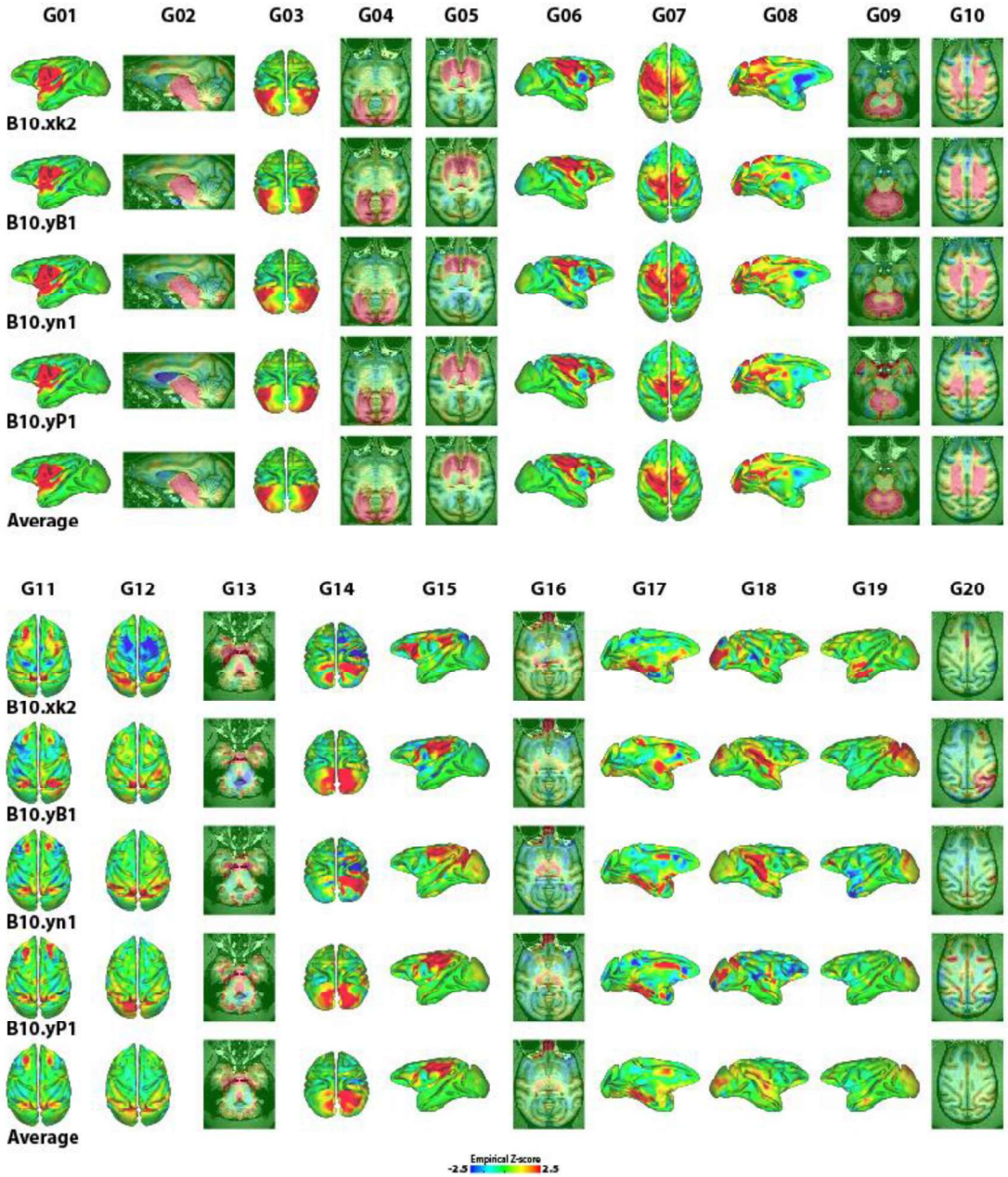

Figure 2. Groups of independent components automatically formed by our custom-written unsupervised network classifier dealing with all four different resting-state sessions of M1. Groups are displayed column-wise and are numbered from G01 to G20, while sessions are displayed row-wise (B10.xk2, B10.yB1, B10.yn1, and B10.yP1). Last row of top and bottom groups contain averages of the four individual components above it. Color scale represents empirical Z-scores outputted by GIFT software, which is a measure of similarity between the timecourse of each voxel with the timecourse of the related independent component (Calhoun et al. 2001).

"From my early youth I have had the strongest desire to understand or explain whatever I observed, –that is, to group all facts under some general laws. These causes combined have given me the patience to reflect or ponder for any number of years over any unexplained problem. As far as I can judge, I am not apt to follow blindly the lead of other men." — Charles Darwin.